DNA-MEDIATED HOLE AND ELECTRON TRANSPORT

Thesis by
Fangwei Shao

In Partial Fulfillment of the Requirements
for the Degree of
Doctor of Philosophy

California Institute of Technology
Pasadena, California

2008

(Defended June 26, 2007)

ACKNOWLEGEMENTS

My five-year studies at Caltech have been one of the most important and memorable periods in my life. I have always felt lucky and honored to become a member of this unique and world-class research institute. I have made acquaintance with so many intelligent and conscientious people who have inspired my enthusiasm for both science and life. They have been the role models in my professional development, as well as friends in my life. I owe an enormous debt of gratitude to each one of them.

First and foremost, I must thank my research advisor, Professor Jacqueline K. Barton. She has always been a great mentor to me. She is the person who led me into the fascinating world of DNA-mediated charge transport. During the first year in the lab, she had great patience to educate and transform me from a theoretical chemist to a handy bioinorganic experimentalist. I am amazed by her undying unyielding enthusiasm for chemistry and science in general. Her encouragement and brilliant ideas about research kept my spirits high as I struggled through the failures in experiments. I have always remembered the exciting spirit fulfilling me after every time that I discussed my projects with her. I admire her high standards for scientific researches and from her I learned to be a better critical thinker. She is truly an inspirational leader who brings together such a wonderful group of intelligent people who have contributed to my thesis work in various ways. Lastly, and perhaps mostly importantly, I thank you for the tremendous help you have provided for my scientific career. I eagerly look forward to our future interaction.

I have many thanks to Mo Renta for all she had done for me over these years. She makes things run smoothly around the lab. She is the person who had big contributions to educate my American style life. Because of Mo, I was able to focus on doing chemistries

and for that I think her immensely. Tom Dunn is able to fix almost everything when I asked for help and revived many instruments over the years. I also thank Dian Buchness who was the first person I talked to in Chemistry department and always a source of a smile. With Lura Howe, two of them made the administrative tasks of my graduate studies so easy.

I must also acknowledge my thesis committee. I thank Professor Dennis Dougherty for serving as chairman of my committee and for presiding over my candidacy and proposal defense. I also value highly the numerous discussions with my committee, including Professor Rudolph A. Marcus and Professor Harry Gray. Their insightful advice during my candidacy, fourth-year meetings and proposal defense are brilliant and inspire my thesis work a lot. I want to also thank my committee for taking time to read my proposal and research reports for all the exams.

Many Barton group members, both past and present, have provided me tremendous help in various ways during my time at Caltech. Dr. Tashica Williams was the person coaching my experimental technique when I first joined the Barton lab. She was extremely nice and patient with me and tolerated my “first-experiment curse” unconditionally. I owe a big thank you to her. I thank Professor Chikara Dohno who kindly shared his wisdom on the cyclopropylguanine project. I would also like to thank Professor Melanie O’Neill and Dr. Katherine Augustyn with whom I had a great collaboration in the cyclopropylamine-substituted base project. I must additionally thank both of them for helping me prepare the manuscripts of my two publications. Because of them, my scientific writing skills were improved. Professor Anne Petijean and Professor Eylon Yavin introduced me to the wonders of organic and inorganic synthesis.

Amazingly, they actually made me enjoy synthesizing transition metal complexes and cyclopropyl-modified bases. I must thank Dr. MiHee Lim for the intelligent discussion about both research and my future career, as well as being such a fantastic friend to me. She offered huge comforts to me, and made the tough graduation time and postdoc hunting endurable. I also thank her for introducing me to the authentic Korean food, and I enjoy that a lot. I am also looking forward to attending her wedding in Soul. Last but not the least, I want to thank rest of the Barton group for making the lab such a happy place to work.

I must present my appreciation to the Caltech Chinese community too. The Chinese students and scholars at Caltech constitute a caring family for me. Their considerations healed my homesickness and helped me go through the loneliness being away from my family. In particular, I want to thank Jie Yang, Yan Chen, and the cell group members, including Yanshun Liu, Rong Cai, Ke Wang and Jing Yang.

Lastly, I must thank my family for their unconditional love and support. Although they are thousands of miles away, their encouragement and care made tough times easier; without them I could never have made it this far. I would like to dedicate this work to my Mom and Dad for your endless sacrifices and support over the years; I am truly thankful.

ABSTRACT

Since the elucidation of the double helical structure of DNA, it has been proposed that the dynamic π-stacking base pair array may mediate charge migration, hole transport (HT), and electron transport (ET). In this thesis work, both DNA-mediated HT and ET are investigated to explore their mechanisms by using kinetically fast electron/hole traps: cyclopropylamine-substituted bases, especially N_4-cyclopropylcytosine (^{CP}C), and N_2-cyclopropylguanine (^{CP}G). Both biochemical reaction with a variety of photooxidants and electrochemistry show that the modified bases, ^{CP}C and ^{CP}G, have similar redox properties as the natural DNA bases and are irreversible kinetic traps by ring opening on the picosecond time scale.

In DNA assemblies containing either $[Rh(phi)_2(bpy')]^{3+}$ (Rh) or an anthraquinone derivative (AQ), two high energy photooxidants, appreciable oxidative damage at a distant ^{CP}C is observed, which shows that hole migration must involve also the higher energy pyrimidine bases. The damage yield is modulated by lower energy guanine sites on the same or complementary strand. Significantly, the efficiency in trapping at ^{CP}C is similar to that at flanking ^{CP}G. Thus, HT is not simply a function of the relative energies of the isolated bases, but instead may require orbital mixing among the bases. Hole migration through DNA involves occupation of all the DNA bases with radical delocalization.

The oxidation of ^{CP}C via distant photooxidants has been found also to be sensitive to intervening structure and sequences. AQ-modified DNA assemblies of identical base composition but different base sequence have been probed. Single and double base substitutions within A-tracts modulate ^{CP}C decomposition. In fact, the entire sequence

within the DNA assembly is seen to govern ^{CP}C oxidation, not simply the bases intervening between ^{CP}C and the tethered photooxidant.

These data are reconciled in a mechanistic model of conformationally gated hole transport through delocalized DNA domains. Oxidation of ^{CP}G separated from a tethered photooxidant by A-tracts with a series of lengths over 50 Å exhibits a nonmonotonically periodic distance dependence and shows that the domain sizes in the A-tract is 4–5 base pairs. Sequence-dependent DNA structure and dynamics are essential to the transient formation of the domains and hole propagation among the domains. This dynamic, delocalized model provides a basis to reconcile and exploit DNA HT chemistry.

Jus as long-range hole transport through DNA has now been established, DNA-mediated electron transport has not been as well characterized. Three iridium complexes have therefore been designed in order to initiate both photooxidative and photoreductive reaction of DNA and allow direct comparison between the two. Redox potentials of excited Ir complexes are determined by both triplet energy ($E_{0\text{-}0}$) and ground state redox potentials. Two of the iridium complexes prepared have excited state potentials that are suffcient to oxidize purines, but not pyrimidines. The excited state oxidation potentials of three Ir complexes are around −1.0 V and would be able to reduce DNA pyrimidines. Both ^{CP}C and ^{CP}G in DNA can be decomposed by photoirradiation with the noncovalently bound iridium complexes. In particular, two of the complexes have the potential to probe oxidation of purines and reduction of pyrimidines in DNA.

Studies were also conducted using one of the iridium complexes covalently tethered to DNA oligonucleotides. Hence the metal complex serves as both a photooxidant and photoreductant in the study of DNA-mediated hole and electron

transport. In the Ir-tethered DNA assemblies, a metal complex stabilizes the DNA duplex through its intercalative, functionalized dppz ligand. Cyclopropylamine-substituted bases, ^{CP}C and ^{CP}G, are used as kinetic fast electron and hole traps to probe the resulting charge migration processes after direct photoirradiation of the assemblies. Reductive decomposition of ^{CP}C via ET as well as the oxidation of ^{CP}G via HT is observed. Thus, the iridium tethered DNA containing cyclopropylamine-substituted bases provides a unique model system to explore the two DNA-mediated charge transport processes through the same DNA bridges. For the first time, ET and HT can be initialized by the same photoredox probe employing the identical electronic interaction mode with DNA.

A flash quench technique was also applied to Iridium-tethered DNA in order to generate the ground state photoreductant and initiate photoreduction using 5'-bromo-uridine (^{Br}U) as the electron trap. Efficiencies of ^{Br}U reduction in Ir-DNA upon flash quench technique was found to be comparable to that of ^{CP}G oxidation upon direct photoirradiation of Ir-DNA. Furthermore, in Ir-tethered DNA assemblies containing ^{CP}G or ^{Br}U as either the hole or electron trap, the sequence dependence of HT versus ET through an A-tract was examed. When ^{CP}G and ^{Br}U are placed in either purine or pyrimidine strands in A-tract, decomposition of both modified bases are observed. Thus, transient electron occupancy during ET, as well as hole occupancy during HT, are distributed onto both purine and pymidine strands in A-tract. Additionally, ^{Br}U decomposes in a more efficient fashion when it is located on a thyime-containing strands, which indicates that DNA-mediated ET prefers to pyrimidine strands rather than purine strands.

Chapter 1

Long Range Hole and Electron Transport through DNA.

1.1. Introduction

The first observation of right-handed double helical structure in B-form DNA was published more than 50 years ago.[1] The salient structure of DNA is simply described as an array of heterocyclic aromatic base pairs, stacked at a distance of 3.4 Å and wrapped within a negatively charged sugar phosphate backbone as shown in Figure 1.1.[2] About 10 years later, Eley and Spivey hypothesized the possibility that DNA can be a charge conduit based upon similarity of DNA structure to one-dimensional aromatic crystals.[3] Generally speaking, DNA-mediated charge transport (CT) includes two types of charge migration processes.[4] One is hole transport (HT), in which DNA is in an electron deficient status and the charge carrier is a radical cation.[5] On the other hand, in electron transport (ET), DNA is reduced and an excess electron is propagated through DNA.[6] The two processes are basically the same except for the involvement of the electronic orbitals of DNA oligonucleotides.

In the past four decades, a variety of biological and spectroscopic experiments have shown that DNA, besides guarding the integrity of our genome codes, is also unambiguously active when it comes to the transport of charge.[7] Among the nucleic acid bases free in solution, guanine has the lowest oxidation potential as shown in Figure 1.1 and thus is the easiest to be oxidized.[8] Reduction potentials of pyrimidines are the most available for DNA reduction.[9] Upon irradiation of photooxidants covalently bound to DNA, oxidative guanine damage can be promoted over a large molecular distance. Hole transport through DNA has been found to occur as far as 200 Å with well electronically coupled photooxidants (Figure 1.2).[10] The ability of DNA CT to repair thymine dimer has been discovered both in solution and on surfaces.[11,12] Donor- bridge-acceptor model

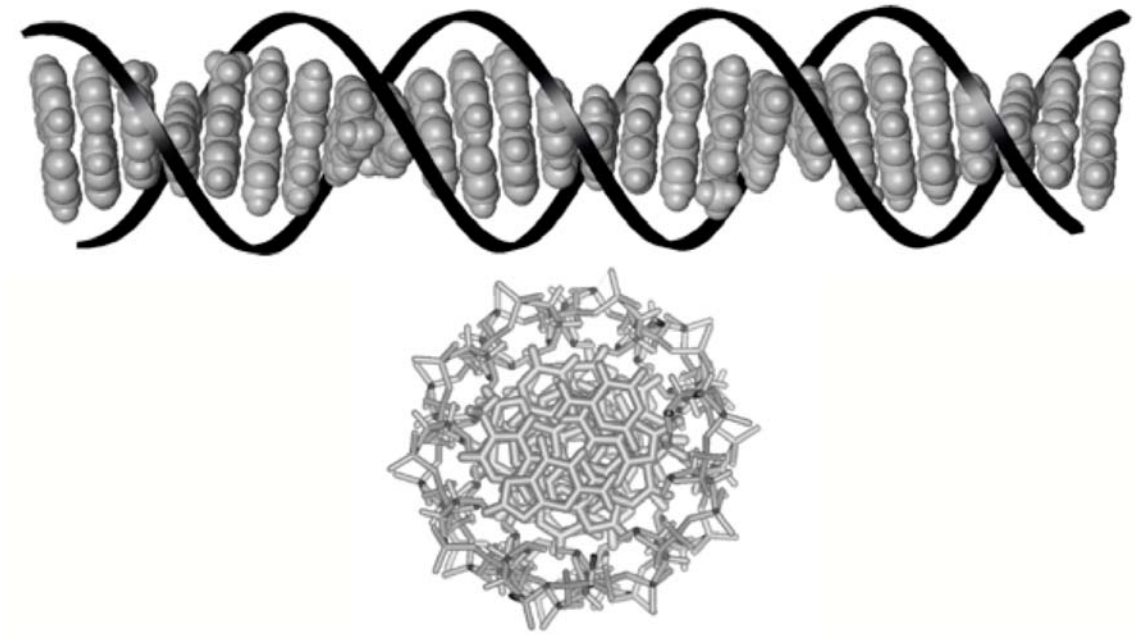

(A)

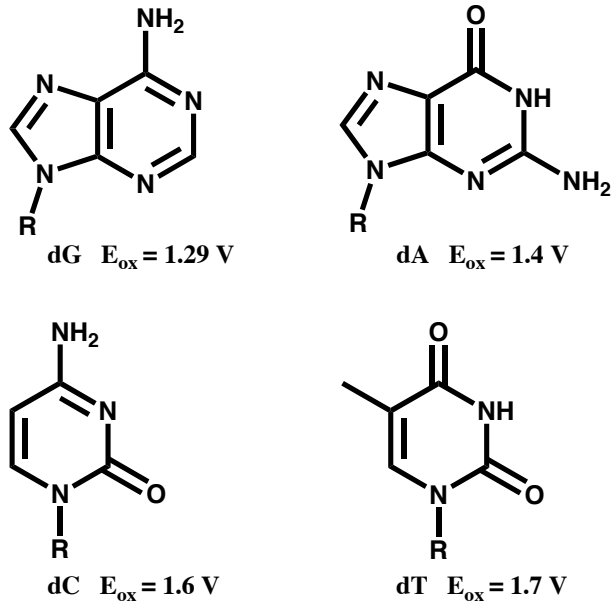

(B)

Figure 1.1. (A) Schematic representation of double helical DNA along the helical axis (*top*) where the array of π-stacked bases is shown in gray and the sugar-phosphate backbone as a ribbon in black and a view down the helical axis (*bottom*). (B) Structures of 2'-deoxynucleosides. R = 2'-deoxyribose. Oxidation potentials of nucleic acids are indicated in figure. The potentials are versus NHE.

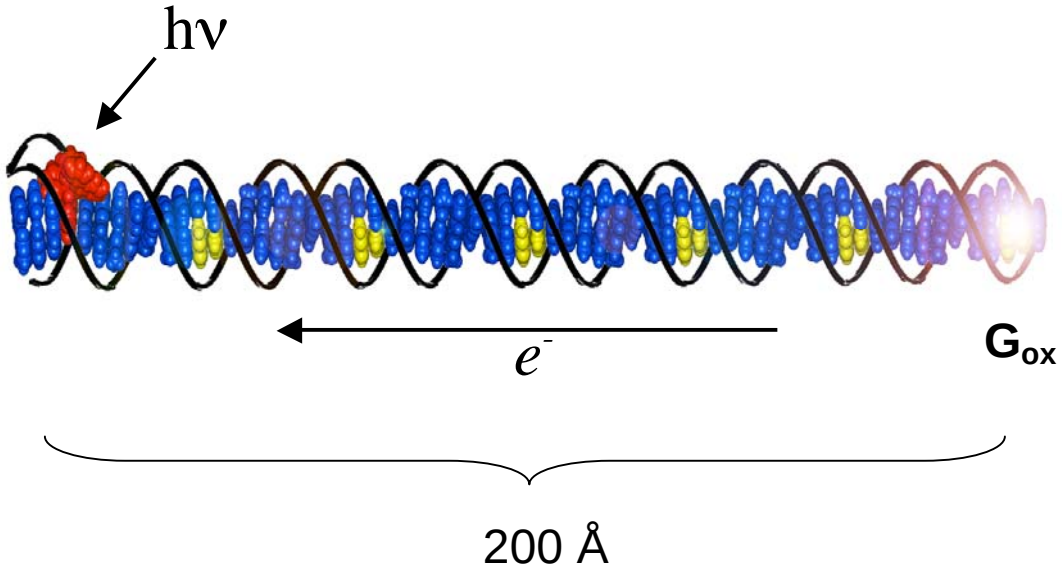

Figure 1.2. Schematic illustration of DNA-mediated hole transport through a 63-mer DNA duplex with covalently tethered Rh complex as photooxidant. Irradiation of Rh intercalator leads to oxidation of 5'-G in six guanine doublets over 200 Å. Figure is adapted from reference 10.

systems for exploiting DNA CT have been established by using a decade of biochemical and spectroscopic assays.[10,13-17] Given the substantial observations on DNA CT, scientists now are interested in the biological relevant applications of this process and also the fundamental mechanisms governing the features of DNA CT.

1.2. Model systems and experimental assays for DNA-mediated CT

1.2.1. Photoredox probes serve as charge donors and acceptors in model systems Charge transport through DNA is studied *in vitro* using external photoredox probes as photooxidants and photoreductants, as well as sometimes charge traps (Figure 1.2). These redox probes, which process well-characterized and varied redox, photophysical and photochemical properties, include metallointercalators, organic intercalators and modified bases.

Several transition metal complexes are used as photooxidants in the study of DNA HT. In particular, phenanthrequinone diimine (phi) ligand of Rh(III) complexes (e.g., $[Rh(phi)_2(bpy')]^{3+}$) and dipyridophenazine (dppz) ligand of Ru(II) complexes (e.g., $[Rh(phen)(bpy')(dppz)]^{2+}$) facilitate tight binding of the octahedral complexes by intercalating into DNA base pair stacking.[18] The interaction modes of these complexes have been well characterized by spectroscopy and crystallography. High-resolution NMR shows the complexes are major groove binders and the ancillary, non-intercalating ligands of the complexes define the sequence specificity of the DNA binding.[19] A 1.2 Å crystal structure of Δ-α-$[Rh(R,R,$-dimethyltrien)(phi)$]^{3+}$ with a DNA octamer demonstrates that the oligonucleotide duplex accommodates the intercalative ligand as an extra base pair without disturbing the overall structure of DNA.[20] Additionally, Ru(II)

Metallointercalators

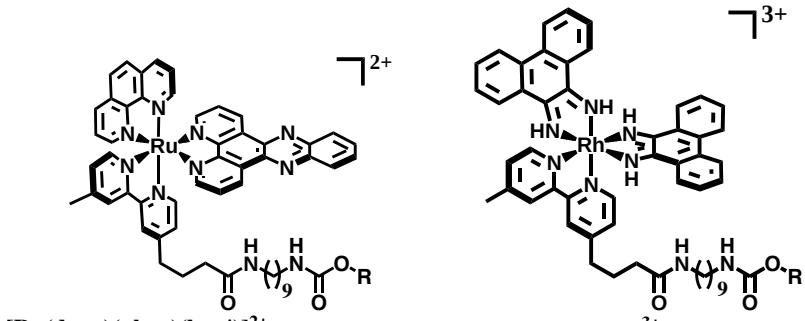

[Ru(dppz)(phen)(bpy')]$^{2+}$ **[Rh(phi)$_2$(bpy')]$^{3+}$**

Organic intercalators

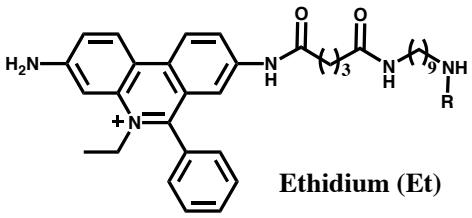

Ethidium (Et)

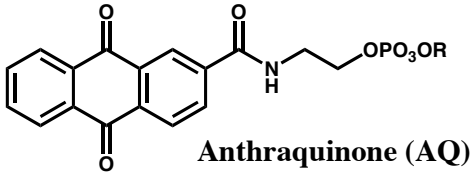

Anthraquinone (AQ)

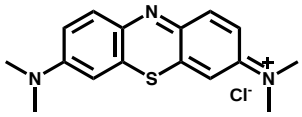

Methylene Blue (MB)

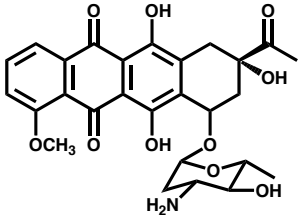

Daunomycin (DM)

Modified bases

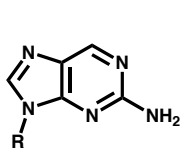

2-Aminopurine (Ap)

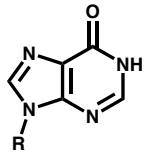

Inosine (I)

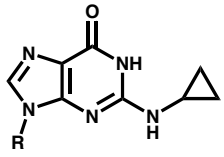

N_2-Cyclopropylguanine (^{CP}G)

1-N^6-Ethenoadenine (εA)

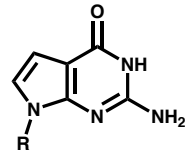

7-Deazaguanine (^{z}G)

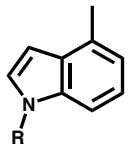

Methylindole (M)

Figure 1.3. Structures of intercalators and modified DNA bases used in studies of DNA-mediated charge transport.

dppz complexes are well known as a “DNA light-switch” due to their intercalative contact mode with DNA.[21] Protonation of the dppz imine in these complexes results a luminescence quench in aqueous solution. Intercalation within the DNA π-stack protects the phenazine nitrogens from water and restores the luminescence of the complex.

Organic intercalators often have optical or electrochemical properties that can be used to exploit either DNA HT or DNA ET. As shown in the middle of Figure 1.3, Ethidium (Et), intercalating into DNA with the similar association constant as metallointercalators ($K \sim 10^6$ M^{-1}),[22] exhibits strong fluorescence in the presence and absence of DNA,[23] which provides extensive application of Et to spectroscopic studies of DNA CT.[24,25] The excited Et can only promote reaction with reagent of low oxidation potentials, such as 7-deazaguanine, which is due to insufficient potential of Et ($E(Et^{*/0} \sim$ 1.2 V versus NHE) compared to natural bases.[26] Another type of organic intercalators, such as methylene blue (MB) and daunomycin (DM) have reversible reduction at negative potentials.[27] Whether covalently cross-linked or non-covalently bound to DNA, these molecules can intercalate tightly to DNA and are used as electrochemical probes in the studies of ground-state DNA-mediated ET on an electrode film.[28] In particular, DM is readily covalently attached to the guanine residues in double stranded DNA and the structure of DM-DNA conjugates are well characterized by crystallography.[29] Additionally, several organic molecules have proper redox potential upon excitation and can be used as photooxidants (e.g., anthraquinone, (AQ: $E^{*/-} \sim 2.0$ V versus NHE)[30] and photoreductants[31] (e.g., flavin and aromatic amines $E^{*/+} \sim -2.6$ V versus NHE) in the investigation of DNA CT. However, their interaction modes with DNA are not well characterized and may not stack with DNA base pairs by intercalation.

Nature generates modified DNA bases by methylation and oxidation of natural DNA bases.[32] In the study of DNA CT, we take advantage of modified bases since they have minimal perturbation on structures and dynamics upon incorporation into DNA and meanwhile modulate the redox properties, chemical reactivity and photophysics of nucleic acid bases. For example, adenine analogues, 2-aminopurine (Ap) and 1-N_6-ethenoadenine (εA), are fluorescent bases that can serve as photooxidants (Ap: $E^{*/-}$ ~ 1.5 V; εA: $E^{*/-}$ ~ 1.4 V versus NHE).[33] The fluorescence quenching of the two bases in DNA was applied to characterize the features of DNA HT. Guanine analogues, such as 7-deazaguanine (^{Z}G) and methylindole (M), are two unnatural bases which have lower potentials than guanine and thus can serve as a thermal hole sink in model system for DNA HT.[26,34] In addition, since methylindole generates a signature radical cation signal upon oxidation, M makes an ideal probe for investigation of CT by transient absorption spectroscopy.[34]

1.2.2. Spectroscopic, biochemical, and electrochemical assays for exploiting DNA-mediated CT

1.2.2.1. Probe DNA-mediated CT by optical spectroscopy A variety of spectroscopic techniques are applied to investigate the optical property variations of either the charge donors and/or acceptors in model systems via DNA CT.[34-36] Time-resolved techniques combined with steady-state spectroscopy allow us to probe DNA CT from femtosecond to millisecond time scales and measure both rate constants and yields.[37] For instance, fluorescence of Ap provides information of both structural dynamics and hole injection in the DNA on a subnanosecond time scale (Figure 1.4).[37] Initially upon base stacking into DNA helix, fluorescence of Ap can be efficiently

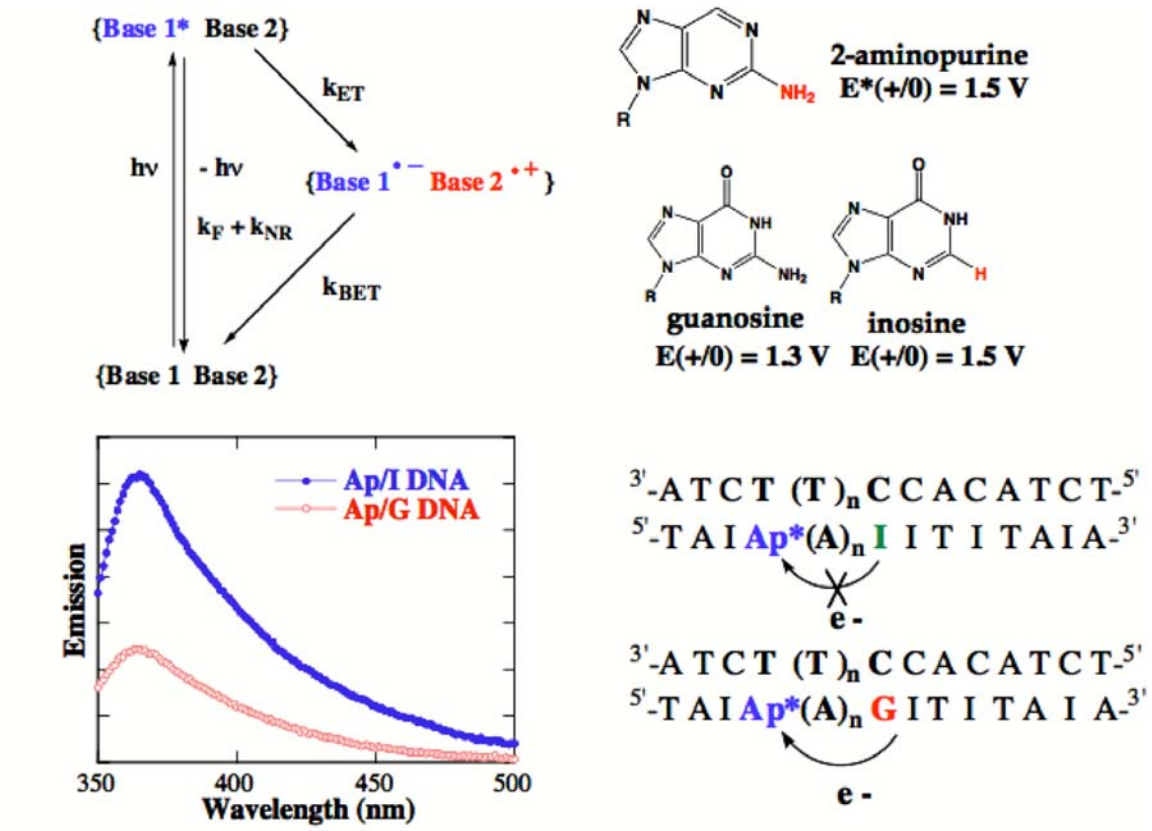

Figure 1.4. Illustration of base-base charge transport between 2-aminopurine and guanine. Excitation of Ap leads to fluorescence quenching when the easily oxidized guanine base, but not inosine, is present. The redox potentials of guanine, Ap and I are indicated under the bases.

quenched. Hole injection to oxidize distant guanine provides an extra HT pathway to quench Ap*. Fractional fluorescence quenching (Fq) of Ap* via HT can be distinguished by comparing the fluorescence of redox-active duplex containing guanine to an identical reference duplex where G is substituted by inosine (I),[33] a guanine analogue with higher oxidation potential ($E^{+/0}$ ~ 1.5 V versus NHE). Thus, HT yield is deduced from the fluorescence quantum yield (Φ) as $F_q = 1 - \Phi_G / \Phi_I$. In DNA assemblies with Ap and G intervened by 0 to 9 AT base pairs, efficient hole injection over above 30 Å was observed.[38]

In addition to the initial steps of DNA HT, the whole process of HT including hole migration and trapping can be probed by fluorescence and transient absorption spectroscopy. In DNA containing methylindole, flash-quenched generated Ru(III) intercalator (*vide infra)* initialized HT to oxidize distant M. The resultant reaction intermediate, M radical cation, was detected by both transient absorption and EPR spectroscopy over long molecular distance (>20 Å).[17]

1.2.2.2. Biochemical observation of long-range oxidative damage. A biochemical assay is used to probe the redox chemistry at distant bases by monitoring the damage of specific hole/electron traps, usually upon photoirradiation of oxidants. As free nucleosides in solution, guanine is the easiest to be oxidized (E_{ox} = 1.29 V, 1.4 V, 1.6 V and 1.7V for G, A, C and T, respectively).[39] Since purine stacking tends to reduce the guanine potential and redistribute electron density among the stacking guanines,[40] guanine doublets (GG) and triplets (GGG) become the prevalent thermal hole traps. Especially the 5'-G in a 5'-GG-3' doublet is more sensitive to permanent oxidation, which is now a characteristic signature of CT.[10] In particular, photochemistry of rhodium

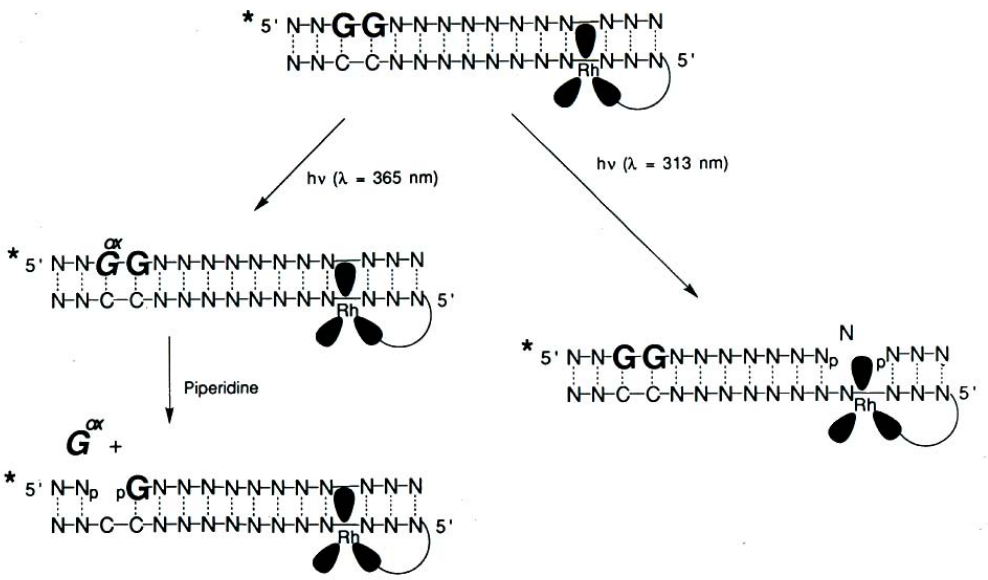

Figure 1.5. Photolysis and DNA-mediated CT initialized by irradiation of covalently tethered $[Rh(phi)_2(bpy')]^{3+}$ and corresponding wavelengths. The complementary strand to Rh-tethered strand is ^{32}P-radioactively labeled. Irradiation at 313 nm triggers direct strand cleavage and the intercalation site is revealed. DNA-mediated hole transport from photoactivated Rh complex is initialized by 365 nm irradiation and oxidative guanine damage is revealed by hot pipiridine treatment and gel electrophoresis. Adapted from reference 13.

phi complexes makes them particularly useful probes in exploring DNA-mediated CT as shown in Figure 1.5. When radioactively labeled Rh-tethered DNA duplexes are excited by UV light (λ = 313 nm), direct strand cleavage is promoted and indicates the intercalation sites of the complex. Alternatively, visible light irradiation at 365 nm generates a powerful excited state oxidant (E ($Rh^{3+*/2+}$) ~ 2 V vs NHE)[41] and initiates HT to oxidize guanine over a long distance. The HT yield as guanine damage can then be revealed by hot pipiridine treatment followed by gel electrophoresis. In a series of Rh-tethered DNA assemblies, proximal guanine doublets were positioned at fixed position to the photooxidant and distal guanine doublets were moved away up to 75 Å. Comparable oxidative damage yield via DNA HT were observed at both GG sites in all the assemblies.[10] A similar assay has been applied to Ru-tethered DNA assemblies, except that a flash quench technique is used because direct photoexcitation of Ru(II) ($E(Ru^{2+*/3+})$ ~ 0.6 V versus NHE) is not sufficient to oxidize DNA bases.[42] Here, excited Ru(II) complex is quenched by electron transfer from a diffusion controlled oxidative quencher (e.g., $Co(NH_3)_5^{2+}$) and yields the ground state oxidant Ru(III) ($E(Rh^{3+/2+})$ ~ 1.6 V vs NHE) *in situ* on the submicrosecond time scale (Figure 1.6).[36] It has been demonstrated that covalently bound Ru(III) complex generated by flash quench technique *in situ* can promote oxidation of guanine doublets via long-range HT over 37 Å.[43]

1.2.2.3. DNA-mediated ET through self-assembled DNA films. DNA-mediated ET is also observed on surfaces electrochemically.[44] As schematically shown in Figure 1.7, well-defined self-assembled DNA monolayers were fabricated on gold by using thiol-modified DNA duplexes and on highly oriented pyrolytic graphite (HOPG) by using pyrene-functionalized DNA duplexes. The morphology of DNA on gold surface was

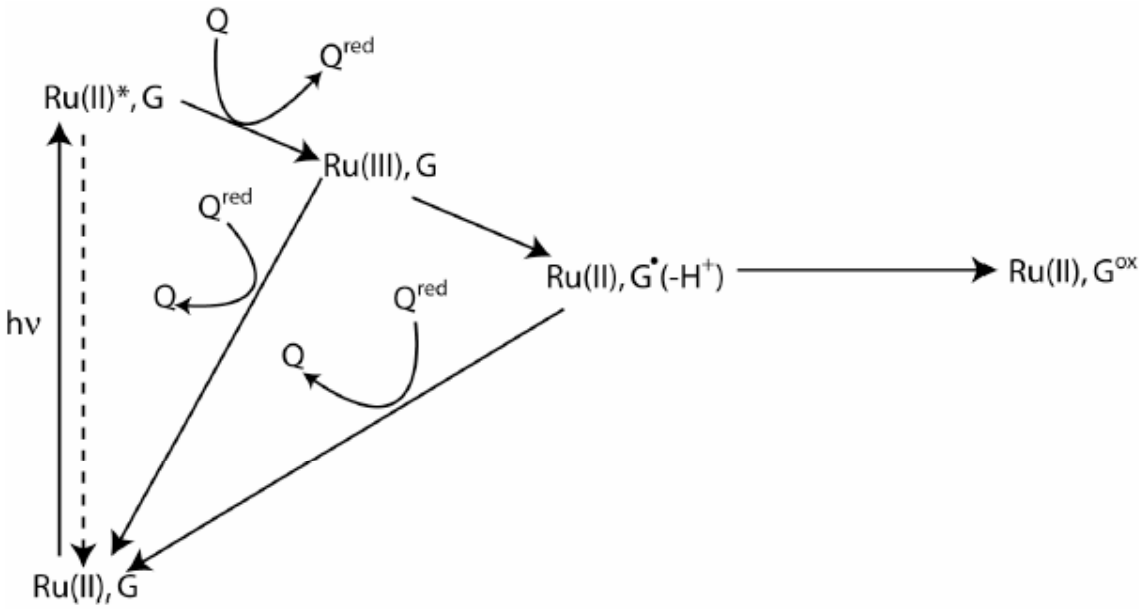

Figure 1.6. Flash-quench technique for generating guanine radicals. The ground-state intercalative oxidant for DNA-mediated HT, Ru^{3+}, is generated *in situ* by electron transfer to a groove-bound quencher, Q, such as $Ru(NH_3)_6^{3+}$ or $Co(NH_3)_5^{2+}$. Once generated, Ru^{3+} promotes oxidation of guanine (G). Recombination reactions with Q^{red} limit the yield, but if Q^{red} is unstable, the yield of damage, G^{ox}, is high. Figure is adapted from reference 43.

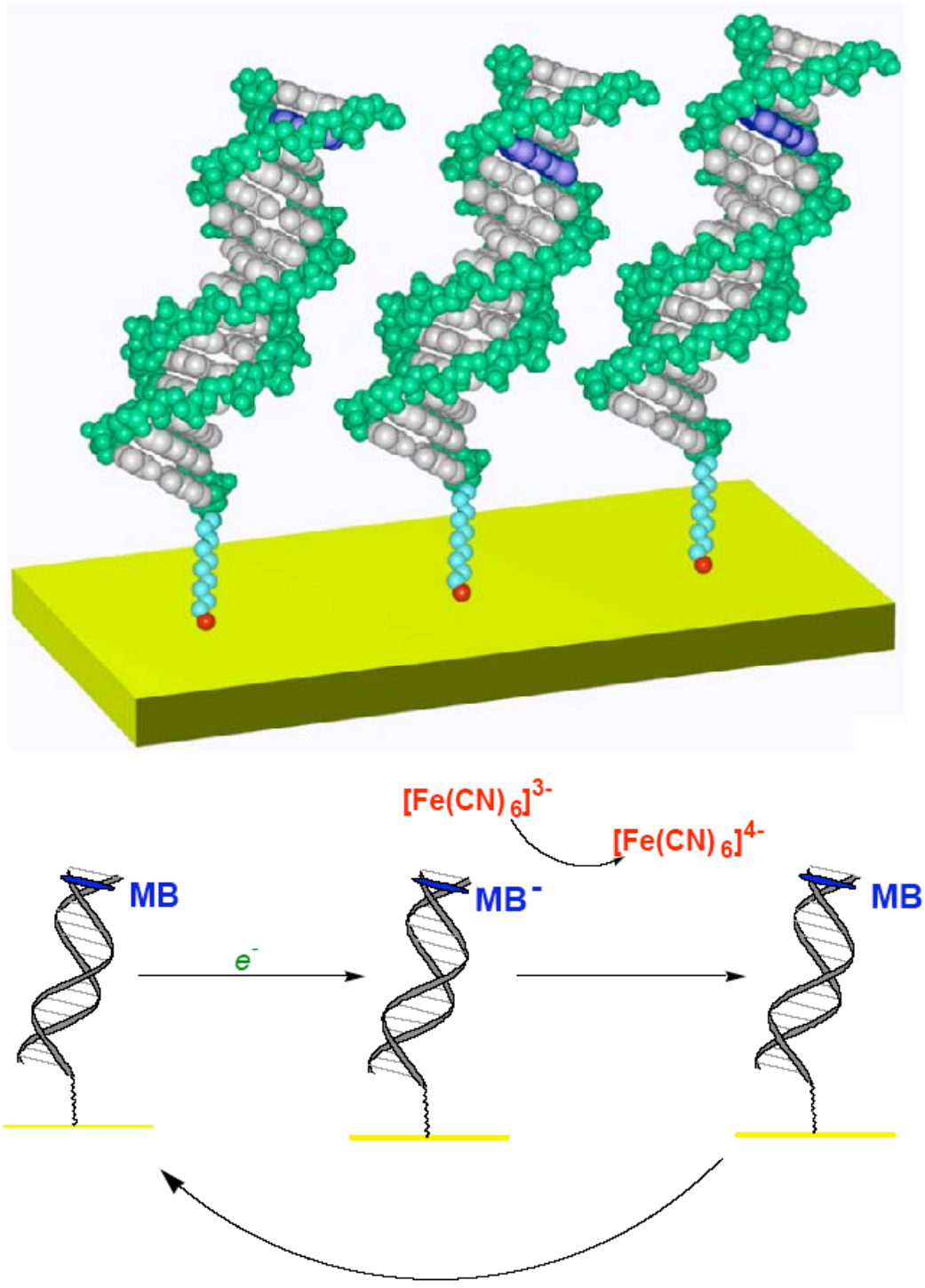

Figure 1.7. Electrochemistry assays for DNA ET. *Upper*: Schematic illustration of alkanethiol functionalized DNA duplexes fabricated on a gold surface for use in electrochemical assays. An intercalator (blue) bound near the top of the DNA monolayer is reduced by electron transport from the electrode surface through the π-stack of DNA. *Bottom*: Scheme of electrocatalytic cycle of MB on DNA-modified gold electrode involving a diffusing redox couple, $[Fe(CN)_6]^{3-}/[Fe(CN)_6]^{4-}$.

characterized by scanning tunneling and scanning probe microscopy.[45] A variety of redox-active species, such as MB and DM, intercalate in the base stack of individual DNA helices at a defined distance from the electrodes and act as electrochemical reporters for ET through the intervening DNA bridge.[46-48] The reduction of the probes monitored by cyclic voltammetry or chronocoulometry should provide a measure of the efficiency of ET through DNA. The first observation of ET through a densely packed DNA film used covalently crosslinked daunomycin as a redox probe.[44] Remarkably, efficient reduction of DM exhibited an distance independence on the position of DM up to 100 Å.[48b] Electron tunneling through the alkyl linker between the electrode and DNA monolayer is the rate-limiting step in ET through DNA films.[47] The sensitivity of ET through DNA-modified films was further explored using electrocatalysis of noncovalent intercalator MB.[46,49] In this study, the reduction signal of MB was significantly enhanced when coupled to the reduction of a freely diffusive ferricyanide as shown in figure 1.7. With electrocatalysis, all the single base mismatches, including the thermodynamically stable GT and GA mismatches, were detected by both cyclic voltammetry and chronocoulometry.[48a]

1.3. Biology application of DNA-mediated CT.

DNA-mediated charge transport has been established in many donor-bridge-acceptor model systems by variety of experiments *in vitro* (*vide supra*) We cannot help thinking whether nature also benefits from this inherent feature of DNA helices. How does nature harness DNA-mediated charge transport?

Before starting to explore the answers for these questions, it is first necessary to demonstrate that CT over long distance can actually occur in DNA within the cell. Unlike typical *in vitro* studies with DNA is free in solution, in eukaryotic cells DNA is packaged and protected in nucleosome core particles (NCP).[50] Would CT proceed through DNA with restricted motion and significant binding in NCP? Using a photoexcited Rh(III) intercalator, oxidative guanine damage within the NCP is observed up to 80 Å.[51] Thus, oxidative damage via inherent DNA CT is not prevented in nucleosome although NCP may protect DNA from solution-mediated damage. Furthermore, the DNA-mediated CT within cell nuclei and mitochondrion is explored by using Rh(III) intercalator as photooxidant.[52,53] CT-charactoristic 5'-G specificity is observed at the oxidation damage site in Hela genomic DNA.[52] In original mitochrondrial DNA, base oxidations via CT is revealed by a primer extension reaction. The oxidation sites in conserved sequence block II overlap with known mitochondrial hot spots for cancers, which indicates the correlation of CT with cancer-related genome damage.[53]

Since the evidence above shows that DNA-mediated CT occurs in cellular milieu, redox reaction with a biological partner of DNA, such as protein, may be able to be initiated by DNA CT. Many base-excision repair proteins, such MutY, possess [4Fe-4S]$^{2+}$ clusters that have no apparent catalytic or structural roles.[54] DNA-mediated CT leads to oxidation of a DNA-bound MutY.[55] Oxidation of the [4Fe-4S]$^{2+}$ cluster in MutY was promoted by a DNA-tethered Ru(III) complex generated by the flash quench technique and degradation of oxidized cluster was observed by EPR spectroscopy.[56] In addition, the electrochemistry conducted on DNA-assemblied gold and HOPG electrodes

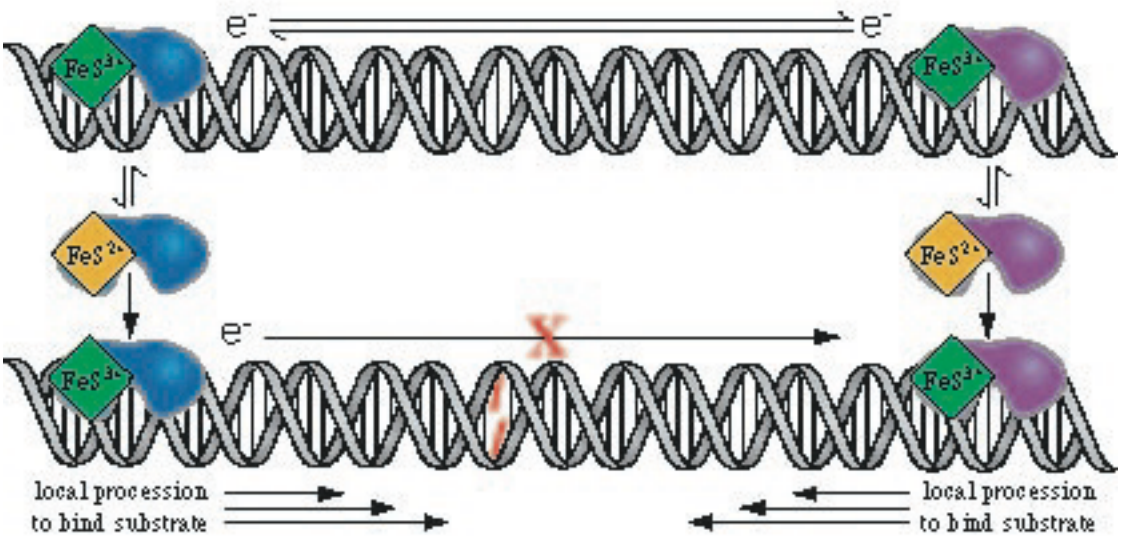

Figure 1.8. Proposed model for long-range DNA signaling between base excision repair enzymes using DNA-mediated charge transfer to detect base lesions. A collaboration among BER enzymes allows for more efficient sorting onto regions of DNA containing base lesions to facilitate substrate detection by these proteins. Figure is adopted from reference 55.

have also detected that oxidation potential of the cluster was shifted when the repair enzymes are bound to DNA.[57] These exciting results of DNA-dependent redox activity provoke the proposition that MutY, as well as other DNA repair enzymes, may employ DNA-mediated CT to locate the lesion in DNA (Figure 1.8). When bound to DNA, the repair enzymes become redox active and charge transfer through well-matched DNA to an alternate bound repair protein can lead to the rapid redistribution of proteins onto genome sites in the vicinity of DNA lesions. This redox-activation model provides a rationale to explain the unbelievable coexistence of the low copy number and high performance of the repair proteins.

1.4. Mechanistic considerations of CT through DNA.

1.4.1. Energetic models. Based upon extensive experimental results that have established DNA-mediated CT over a long molecular distance (*vide supra*), the focus of research currently has shifted from asking *whether* long-range CT can occur through DNA to *how* electrons and holes propagate through the base stack. Generally, there are two basic models for one-dimensional charge migration, which are simply based upon the energetics of donor, bridge and acceptor (Figure 1.9).[58] One is the *superexchange* model, in which the donor and acceptor have lower potentials than the bridge bases and charge tunnels through bridge without formally occupying it. Without virtual occupation of the bridge, the CT rate would exhibit an exponential decay according to the donor/acceptor separation. The other model is called “thermal-hopping”. Here, donor and acceptor have orbitals energetically close to that of bridge. Charge hops between discrete bridge bases and a shallower distance dependence is often predicted in this model. When it comes to

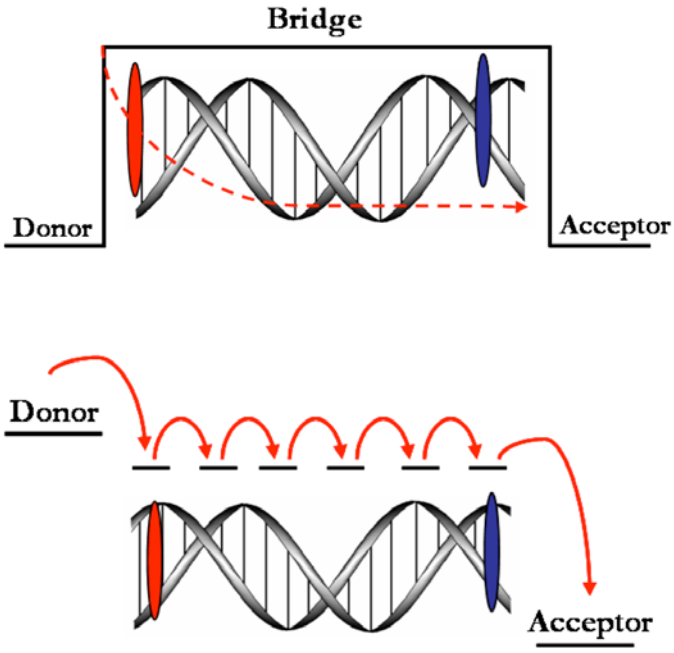

Figure 1.9. Schematic representation of energetic models of electron migration through one-dimensional π-system. In superexhange model (*top*), charge tunnels from the donor (D) to the acceptor without virtual occupation of the bridge. In the thermal-hopping model (*bottom*), donor orbitals are energetically close to those of the bridge. Charge occupies the bridge hopping between discrete molecular orbitals.

DNA-mediated CT, Bixon and Jortner initially proposed a model which combines the two simple models above based upon only the energies of the isolated nucleic acid bases.[59] In this model, charge sequentially hops between low energy guanine sites with tunneling through AT base pairs. However, none of the models above that are purely based upon energetic factors of isolated bases can account for the unique features of CT through DNA, especially for those results obtained by probing DNA CT on fast time scales (*vide infra*). This is presumably due to the ignorance of the signature characteristics possessed by DNA π-system.

1.4.2. Base π-stack mediates CT. The analogy between base pair stack along DNA helices and solid-state π-systems provides the possibility of CT existence in DNA. The interactions between the π-electrons of base pairs generate the electron-coupling requisite for CT to occur. One way to test that is to disturb the π-stacking by mismatch base pairs or by the interaction with DNA physiological partners, such as proteins. For instance, rapid (10 ns) luminescence quenching of Et^{*} via DNA CT from a distant Rh(III) intercalator was observed over fully matched DNA bridge.[60] However, incorporation of a single C-A mismatch in the intervening DNA bridge remarkably reduced the overall yield of CT. In an analogous experiment, formation of methyindole radical cation by HT from a Ru(III) complex generated by flash-quench technique is detected by both EPR and transient absorption spectroscopy.[17] In the assemblies without intervening guanines, the formation rate of M radical by CT is too fast to be resolved even over a distance of >40 Å. However, a single C-A mismatch in the DNA bridge essentially eliminated the formation of M radical cation and the subsequent damage products.[61] In addition, in the DNA assemblies containing a protein-binding site between two guanine doublets,

significant attenuation of damage over long distance occurs in presence of DNA-binding protein M.*Hha*I or TBP, which disrupt DNA base stacking by base flipping or dramatically kinking the DNA.[62] Furthermore, the suspicion that CT may undergo DNA sugar-phosphate backbone is eliminated by examining ET through self-assembled DNA films.[63] Introduction of one or even two nicks on DNA backbones yields nondetectable effects on electron transfer, while single CA mismatch significantly diminishes ET efficiency. These results obtained by spectroscopic, biochemical and electrochemical assays, confirm that the pathway of CT through DNA is indeed the base pair stack, not via the sugar-phosphate backbone. The considerations of including the structural dynamics of DNA base pair stacking, as well as the stacking of photoredox probes within the π-stacking, into the mechanism of DNA CT, are invoked.

1.4.3. Stacking redox probes into DNA plays a role in CT. Given that DNA-mediated CT undergoes primarily through base pair stacking, it is not unexpected that the way photoredox probes interact with the DNA π-system also could be crucial to the charge migration. In fact we found it is true in many of the model systems for CT studies. The luminescence of Ru(II) intercalator was reported to be quenched by a Rh(III) intercalator over a distance of 40 Å, while the quenching reaction was not observed with non-intercalating tethered Ru(II) and Rh(III) complexes.[26] The unambiguous correlation between the strength of intercalative binding and yield of distant guanine damage was also observed when examining the oxidative damage induced by a series of Ru(II) complexes with similar redox potentials.[64] Moreover, using both steady-state and nanosecond and femtosecond fluorescence to study base-base CT in Ap or εA containing DNA assemblies, two adenine analogues with comparable excited state potentials

exhibited dramatically different rates and yields of CT.[33] Ap, which can base pair with T and stack as a normal base in DNA helices, has a rapid CT rate ($k \sim 10^{10}$–10^{11} s^{-1}) with shallow distance dependence. Conversely, CT involving εA* is several orders of magnitude slower and decreases steeply in both the rate constant and the yield over 13.6 Å. A high-resolution NMR structure of εA-containing duplex shows a non-rigid conformation of bulky εA that prevents it from effective stacking with the flanking DNA bases, which makes resulting CT efficiency of εA* significantly differentiate from that of Ap*. Thus, although CT is an intrinsic feature of DNA itself, it has to been also noted that the difference among the redox probes in the model systems of CT cannot be neglected. Distinctions in the interaction modes with DNA π-stacking adopted by photoredox probes exert significant impacts on the rate and yield of CT; the diverse features of redox probes makes it difficult to reconcile the fundamental mechanism of CT.

1.4.4. Conformational dynamics of DNA bases. Unlike solid-state π-stacks, double helical DNA is a dynamic structure.[65] The conformational rearrangements within DNA molecules are on the time scales from at least pico- to milliseconds.[65] Since the base stacks provide the conduit for CT, most likely their conformational motion will have essential influences on the rate constants, yields, distance and sequence dependence of DNA CT. It is not surprising that the energetic models that do not consider the dynamic conformation of DNA bases cannot account for most of the CT results. The investigation of DNA CT between Et* and Rh(III) complex demonstrates that increasing the number of bridge bases diminishes the population portion of Et* quenched by CT, but with no concomitant decrease in CT rate.[60] In addition, fluorescence decay of covalently tethered

Et* in DNA assemblies containing ^{Z}G showed two characteristic decay rate constants, 5 ps and 75 ps. The short component was assigned as the rate of direct CT between Et* and ^{Z}G and, while the longer decay (75 ps) was proposed to be reorientational motion of Et* to a CT-favored conformation within its binding site. None of rate constants varied according to the distance between Et and ^{Z}G over 17 Å, while the yield of CT (as ^{Z}G damage) exhibited a shallow distance dependence. It was hypothesized that Et undergoes a conformation rearrangement within DNA π-stacking (75 ps) when the favorable conformation required for CT on 5 ps was not accessible. Although gating by the dynamic motion of photooxidant within DNA base stack explains the constant CT rate, it cannot reconcile the shallow distance dependence of the CT yield. Dynamic motion of bases on the intervening DNA bridge should be also included. Femtosecond spectroscopy of Ap-containing 35-mer duplexes, in which Ap and the electron donor G are either flanked (ApG) or separated by one adenine (ApAG) exhibits multiple components of Ap* decay.[66] Fast decay rate represents the CT rate (k_{CT}) between Ap* and G. The temperature dependence of k_{CT} directly characterizes the modulation of DNA CT from dynamic motion of base pairs. Both k_{CT} of ApG and ApAG increased weakly with temperature, resulting in less variation in k_{CT} at higher temperature. The complete loss of k_{CT} after DNA assemblies were denatured, confirmed again that the CT is an inherent feature of DNA duplex. The increase in k_{CT} deviates from the prediction of standard Marcus theory for ET, since the conventional theory has not considered the dynamics of DNA base motion. More remarkable, the dichotomy between experiment and theory was more pronounced in ApAG, in which CT requires to overcome an intervening base and relies on dynamic motion of bases more than that in ApG.

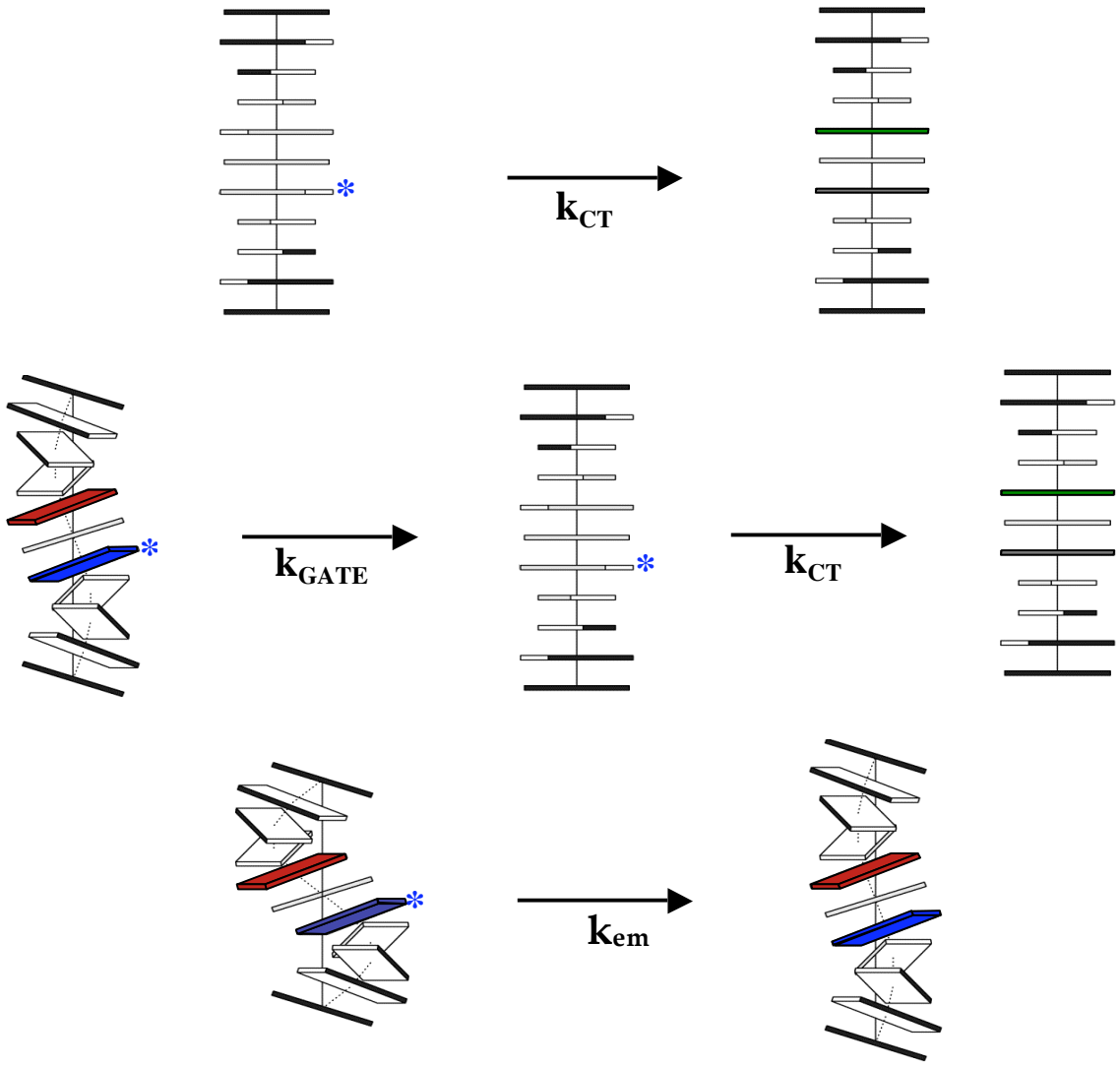

Figure 1.10. Schematic illustration of how fluctuations in the π-stacking of DNA affects DNA charge transport. CT is rapid in a perfectly stacked DNA (*top*), is gated by conformational alignment in an imperfectly stacked DNA (*middle*), and does not occur at all in a poorly stacked DNA (*bottom*), where CT-active conformation cannot be accessed within the lifetime of of the excited probe molecule. Figure is adopted from reference 66.

We attentively propose that DNA CT needs to undergo a CT-active conformation: specific, well-coupled arrangements of DNA base achieved by dynamic motion of DNA bases with stacking. The yield of CT reflects the probability of DNA assemblies accessing the active conformation as shown in Figure 1.10. At the excitation time, a portion of assemblies is properly aligned and can undergo directly CT, while other assemblies do not assume such conformation, but can reorganize the base conformation gated by dynamic motion (k_{ET}) during the lifetime of Ap*. If the assemblies cannot attain the CT-active conformation, Ap* decays through non-CT pathway such as emission (k_{em}). An investigation of CT between Ap* and G in rigid LiCl glasses at 77 K provided further evidence for comforationally gated CT.[67] No fractional fluorescence quenching of Ap* via CT was observed at 77 K, since the reorganization of DNA conformation is "turned off" in the solid glass. A further testimony to the impact of DNA dynamic structure on CT is sequence and distance dependence. DNA-mediated CT should be strongly modulated by the intervening distance and sequence, as well as by temperature, since dynamic motion of DNA bases is sensitive to base sequence and become more important when the number of bridge bases increases. In fact, in DNA assemblies (35-mers), Ap and G is separated by 0-9 adenine bases or mix bridges, such as AAIA and ATAT.[38] Fractional fluorescence quenching of Ap* by CT from G in all the assemblies was enhanced with increased temperature, and a more dramatic effect of temperature was observed for longer bridges and more flexible bridges (ATAT). These results indicate that DNA CT is regulated by the lengths and the sequences of the bridge bases, rather than the energetics, which matches precisely the prediction of conformationally gated CT.

1.4.5. Trapping rates of electron acceptors versus back electron transfer. Except for several observations of intermediate reaction radicals by transient absorption spectroscopy,[17,68] CT yield reported by the redox reaction over long molecular distances is based on the oxidative damage at a thermal hole trap, guanine or its analogues.[13,26] However, the guanine radical has a relatively long lifetime (millisecond time scale)[36] compared to the gating process of CT: the dynamic motion of DNA bases. Before being trapped as permanent guanine damage, charge can undergo many pathways, which inevitably convolute the concomitant CT process. In particular, fast back electron transfer (BET) within the initially generated radical ion/ion pair can severely diminish the amount of charge that remains. For instance, no detectable permanent guanine damage was observed when Ap or thionin (Th), a DNA intercalator, were used as covalently incorporated photooxidants to DNA.[69] Although the charge injection for the two oxidants occurs on picosecond time scale or even faster,[35,70] BET, with a significantly faster rate than the trapping of guanine radial cation by water and/or oxygen, depletes the hole density in duplex DNA. A complementary experiment by using a kinetic fast hole trap, N_2-cyclopropylguanine (^{CP}G), supportes this rationale. The cyclopropyl ring on the exocyclic amine of guanine can undergo a rapid ring-opening reaction on the picosecond time scale upon one-electron oxidation.[71] Indeed, oxidative decomposition of ^{CP}G was observed by photolysis of both Ap and Th containing DNA duplexes.[69a,72] Thus, accurate evaluation of CT yield also requires the trapping rate of charge acceptor to match the time scale of DNA CT gated by the dynamic motion of DNA bases.

1.4.6. Conformationally gated domain model for DNA HT. Given all the considerations about dynamic structures of the inherent DNA π-stacking, the coupling of

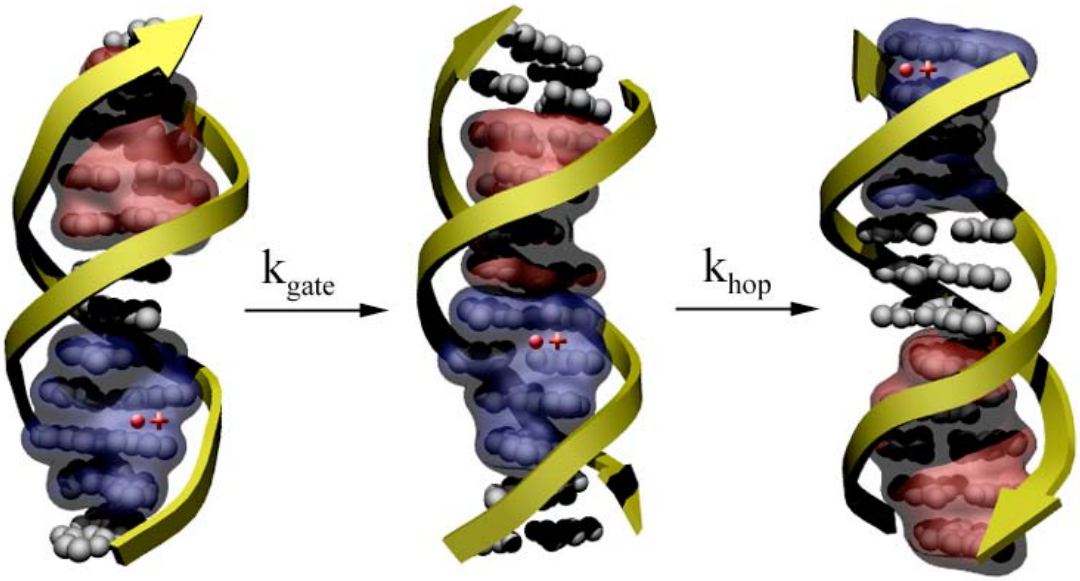

Figure 1.11. Illustration of conformationally gated domain model for DNA-mediated CT. A radical cation, hole, is injected into a domain over 4-5 base pairs and delocalizes transiently onto all the bases within the domain. Hole propagation occurs when the two neighboring domain access to a CT-active formation. The formation of domains and hole migration is gated by the dynamic motion of the DNA bases.

redox probes, as well as the trapping of electron acceptors, we proposed a mechanistic model for DNA-mediated hole transport: conformationally gated domain hopping model (Figure 1.11). A domain is a transiently extended π-orbital over 4–5 base pairs (Chapter 4). A hole can be propagated from one domain to the next domain when the two neighboring domains achieve a CT-active conformation. During migration, the hole delocalizes onto all the bases within a domain transiently, but not simultaneously (Chapter 2). The formation and breakup of a domain is gated by the dynamic motion of DNA bases and is sensitive to the sequence of the DNA bridges (Chapter 3). This dynamic delocalized model accounts for the sensitivity of the process to sequence-dependent DNA structure and provides a basis to reconcile and exploit DNA HT chemistry and physics. Although the orbitals involved in ET and HT are different, the fundamental features described in DNA HT may be able to apply to migration of charge in general, including both electron and hole. In chapters 5 and 6, DNA-mediated ET is explored by a novel series of Ir(III) cyclometalated complex. As a result, HT and ET may be compared using the model system with identical photoredox probes.

1.5. References

1. Watson, J. D., Crick, F. C. H. A structure for deoxyribonucleic acid. *Nature* **1953**, *171*, 737-738.

2. Sanger, W. *Principles of Nucleic Acid Structure* Cator, C. R., ed.; Springer-Verlag: New York. **1984**.

3. Eley, D. D., Spivey, D. I. Semiconductivity of organic substances: Nucleic acids in the dry state. *Trans. Faraday Soc.* **1962**, *58*, 411.

4. (a) Delaney, S., Barton, J. K. Long-range DNA charge transport *J. Org. Chem.* **2003**, *68*, 6475-6483; (b) Rokita, S. E., Ito, T. Chemical probing of reductive electron transfer in DNA *Charge Transfer in DNA: From Mechanism to Application*, Wagenknecht, H. A., ed.; Wiley, **2005**, 133-152.

5. O'Neill, M. A., Barton, J. K. Sequence-dependent DNA Dynamics: The regulator of DNA-mediated charge transport In *Charge Transfer in DNA: From Mechanism to Application*, Wagenknecht, H. A., ed.; Wiley, **2005**, 27-75.

6. Carell, T., Meltzer, M. Excess electron transfer in DNA probed with flavin- and thymine dimer-modified oligonucleotides *Charge Transfer in DNA: From Mechanism to Application*, Wagenknecht, H. A., ed.; Wiley, **2005**, 77-92.

7. (a) *Topics in Current Chemistry: Long-Range Electron Transfer in DNA:1*, Schuster, G. B., ed.; Springer-Verlag: New York, **2004**, *236*; (b) Schuster, G. B. Long-range charge transfer in DNA: transient structural distortions control the distance dependence. *Acc. Chem. Res.* **2000**, *33*, 253-260; (c) Giese, B. Long-distance electron transfer through DNA. *Ann. Rev. Biochem.* **2002**, *71*, 51-70; (d) Lewis, F. D., Letsinger, R. L., Wasielewski, M. R. Dynamics of photoinduced charge transfer and hole transport in synthetic DANN hairpins. *Acc. Chem. Res.* **2001**, *34*, 159-170.

8. Oxidation potentials of the four isolated bases are estimated as follows: G: E_{ox} = 1.3 eV; A: E_{ox} = 1.4 eV; C: E_{ox} > 1.6 eV; T: E_{ox} > 1.7 eV. See Steenken, S., Jovanovic, S.V. How easily oxidizable is DNA? One-electron reduction potentials of adenosine and guanosine radicals in aqueous solution *J. Am. Chem. Soc*. **1997**, *119*, 617-618.

9. Steenken, S., Telo, J. P., Novais, H. M., Candeias, L. P. One-electron-reduction potentials of pyrimidine bases, nucleosides, and nucleotides in aqueous solution. Consequences for DNA redox chemistry *J. Am. Chem. Soc.* **1992**, *114*, 4701-4709.

10. (a) Núñez, M. E., Hall, D. B., Barton, J. K. Long range oxidative damage to DNA: effects of distance and sequence *Chem. Biol.* **1999**, *6*, 85-97; (b) Henderson, P.T., Jones, D., Hampikian, G., Kan, Y. Z., Schuster, G. Long-distance charge transport in duplex DNA: the phonon-assisted polaron-like hopping mechanism *Proc. Natl. Acad. Sci. USA* **1999**, *96*, 8353-8358.

11. Dandliker, P. J., Holmlin, R. E., Barton, J. K. Oxidative thymine dimer repair in the DNA helix *Science*, **1997**, *275*, 1465-1468.

12. DeRosa, M. C., Sancar, A., Barton, J. K. Electrochemically monitoring DNA repair by photolyase *Proc. Nat. Acad. Sci. USA* **2005**, *102*, 10788-10792.

13. Hall, D. B., Holmlin, R. E., Barton, J. K. Oxidative DNA damage through long range electron transfer *Nature* **1996**, *382*, 731-735.

14. Takada, T., Kawai, K., Cai, X., Sugimoto, A., Fujitsuka, M., Majima, T. Direct observation of hole transfer through double-helical DNA over 100 Å *J. Am. Chem. Soc.* **2004**, *126*, 1125-1129.

15. Nakatani, K., Dohno, C., Saito, I. Modulation of DNA-mediated hole-transport efficiency by changing superexchange electronic interaction *J. Am. Chem. Soc.* **2000**, *122*, 5893-5894.

16. Yoo, J., Delaney, S., Stemp, E., Barton, J. K. Rapid radical formation by DNA charge transport through sequences lacking intervening guanines *J. Am. Chem. Soc.* **2003**, *125*, 6640-6641.

17. Delaney, S., Yoo, J., Stemp, E. D. A., Barton, J. K. Charge equilibration between two distinct sites in double helical DNA *Proc. Nat. Acad. Sci. USA* **2004**, *101*, 10511-10516.

18. Núñez, M. E., Barton, J. K. Probing DNA charge transport with metallointercalators *Curr. Opin. Chem. Biol.* **2000**, *4*, 199-206.

19. (a) David, S. S., Barton, J. K. NMR evidence for specific intercalation of Δ-$[Rh(phen)_2phi]^{3+}$ in $[d(GTCGAC)]_2$ *J. Am. Chem. Soc.* **1993**, *115*, 2984-2985; (b) Hudson, B. P., Barton, J. K. Solution structure of a metallointercalator bound site-specifically to DNA *J. Am. Chem. Soc.* **1998**, *120*, 6877-6888.

20. Kielkopf, C. L., Erkkila, K. E., Hudson, B. P., Barton, J. K., Rees, D. C. Structure of a photoactive rhodium complex intercalated into DNA *Nature Struc. Biol.* **2000**, *7*, 117-121.

21. Jenkins, Y., Friedman, A. E., Turro, N. J., Barton, J. K. Characterization of dipyridophenazine complexes of ruthenium (II): the light switch effect as a function of nucleic acid sequence and conformation *Biochemistry*, **1992**, *31*, 10809-10816.

22. Waring, M. J. Complex formation between ethidium bromide and nucleic acids *J. Mol. Biol.* **1965**, *13*, 269-282.

23. Olmsted, J., Kearns, D. R. Mechanism of ethidium bromide fluorescence enhancement on binding to nucleic acids *Biochemistry*, **1977**, *16*, 3647-3654.

24. Wan, C. Z., Fiebig, T., Kelley, S. O., Treadway, C. R., Barton, J. K., Zewail, A. H. Femtosecond dynamics of DNA-mediated electron transfer. *Proc. Natl. Acad. Sci. USA* **1999**, *96*, 6014-6019.

25. Fiebig, T., Wan, C. Z., Kelley, S. O., Barton, J. K. Femtosceond dynamics of the DNA intercalator, eithidium and electron transfer with mononucleotides in water *Proc. Natl. Acad. Sci. USA* **1999**, *96*, 1187-1192.

26. Kelley, S. O., Barton, J. K. DNA-mediated electron transfer from a modified base to ethidium: π-Stacking as a modulator of reactivity *Chem. Biol.* **1998**, *5*, 413-425.

27. Kelley, S. O., Barton, J. K., Jackson, N., Hill, M. G. Electrochemistry of methylene blue bound to a DNA-modified electrode *Bioconjug. Chem.* **1997**, *8*, 31-37.

28. (a) Norden, B, Tjerneld, F. Structure of methylene-blue DNA complexes studied by linear and circular-dichroism spectroscopy *Biopolymers* **1982**, *21*, 1713-1734. (b) Tuite, E, Kelly, J. M. The interaction of methylene-blue with polynucleotides and DNA – a spectroscopic study *J. Am. Chem. Soc.* **1994**, *116*, 7548-7556.

29. (a) Wang, A. H. J., Gao, Y. G., Liaw, Y. C., Li, Y. K. Formaldehyde cross-links daunorubicin and DNA efficiently – HPLC and X-ray-diffraction studies *Biochemistry* **1991**, *30*, 3812-3815. (b) Leng, F. F., Savkur, R., Fokt, I., Przewloka, T., Priebe, W., Chaires, J. B. Base specific and regioselective chemical cross-linking of daunorubicin to DNA *J. Am. Chem. Soc.* **1996**, *118*, 4731-4738.

30. Schuster, G. B. Long-range charge transfer in DNA: Transient structural distortions control the distance dependence *Acc. Chem. Res.* **2000**, *33*, 253-260.

31. Behrens, C. Burgdorf, L. T., Schwögler, A., Carell, T. Weak distance dependence of excess electron transfer in DNA *Angew. Chem. Int. Ed.* **2002**, *41*, 1763-1766.

32. Bestor, T. H. The DNA methyltransferases of mammals *Human Molecular Genetics* **2000**, *9*, 2395-2402.

33. Kelley, S.O., Barton, J. K. Electron transfer between bases in double helical DNA *Science* **1999**, *283*, 375-381.

34. Delaney, J. Y., Stemp, E. D. A., Barton, J. K. Charge equilibration between two distinct sites in double helical DNA *Proc. Nat. Acad. Sci. USA* **2004**, *101*, 10511-10516.

35. Wan, C., Fiebig, T., Schiemann, O., Barton, J. K., Zewail, A. H. Femtosecond direct obaservation of charge transfer between bases in DNA *Proc. Nat. Acad. Sci. USA* **2000**, *97*, 14052-14055.

36. Stemp, E. D. A., Arkin, M. R., Barton, J. K. Oxidation of guanine in DNA by $Ru(phen)_2dppz^{2+}$ using the flash-quench technique *J. Am. Chem. Soc.* **1997**, *119*, 2921-2925.

37. O'Neill, M. A., Barton, J. K. 2-Aminopurine: A probe of structural dynamics and charge transfer in DNA and DNA:RNA hybrids *J. Am. Chem. Soc.* **2002**, *124*, 13053-13066.

38. O'Neill, M.A., Barton, J. K. DNA charge transport: conformationally gated hopping through stacked domains *J. Am. Chem. Soc.* **2004**, *126*, 11471-11483.

39. Steenken, S., Jovanovic, S. V. How easily oxidizable is DNA? One-electron reduction potentials of adenosine and guanosine radicals in aqueous solution *J. Am. Chem. Soc*. **1997**, *119*, 617-618.

40. Sugiyama, H., Saito, I. Theoretical studies of GG-specific photocleavage of DNA via electron transfer: significant lowering of ionization potential and 5'-localization of HOMO of stacked GG bases in B-Form DNA *J. Am. Chem. Soc.***1996**, *118*, 7063-7068.

41. Turro, C., Evenzahav, A., Bossmann, S. H., Barton, J. K. Turro, N. J. Excited state properties of $Rh(phi)_2(phen)^{3+}$ and related complexes: A strong photooxidant *Inorg. Chim. Acta.* **1996**, *243*, 101-108.

42. Murphy, C. J., Arkin, M. R., Ghatlia, N. D., Bossmann, S., Turro, N. J., Barton, J. K. Fast photoinduced electron transfer through DNA intercalation *Proc. Nat. Acad. Sci. USA* **1994**, *91*, 5315-5319.

43. Arkin, M. R., Stemp, E. D. A., Pulver, S. C., Barton, J. K. Long-range oxidation of guanine by Ru(III) in duplex DNA *Chem. Biol.* **1997**, *4*, 389-400.

44. Kelley, S. O., Jackson, N. M., Hill, M. G., Barton, J. K. Long-range electron transfer through DNA film *Angew. Chem. Int. Ed.* **1999**, *38*, 941-945.

45. (a) Ceres, D. M., Barton, J. K. *In situ* scanning tunneling microscopy of DNA-modified gold surfaces: bias and mismatch dependence *J. Am. Chem. Soc.* **2003**, *125*, 14964-14965. (b) Sam, M., Boon, E. M., Barton, J. K., Hill, M. G., Spain, E. M. Morphology of 15-mer duplexes tethered to Au(111) using scanning probe microscopy *Langmuir*, **2001**, *17*, 5727-5730.

46. Boon, E. M., Ceres, D. M., Drummond, T. G., Hill, M. G., Barton, J. K. Mutation detection by electrocatalysis at DNA-modified electrodes *Nature Biotechnology* **2000,** *18*, 1096-1100.

47. Drummond, T. G., Hill, M. G., Barton, J. K. Electron transfer rates in DNA films as a function of tether length *J. Am. Chem. Soc.* **2004**, *126*, 15010-15011.

48. (a) Boon, E.M., Jackson, N. M., Wightman, M. D., Kelley, S. O., Hill, M. G., Barton, J. K. Intercalative stacking: A critical feature of DNA charge-transport electrochemistry *J. Phys. Chem. B* **2003**, *107*, 11805-11812. (b) Liu, T. thesis for Ph.D. Electrochemical studies of electron transfer in DNA films with covalently tethered intercalators. **2007**, Caltech.

49. Kelley, S. O., Boon, E. M., Barton, J. K., Jackson, N. M., Hill, M. G. Single-base mismatch detection based on charge transduction through DNA *Phys. Rev. E* **1997**, *55*, 7390-7395.

50. Luger, K., Mäder, A., Richmond, R., Sargent, D., Richmond, T. J. Crystal structure of the nucleosome core particle at 2.8 Å resolution *Nature* **1997**, *389*, 251-260.

51. Núñez, M. E., Noyes, K.T., Barton, J. K. Oxidative charge transport through DNA in nucleosome particles J. K. *Chem. Biol.* **2002**, *9*, 403-415.

52. Núñez, M. E, Holmquist, G. P., Barton, J. K. Evidence for DNA charge transport in the nucleus *Biochemstry* **2001**, *40*, 12465-12471.

53. Merino, E. J., Barton, J. K. Oxidation by DNA charge transport damages conserved sequence block II, a regulatory element in mitochondrial DNA *Biochemstry* **2007**, *46*, 2805-2811.

54. (a) Cunningham, R. P., Asahara, H., Bank, J. F., Scholes, C. P., Salerno, J. C., Surerus, K., Munck, E., McCracken, J., Peisach, J., and Emptage, M. H. Endonuclease III is an iron-sulfur protein, *Biochemistry* **1989**, *28*, 4450-4455. (b) Hinks, J. A, Evans, M. C. W., de Miguel, Y., Sartori, A. A., Jiricny, J., and Pearl, L. H. (2002) An iron-sulfur cluster in the family 4 uracil-DNA glycosylases, *J. Biol. Chem.* **2002**, 277, 16936-16940. (c) Rebeil, R., Sun, Y., Chooback, L., Pedraza-Reyes, M., Kinsland, C., Begley, T. P., and Nicholson, W. L. Spore photoproductlyase from *Bacillus subtilis* spores is a novel iron-sulfur DNA repair enzyme which shares features with proteins such as class III anaerobic ribonucleotide reductases and pyruvate-formatelyases *J. Bacteriol.* **1998**, 180, 4879-4885. (d) Lee, C. H., Kim, S. H., Choi, J. I., Choi, J. Y., Lee, C. E., and Kim, J. Electron paramagnetic resonance study reveals a putative iron-sulfur cluster in human rpS3 protein, *Mol. Cells* **2002**, *13*, 154-156.

55. Boal, A. K., Yavin, E., Lukianova, O. A., O'Shea, V. L., David, S. S., Barton, J. K. DNA-bound redox activity of DNA-repair glycosylases containing [4Fe-4S] clusters *Biochemistry* **2005**, *44*, 8397-8407.

56. Yavin, E., Boal, A. K., Stemp, E. D. A., Boon, E. M., Livingston, A. L., O'shea, V. L., David, S. S., Barton, J. K. Protein-DNA charge transport: Redox activation of a

DNA repair protein by guanine radical *Proc. Nat. Acad. Sci. USA* **2005**, *102*, 3546-3551.

57. Gorodesky, A. A., Barton, J. K. DNA-mediated electrochemistry of disulfides on graphite *J. Am. Chem. Soc.* **2007**, *129*, 6074-6075.

58. Marcus, R. A., Sutin, N. Electron transfer in chemistry and biology *Biochim. Biophys. Acta.* **1985**, *811*, 265-

59. (a) Bixon, M., Jortner, J. Long-range and very long-range charge transport in DNA *Chem. Phys.* **2002**, *281*, 393-408. (b) Jortner, J., Bixon, M., Voityuk, A. A., Rösch, N. Superexchange mediated charge hopping in DNA *J. Phys. Chem. A.* **2002**, *106*, 7599-7606.

60. Kelley, S. O., Holmlin, R. E., Stemp, E. D. A., Barton, J. K. Photoinduced electron transfer in eithidium modified DNA duplexes: Dependence on distance and base stacking *J. Am. Chem. Soc.* **1997**, *119*, 9861-9870.

61. Yoo, J., Delaney, S., Stemp, E. D. A., Barton, J. K. Rapid radical formation by DNA charge transport through sequences lacking intervening guanines *J. Am. Chem. Soc.* **2003**, *125*, 6640-6641.

62. (a) Rajski, S. R., Kumar, S., Roberts, R. J., Barton J. K. Protein-modulated DNA electron transfer *J. Am. Chem. Soc.* **1999**, *121*, 5615-5616. (b) Rajski, S. R., Barton, J. K. How different DNA-binding proteins affect long-range oxidative damage to DNA *Biochemistry* **2001**, *40*, 5556-5564.

63. Liu, T., Barton, J. K. DNA electrochemistry through the base pairs not the sugar-phosphate backbone *J. Am. Chem. Soc.* **2005**, *127*, 10160-10161.

64. Delaney, S., Pascaly, M., Bhattacharya, P. K., Ham, K., Barton, J. K. Oxidative damage by ruthenium complexes containing the dipyridophenazine ligand or its derivatives: A focus on intercalation *Inorg. Chem.* **2002**, *41*, 1966-1974.

65. (a) Mordlund, T. M., Andersson, S., Nilsson, L., Rigler, R., Graeslund, A., Mclaughlin, L. W. Structure and dynamics of a fluorescent DNA oligomer containing the EcoRI recognition sequence: Fluorescnece molecular dynamics, and NMR studies *Biochemistry* **1989**, *28*, 9095-9013. (b) Giudice, E., Lavery, R. Simulations of nucleic acids and their complexes *Acc. Chem. Res.* **2002**, *35*, 350-357.

66. O'Neill, M. A., Becker, H., Wan, C., Barton, J. K., Zewail, A. H. Ultrafast dynamics in DNA-mediated electron transfer: base gating and the role of temperature *Angew. Chem. Int. Ed.* **2003**, *42*, 5896-5900.

67. O'Neill, M. A., Barton, J. K. DNA-mediated charge transport requires conformational motion of the DNA bases: elimination of charge transport in rigid glasses at 77K *J. Am. Chem. Soc.* **2004**, *126*, 13234-13235.

68. Takada, T., Kawai, K., Fujistuka, M., Majima, T. Rapid long-distance hole transfer through consecutive adenine sequence. *J. Am. Chem. Soc.* **2006**, *128*, 11012-11013.

69. (a) O'Neill, M. A., Dohno, C., Barton, J. K. Direct chemical evidence for charge transfer between photoexcited 2-aminopurine and guanine in duplex DNA *J. Am. Chem. Soc.* **2004**, *126*, 1316-1317. (b) Dohno, C., Stemp, E. D. A., Barton, J. K. Fast back electron transfer prevents guanine damage by photoexcited thionine bound to DNA *J. Am. Chem. Soc.* **2003**, *125*, 9586-9587.

70. Reid, G. D., Whittaker, D. J., Day, M. A., Turton, D. A., Kayser, V., Kelly, J. M., Beddard, G. S. Femtosecond electron-transfer reactions in mono- and polynucleotides and in DNA *J. Am. Chem. Soc.* **2002**, *124*, 5518-5527.

71. Nakatani, K., Dohno, C., Saito, I. Design of a hole-trapping nucleobase: termination of DNA-mediated hole transport at N^2-cylcopropyldeoxyguanosine *J. Am. Chem. Soc.* **2001**, *123*, 9681-9682.

72. Williams, T. T., Dohno, C., Stemp, E. D. A., Barton, J. K. Effects of the photooxidant on DNA-mediated charge transport *J. Am. Chem. Soc.* **2004**, *126*, 8148–8158.

Chapter 2

Long Range Oxidative Damage to Cytosines in Duplex DNA

Adapted from: Shao, F., O'Neill, M. A., and Barton, J. K. *Proc. Nat. Acad. Sci. USA* **2004**, *101*, 17914–17919.

2.1. Introduction.

Oxidative damage to DNA from a distance through long range migration of charge has now been established in many DNA assemblies using different pendant photooxidants through both biochemical and spectroscopic assays.[1-8] The DNA base pair stack can mediate hole transport (HT) over at least 200 Å,[2,3] and the reaction is exquisitely sensitive to the dynamic structure and stacking within the DNA duplex.[9,10] This sensitivity to perturbations in base pair stacking has been advantageous in the development of DNA-based sensors for mutational analysis,[11] and may provide a role for DNA-mediated HT within the cell,[11,12] but it has limited the application of physical techniques to explore HT mechanistically.

While not a robust molecular wire, the DNA duplex has in some experiments been characterized as a wide band gap semiconductor.[13,14] More prevalent have been models of incoherent HT involving a mixture of localized charge hopping among low energy sites, guanines and sometimes adenines, and tunneling through higher energy pyrimidine bases.[15-18] These mechanisms do not provide a rationale, however, for the sensitivity of HT to DNA structure. We have observed that DNA HT is gated by the dynamical motions of the DNA bases[9,19] and have described DNA HTas conformationally gated hopping through transient, well-stacked DNA domains.[20]

Our experimental strategy to probe for hole occupancy of pyrimidines exploits the rapid (ns-ps) ring opening of cyclopropylamine radical cations.[21] Saito and co-workers have developed kinetic traps for holes residing on G[22] and A[23] based on the rapid ring opening of N_2-cyclopropylguanosine (^{CP}G) and N_6-cyclopropyladenine (^{CP}A) upon oxidation through DNA-mediated HT. These kinetic traps have been useful also in

establishing HT for those photooxidants that produce limited oxidative DNA damage owing to rapid back CT.[24,25] Guanine, although a low energy site, provides a relatively slow (ms)[26] hole trap through irreversible reaction with water and/or oxygen.[27] Significantly, in experiments using ^{CP}A, HTinvolving adenines has been documented.[23]

Here, using the kinetically fast electron hole trap, N_4-cyclopropylcytosine (^{CP}C), we demonstrate that hole migration involves not only low energy purine sites but also the higher energy pyrimidine bases. We examine long range HT in DNA assemblies containing two different high energy photooxidants, and we find appreciable oxidative damage at a distant ^{CP}C. The yield of ^{CP}C decomposition is modulated by lower energy guanine sites within the assembly and is comparable in magnitude to that for a neighboring ^{CP}G. Thus, during the course of HT through DNA, appreciable hole density must reside also on high energy pyrimidine sites. HTthrough DNA involves all the DNA bases.

2.2. Materials and methods.

2.2.1. Modified bases. N_4-Cyclopropylcytidine (r^{CP}C) and N_4-cyclopropyl-cytosine (^{CP}C) were synthesized by stirring 4-thiouridine or 4-thiouracil, respectively in 1:2 cyclopropylamine:ethanol solution at 55 ^{o}C for 2 days. Following purification by reverse phase HPLC, the product was confirmed by ^{1}H NMR and ESI-TOF mass spectrometry. Cyclic voltammetry was carried out in aqueous solution (pH 7) using a glassy carbon electrode with Ag/AgCl as reference.

2.2.2. Oligonucleotides. All DNA oligonucleotides were synthesized on an ABI DNA Synthesizer (trityl on), twice purified by HPLC (Rainin Dynamax 300 Å C18

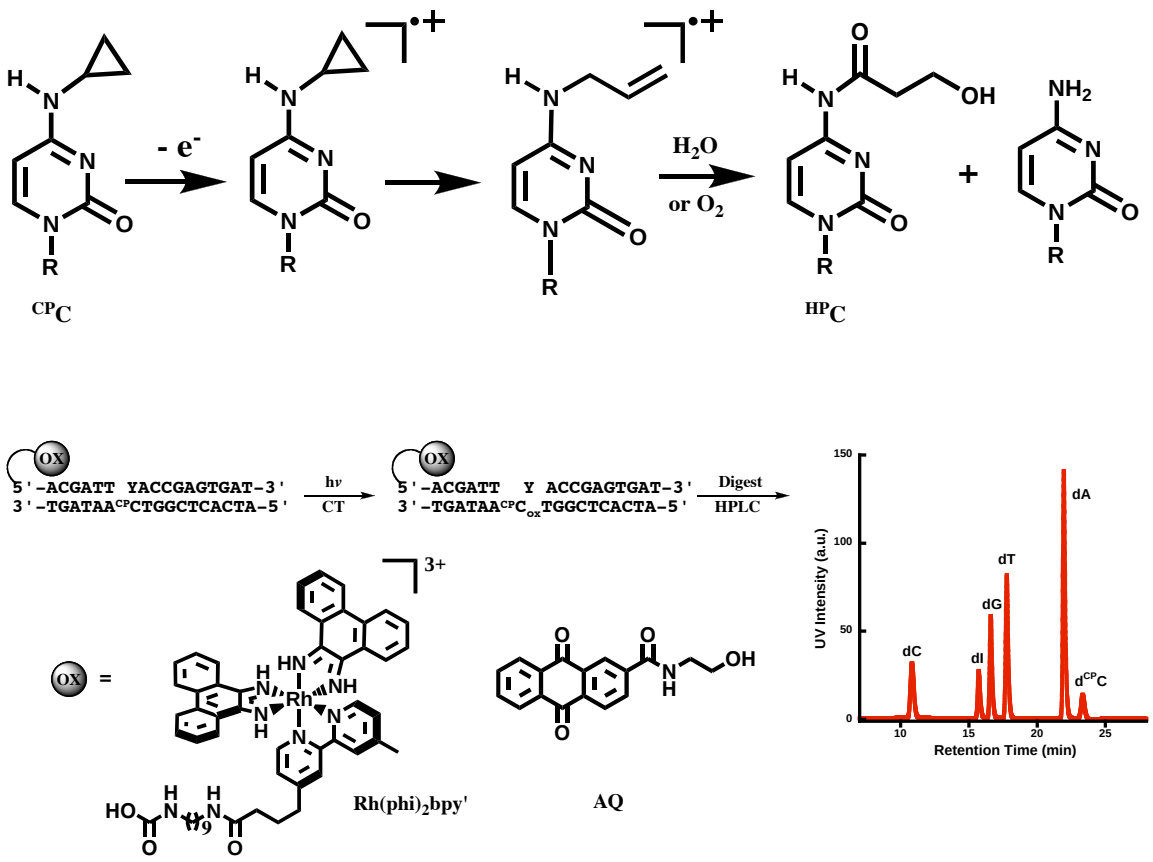

Figure 2.1. Experimental assay to test for hole occupation of pyrimidines during HT through duplex DNA. (*top*) Oxidation of ^{CP}C leads to rapid decomposition through ring scission and subsequent generation of two characteristic products. (*bottom*) Two potent photooxidants, $[Rh(phi)_2(bpy')]^{3+}$, Rh, and an anthraquinone derivative, AQ, positioned remote from ^{CP}C (covalently appended to the DNA with a C9 linker) initiate hole injection into DNA. Photooxidation of ^{CP}C in DNA, detected by HPLC analysis of the enzymatically digested duplexes, requires that the hole first migrate through the lower energy intervening bases.

reverse-phase column; for trityl on 5% ~ 35% and for trityl off 5% ~ 20% MeCN in 50 mM NH_4OAc over 30 min), and analyzed by mass ESI-TOF spectrometry. ^{CP}C- or ^{CP}G-containing strands were obtained by incubating oligonucleotides possessing 4-thiouridine, or 2-fluoroinosine, respectively, in 6M aqueous cyclopropylamine at 60 ºC for 16 hours prior to HPLC purification. The photooxidants, $Rh(phi)_2(bpy')^{3+}$ (phi = 9,10-phenanthrenequinone diimine; bpy' = 4-methyl-4'(butyric acid)-2,2'-bipyridine) (Rh) and an anthraquinone derivative (anthraquinone-2-carboxylic acid (2-hydroxyethyl) amide) (AQ) were synthesized and tethered to the complementary strands as previously described;[25] Rh-tethered assemblies are purified by RP-HPLC (Rainin Dynamax 300 Å C4 column, same solvents as DNA purification, 5% ~ 15% over first 20 min followed by 15% ~ 30% over 30 min). AQ-tethered DNA is purified as regular oligonucleotides. Rh-tethered assemblies, only the Δ-isomers (determined from CD spectroscopy) were used.

DNA oligonucleotides were quantitated by UV-visible spectroscopy. Duplex solutions (5 μM in 10mM sodium phosphate, 50 mM NaCl, pH 7) were prepared by combining equimolar amounts of the desired DNA complements and annealing with regulated cooling from 90 ºC to ambient temperature over a period of 2 hours. Under our experimental conditions the duplexes melt between 53 and 60 ºC (2 μM duplexes in 10 mM sodium phosphate, 50 mM NaCl, pH 7), depending upon the DNA sequence. The presence of ^{CP}C depresses the duplex melting temperature by ≤ 1 ºC.

2.2.3. Photooxidation. Aliquots of Rh tethered duplexes were irradiated at 365 nm with a 1000W Hg/Xe lamp equipped with a 320 nm LP filter and a monochromator. Aliquots of AQ tethered duplexes were irradiated at 350 nm using the same apparatus. Light controls were conducted by irradiating duplexes in the absence of tethered

photooxidant. Interduplex controls were conducted by irradiating a mixture of duplexes containing both photooxidant without ^{CP}C and ^{CP}C without photooxidant. Experiments reported here were carried out aerobically, however similar results were obtained in the absence of oxygen. After irradiation (0-40 minutes), duplex samples were digested by 37 ^{o}C incubation with phosphodiesterase, S1 endonuclease and alkaline phosphatase for 4 hours in order to yield the free nucleosides, and the samples were analyzed by reverse phase HPLC (Chemcobond 5-ODS-H, 4.6 * 100 mm). Oxidation of r^{CP}C (250 μM) by Rh or AQ (25 μM) and subsequent HPLC analyses were carried out under the same conditions described for the DNA samples. The oxidation products of r^{CP}C nucleoside were characterized by ESI-TOF MS.

2.3. Results.

2.3.1. The pyrimidine hole trap and its oxidation. We have prepared ^{CP}C by reaction of cyclopropylamine with 4-thiouracil. Just as the oxidation potential of ^{CP}G does not differ significantly from that of G,[22,28] the oxidation potential of ^{CP}C is expected to be very similar to unmodified C. Cyclic voltammetry reveals no oxidation of ^{CP}C at potentials of <1.6 V versus NHE in aqueous solution (pH 7), while oxidation of G was observed at ~1.3 V versus NHE. Thus the cyclopropyl moiety does not significantly reduce the oxidation potential of C. For the isolated nucleosides, then, ^{CP}C, like C, is significantly harder to oxidize than G.

Two potent photooxidants, Rh and AQ, are used to initiate the chemistry. Both have sufficient excited state reduction potentials (2.0 and 1.9 V vs NHE, respectively)[29,30] to oxidize each of the four natural DNA bases, and neither photoreduces DNA bases.[31,32]

Table 2.1. Assemblies to test long range oxidative damage to ^{CP}C in duplex DNA

Duplex[a]	Sequence[b]	% Decomposition of ^{CP}C[c]
Rh-G-1	Rh – 5′–ACGATT **G**ACCGAGTCAT–3′	36
Cp-1	3′–TGCTAA^{CP}**C**TGGCTCAGTA–5′	
Rh-I-1	Rh – 5′–ACGATT **I**ACCGAGTCAT–3′	92
Cp-1	3′–TGCTAA^{CP}**C**TGGCTCAGTA–5′	
Rh-G-2	Rh – 5′–ACGACC **G**ATTGAGTCAT–3′	5
Cp-2	3′–TGCTGG^{CP}**C**TAACTCAGTA–5′	
Rh-I-2	Rh – 5′–ACGACC **I**ATTGAGTCAT–3′	23
Cp-2	3′–TGCTGG^{CP}**C**TAACTCAGTA–5′	
AQ-G-1	AQ – 5′–ACGATT **G**ACCGAGTCAT–3′	10[d]
Cp-1	3′–TGCTAA^{CP}**C**TGGCTCAGTA–5′	
AQ-I-1	AQ – 5′–ACGATT **I**ACCGAGTCAT–3′	36[d]
Cp-1	3′–TGCTAA^{CP}**C**TGGCTCAGTA–5′	
AQ-A-1	AQ – 5′–ACGATT **A**ACCGAGTCAT–3′	15[d]
Cp-1	3′–TGCTAA^{CP}**C**TGGCTCAGTA–5′	
AQ-I-3	AQ – 5′–ACIATT **I**TTACCIAITCAT–3′	86
Cp-3	3′–TICTAA^{CP}**C**AATGGCTCAITA–5′	
AQ-I-4	AQ – 5′–ACIATT **IC**TTACCIAITCAT–3′	93
Cp-4	3′–TICTAA^{CP}**CG**AATGGCTCAITA–5′	
AQ-I-4	AQ – 5′–ACIATT**I C**TTACCIAITCAT–3′	100[e]
Cp-5	3′–TICTAA**C**^{CP}**G**AATGGCTCAITA–5′	
AQ-7	AQ – 5′–ACIATT **I C**TTACCIAITCAT–3′	90[f]/100[g]
Cp-7	3′–TICTAA^{CP}**C**^{CP}**G**AATGGCTCAITA–5′	
AQ-8	AQ – 5′–ACIATT **C I**TTACCIAITCAT–3′	86/98
Cp-8	3′–TICTAA^{CP}**G**^{CP}**C**AATGGCTCAITA–5′	

a. See Figure 2.1.

b. The ^{CP}C or ^{CP}G substitutions alter the melting temperatures (T_m) by ≤ 1 °C, e.g., the T_ms of 2 μM G-1/Cp-1 and G-1/C-1 are both 58 °C in 10 mM sodium phosphate and 50 mM sodium chloride, pH 7.

c. After 10 min of irradiation unless indicated (see *materials and methods*). Relative uncertainties are ±5%.

d. After 40 min of irradiation.

e. Percent decomposition of ^{CP}G.

f. Decomposition of ^{CP}C after 10 min of irradiation.

g. Decomposition of ^{CP}G after 10 min of irradiation.

Photoinduced electron transfer from N_4-cyclopropylcytidine ($r^{CP}C$) to each of these oxidants is observed in solution. The oxidation products are completely analogous to those found upon oxidation of ^{CP}G.[22] Irradiation of either Rh or AQ in the presence of $r^{CP}C$ induces efficient decomposition of the nucleoside and leads exclusively to the products of one electron oxidation followed by ring scission and trapping with water and/or oxygen (Figure 2.1).

2.3.2. Assay for pyrimidine radical formation. Our experimental assay to test for hole occupation of pyrimidines is also shown schematically in Figure 2.1. This assay employs duplex DNA assemblies containing ^{CP}C positioned remotely from a covalently tethered photooxidant. Irradiation initiates hole injection and migration through the duplex; the presence of hole density on ^{CP}C can be detected by its decomposition monitored via HPLC after enzymatic digestion. As with ^{CP}A and ^{CP}G,[22,23] substitution of the cyclopropyl moiety onto C causes little structural perturbation in the duplex. It is readily accommodated in B-DNA, with little change in duplex melting temperature ($\leq$1 ^{o}C) and no change in hypochromism.

In the DNA sequences employed (Table 2.1), ^{CP}C is positioned 5' to either an AA or a GG site, and is base paired with G or inosine (I). Importantly, ^{CP}C is 4-7 base pairs away from the site of the tethered photooxidant; in order to oxidize ^{CP}C, a hole must first traverse this intervening low energy bridge. Based upon current mechanistic models involving hopping among low energy bases, one would expect essentially no reaction at ^{CP}C in these duplexes.[28]

2.3.3. Hole trapping on ^{CP}C with HT through DNA. Figure 2.2 shows evidence of the long range oxidative damage to cyclopropylamine-substituted cytosines in the

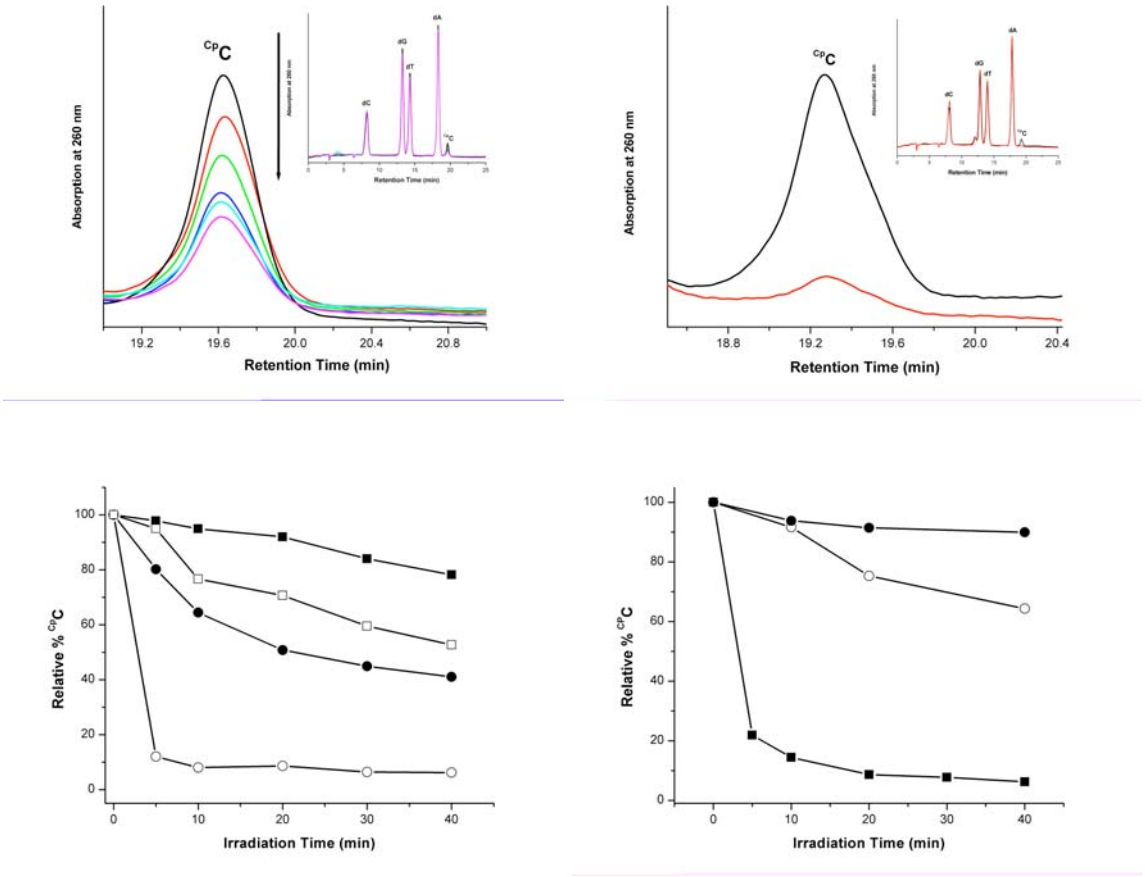

Figure 2.2. Long range oxidative damage to cytosines in duplex DNA. HPLC traces show the oxidative decomposition of ^{CP}C with increasing irradiation, 0-40 minutes for Rh-G-1 (*top left*) and 0 (black) versus 5 (red) minutes for Rh-I-1 (*top right*). Insets show the full HPLC traces. Plots of the amount of ^{CP}C as a function of irradiation time reveals the sequence dependence of ^{CP}C decomposition with Rh (*bottom left*) and AQ (*bottom right*): Rh-G-2 (closed circles), Rh-I-2 (open circles), Rh-G-1 (closed squares), Rh-I-1 (open squares), and in (d), AQ-G-1 (closed circles), AQ-I-1 (open circles), and AQ-I-3 (closed squares). For AQ, note the dramatic increase in efficiency of ^{CP}C photooxidation when the intervening guanines (AQ-I-1) are replaced with inosines (AQ-I-3). Decomposition of ^{CP}C is an intraduplex reaction that requires light and photooxidant.

DNA duplex. Despite the significant energetic differences among the intervening DNA bases, decomposition of ^{CP}C is clearly observed upon irradiation of the Rh-tethered DNA assemblies (Table 2.1). This observation provides direct HT chemical evidence for the existence of hole density on the pyrimidines.

The extent of hole occupation on the pyrimidine, moreover, is modulated by the energetics of the full duplex. When ^{CP}C is base paired with G, limited oxidation of ^{CP}C (~5 %) is observed in the sequence context 3'-GG^{CP}CT-5' (Rh-G-2) after 10 minutes of irradiation at 365 nm. However, the yield of ^{CP}C photodecomposition after 10 minutes of irradiation increases by 7-fold when the sequence context around ^{CP}C is altered to 3'-AA^{CP}CT-5' (Rh-G-1). This difference in yield of ^{CP}C decomposition is attributed to the sequence dependence of hole distribution; in 3'-GG^{CP}CT-5', the hole density is likely more localized on the GG doublet, while in 3'-AA^{CP}CT-5' the hole density is more diffuse, and there is thus a greater distribution on the ^{CP}C.

A similar but even more dramatic modulation is apparent when we replace the G base paired to ^{CP}C with an I. For the 3'-AA^{CP}CT-5' assembly (Rh-I-1), we observe rapid photodecomposition (> 90% after 10 minutes) of ^{CP}C. As seen with the Rh-G duplexes, the efficiency of photodecomposition is attenuated somewhat when the sequence context is changed to 3'-GG^{CP}CT-5' (Rh-I-2). However in both cases, when ^{CP}C is base paired with I, the efficiency of decomposition is significantly greater than when ^{CP}C is based paired with G. This again can be reconciled based on different distributions of hole density; owing to the higher oxidation potential of I (~1.5 V versus NHE),[30] the hole distribution is altered with greater hole density on ^{CP}C. Thus the modulation by base sequence is apparent both with intra- and interstrand substitutions. Importantly, this

modulation also establishes that the ring opening of the cyclopropyl-amine radical does not drive the reaction; variations in ring opening are instead dependent upon the sequence of the DNA assembly and its energetics.

Note that control experiments have also been conducted under parallel conditions where ^{CP}C-substituted assemblies lacking Rh are mixed with Rh-tethered assemblies lacking ^{CP}C. This control provides a test of whether any interduplex reaction occurs, as might be expected if a diffusible species were involved rather than long range DNA-mediated CT. In these control experiments, no photodecomposition of ^{CP}C is observed. Hence the oxidative reaction is intraduplex.

Sequence-dependent oxidation of ^{CP}C is an inherent feature of DNA CT, irrespective of oxidant. Covalently tethered AQ is therefore also found to be effective at photooxidation of ^{CP}C from a distance (Table 2.1, Figure 2.2), albeit at a somewhat lower efficiency. Noteworthy here is the fact that in these duplexes AQ is restricted to capping the duplex terminus, while the Rh photooxidant intercalates predominantly between the third and fourth bases. Photooxidation of ^{CP}C by AQ is also found to be an intraduplex reaction.

As with Rh, photooxidation of ^{CP}C by AQ is more efficient when ^{CP}C is based paired with I than with G (Table 2.1). In assemblies AQ-I-3/Cp-3 and AQ-I-4/Cp-4, containing only I between ^{CP}C and AQ, extensive photodecomposition of ^{CP}C is observed. Again this can be attributed to the modulation of hole density distribution through base pairing. This consistent modulation by sequence shows that the fast trapping reaction probes hole density rather than driving a redistribution. The cyclopropylamine kinetic trap does not determine the hole density, but simply reports it.

It is also noteworthy that H-bonding to ^{CP}C is not required for long range oxidation of ^{CP}C. We still find significant oxidation of ^{CP}C in assemblies where ^{CP}C opposes A, creating a non-hydrogen bonded mismatch (Table 2.1, AQ-A-1/Cp-1). The extent of reaction at ^{CP}C is therefore governed by intrinsic sequence dependent variations in the distribution of hole density in double stranded DNA.

2.3.4. Comparisons in photooxidation of ^{CP}C and ^{CP}G, modified bases with equal trapping rates but different energetics. To compare further the hole occupancy on purines and pyrimidines, we examined two duplexes of equivalent sequence, one containing ^{CP}C and the other containing ^{CP}G at the neighboring site (^{CP}G in AQ-I-4/Cp-5 and ^{CP}C in AQ-I-4/Cp-4 in Table 2.1). Based upon a thermal equilibration of charge, given a conservative difference in potential between C and G of ~ 0.3–0.5 V, the relative hole occupancy on ^{CP}C versus ^{CP}G should be ~1:10^5–10^8. As evident in Table 2.1, however, ^{CP}G and ^{CP}C in these two duplexes are seen to decompose with similar efficiency.

As shown in Figure 2.3, we also examined photooxidation of duplexes containing both ^{CP}G and ^{CP}C in the same assembly. Here, then, trapping times for the two modified bases should be equal, and one would expect the relative energetics of the fast traps to determine their relative efficiencies in photodecomposition. Remarkably, however, in these duplexes (AQ-7/Cp-7 and AQ-8/Cp-8), when ^{CP}G and ^{CP}C are incorporated as neighboring bases on the same strand, their efficiency of photodecomposition is comparable, although not identical (Figure 2.3, Table 2.1).

These data provide unequivocal evidence that hole density is transported onto the pyrimidines, and that hole density is appreciable. The hole distribution on the DNA

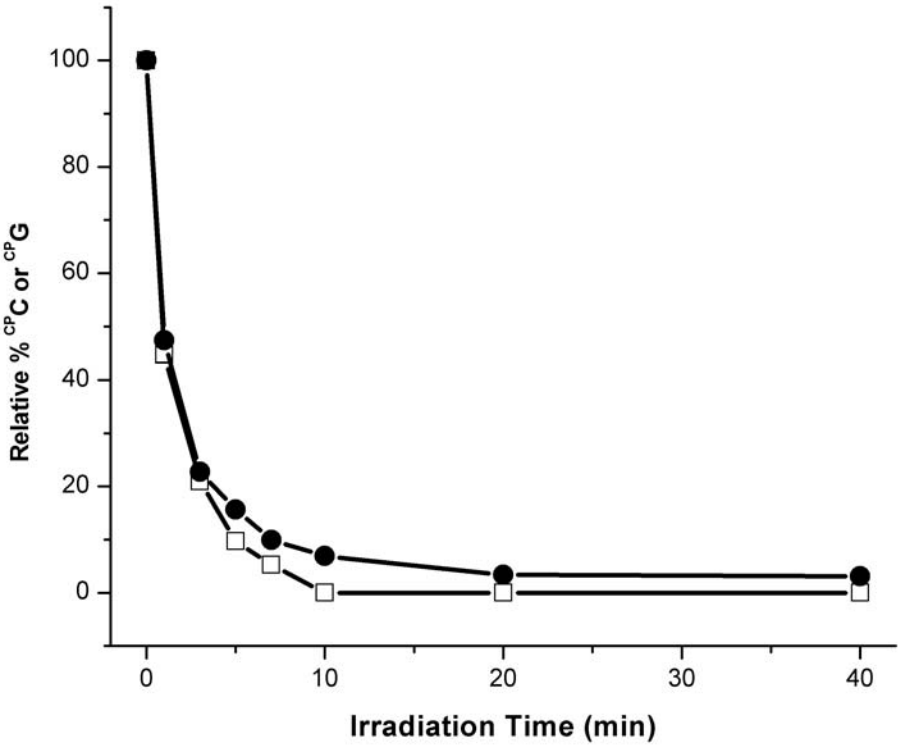

Figure 2.3. Hole distribution on the DNA bridge does not reflect the relative energies of the individual bases. Shown is a plot of the amount of ^{CP}C (closed circles) or ^{CP}G (open squares) as a function of irradiation time in AQ-7/Cp-7. This duplexes contain ^{CP}C and ^{CP}G at neighboring sites, 3'- ^{CP}C^{CP}G -5'. Similar results were observed for AQ-8/Cp-8 possessing a 3'- ^{CP}G^{CP}C-5' sequence within an otherwise identical duplex.

bridge does not reflect the relative energies of the isolated bases.

2.4. Discussion.

2.4.1. Mechanistic models for long range DNA CT. In many experiments characterizing DNA CT, a shallow distance dependence in the reaction has been demonstrated,[1-8] and this shallow distance dependence has been reconciled through models primarily involving long range diffusive charge hopping.[15,16] Models involving a mixture of hopping among low energy guanine sites and tunneling through AT tracts have provided a useful starting point for reconciling many experiments. Once experiments demonstrated rapid, long range DNA HT across assemblies containing adenine tracts,[5,7,34,35] however, the model was modified to also include hopping on low energy adenines.[18] These models, however, consistently explain DNA HT in the context solely of base energetics. Yet many experiments have underscored the sensitivity of DNA HT to DNA structure and dynamics.[9-11,19,20] Indeed it is now apparent that conformational motions of the DNA bases are required for effective CT; indeed increased rigidity of DNA assemblies limits CT.[36]

The results shown here cannot be understood through descriptions for DNA HT that are defined primarily by the energetics of individual bases. We find that, during the course of DNA CT, holes must occupy both the pyrimidine as well as purine bases, despite the fact that the HOMOs of isolated pyrimidines are ~0.5 eV higher in energy than purines. Clearly, then, the current descriptions of DNA-mediated HT in terms of incoherent G or A hopping cannot account for these data. Certainly base energetics do affect the reaction. Hole density on the pyrimidines found to be modulated by relative

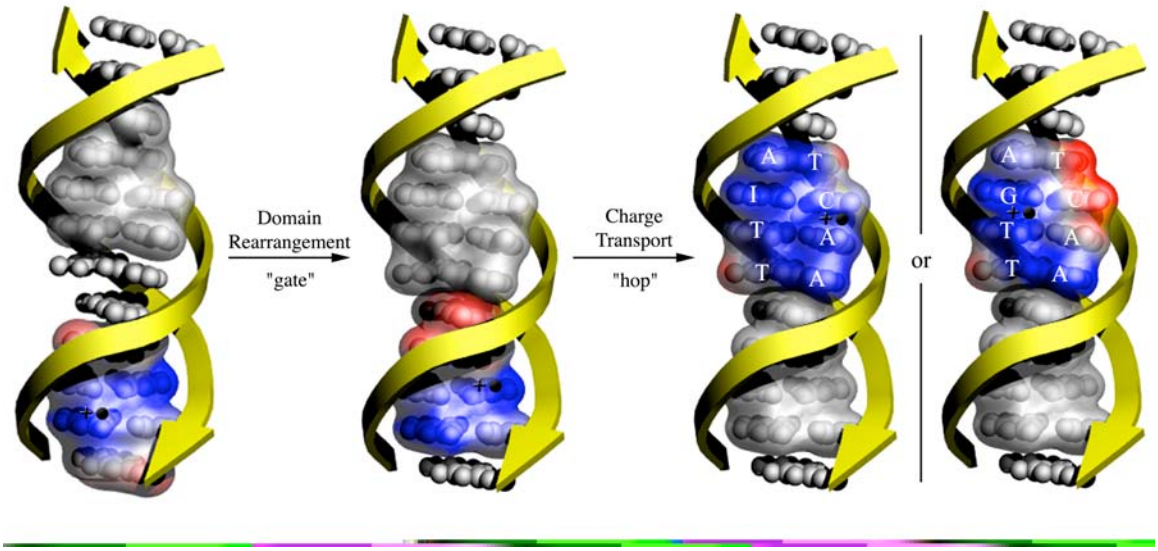

Figure 2.4. Schematized delocalized domain model for DNA charge transport. Charge migrates through the DNA bridge by hopping among domains, extended π-orbitals formed transiently in a manner governed by DNA sequence and dynamics. DNA domains form transiently irrespective of charge. Base motion, causes domains to form and break up, and consequently, migration of charge among domains is conformationally gated. In duplex DNA hole density is distributed through the domain (high-low, blue-white-red) in a sequence dependent fashion, as shown for instance when a I-C base pair is replaced by an G-C base pair. Here hole density distribution in the domains is shown schematically by static snapshots, but it will fluctuate in time with the dynamic motion of the DNA bases.

energies of bases on the same and opposite strand. Indeed theoretical predictions have been made indicating the modulation of baseionization potentials in DNA by sequence dependent structure[37] and dynamics.[38] In this context it is also interesting to consider the asymmetrical distribution of oxidative damage at the 5'-G of 5'-GG-3' doublets,[39] observed after relatively slow secondary reactions leading to trapping of the G radical and ultimately DNA strand cleavage. Yet these modulations do not provide sufficient energetic fluctuations to account for differences in oxidation potential between C and G. Here, experimentally, once the rate of trapping at C and G are made comparable by cyclopropyl substitution, the data indicate that the radical is delocalized comparably over the two neighboring bases. Thus, not only is there modulation, in fact there must necessarily be orbital mixing among the purines and pyrimidines to generate extended π-orbitals.

Models involving superexchange tunneling through pyrimidines are also unsatisfactory, since these data establish that the hole occupies the full DNA bridge, both pyrimidines as well as purines.[15,40] Models derived solely upon base energetics furthermore do not provide a reasonable rationale for the sensitivity of HT to sequence-dependent structure and dynamics. An alternative mechanistic description is required.

2.4.2. Charge transport through transient, delocalized domains. As illustrated in Figure 2.4, we propose a model where charge migrates through the DNA bridge among delocalized domains. Our data require occupation of all bases of the DNA bridge, although not necessarily simultaneously. These DNA domains can be described as extended π-orbitals formed transiently depending upon DNA sequence and dynamics. Spectroscopic investigations of base-base HT with 2-aminopurine as a function of bridge

length and temperature have provided evidence for a domain size of ~ 4 base pairs,[20] and distinguish a domain from a polaron.[3,41] Recently, a variable-range hopping model was developed and it was found to that delocalized bridge states are required to account for experimental yields of DNA hole transport.[42] Data here, where comparable efficiency of reaction at ^{CP}C and a neighboring ^{CP}G are observed, provide direct support for delocalization of charge.

However, delocalization clearly does not occur over the entire duplex. The transport is partly incoherent since we have found also that HT is gated by base motions.[9] Thus these delocalized domains form and break up transiently, facilitating and limiting HT. This model accounts well for the attenuation in HT seen in AT-rich sequences, owing to their inherent flexibility, and tunneling through AT sequences need not be invoked.[15,16] It also explains oxidative repair of thymine dimers at a distance, another fast trap.[43,44] While this model is more challenging to test experimentally, and describe theoretically, than superexchange or localized hopping, these and other data[45,46] show that DNA-mediated HT requires a more complete treatment.

Importantly, delocalized DNA domains reflect the rich sequence-dependent structure and dynamics of nucleic acids, known to be essential for DNA function. It is the sequence, with its inherent structure and dynamics, that defines a domain. Moreover, it is precisely this dependence upon nucleic acid structure and dynamics that is required for DNA-mediated HT to be exploited in molecular electronics and sensors, as well as to discover how it may be utilized in a biological context.

2.5. References

1. Hall, D. B., Holmlin, R. E., Barton, J. K. Oxidative DNA damage through long range electron transfer *Nature* **1996**, *382*, 731-735.

2. Núñez, M. E., Hall, D. B., Barton, J. K. Long range oxidative damage to DNA: effects of distance and sequence *Chem. Biol.* **1999**, *6*, 85-97.

3. Henderson, P. T., Jones, D., Hampikian, G., Kan, Y. Z., Schuster, G. Long-distance charge transport in duplex DNA: the phonon-assisted polaron-like hopping mechanism *Proc. Natl. Acad. Sci. USA* **1999**, *96*, 8353-8358.

4. Giese, B. Long-dstance electron transfer through DNA *Annu. Rev. Biochem.* **2002**, *71*, 51-70.

5. Takada, T., Kawai, K., Cai, X., Sugimoto, A., Fujitsuka, M., Majima, T. Direct observation of hole transfer through double-helical DNA over 100 Å *J. Am. Chem. Soc.* **2004**, *126*, 1125-1129.

6. Nakatani, K., Dohno, C., Saito, I. Modulation of DNA-mediated hole-transport efficiency by changing superexchange electronic interaction *J. Am. Chem. Soc.* **2000**, *122*, 5893-5894.

7. Yoo, J., Delaney, S., Stemp, E., Barton, J. K. Rapid radical formation by DNA charge transport through sequences lacking intervening guanines *J. Am. Chem. Soc.* **2003**, *125*, 6640-6641.

8. Delaney, S., Yoo, J., Stemp, E. D. A., Barton J. K. Charge equilibration between two distinct sites in double helical DNA *Proc. Nat. Acad. Sci. USA* **2004**, *101*, 10511-10516.

9. O'Neill, M. A., Becker, H. C., Wan, C., Barton, J. K., Zewail, A. H. Ultrafast dynamics in DNA-mediated electron transfer: base gating and the role of temperature *Angew. Chem. Int. Ed.* **2003**, *42*, 5896-5900.

10. Bhattacharya, P., Barton, J. K. The influence of intervening mismatches on long-range guanine oxidation in DNA duplexes *J. Am. Chem. Soc.* **2001**, *123*, 8649-8656.

11. Boon, E. M., Ceres, D. M., Drummond, T. G., Hill, M. G., Barton J. K. Mutation detection by electrocatalysis at DNA-modified electrodes *Nature Biotechnology* **2000**, *18*, 1096-1100.

12. Boon, E. M., Livingston, A. L., Chmiel, N. H., David, S. S., Barton J. K. DNA-mediated charge transport for DNA repair *Proc. Natl. Acad. Sci. USA* **2003**, *100*, 12543-12546; *ibid* **2004**, *101*, 4718-4718.

13. Porath, D., Bezryadin, A., Vries, S. D., Dekker, C. Direct measurement of electrical transport through DNA molecules *Nature* **2000**, *403*, 635-638.

14. Fink, H., Schonenberger, C. Electrical conduction through DNA molecules *Nature* **1999**, *398*, 407-410.

15.Bixon, M., Giese, B., Wessely, S., Langenbacher, T. Michel-Beyerle, M. E., Jortner, J. Long-range charge hopping in DNA *Proc. Natl. Acad. Sci. USA* **1999**, *96*, 11713-11716.

16. Berlin, Y. A., Burin A. L., Ratner M. A. Elementary steps for charge transport in DNA: thermal activation vs. tunneling *Chem. Phys.* **2002**, *275*, 61-74.

17. Lewis, F. D., Liu, J. Q., Zuo, X. B., Hayes R. T., Wasielewski, M. R. Dynamics and energetics of single-step hole transport in DNA hairpins *J. Am. Chem. Soc.* **2003**, *125*, 4850-4861.

18. Giese, B., Amaudrut, J., Kohler, A. K., Spormann M., Wessely, S. Direct observation of hole transfer through DNA by hopping between adenine bases and by tunnelling *Nature*, **2001**, *412*, 318-320.

19. Wan, C. Z., Fiebig, T., Kelley, S. O., Treadway, C. R., Barton, J. K., Zewail, A. H. Femtosecond dynamics of DNA-mediated electron transfer *Proc. Natl. Acad. Sci. USA* **1996**, *96*, 6014-6019.

20. O'Neill, M. A., Barton, J. K. DNA charge transport: conformationally gated hopping through stacked domains *J. Am. Chem. Soc.* **2004**, *126*, 11471-11483.

21. Musa, O. M., Horner, J. H., Shahin, H., Newcomb, M. A kinetic scale for dialkyl-aminyl radical reactions *J. Am. Chem. Soc.* **1996**, *118*, 3862-3868.

22. Nakatani, K., Dohno, C., Saito, I. Design of a hole-trapping nucleobase: termination of DNA-mediated hole transport at N^2-cylcopropyldeoxyguanosine *J. Am. Chem. Soc.* **2001**, *123*, 9681-9682.

23. Dohno, C., Ogawa, A., Nakatani, K., Saito, I. Hole trapping at N^6-cyclopropyldeoxyadenosine suggests a direct contribution of adenine bases to hole transport through DNA *J. Am. Chem. Soc.* **2003**, *125*, 10154-10155.

24. O'Neill, M. A., Dohno, C., Barton, J. K. Direct chemical evidence for charge transfer between photoexcited 2-aminopurine and guanine in duplex DNA *J. Am. Chem. Soc.* **2004**, *126*, 1316-1317.

25. Williams, T.T., Dohno, C., Stemp, E.D.A & Barton, J.K. Effects of the photooxidant on DNA-mediated charge transport *J. Am. Chem. Soc.* **2004**, *126*, 8148–8158.

26. Stemp, E. D. A, Arkin, M., Barton, J. K. Oxidation of guanine in DNA by $Ru(phen)_2dppz^{3+}$ using the flash-quench technique *J. Am. Chem. Soc.* **1997**, *119*, 2921-2925.

27. Burrows, C. J., Muller, J. G. Oxidative nucleobase modifications leading to strand scission *Chem. Rev.* **1998**, *93*, 1109-1151.

28. Steenken, S., Jovanovic, S. V. How easy oxidizable is DNA? One-electron reduction potentials of adenosine and guanosine radicals in aqueous solution *J. Am. Chem. Soc.* **1997**, *119*, 617-618.

29. Turro, C., Evenzahav, A., Bossmann, S. H., Barton, J. K., Turro, N.J. Excited state properties of $Rh(phi)_2(phen)^{3+}$ and related complexes: a strong photooxidant *Inorg. Chim. Acta.* **1996**, *243*, 101-108.

30. Armitage, B., Yu, C., Devadoss, C., Schuster, G. B. Cationic anthraquinone derivatives as catalytic DNa photonucleases: mechanism for DNA damage and quinone recycling *J. Am. Chem. Soc.* **1994**, *116*, 9847-9859.

31. Turro, C., Hall, D. B., Chen, W., Zuilhof, H., Barton, J. K., Turro, N.J. Solution Photoreactivity of phenanthrenequinone diimine complexes of rhodium and correlations with DNA photocleavage and photooxidation *J. Phys. Chem. A* **1998**, *102*, 5708-5715.

32. Ma, J. H., Lin, W. Z., Wang, W. F., Han, Z. H., Yao, S. D., Lin, N. Y. Characterization of reactive intermediates in laser photolysis of nucleoside using of sodium salt anthraquinone-2-sulfonic acid as photosensitizer *Radiat. Phys. Chem.* **1999**, *54*, 491-497.

33. Kelley, S. O., Barton, J. K. Electron transfer between bases in double helical DNA J.K. *Science* **1999**, *283*, 375-381.

34. Williams, T. T., Odom, D. T., Barton, J. K. Variations in DNA charge transport with nucleotide composition and sequence *J. Am. Chem. Soc.* **2000**, *122*, 9048-9049.

35. Schuster, G. B. Long-range charge transfer in DNA: transient structural distortions control the distance dependence *Acc. Chem. Res.* **2000**, *33*, 253-260.

36. O'Neill M. A., Barton, J. K. DNA-mediated charge transport requires conformational motion of the DNA bases: elimination of charge transport in rigid glasses at 77K *J. Am. Chem. Soc.* **2004**, *126*, 13234-13235.

37. Voityuk, A. A., Jortner, J., Bixon, M., Rösch, N. Energetics of hole transfer in DNA *Chem. Phys. Lett.* **2000**, *324*, 430-434.

38. Voityuk, A. A., Siriwong, K., Rösch, N. Environmental fluctuations facilitate electron-hole transfer from guanine to adenine in DNA π stacks *Angew. Chem. Int. Ed.* **2004**, *43*, 624-627.

39. Sugiyama, H., Saito, I. Theoretical studies of GG-specific photocleavage of DNA via electron transfer: significant lowering of ionization potential and 5'-localization of HOMO of stacked GG bases in B-form DNA *J. Am. Chem. Soc.* **1996**, *18*, 7063-7068.

40. Lewis, F. D., Letsinger, R. L., Wasielewski, M. R. Dynamics of photoinduced charge transfer and hole transport in synthetic DNA hairpins *Acc. Chem. Res.* **2001**, *34*, 159-170.

41. Barnett, R. N., Cleveland, C. L., Joy, A., Landman, U., Schuster, G. B. Charge migration in DNA: ion-gated transport *Science* **2001**, *94*, 567-571.

42. Renger, T., Marcus, R. A. Variable-range hopping electron transfer through disordered bridge states: application to DNA *J. Phys. Chem. A* **2003**, *107*, 8404-8419.

43. Dandliker, P. J., Holmlin, R. E., Barton, J. K. Oxidative thymine dimer repair in the DNA helix *Science* **1997**, *275*, 1465-1467.

44. Dandliker, P. J., Núñez, M. E., Barton, J. K. Oxidative charge transfer to repair thymine dimers and damage guanine bases in DNA assemblies containing tethered metallointercalators *Biochemistry* **1998**, *37*, 6491-6502.

45. Ceres D. M., Barton, J. K. *In situ* scanning tunnelling microscopy of DNA-modified gold surfaces: bias and mismatch dependence *J. Am. Chem. Soc.* **2003**, *125*, 14964-14965.

46. Drummond, T. D., Hill, M. G., Barton, J. K. Electron transfer rates in DNA films as a function of tether length *J. Am. Chem. Soc.* **2004**, *126*, 15010-15011.

Chapter 3

Sequence Dependence of Hole Transport through DNA Domains

Adapted from Shao, F., Augustyn, K., Barton, J. K. *J. Am. Chem. Soc.* **2005**, *117*, 17445-17452.

** Photooxidation of DNA with non-covalently bound Ru and Rh complexes were conducted by Dr. K. Augustyn.

3.1. Introduction.

Hole transport (HT) through double helical DNA to promote oxidative damage from a distance has been demonstrated through biochemical and spectroscopic assays in many DNA assemblies containing different pendant photooxidants.[1-6] The DNA base pair stack mediates hole transport over at least 200 Å,[7,8] and the reaction is remarkably sensitive to the dynamic structure and stacking within the DNA duplex.[2,9] Given this exquisite sensitivity to stacking, DNA-mediated HT chemistry uniquely provides a means to detect anomalies in the base pair stack. Thus DNA HT has provided the basis for novel electrochemical sensors for mutational analysis,[10] and indeed, DNA HT may play a role in the detection of mismatches and lesions within the cell.[11]

While DNA hole transport is now well accepted based upon experiment, mechanistic descriptions of how hole migration through DNA proceeds is still not well established. Physical measurements have been used to characterize DNA as a wide band gap semiconductor,[12-14] but in many of these studies, the integrity of the base pair stack has been unclear. Mechanistic descriptions have focused on one-step superexchange-mediated tunneling or incoherent multistep hopping of localized charge (generally holes).[4, 15-17] The fundamental difference between these two mechanisms is whether the hole actually occupies the DNA bridge.[18] For HT through donor-bridge-acceptor systems, occupancy of the bridge depends upon the energetic barrier for hole injection from the donor to the bridge.[19] More recently, models of incoherent HT have been considered as involving a mixture of localized hole hopping among low energy sites, guanines and sometimes adenines, and tunneling through higher energy pyrimidine bases.[20] These

mechanisms do not provide a rationale, however, for the sensitivity of HT to DNA stacking.

We have found that DNA HT is gated by the dynamical motions of the DNA bases[21] and have described DNA HT as conformationally gated hopping through transient, well stacked DNA domains.[22] Dynamical motion is, in fact, necessary to promote HT through the base stack; experiments at 77K show no detectable HT between bases.[23]

Most recently, we have obtained experimental evidence in support of partial delocalization using cyclopropylamine-substituted bases as fast hole traps to monitor radical occupation on the DNA bridge.[24] Despite a significant difference in oxidation potential between purines and pyrimidines, within the base pair stack we observed comparable efficiency of oxidation of N_4-cyclopropylamine-cytosine (^{CP}C) and a neighboring N_2-cyclopropylamine-guanosine (^{CP}G) in chapter 2. This comparable reactivity points to orbital mixing between these neighboring bases in the stack. Delocalization clearly does not occur over the entire duplex, however. Spectroscopic investigations with 2-aminopurine of base-base HT as a function of bridge length and temperature show evidence for a domain size of ~ four base pairs.[22] It should be noted that a partially delocalized model for DNA HT was also recently supported by calculations of a variable-range hopping model, in which it was found that delocalized bridge states are required to account for experimental yields of DNA hole transport.[25]

Thus we have considered that the extent of delocalization within the DNA duplex depends upon the sequence-dependent dynamics of DNA. We distinguish our model of conformationally gated delocalized domains from polaron models[3,26,27] for hole transport,

since polarons are expected to form as a result of structural distortions in response to the migrating hole.[26] We consider instead that it is the sequence-dependent motions of DNA that lead to delocalized domains that form and break up transiently, facilitating and limiting HT.

Here we look in more detail at the energetics and sequence dependence of HT using cyclopropylamine substituted bases as fast kinetic traps to probe hole occupation. These cyclopropylamine-modified bases allow us to examine how domains vary as a function of base sequence, position, and length, and perhaps also allow us to distinguish dynamical domains from polarons. Certainly these data allow us to characterize features of the rich sequence-dependent dynamical structure of DNA and its consequences with respect to DNA HT.

3.2. Materials and methods.

3.2.1. Synthesis and characterization of the oligonucleotides and photooxidants.

Oligonucleotides containing ^{CP}C and ^{CP}G. All DNA oligonucleotides containing ^{CP}C and ^{CP}G, were synthesized with the terminal dimethoxytrityl group intact on an Applied Biosystems 394 DNA synthesizer, using 4-thio-uracil and 2-fluoro-inosine phosphoramidites as the ^{CP}C and ^{CP}G precursors respectively.[24,28] The DNA resin was reacted with 1M diaza(1,3)bicyclo[5.4.0]-undecane (DBU) in acetonitrile in order to remove the protecting groups on the precursor bases. The DNA oligonucleotides were incubated for 16 h in 6M aqueous cyclopropylamine at 60 ^{o}C and simultaneously deprotected and cleaved from the resin. The cleaved DNA strands were dried *in vacuo*, and resuspended in buffer prior to purification by HPLC. Following the first purification,

the dimethoxytrityl group was removed with 80% acetic acid and the strands were repurified by HPLC. MALDI-TOF mass spectrometry was used to characterize the strands.

Anthraquinone-tethered oligonucleotides. An anthraquinone derivative [anthraquinone-2-carboxylic acid (2-hydroxyethyl) amide] (AQ) was synthesized and converted into its respective phosphoramidite.[29] The AQ phosphoramidite was incorporated onto the 5' end of the DNA oligonucleotides employing a 15 min coupling time. The DNA was deprotected and cleaved from the resin overnight at 60 ^{o}C in ammonium hydroxide and dried *in vacuo*. The resulting oligonucleotides were purified once by HPLC and characterized by MALDI-TOF mass spectrometry.

DNA Duplexes. The DNA oligonucleotides were suspended in a buffer containing 50 mM NaCl, 20 mM sodium phosphate, pH 7.0 and quantified by UV-visible spectroscopy. DNA duplexes were annealed by combining equal moles of the desired DNA complements in the buffer and heating at 90 ^{o}C for 5 min, followed by cooling to ambient temperature over 2 h. Melting temperatures were determined for all substituted DNA duplexes prepared. Cyclopropylamine substitution on the DNA bases leads to changes in melting temperature of <2 ^{o}C, indicating that substitution causes little destabilization of the duplex.[24]

Metal photooxidants. The metal complexes [Ru(phen)(dppz)(bpy')]Cl_2 (phen = 1,10-phenanthroline, dppz = dipyrido[3,2-a:2'-3'-c]phenazine, bpy' = 4-(4'-methyl-2,2'-bipyridyl valerate) and [Rh(phi)2(bpy)]Cl_3 (phi = phenanthrenequinone diimine) were synthesized as previously described[30] and characterized by ESI mass spectrometry and 1H NMR.

3.2.2. Photooxidations. For ruthenium oxidations, aliquots (30 μl) contained 5 μM DNA duplex, 5 μM $[Ru(phen)(dppz)(bpy')]^{2+}$, and 50 μM $[Ru(NH3)6]Cl_3$. Anaerobic samples were prepared by utilizing the freeze-pump-thaw method in air tight cuvettes under Ar. Flash quench generated oxidation was accomplished by irradiation for 0 – 30 min using a Liconix He:Cd laser (~12 mW) at 442 nm. For rhodium oxidations, aliquots contained 5 μM DNA duplex and 5 μM $[Rh(phi)2(bpy)]^{3+}$. Rhodium samples were irradiated for 0 to 10min at 365 nm, using a 1000 W Hg/Xe lamp equipped with a 320 nm long pass filter and a monochromator. For anthraquinone-DNA oxidations, aliquots of 10 or 15 μM AQ tethered duplexes were irradiated at 350 nm for 0 - 10 minutes, using the same apparatus as for the rhodium oxidations.

3.2.3. HPLC analysis of base products. Following irradiation, the samples were digested by phosphodiesterase I and alkaline phosphatase at 37 ^{o}C for 4.5-24 h to generate individual nucleosides. Reverse-phase HPLC (Chemcobond 5-ODS-H, 4.6×100mm) was applied to analyze the oxidation of ^{CP}C and ^{CP}G nucleosides. Oxidation yields of ^{CP}C and ^{CP}G were determined by the peak area from HPLC analysis normalized to that of thymidine. All photooxidations were carried out at least three times, and the results were averaged.

3.3. Results.

3.3.1. Design of DNA Assemblies. A range of DNA assemblies was prepared that contain tethered AQ on one strand and either or both ^{CP}G and ^{CP}C on the other strand. In these assemblies, it is considered that AQ stacks at the end of the helix. Thus the photooxidant, AQ, is spatially well separated from the hole traps, ^{CP}G and ^{CP}C. In order

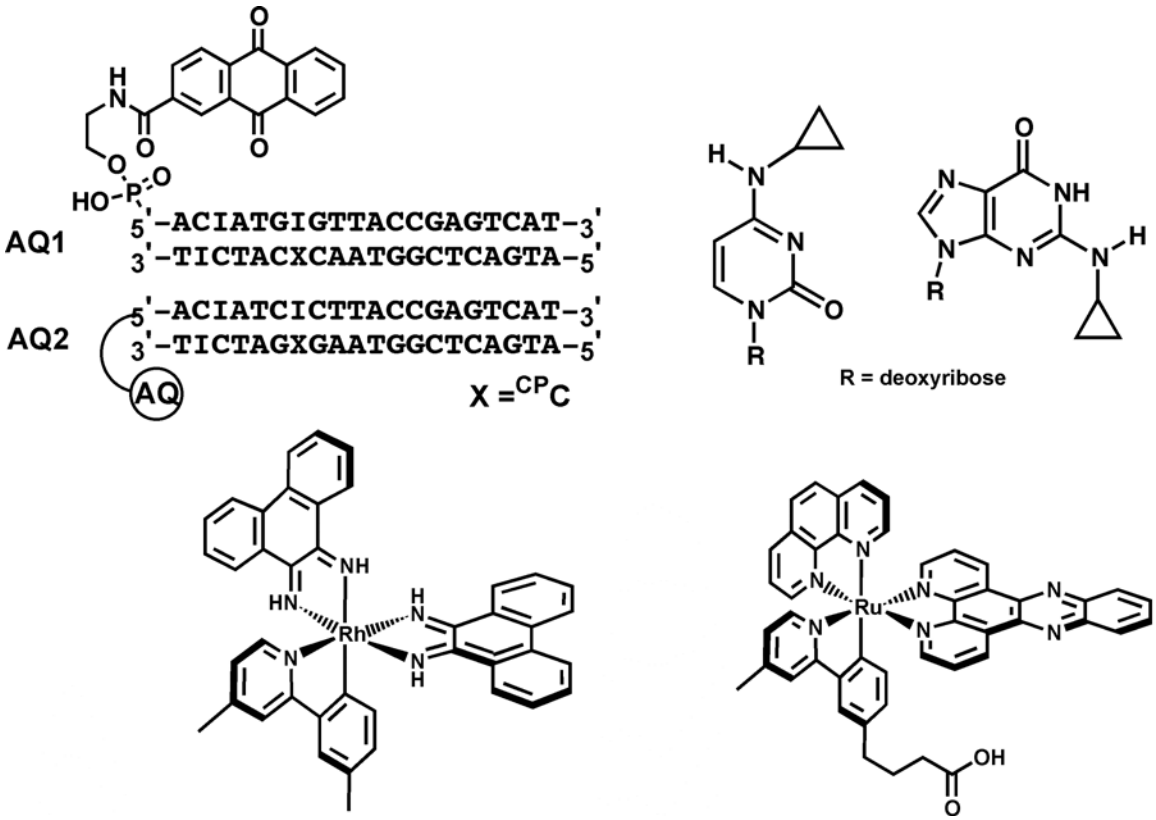

Figure 3.1. Shown are some DNA assemblies used to explore DNA HT as well as photoxidants and modified bases as hole traps. In **AQ1** and **AQ2**, an anthraquinone derivative is covalently tethered through the phosphate backbone to the 5' end of the complements to ^{CP}C-containing DNA strands. The sequences of the DNA assemblies are shown either with the structure of the photooxidant in **AQ1**, or schematically in **AQ2**. The structures of ^{CP}C, ^{CP}G, $[Ru(phen)(dppz)(bpy')]^{2+}$ and $[Rh(phi)_2(bpy)]^{3+}$ are also shown.

to limit competition with hole trapping at guanine sites and therefore to provide the largest possible window through which to monitor decomposition of ^{CP}C, inosines, rather than guanosines, are utilized at many sites in the duplexes, particularly base paired to ^{CP}C. Figure 3.1 shows two representative assemblies. We also examined photooxidation of DNA assemblies containing ^{CP}C and ^{CP}G using the non-covalent intercalators, $[Ru(phen)(bpy')(dppz)]^{3+}$ and $[Rh(phi)_2(bpy)]^{3+}$.

3.3.2. Photooxidation of ^{CP}C in 5'-C^{CP}CC-3' and 5'-G^{CP}CG-3'. In order to probe the effects of the flanking bases in a DNA duplex, two assemblies, **AQ1** and **AQ2** were designed (Figure 3.1). **AQ1** and **AQ2** are similar in sequence, except that in **AQ1** a 5'-C^{CP}CC-3' segment is placed six base pairs away from the AQ-tethered end, while in **AQ2** a 5'-G^{CP}CG-3' segment is at the corresponding position. ^{CP}C decomposes efficiently after 10 minutes of irradiation in both assemblies: 92% in **AQ1** and 96% in **AQ2**. Moreover, as shown in Figure 3.2, ^{CP}C in **AQ1** and **AQ2** have similar but not identical decomposition profiles over time. When the two flanking bases are guanines, ^{CP}C decomposes slightly more efficiently as compared to the case when ^{CP}C is flanked by two cytosines. Thus flanking bases have a small but significant effect on ^{CP}C decomposition.

3.3.3. Variation in sequences across strands. In order to probe variations between the complementary strands, we utilized four assemblies, **AQ3** through **AQ6** as shown in Table 3.1. All four assemblies are identical with respect to base content and position but are different with respect to the sequence of their single strands. In all cases, ^{CP}C is located on the complement to the AQ-tethered strand, nine bases away, and is base paired to inosine (I). ^{CP}C-I is flanked by four AT base pairs on either side. In **AQ3**, the

Table 3.1. The effect of A_n and T_n tracts on ^{CP}C decomposition in DNA duplexes.

DNA #	Sequence[a,b]	% Decomposition of ^{CP}C[c,d]
AQ3	5′-AQ-ACIATTTT ITTTTCCAGTCAT-3′ 3′-TICTAAAA^{CP}CAAAAGGTCAGTA-5′	88
AQ4	5′-AQ-ACIAAAAA IAAAACCAGTCAT-3′ 3′-TICTTTTT^{CP}CTTTTGGTCAGTA-5′	13
AQ5	5′-AQ-ACIATTTT IAAAACCAGTCAT-3′ 3′-TICTAAAA^{CP}CTTTTGGTCAGTA-5′	92
AQ6	5′-AQ-ACIAAAAA ITTTTCCAGTCAT-3′ 3′-TICTTTTT^{CP}CAAAAGGTCAGTA-5′	71

a. AQ refers to the anthraquinone derivative as described in materials and methods.
b. Melting temperatures for duplexes are 51 ± 2 ^{o}C.
c. Following 5 minutes of irradiation. Duplexes (5μM) were irradiated in 50mM NaCl and 20mM sodium phosphate buffer. Details are in materials and methods.
d. Data are averaged over at least 3 data sets. Deviations are less than 5%.

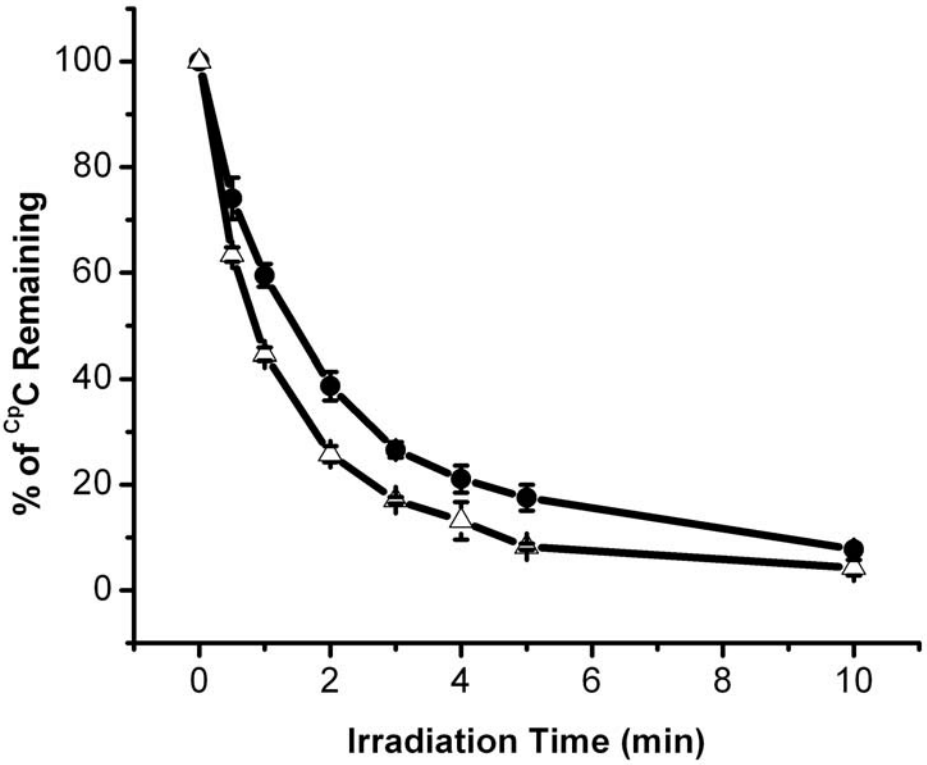

Figure 3.2. Plot of the % of ^{CP}C remaining in **AQ1** (dark circles) and **AQ2** (open triangles) as a function of irradiation time. Standard errors based upon three trials are shown. ^{CP}C is flanked by cytosines in **AQ1** and guanines in **AQ2**, while the remainder of the sequence is identical in both assemblies.

four-base segments surrounding ^{CP}C are all adenines, whereas in **AQ4** they are all thymines. **AQ5** has ^{CP}C flanked by one adenine segment, A4, and one thymine segment, T4, while A4 and T4 are reversed in **AQ6**.

AQ3 and **AQ5**, both containing an A4 tract in front of ^{CP}C, have similar decomposition efficiencies of 88% and 92% respectively. However, both assemblies show greater reactivity on ^{CP}C than in **AQ4** and **AQ6**, both of which contain a proximal T4. In fact, **AQ4** has both a proximal and distal T4 segment and the ^{CP}C decomposition is significantly diminished to only 13%, seven times less than in **AQ5**. Replacing the distal T4 with A4 in **AQ6** results in a five-fold increase in ^{CP}C decomposition. It is therefore apparent that the full sequence of DNA, both before and after the kinetic trap, affect the efficiency of hole trapping.

3.3.4. Reactivity in adenine tracts. The effects of repetitive adenines are monitored using two sets of assemblies, as shown in Table 3.2. The first type of perturbation we examined is a single base substitution within the A-tract. In **AQ7**, ^{CP}C is placed after the sixth base in an eight base-pair adenine tract. The structural coherence of the adenine tract is then disrupted by replacing the fourth adenine with either a T, G, or C in **AQ8**, **AQ9** and **AQ10**, respectively. As is evident, trapping reactivity is mildly affected by a single base interruption in adenine stacking. Following irradiation, **AQ8**, **AQ9** and **AQ10** show somewhat less decomposition of ^{CP}C than **AQ7**, in which the A-tract remains intact. Interestingly, the base substitution with the most pronounced effect in diminishing the decomposition of ^{CP}C is guanine in **AQ9**; **AQ9** shows only 72% decomposition of ^{CP}C after 5 minutes of irradiation as compared with 91% for **AQ7**. This result may reflect the lower oxidation potential of guanine. Upon irradiation, **AQ8** and

Table 3.2. The Effect of coherence of the A-tract on ^{CP}C decomposition in DNA duplex.

DNA #	Sequence[a,b]	% Decomposition of ^{CP}C[c,d]
AQ7	5′-AQ-ACIATTTTTT ITTCCAGTCAT-3′ 3′-TICTAAAAAA^{CP}CAAGGTCAGTA-5′	91
AQ8	5′-AQ-ACIATTTATT ITTCCAGTCAT-3′ 3′-TICTAAATAA^{CP}CAAGGTCAGTA-5′	81
AQ9	5′-AQ-ACIATTTCTT ITTCCAGTCAT-3′ 3′-TICTAAAGAA^{CP}CAAGGTCAGTA-5′	72
AQ10	5′-AQ-ACIATTTGTT ITTCCAGTCAT-3′ 3′-TICTAAACAA^{CP}CAAGGTCAGTA-5′	78
AQ11	5′-AQ-ACIATTAATT ITTCCAGTCAT-3′ 3′-TICTAATTAA^{CP}CAAGGTCAGTA-5′	85
AQ12	5′-AQ-ACIATATATT ITTCCAGTCAT-3′ 3′-TICTATATAA^{CP}CAAGGTCAGTA-5′	71
AQ13	5′-AQ-ACIATATATA ITTCCAGTCAT-3′ 3′-TICTATATAT^{CP}CAAGGTCAGTA-5′	41

a. AQ refers to the anthraquinone derivative as described in materials and methods.
b. Melting temperatures for duplexes are 50 ± 2 ^{o}C.
c. Following 5 minutes of irradiation. Duplexes (5μM) were irradiated in 50mM NaCl and 20mM sodium phosphate buffer. Details are in materials and methods.
d. Data are averaged over at least 3 data sets. Deviations are less than 5%.

AQ10 with T and C substitutions, respectively, show similar efficiencies of ^{CP}C decomposition (81% and 78%).

In addition to a single base substitution, the coherence of the six-adenine tract preceding ^{CP}C can be disrupted by decreasing the number of adenine doublets in the A-tract. In **AQ11**, **AQ12**, and **AQ13**, the six adenines preceding ^{CP}C are modified to contain either two (**AQ11**), one (**AQ12**), or no (**AQ13**) adenine doublets. As shown in Table 3.2, **AQ7**, with three adenine doublets yields more decomposition of ^{CP}C than **AQ11**, **AQ12** and **AQ13**, which contain two, one or no adenine doublets in the proximal A-tract. When no adenine doublets are present, decomposition of ^{CP}C is significantly reduced to 41% in **AQ13** compared with 91% in **AQ7**. When one or two adenine doublets are present, decomposition is mildly reduced (85% for **AQ11** and 71% for **AQ12**).

3.3.5. Competition between ^{CP}C and ^{CP}G. To investigate the domain size in an adenine tract, sequences **AQC0**-**AQC5** were designed. All assemblies contain a seven base-pair adenine tract and have one ^{CP}C and ^{CP}G separated by various numbers of adenines (0-5) within the tract. Although the position of ^{CP}C remains fixed after the second adenine in the tract, ^{CP}G is placed at distances further along the tract, as shown in Table 3.3.

The decomposition of ^{CP}C in all six assemblies shows similar efficiencies, ranging from 77% to 89%. A small increase in decomposition of ^{CP}C occurs when ^{CP}G is moved two or more adenines away. In contrast, ^{CP}G decomposition can be divided into two distinct regions, the efficient region seen with **AQC0** and **AQC1** assemblies versus the inefficient region found with **AQC2**, **AQC3**, **AQC4**, and **AQC5** as shown in Figure 3.2. ^{CP}G is most efficiently decomposed in **AQC0**, where ^{CP}G is neighboring ^{CP}C. A 10%

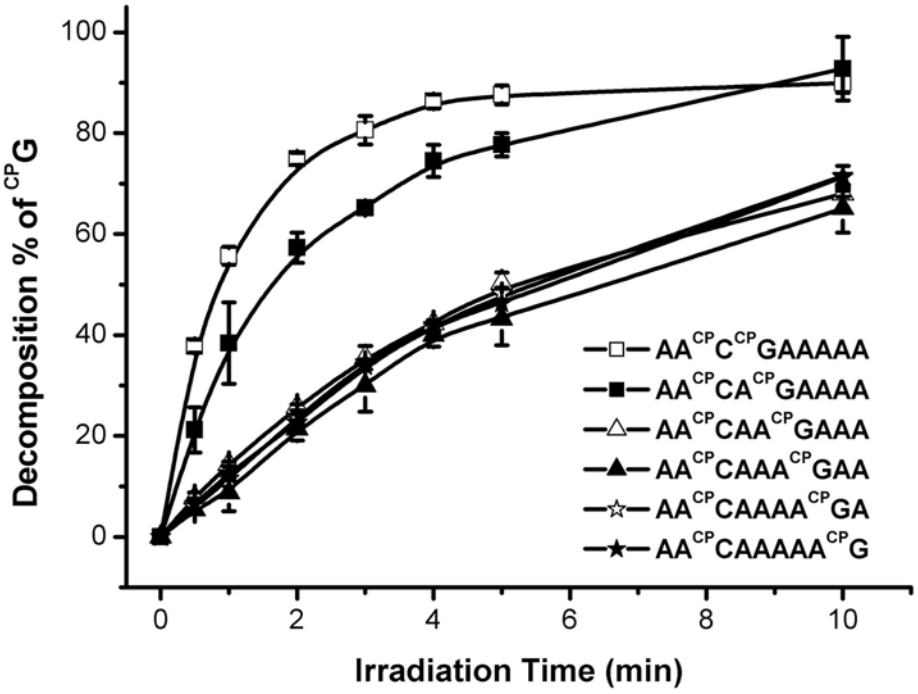

Figure 3.3. Plot of the % decomposition of ^{CP}G in **AQCn** assemblies as a function of irradiation time. In **AQCn** assemblies, ^{CP}G is place n adenines away from ^{CP}C, while the position of ^{CP}C is fixed. The data with standard errors are shown as **AQC0** (open squares), **AQC1** (closed squares), **AQC2** (open triangles), **AQC3** (closed triangles), **AQC4** (open stars) and **AQC5** (closed stars).

Table 3.3. Sequence and base decomposition in assemblies containing ^{CP}C and ^{CP}G

DNA #	Sequence[a,b]	% Decomposition of ^{CP}C and ^{CP}G[c]
AQC0	5′-AQ-ACIATT I CTTTTTACCGAGTCAT-3′ 3′-TICTAA^{CP}C^{CP}GAAAAATGGCTCAGTA-5′	79[d]/88[e]
AQC1	5′-AQ-ACIATT IT CTTTTACCGAGTCAT-3′ 3′-TICTAA^{CP}CA^{CP}GAAAATGGCTCAGTA-5′	77/78
AQC2	5′-AQ-ACIATT ITT CTTTACCGAGTCAT-3′ 3′-TICTAA^{CP}CAA^{CP}GAAATGGCTCAGTA-5′	88/50
AQC3	5′-AQ-ACIATT ITTT CTTACCGAGTCAT-3′ 3′-TICTAA^{CP}CAAA^{CP}GAATGGCTCAGTA-5′	83/43
AQC4	5′-AQ-ACIATT ITTTT CTACCGAGTCAT-3′ 3′-TICTAA^{CP}CAAAA^{CP}GATGGCTCAGTA-5′	89/48
AQC5	5′-AQ-ACIATT ITTTTT CACCGAGTCAT-3′ 3′-TICTAA^{CP}CAAAAA^{CP}GTGGCTCAGTA-5′	88/46

a. AQ refers to the anthraquinone derivative as described in materials and methods.
b. Melting temperatures for duplexes are 55 ± 2 ^{o}C.
c. Data are averaged over at least 3 data sets. Deviations are less than 5%.
d. Decomposition of ^{CP}C after 5 minutes of irradiation. Duplexes (10μM) were irradiated in 50mM NaCl and 20mM sodium phosphate buffer. Details are in materials and methods.
e. Decomposition of ^{CP}G after 5 minutes of irradiation. Duplexes (10μM) were irradiated in 50mM NaCl and 20mM sodium phosphate buffer. Details are in materials and methods.

decrease in decomposition of ^{CP}G is observed in **AQC1**, in which ^{CP}G is moved one adenine base away from ^{CP}C. **AQC2-AQC5**, in which ^{CP}G is at least two adenines away from ^{CP}C, results in dramatically diminishing the decomposition of ^{CP}G to about 50%, regardless of the position of ^{CP}G. A similar but less pronounced trend is observed when these experiments are repeated using the **AQGn** series, which have the same sequence as the corresponding **AQCn**, but with the positions of ^{CP}G and ^{CP}C switched (data not shown). It should be noted in Table 3.3 that the decomposition ratio of the two traps is inverted after more than one adenine is inserted between ^{CP}G and ^{CP}C. When ^{CP}G is next to ^{CP}C in **AQC0**, there is more decomposition of ^{CP}G than ^{CP}C. In **AQC1**, decomposition profiles of ^{CP}C and ^{CP}G overlap. Decomposition of ^{CP}C becomes more pronounced than on ^{CP}G in **AQC2~AQC5**, in which ^{CP}G is two or more adenines away from ^{CP}C.

3.3.6. Decomposition of ^{CP}C and ^{CP}G in DNA assemblies by non-covalently bound oxidants. In order to vary the energy of the photooxidant relative to that of the isolated bases, a ground state ruthenium photooxidant with known potential was used to probe the DNA duplex ring opening reaction. Both the rhodium and anthraquinone photooxidants have excited state potentials higher than that of the individual bases,[31,32] whereas the ruthenium(III) has a potential sufficient to oxidize only guanine.[33] As shown in Table 3.4, sequences containing either ^{CP}C (**C-1**) or ^{CP}G (**G-2**) in roughly the same position within the oligonucleotide were irradiated at 442 nm in the presence of the $[Ru(phen)(dppz)(bpy')]^{2+}$ complex and $[Ru(NH_3)_6]^{3+}$ quencher in order to initiate oxidation via the flash-quench technique.[34]

First we consider oxidative decomposition by $[Ru(phen)(dppz)(bpy')]^{3+}$. Since singlet oxygen is generated upon photolysis of the ruthenium complex in the absence of

Table 3.4. % of ^{CP}C and ^{CP}G decomposition with non-covalently bound $[Ru(phen)(dppz)(bpy')]^{2+}$ and $[Rh(phi)_2(bpy)]^{3+}$

DNA #	Sequence[a]	Photooxidant		% Decomposition of ^{CP}C or ^{CP}G[b]
C-1	3′-TGCTCGGCATCAGT^{CP}CGGCATA-5′ 5′-ACGAGCCGTAGTCA GCCGTAT-3′	$[Rh(phi)_2(bpy)]^{3+}$		57.6[c]
		$[Ru(phen)(dppz)(bpy')]^{2+}$ [d]	-Q[e]	2.5[f]
			+Q	4.8
G-2	3′-TGCTCGGCATCAGTCG^{CP}GCATA-5′ 5′-ACGAGCCGTAGTCAGC CGTAT-3′	$[Rh(phi)_2(bpy)]^{3+}$		100
		$[Ru(phen)(dppz)(bpy')]^{2+}$ [d]	-Q	9.1
			+Q	87.5

a. DNA strands were synthesized as described in materials and methods.
b. Ru photooxidations are averaged over at least 3 data sets. Deviations are less than 10%.
c. Amount of cyclopropylamine-modified nucleoside remaining after 10 minutes of irradiation. Duplexes (5μM) were irradiated with 5μM $[Rh(phi)_2(bpy)]^{3+}$ in 50mM NaCl and 20mM sodium phosphate buffer. Details are in materials and methods.
d. All ruthenium experiments were carried out anaerobically under Ar. See experimental for details.
e. Q refers to quencher, $Ru(NH_3)_6^{3+}$. Details are in materials and methods.
f. Amount of cyclopropylamine-modified nucleoside remaining after 30 minutes of irradiation. Duplexes (5μM) were irradiated in 50mM NaCl and 20mM sodium phosphate buffer. Concentration of $[Ru(phen)(dppz)(bpy')]^{2+}$ is 5μM and that of $Ru(NH_3)_6^{3+}$ is 50μM if added. Details are in materials and methods.

quencher,[35,36] and singlet oxygen can potentially contribute to ring opening, all ruthenium samples were irradiated under anaerobic conditions. When oxygen is eliminated from the system, damage patterns solely resulting from hole transfer events are revealed.[37] Table 3.4 shows that considerable ring opening occurs only with quencher in **G-2**, which contains ^{CP}G, while the ^{CP}C in **C-1** remains essentially intact. When no quencher is added to the irradiated samples, a small amount of ring opening occurs in **G-2** but not **C-1**. ^{CP}C, incorporated in DNA, shows little reaction with $[Ru(phen)(dppz)(bpy')]^{2+}$ in the presence or absence of quencher. In contrast, ^{CP}G decomposes completely within 30 minutes of irradiation in the presence of $[Ru(phen)(dppz)(bpy')]^{2+}$ and quencher and to a small extent if the quencher is excluded.

For comparison, we also examined base decomposition using non-covalent $[Rh(phi)_2(bpy)]^{3+}$ as the photooxidant, since the rhodium complex is a far more potent photooxidant. As shown in Table 3.4, ^{CP}G in **G-2** decomposes completely after 10 minutes of irradiation. Decomposition of ^{CP}C in **C-1** is also significant, 58%, as compared to the case of ruthenium. Although the decomposition of ^{CP}C is less pronounced than that of ^{CP}G, both of the cyclopropylamine bases are oxidized by $[Rh(phi)_2(bpy)]^{3+}$.

3.4. Discussion

3.4.1. Application of fast hole traps as a measure of hole delocalization. The experiments described here provide a sensitive assay for radical occupation in the DNA bridge during the course of hole transport. Most mechanistic studies of long range oxidative DNA damage have utilized guanine damage as a reporter of the efficiency of

hole transport.[1-5] However, these studies actually measure the yield of a mixture of irreversible guanine oxidation products several steps removed from the guanine radical. In fact, the guanine radical lifetime itself is quite long (ms),[34] and on that timescale other reactions, including back electron transfers,[38] may proceed. Here instead we utilize a kinetically fast hole trap, cyclopropylamine-substituted cytosine and guanosine. Although the kinetics of ring-opening upon oxidation within DNA have not yet been measured, model studies suggest the ring-opening time to be on the timescale of 10^{-11} s.[39,40] It is because of this fast timescale for ring-opening that the cycloproplyamine-substituted bases can provide a snapshot of radical occupation during the course of hole transport. Significantly, these measurements can be made in solution under physiological conditions on well characterized DNA duplexes.

Indeed, cyclopropylamine-substituted adenosines in DNA were first used to establish that hole transport through DNA cannot involve hopping only amongst low energy guanine sites.[41] Our own first studies using ^{CP}C showed furthermore that hole occupation is not restricted to purines in DNA.[24] Instead a significant population of radical density on the cytosines must also occur, despite the relatively high oxidation potential of isolated pyrimidine nucleosides. Because of these experiments, we have proposed that radicals must delocalize within transient domains of the DNA duplex, domains that include pyrimidines as well as purines. The relative efficiencies of decomposition of the cyclopropylamine-substituted bases can therefore be used to probe these domains and the relative extent of hole delocalization into domains as a function of sequence.

A consideration in utilizing such trapping chemistry is whether the trapping reaction itself serves as a driver, thus perturbing rather than reporting upon hole occupation. The range of efficiencies reported here as a function of even subtle variations in sequence indicate that the ring-opening reaction cannot be driving hole transport; if that were the case, decomposition efficiencies would all be the same. Instead we can, therefore, utilize the reaction as a reporter of hole occupancy and thus, for ^{CP}C, of hole delocalization.

3.4.2. Energetic considerations. It has been proposed that flanking bases can serve to modulate oxidation potentials.[42] Based upon theoretical calculations by Voityuk et al.,[42] a hole on the middle cytosine in the trinucleotide, 5'-CCC-3', has an energy ~0.5 eV higher than that in 5'-GCG-3'. Here we have compared the decomposition efficiency of ^{CP}C in the 5'-C^{CP}CC-3' and 5'-G^{CP}CG-3' segments and we find that ^{CP}C decomposes slightly more efficiently with flanking guanines. The result is, then, not inconsistent with the calculation. The magnitude of energy lowering of cytosines by flanking bases, nonetheless, is not sufficient to account for the similarity in efficiency of decomposition of ^{CP}C and ^{CP}G within the duplex.

In an effort to obtain some limit on the extent of stabilization of cytosines within DNA, we examined ^{CP}C ring opening by two non-covalently bound oxidants, a ruthenium(III) oxidant, generated *in situ* by flash-quench technique, and our rhodium photooxidant, $[Rh(phi)_2(bpy)]^{3+}$. With a reduction potential of 1.6 eV, the Ru(III) complex is able to promote oxidation of guanine in DNA;[33] with rhodium as a photooxidant (>1.9 eV), all bases can be oxidized.[31]

With the non-covalently bound intercalators, consistent with these potentials, both are able to promote ring opening of ^{CP}G in **G-2**. However only the rhodium complex can promote efficient decomposition of ^{CP}C in **C-1**. These results suggest that, while the energy of ^{CP}C may be lowered significantly owing to delocalization, the energy of ^{CP}C is still higher than that of ^{CP}G.[43]

3.4.3. Domain formation is sensitive to DNA sequence. Although some experimental results showing the sequence and distance dependence in DNA-mediated HT can be rationalized using models based upon energetics alone,[4,15] others do not directly fit these models.[9,45,46,47] Our experiments utilizing ^{CP}C as a probe of hole occupancy demonstrate that the hole occupies both purines and pyrimidines during the course of HT through DNA.[24] All the bases in DNA duplexes are involved in HT, not only guanines and adenines. But what determines the extent of delocalization? Do some sequences promote greater delocalization, and hence greater stabilization of pyrimidine radicals than do others?

Domain formation is sensitive to the sequence of DNA. Our data show, for example, that the arrangement of the A-tract modulates the hole density on ^{CP}C. As evidenced in Tables 3.1 and 3.2, holes delocalize not only over the purine-containing strands, but also over those containing pyrimidines, although the holes are not equally distributed between the strands. ^{CP}C surrounded by two A4 segments decomposes five times faster than that with two flanking T4 segments. In **AQ13**, an alternatively stacked (purine-pyrimidine)$_3$ segment dramatically attenuates the hole density on ^{CP}C. A HT active conformation facilitating HT across a domain is easily accessed in the A-tract of **AQ7**, which contains only purine stacking. In contrast, when purine-purine stacking is

interrupted by pyrimidines, such as in **AQ13**, larger domains facilitating HT are less likely to be reached.

Among the most noteworthy results is that seen in comparing ^{CP}C decomposition between **AQ4** and **AQ6**. These two assemblies have identical sequences intervening between the photooxidant and ^{CP}C; they differ in that **AQ4** contains a T4 tract distal to ^{CP}C whereas **AQ6** contains an A4 tract. Yet ^{CP}C decomposition and therefore hole density on ^{CP}C is markedly attenuated for **AQ4** versus **AQ6**. Thus it must be the larger DNA sequence of the assembly that governs HT, not just the intervening bases. Earlier we had seen that ^{CP}C decomposition is affected also by base substitutions on both strands.[24] These effects can be understood in the context of dynamic delocalized domains in the duplex that form and dissolve over time. The results here underscore the fact that the full sequence of the assembly must govern such dynamical interchanges.

The adenine tract can tolerate small perturbations without disrupting domain formation. As seen in Table 3.2, a one base perturbation of a six-base A-tract slightly attenuates the hole density on the following ^{CP}C. The most pronounced effect we observe here occurs with guanine substitution, which is likely the result of a combination of energetic factors, guanine competing for the hole, and the disruption of adenine stacking.

Domain sizes in adenine tracts have been found to be four to five bases in length based upon the aminopurine fluorescence quenching experiments in DNA.[22] In the **AQCn** assemblies (Table 3.3), ^{CP}C is placed after the second adenine in a seven base adenine tract. Based on ^{CP}G decomposition, it is apparent that ^{CP}C and ^{CP}G affect one another in the same domain when there are fewer than two bridging adenines. However, when more than two adenines separate ^{CP}G from ^{CP}C, the decomposition efficiency of

^{CP}G is attenuated to half of that in **AQC0**. We understand this result in terms of the lack of interchange between cyclopropylamine-nucleosides in these assemblies with longer distances separating cyclopropylamine-substituted bases; the cyclopropylamine-substituted bases must now fall into separate domains. This observation then supports the domain size in the A-tract being at least 3 bases.

3.4.4. The delocalized domain model for HT. Two mechanisms of hole transfer in DNA have been proposed that incorporate dynamic structural distortions. The first one is ion-gated polaron hopping.[26,27] This mechanism describes a structural distortion over several DNA base pairs to self-trap the hole and generate a polaron-like species in response to charge injection.[26] In this model, hole is transported from one polaron to the next by thermal activation. The second mechanism, our model,[22,24] involves HT among sequence-dependent delocalized domains. Domains are transiently formed extended π-orbitals that depend on the dynamics and sequence of DNA. Contrary to the polaron model as first described,[26] here domains are related to the structure and the internal dynamical motion of bases across the DNA duplex. Holes and electrons are transported as delocalized domains form and dissolve depending upon the sequence-dependent stacking within the duplex.

Figure 3.4 shows our model for HT through delocalized domains. In this model a hole is injected into a domain and delocalizes over the transiently extended π-orbitals without distorting the domain structure. The hole can then either be trapped by a cyclo-propylamine base if the domain contains one, or be transported through delocalization into the next domain. The transport is gated by coherent base motion. When two domains come together, forming a well-stacked HT-active conformation, transport can occur. It is

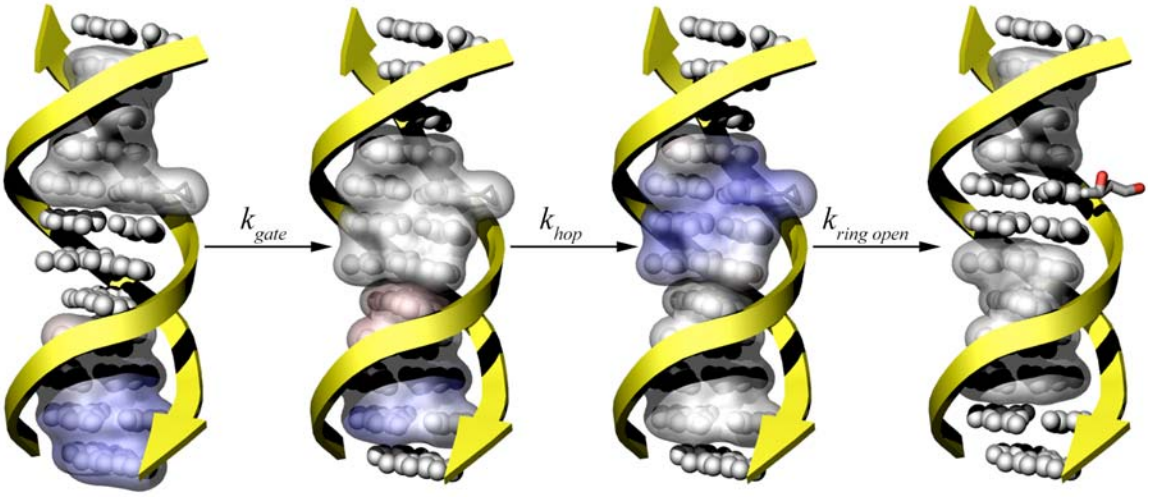

Figure 3.4. Schematized model for conformationally gated DNA HT among delocalized domains. The hole delocalizes over transiently extended π-orbitals within a domain (blue); as the domain enlarges and dissolves, hole is transported, gated by coherent base motions. DNA domains form transiently, governed by DNA sequence and dynamics. When the radical reaches the cyclopropylamine-substituted base, hole density is reported through ring opening.

the sequence-dependent and dynamic structure of DNA that determines the efficiency of HT in this model. The dynamical motion of DNA base pairs helps to achieve the HT active conformations. In this model, then, time-dependent structural distortions in DNA should vary with DNA sequence, irrespective of whether or not hole is being transported. Our time-resolved kinetic studies of base-base HT as a function of temperature have been consistent with this model, where HT is gated by base motions,[21] and our HT studies at 77K have earlier shown the requirement for conformational motion for HT.[23] Here it is apparent that HT is furthermore remarkably sensitive to DNA sequence, and not owing to energetic considerations alone.

Can we distinguish between the polaron and domain model based upon these data? As described above, previous studies[1-5] have used double or triple guanine sites as traps for hole transfer events, but this method has a shortcoming of an extremely slow trapping rate, and thus leads to data representing the average of HT events occurring over many timescales. In the study here we make use of a much faster trap, cyclopropylamine substituted bases, which can be oxidized and ring-opened within ~10^{-11} s;[39] this fast trap allows us to monitor hole delocalization over even transiently formed domains. What we observe with this fast trap is that the entire sequence of the DNA duplex contributes to the formation and disintegration of domains. Furthermore, in the polaron hopping model, hole is transferred by thermal activation among low energy purine sites, and what is usually measured is the result of trapping at these low energy sites. Here we measure instead hole density on the bridge, kinetically trapped by the ring-opening reaction.
It should be noted that recently a solvated polaron model[27] has been distinguished from that described earlier based upon charge-dependent distortions in the DNA.[26] Here, the

solvated polaron state is formed by injection of a charge carrier into an appropriate configuration reached by fluctuation of the DNA bases and solution environment surrounding the DNA. Our results are not sufficient to differentiate between these models.

We can, however, consider some differences expected based upon these various proposals. For example, in considering the series of assemblies **AQ9**, **AQ10**, **AQ8**, and **AQ11** (Table 3.2), while the G inserted in **AQ9** would be expected to stabilize polaron formation, the higher energy C, T, and T2 inserts should interfere with propogation of the polaron. Yet when we measure hole density at the distal site along the bridge through ^{CP}C decomposition, the opposite trend is revealed. An increase in ^{CP}C decomposition is seen along the series **AQ9**, **AQ10**, **AQ8**, **AQ11**. In addition, for the polaron hopping model, polarons in an adenine tract are considered to drift step by step; as one adenine adds to the polaron, another is released. Therefore, as long as the A-tract remains intact, the oxidation yield should be constant. However, here, we clearly see differences of decomposition efficiency in **AQCn** assemblies, even with the fast hole trap. In fact not only does a distal change in sequence affect the hole delocalization of nearby ^{CP}C, but also the distance between ^{CP}C and ^{CP}G along the tract affects the decomposition in a discrete way. We consider that these observations can best be rationalized through a delocalized domain model.

Here we have illustrated the rich and remarkable dependence of DNA HT upon sequence. Importantly, our model of conformationally gated HT among delocalized domains predicts a rich sequence and structure dependence. Certainly, then, we can understand both the data presented here as well as earlier data showing the sensitivity of

DNA HT to stacking in the context of our model; other models based largely upon energetic considerations associated with base oxidation do not provide a similar reconciliation of the data. Clearly, the sequence dependence of DNA HT must be taken into account in any mechanistic descriptions going forward and in viewing the possible applications and biological implications of DNA HT.

3.5. References

1. Hall, D. B., Holmlin, R. E., Barton, J. K. Oxidative DNA damage through long range electron transfer *Nature* **1996**, *382*, 731-735.

2. (a) Delaney, S., Barton, J. K. Long-range DNA charge transport *J. Org. Chem.* **2003**, *68*, 6475-6483; (b) O'Neill, M. A., Barton, J. K. *Charge Transfer in DNA: From Mechanism to Application*, Wagenknecht, H. A., ed.; Wiley, **2005**, 27-75.

3. (a) Schuster, G. B. Long-range charge transfer in DNA: transient structural distortions control the distance dependence *Acc. Chem. Res.* **2000**, *33*, 253-260; (b) Schuster, G. B., Landman, U. The mechanism of long-distance radical cation transport in duplex DNA: ion-gated hopping of polaron-like distortions *Top. Curr. Chem.* **2004**, *236*, 139-162.

4. (a) Giese, B. Long-distance charge transport in DNA: the hopping mechanism *Acc. Chem. Res.* **2000**, *33*, 631-636; (b) Giese, B. Hole injection and hole transfer through DNA: the hopping mechanism *Top. Curr. Chem.* **2004**, *236*, 27-44.

5. Nakatani, K., Saito, I. Charge transport in duplex DNA containing modified nucleotide bases *Top. Curr. Chem.* **2004**, *236*, 163-186.

6. Lewis, F. D., Wasielewski, M. R. Dynamics and equilibrium for single step hole transport processes in duplex DNA *Top. Curr. Chem.* **2004**, *236*, 45-65.

7. Núñez, M. E., Noyes, K. T., Barton, J. K. Oxidative charge transport through DNA in nucleosome particles J. K. *Chem. Biol.* **2002**, *9*, 403-415.

8. Henderson, P. T., Jones, D., Hampikian, G., Kan, Y. Z., Schuster, G. B. Long-distance charge transport in duplex DNA: the phonon-assisted polaron-like hopping mechanism *Proc. Natl. Acad. Sci. USA* **1999**, *96*, 8353-8358.

9. (a) Bhattacharya, P. K., Barton, J. K. The influence of intervening mismatches on long-range guanine oxidation in DNA duplexes *J. Am. Chem. Soc.* **2003**, *123*, 8649-8656; (b) Hall, D. B., Barton, J. K. Sensitivity of DNA-mediated electron transfer to the intervening pi-stack: a probe for integrity of the DNA base stack *J. Am. Chem. Soc.* **1997**, *119*, 5045-5046.

10. (a) Drummond, T. G., Hill, M. G., Barton, J. K. Electrochemical DNA sensors *Nature Biotechnology* **2003**, *21*, 1192-1199; (b) Boon E.M., Ceres D.M., Drummond T.G., Hill M.G., Barton J.K. Mutation detection by electrocatalysis at DNA-modified electrodes *Nat. Biotech.* **2000**, *18*, 1096-1100; (c) Boon E.M., Salas J.E., Barton J.K. An electrical probe of protein-DNA interactions on DNA-modified surfaces *Nat. Biotech.* **2002**, *20*, 282-286.

11. (a) Boon, E. M., Livingston, A. L., Chmiel, N. H., David, S. S., Barton, J. K. DNA-mediated charge transport for DNA repair *Proc. Natl. Acad. Sci. USA.* **2003,** *100*, 12543-12547; **2004,** *101*, 4718; (b) Yavin, E., Boal, A. K., Stemp, E. D. A., Boon, E. M., Livingston, A. L., O'Shea, V. L., David, S. S., Barton, J. K. Protein-DNA charge transport: redox activation of a DNA repair protein by guanine radical *Proc. Natl. Acad. Sci. USA* **2005,** *102*, 3546-3551; (c) Boal, A. K., Yavin, E., Lukianova, O. A., O'Shea, V. L., David, S. S., Barton, J. K. DNA-bound redox activity of DNA repair clycosylases containing [4Fe-4S] clusters *Biochem.* **2005,** *44*, 8397-8407.

12. Fink, H., Schönenberger, C. Electron conduction through DANN molecules *Nature* **1999**, *398*, 407-410.

13. (a) Porath, D., Bezryadin, A., Vires, S., Dekker, C. Direct measurement of electrical transport through DNA molecules *Nature* **2000**, *403*, 635-638; (b) Porath, D., Cuniberti, G., Di Felice, R. Charge transport in DNA-based devices *Top. Curr. Chem.* **2004,** *237*, 183-227.

14. Ceres, D. M., Barton, J. K. *In situ* scanning tunneling microscopy of DNA-mediated gold surfaces: bias and mismatch dependence *J. Am. Chem. Soc.* **2003**, *125*, 14964-14965.

15. (a) Bixon M, Giese B, Wessely S, Langenbacher T, Michel-Beyerle ME, Jortner, J. Long-range charge hopping in DNA *Proc. Natl. Acad. Sci. USA* **1999**, *96* 11713-11716; (b)Bixon, M., Jortner, J. Long-range and very long-range charge transport in DNA *Chem. Phys.* **2002**, *281*, 393-408.

16. Lewis F. D., Liu, J., Weigel, W., Rettig, W., Kurnikov, I. V., Beratan, D. N. Donor-bridge-acceptor energetics determine the distance dependence of electron tunneling in DNA *Proc. Nat. Acad. Sci. USA* **2002**, *99*, 12536-12541.

17. Berlin, Y. A., Burin, A. L., Ratner, M. A. Elementary steps for charge transport in DNA: thermal activation vs. tunneling *Chem. Phys.* **2002**, *275*, 61-74.

18. O'Neill, M. A., Barton, J. K. DNA-mediated charge transport chemistry and biology *Top. Curr. Chem.* **2004**, *236*, 67-115.

19. Oxidation potentials of the four isolated bases are estimated as follows: G: E_{ox} = 1.3 eV; A: E_{ox} = 1.4 eV; C: E_{ox} > 1.6 eV; T: E_{ox} > 1.7 eV. See (a) Steenken, S., Jovanovic, S.V. How easily oxidizable is DNA? One-electron reduction potentials of adenosine and guanosine radicals in aqueous solution *J. Am. Chem. Soc*. **1997**, *119*, 617-618. (b) Johnston, D. H., Cheng, C. -C., Campbell, K. J., Thorp, H. H. Trans-dioxorhenium(V)-mediated electrocatalytic oxidation of DNA at indium Tin-oxide electrodes: voltammetric detection of DNA cleavage in solution *Inorg. Chem*. **1994**, *33*, 6388-6390; (c) Brabec, V., Dryhurst, G. Electrochemical behavior of natural and biosynthetic polynucleotides at the pyrolytic graphite electrode A new probe for studies of polynucleotide structure and reactions *J. Electroanal. Chem*. **1978**, *89*, 161-

173; (d) Brabec, V. Interaction of nucleic acids with electrically charged surfaces: VI. A comparative study on the electrochemical behaviour of native and denatured DNAs at graphite electrodes. *Biophys. Chem*. **1979**, *9*, 289-297; (e) Seidel, C. A. M., Schulz, A., Sauer, M. H. M. Nucleobase-specific quenching of fluorescent dyes. 1. Nucleobase one-electron redox potentials and their correlation with static and dynamic quenching efficiencies *J. Phys. Chem***. 1996**, *100*, 5541-5553.

20. Giese, B., Amaudrut, J., Köhler, A., Spormann, M., Wessely, S. Direct observation of hole transfer through DNA by hopping between adenine bases and by tunnelling *Nature* **2001**, *412*, 318-320.

21. (a) Fiebig, T., Wan, C., Kelley, S. O., Barton, J. K., Zewail, A.H. Femtosecond dynamics of the DNA intercalator, ethidium, and electron transfer with mononucleotides in water *Proc. Natl. Acad. Sci. USA* **1999**, *96*, 1187-1192; (b) O'Neill, M. A., Becker, H., Wan, C., Barton, J. K., Zewail, A. H. Ultrafast dynamics in DNA-mediated electron transfer: base gating and the role of temperature *Angew. Chem. Int. Ed.* **2003**, *42*, 5896-5900.

22. O'Neill, M.A., Barton, J.K. DNA charge transport: conformationally gated hopping through stacked domains *J. Am. Chem. Soc.* **2004**, *126*, 11471-11483.

23. O'Neill, M. A., Barton, J. K. DNA-mediated charge transport requires conformational motion of the DNA bases: elimination of charge transport in rigid glasses at 77K *J. Am. Chem. Soc.* **2004**, *126*, 13234-13235.

24. Shao, F., O'Neill, M. A., Barton, J. K. Long-range oxidative damage to cytosines in duplex DNA *Proc. Natl. Acad. Sci. USA* **2004**, *101*, 17914-17919.

25. Renger, T., Marcus, R. A. Variable-range hopping electron transfer through disordered bridge states: application to DNA *J. Phys. Chem. A* **2003**, *107*, 8404-8419.

26. Henderson, P.T., Jones, D., Hampikian, G., Kan, Y.Z., Schuster, G. Long-distance charge transport in duplex DNA: the phonon-assisted polaron-like hopping mechanism *Proc. Natl. Acad. Sci. USA* **1999**, *96*, 8353-8358.

27. (a) Conwell, E. M., Rakhmanova, S. V. Polarons in DNA *Proc. Natl. Acad. Sci. USA* **2000**, *97*, 4556-4560; (b) Conwell, E. M. Charge transport in DNA in solution: The role of polarons *Proc. Natl. Acad. Sci. USA* **2005**, *102*, 8795-8799.

28. Nakatani, K., Dohno, C., Saito, I. Design of a hole-trapping nucleobase: termination of DNA-mediated hole transport at N^2-cylcopropyldeoxyguanosine *J. Am. Chem. Soc.* **2001**, *123*, 9681-9682.

29. Gasper, S. M., Schuster, G. B. Intramolecular photoinduced electron tranfer to anthrquinones linked to duplex DAN: The effect of gaps and traps on long-range radical cation migration *J. Am. Chem. Soc.* **1997**, *119*, 12762-12771.

30. Pyle, A. M., Chiang, M. Y., Barton, J. K. Synthesis and characterization of physical, electronic, and photochemical aspects of 9,10-phenanthrenequinone diimine complexes of ruthenium(II) and rhodium(III) *Inorg. Chem.* **1990**, *29*, 4487-4495.

31. Turro, C., Hall, D. B., Chen, W., Zullhof, H., Barton, J. K., Turro, N.J. Solution photoreactivity of phenanthrenequinone diimine complexes of rhodium and correlations with DAN photocleavage and photooxidation *J. Phys. Chem. A* **1998**, *102*, 5708-5715.

32. Armitage, B., Yu, C., Devadoss, C., Schuster, G. B. Cationic anthraquinone derivatives as catalytic DNA photonucleases: Mechanisms for DNA damage and quinone recycling *J. Am. Chem. Soc.* **1994**, *116*, 9847-9859.

33. Murphy, C. J., Arkin, M. R., Ghatlia, N. D., Bossman, S., Turro, N. J., Barton, J. K., Fast photoinduced electron transfer through DNA intercalation *Proc. Natl. Acad. Sci. USA* **1994**, *91*, 5315-5319.

34. Stemp, E. D. A., Arkin, M. R., Barton, J. K. Oxidation of guanine in DNA by $Ru(phen)_2dppz^{3+}$ using the flash-quench technique *J. Am. Chem. Soc.* **1997**, *119*, 2921-2925.

35. Mei, H. Y., Barton, J. K., A chiral probe for A-form helices of DANN and RNA: Tris(tetramethylphenanthroline)ruthenium(II) *J. Am. Chem. Soc.* **1986**, *108*, 7414-7416.

36. Mei, H. Y., Barton, J. K., Tris(tetramethylphenanthroline)ruthenium(II): A chiral probe that cleaves A-DNA conformations *Proc. Natl. Acad. Soc. USA* **1988**, *85*, 1339-1343.

37. In the presence of oxygen, ^{CP}C and ^{CP}G ring opening is observed with and without $[Ru(NH_3)_6]^{3+}$ quencher, although the effect is more pronounced in the case of ^{CP}G. As ruthenium is a known sensitizer for singlet oxygen, this effect can be eliminated if the samples are irradiated under argon.

38. Williams, T. T., Dohno, C., Stemp, E.D.A, Barton, J.K. Effects of the photooxidant on DNA-mediated charge transport *J. Am. Chem. Soc.* **2004**, *126*, 8148–8158.

39. Musa, O. M., Horner, J. H., Shahin, H., Newcomb, M. A kinetic scale for dialkylaminyl radical reactions *J. Am. Chem. Soc.*, **1996**, *118*, 3862-3868.

40. Although we have not measured the ring opening time for the cyclopropylamine substituted bases, femtosecond spectroscopy shows cyclopropylamine substitutions in trinucleoside segments do not affect the charge transfer rate and therefore potential. Unpublished results, T. Fiebig (2005).

41. Dohno, C., Ogawa, A., Nakatani, K., Saito, I. Hole trapping at N^6-cyclopropyldeoxyadenosine suggests a direct contribution of adenine bases to hole transport through DNA *J. Am. Chem. Soc.* **2003**, *125*, 10154-10155.

42. Voityuk A. A., Jortner J., Bixon M., Rösch N. Energetics of hole transfer in DNA *Chem. Phys. Lett.*, **2000**, *324*, 430-434.

43. Since we have employed non-covalently bound metal complexes here, the issue of long range charge transport cannot be considered. Since both intercalators show little sequence-selectivity, in fact, intercalator binding may to some extent interrupt domains.

44. Since AQ binds DNA non-covalently only very weakly, photooxidation of DNA with non-covalently bound AQ cannot be examined.

45. Williams, T. T., Odom, D. T., Barton, J. K. Variations in DNA charge transport with nucleotide composition and sequence *J. Am. Chem. Soc.* **2000**, *122*, 9048-9049.

46. Joy, A., Schuster, G. B. Long-range radical cation migration in DNA: Investigation of the mechanism *Chem. Comm.* **2005**, 2778-2784.

47. Liu, C., Schuster, G. B. Base sequence effects in radical cation migration in duplex DNA: Support fort he polaron-like hopping model *J. Am. Chem. Soc.* **2003**, *125*, 6098-6102.

Chapter 4

Periodicities in DNA Hole Transport Probed with N_2-Cyclopropylguanine, a Kinetically Fast Hole Trap

Adapted from: Augustyn, K. E., Shao, F., Genereux, J. C., Barton, J. K. Submitted for publication in 2007.

** Photoirradiation of Rh(III) tethered ^{CP}G-contianing DNA assemblies were performed by Dr. K. Augustyn, and the decomposition data are fit by Jeoy Genereux.

4.1. Introduction.

Hole transport (HT) through the DNA double helix has been extensively studied over a wide range of distances using various pendant photooxidants and hole acceptors.[1-9] HT through the π-stacked array of bases can proceed over distances of 200 Å with a shallow distance dependence.[10,11] This shallow distance dependence coupled with a sensitivity to perturbations in base pair stacking has led to the development of sensitive DNA-based diagnostic sensors.[12] This chemistry has further prompted the consideration of biological roles for HT in the context of how DNA is damaged and repaired in the cell.[13,14]

Despite a wide range of measurements of DNA HT using a variety of techniques, there is still debate over the mechanistic description of this phenomenon.[15-23] Models for HT commonly fall within two extremes, tunneling, where the hole only virtually occupies the DNA bridge, and hopping, where, in an incoherent process, discrete radicals occupy and migrate across the bridge. An interesting proposal was made to account for the varied behavior of DNA HT by including both components of hopping among low energy guanine sites and tunneling through higher energy bases.[24] Many studies showing significant oxidative guanine damage across long tracts of adenines, however, sharply contrasted this model.[4,25,26] More recently we have found that discrete radical density also arises on intervening pyrimidines and with occupancies quite comparable to neighboring guanine sites.[27] We have also seen that DNA HT is conformationally gated by motions of the hole donor and bases within the bridge.[28-30] We have therefore developed a model in which four to five neighboring bases act in concert to form an extended π-orbital that can accept a migrating hole.[27-31] These delocalized domains, forming and dissolving as a

function of sequence-dependent dynamics, facilitate hole transport through the DNA duplex.

The fast cyclopropylamine radical trap has been used effectively in a variety of studies to probe the mechanism of DNA HT.[27,32-36] Model studies suggest that the oxidative ring opening occurs on a timescale of ~10^{-12} s.[37] The ring opening reaction of cyclopropylamine-substituted bases upon oxidation is conveniently monitored by enzymatic DNA digestion followed by HPLC analysis of the resulting deoxynucleosides. Moreover, this hole is trapped much more rapidly than on the guanine radical, which decays in aerated aqueous solution in 10^{-4}–10^{-3} s.[38] While biochemical studies of guanine damage have been fruitful in establishing that the reaction occurs at long range and is sensitive to mismatches and protein binding, studies of mechanism and inferences of relative HT rates cannot be reliably made with such a slow radical trap. Indeed, biochemical measurements actually monitor the formation of irreversible products of guanine oxidation several steps removed from the formation of its radical.[39]

Saito and co-workers first examined long-range DNA HT using N_2-cyclopropylguanine (^{CP}G) to provide a faster hole trap for mechanistic investigations.[32] They went on to show definitively that the hole does not tunnel through adenines in studies using N_6-cyclopropyladenine (^{CP}A) to trap radicals in the bridge.[33] In our laboratory, we first applied ^{CP}G in DNA HT studies to show chemically that the photoinduced quenching of 2-aminopurine (Ap) by guanine in DNA duplexes is the result of DNA HT.[34] We then utilized ^{CP}G to compare DNA HT with different photooxidants.[35] We demonstrated that some potent photooxidants, including thionine and our rhodium intercalator, which give low yields in guanine damage due to competitive back electron

transfer (BET) relative to radical trapping, exhibit higher HT yields with the fast ^{CP}G trap. Most importantly, in the context of mechanism, we recently carried out DNA HT studies using *N*$_4$-cyclopropylcytosine (^{CP}C). In this work, it was evident that in DNA HT, not only does the hole occupy low energy purines, but a comparable amount of hole density is found on pyrimidines.[27,36]

Given the utility of the fast cyclopropylamine-substituted base trap in mechanistic studies, we have now reinvestigated DNA HT as a function of sequence and distance using ^{CP}G. For repetitive adenine tracts, we find a remarkable periodic dependence in the decay with distance, and for most other repetitive sequences, the decay is not monotonic. It is worthwhile noting that a periodic decay with distance has been seen previously in studies of DNA HT using fluorescence quenching of Ap by guanine to determine HT yield which reports on a subnanosecond time scale.[31] Here a period of 4-5 bases was observed. This assay of fluorescence quenching, like ^{CP}G ring opening, provides a measurement of HT on a fast time scale, but unlike ^{CP}G ring opening, Ap quenching measures hole injection into the DNA bridge. When normalized to duplexes with inosine replacing guanine, coherent HT events are revealed. Using ^{CP}G as the hole trap, we find here a periodicity of 4-5 bases, consistent with HT through delocalized domains.

4.2. Materials and methods.

4.2.1.Oligonucleotide synthesis. DNA oligonucleotides were synthesized using standard phosphoramidite chemistry on an ABI DNA synthesizer. Cyclopropyl-amine-substituted sequences were prepared by incorporating the precursor base, 2-fluoroinosine at the desired position for substitution and, during synthesis, leaving the

trityl group intact. The resin was then reacted with 1M diaza(1,3)bicyclo[5.4.0]undecane (DBU) in acetonitrile to effectively remove the oxygen protecting group. The oligonucleotides were subsequently incubated overnight in 6 M aqueous cyclopropylamine at 60 ^{o}C, resulting in substitution and simultaneous cleavage from the resin. The cleaved strands were dried *in vacuo* and purified by reverse-phase HPLC. The trityl group was then removed by treatment in 80% acetic acid for 15 minutes. The detritylated strands were repurified by reverse-phase HPLC. Oligonucleotides were characterized by MALDI-TOF mass spectrometry.

Rhodium-modified oligonucleotides were synthesized as described previously.[40] The detritylated resin-bound oligonucleotides were first modified with a nine carbon amine linker by reaction with carbonyldiimidazole and diaminononane in dioxane. The amine-modified strands were then reacted with $[Rh(phi)_2(bpy')]Cl_3$ (bpy' = 4-(4'-methyl-2,2'-bipyridyl) valerate) in 1:1:1 methanol:acetonitrile:isopropanol using O-(N-succinimidyl)-1,1,3,3-tetramethyl uranium tetrafluoroborate (TSTU) as the coupling reagent. Cleavage from the resin was accomplished by incubation in NH_4OH at 60 ^{o}C for 6 hours. Strands were HPLC-purified using a Varian C_4 reverse-phase column. The two diasteromeric conjugates, differing in configuration at the metal center, have different retention times. However, both isomers were collected together and used for subsequent experiments. MALDI-TOF mass spectrometry was used to characterize the metallated DNA conjugates.

Anthraquinone (AQ)-tethered oligonucleotides were synthesized as described previously by incorporating an anthraquinone phosphoramidite at the 5'-end of the oligonucleotide.[41] The DNA was deprotected in NH_4OH at 60 ^{o}C overnight. The resulting

oligonucleotides were purified once by reverse-phase HPLC and characterized by MALDI-TOF mass spectrometry.

Oligonucleotides containing 2-aminopurine were synthesized on the DNA synthesizer using an aminopurine phosphoramidite (Glen Research). Ap-containing strands were synthesized leaving the trityl group intact, and purified twice by reverse-phase HPLC. The strands were characterized by MALDI-TOF mass spectrometry.

All oligonucleotides were suspended in a buffer containing 50 mM NaCl, 20 mM sodium phosphate, pH 7 and quantified using UV-visible spectroscopy. Duplexes were prepared by heating equal concentrations of complementary strands to 90 ^{o}C for 5 minutes and slow cooling to ambient temperature. Melting temperatures (T_m) were obtained for all duplexes. All duplexes melted between 55 and 60 ^{o}C at a 1.5 μM concentration in 20 mM sodium phosphate, 50 mM NaCl, pH 7.

4.2.2. Photooxidation experiments. Photooxidations of Rh-tethered oligonucleotides were carried out by irradiating 30 μL aliquots of 10 μM duplex in a buffer containing 20 mM sodium phosphate, 50 mM NaCl, pH 7, for 30 seconds at 365 nm on a 1000 W Hg/Xe lamp equipped with a 320 nm long pass filter and monochromator. AQ-containing duplexes in the same buffer (30 μL, 10 μM) were irradiated at 350 nm using the same apparatus for 5 minutes. Irradiation times were varied and the decomposition was linear over the times used. Samples were irradiated at various temperatures ranging from 20 to 80 ^{o}C.

To analyze for ^{CP}G ring opening following irradiation, the samples were digested by phosphodiesterase I (USB) and alkaline phosphatase (Roche) at 37 ^{o}C for 24 hours.

The resulting deoxynucleosides were analyzed by reverse-phase HPLC using a Chemcobond 5-ODS-H, 4.6 mm × 100 mm column. The amount of ^{CP}G decomposition (Y) was determined by subtracting the ratio of the area under the ^{CP}G peak in an irradiated sample over that in a non-irradiated sample from one using thymidine as an internal standard for all HPLC traces. Irradiations were repeated three times and the results averaged.

To analyze for guanine oxidation, reactions were carried out analogously to those previously described.[1,10,35] DNA strands were first labeled at the 5'-end with [^{32}P] γ-ATP using polynucleotide kinase and purified on a 20% denaturing polyacrylamide gel (Sequagel). The desired band was identified by autoradiography, excised from the gel and eluted into 500 mM ammonium acetate. Labeled DNA was isolated using Micro Bio-Spin 6 columns (BioRad) and hybridized to complementary strands in a buffer containing 20 mM sodium phosphate, 50 mM NaCl, pH 7. AQ-containing duplexes (4 μM) were irradiated for 1 hour at 350 nm using a 1000 W Hg/Xe lamp containing a 320 nm long pass filter and monochromator. Following irradiation, samples were treated with 10% piperidine, heated to 90 ^{o}C for 30 minutes, and dried *in vacuo*. Samples were eluted through a 20% denaturing polyacrylimide gel for 1.5 hours at 90 W and imaged on a Storm 820 phosphoimager (Molecular Dynamics/ GE Healthcare). Oxidative damage products were quantified by phosphoimagery using Image Quant 5.2 (Molecular Dynamics).

4.2.3. Fluorescence quenching experiments. Steady-state fluorescence measurements of Ap-containing DNA oligonucleotides were conducted using an ISS K2 spectrofluorimeter (5 mm path length) equipped with a Peltier-controlled thermostated

sample holder (Quantum Northwest). Aliquots (300 μl) were prepared by annealing Ap-containing DNA strands (50 μM) and their complements in 100 mM sodium phosphate buffer (pH 7.0). Emission spectra were obtained by exciting at 325 nm and monitoring the integrated emission between 340 and 500 nm. Temperature fluctuations during spectral acquisition were less than +/- 0.02 ^{o}C. HT yields were obtained from emission spectra by comparing the observed fluorescence intensity of the redox-active duplexes containing guanine to that of the redox-inactive duplexes containing inosine.[31,42] The redox-inactive reference was employed to delineate HT from other modes of quenching. The fraction of fluorescence quenching, F_q, due to HT was quantified as $F_q = 1 - (\Phi_G/\Phi_I)$. Relative quantum yields (Φ_G and Φ_I) at each temperature were determined from the ratio of the integrated emission of the Ap-containing DNA to 50 mM free Ap in 100 mM sodium phosphate, pH 7.0 in at least three trials.

4.3. Results.

4.3.1. Experimental design. These studies utilize a variety of modified oligonucleotides and techniques to probe HT through DNA. Figure 4.1 illustrates some of the assemblies we have synthesized. For the ^{CP}G decomposition studies, six sets of duplexes were prepared. The **Rh-A$_n$** and **AQ-A$_n$** series contain rhodium or anthraquinone separated from ^{CP}G by a bridge containing increasing numbers of adenine base pairs (Table 4.1). For all Rh-modified assemblies there is a four base pair segment surrounding the rhodium binding site to provide optimum intercalation for the photooxidant. In Figure 4.1, the rhodium is shown intercalated two base pairs from the terminus but likely a mixture of binding sites are available to the diastereomers. On the side distal to the hole

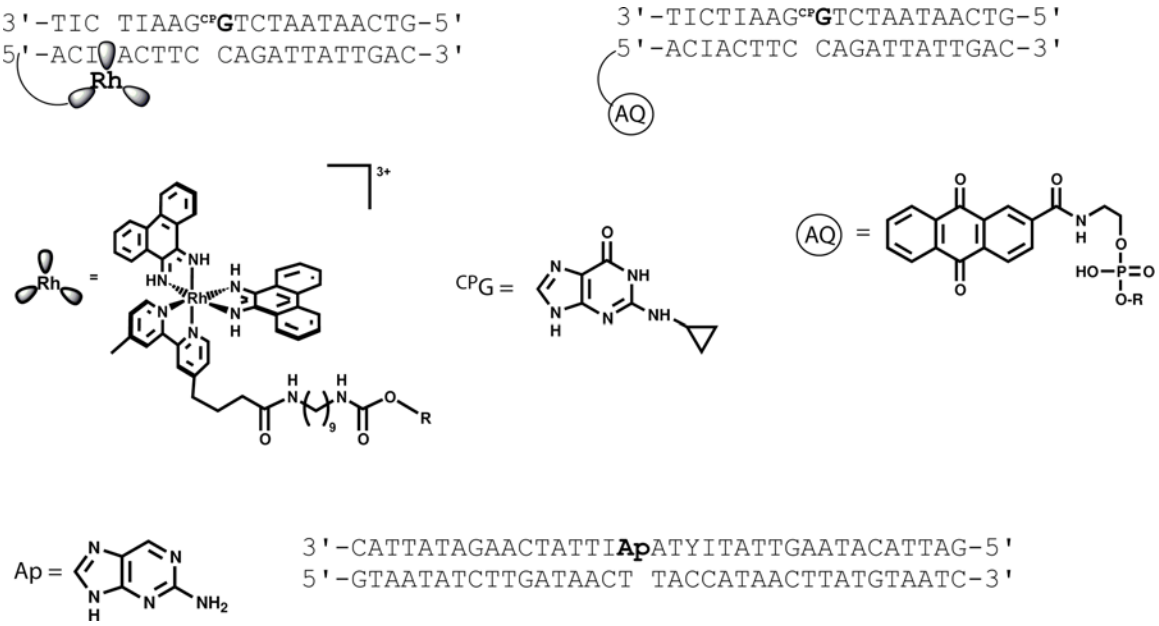

Figure 4.1. Photooxidants, modified bases, and assemblies used to probe HT events in DNA. Shown on the top are representative assemblies containing either rhodium (top left) or anthraquinone (top right) as the photooxidant and ^{CP}G as the trap. The rhodium complex is tethered to the 5'- end of amino modified DNA by a nine carbon linker as represented in the center left and the anthraquinone is capped on the 5' end through the phosphate. A representative aminopurine assembly is shown on the bottom.

Table 4.1. DNA assemblies used for oxidative decomposition studies

DNA #[a]	Sequence[b]
PhO-A_2	3′-TICTI-AA-G**X**TCTAATAACTG-5′ 5′-PhO-ACIAC-TT-CCAGATTATTGAC-3′
PhO-A_4	3′-TICTI-AAAA-G**X**TCTAATCTG-5′ 5′-PhO-ACIAC-TTTT-CCAGATTAGAC-3′
PhO-A_6	3′-TICTI-AAAAAA-G**X**TCTTCTG-5′ 5′-PhO-ACIAC-TTTTTT-CCAGAAGAC-3′
PhO-A_8	3′-TICTI-AAAAAAAA-G**X**TCTTG-5′ 5′-PhO-ACIAC-TTTTTTTT-CCAGAAC-3′
PhO-A_8’	3′-TICTI-AAAAAAAA-G**X**TCTCTATCTTG-5′ 5′-PhO-ACIAC-TTTTTTTT-CCAGAGATAGAAC-3′
PhO-A_{10}	3′-TICTI-AAAAAAAAAA-G**X**TCTATCTTG-5′ 5′-PhO-ACIAC-TTTTTTTTTT-CCAGATAGAAC-3′
PhO-A_{12}	3′-TICTI-AAAAAAAAAAAA-G**X**TCTCTTG-5′ 5′-PhO-ACIAC-TTTTTTTTTTTT-CCAGAGAAC-3′
PhO-A_{14}	3′-TICTI-AAAAAAAAAAAAAA-G**X**TCTTG-5′ 5′-PhO-ACIAC-TTTTTTTTTTTTTT-CCAGAAC-3′
Rh-AT_2	3′-TICTI-AT-G**X**TCTAATAACTG-5′ 5′-Rh-ACIAC-TA-CCAGATTATTGAC-3′
Rh-AT_4	3′-TICTI-ATAT-G**X**TCTAATCTG-5′ 5′-Rh-ACIAC-TATA-CCAGATTAGAC-3′
Rh-AT_6	3′-TICTI-ATATAT-G**X**TCTTCTG-5′ 5′-Rh-ACIAC-TATATA-CCAGAAGAC-3′
Rh-AT_8	3′-TICTI-ATATATAT-G**X**TCTTG-5′ 5′-Rh-ACIAC-TATATATA-CCAGAAC-3′
Rh-$ATIC_2$	3′-TICTI-AT-G**X**TCTAATAATCTATCTTG-5′ 5′-Rh-ACIAC-TA-CCAGATTATTAGATAGAAC-3′
Rh-$ATIC_4$	3′-TICTI-ATIC-G**X**TAATAATCTATCTTG-5′ 5′-Rh-ACIAC-TACG-CCATTATTAGATAGAAC-3′
Rh-$ATIC_6$	3′-TICTI-ATICAT-G**X**ATAATCTATCTTG-5′ 5′-Rh-ACIAC-TACGTA-CCTATTAGATAGAAC-3′

Rh-ATIC$_8$	3′-TICTI-ATICATIC-G**X**AATCTATCTTG-5′ 5′-Rh-ACIAC-TACGTACG-CCTTAGATAGAAC-3′
Rh-ATIC$_{10}$	3′-TICTI-ATICATICAT-G**X**TCTATCTTG-5′ 5′-Rh-ACIAC-TACGTACGTA-CCAGATAGAAC-3′
Rh-ATIC$_{12}$	3′-TICTI-ATICATICATIC-G**X**TATCTTG-3′ 5′-Rh-ACIAC-TACGTACGTACG-CCATAGAAC-5′
Rh-AITC$_2$	3′-TICTI-AI-G**X**TCTAATAATCTATCTTG-5′ 5′-Rh-ACIAC-TC-CCAGATTATTAGATAGAAC-3′
Rh-AITC$_4$	3′-TICTI-AITC-G**X**TAATAATCTATCTTG-5′ 5′-Rh-ACIAC-TCAG-CCATTATTAGATAGAAC-3′
Rh-AITC$_6$	3′-TICTI-AITCAI-G**X**ATAATCTATCTTG-5′ 5′-Rh-ACIAC-TCAGTC-CCTATTAGATAGAAC-3′
Rh-AITC$_8$	3′-TICTI-AITCAITC-G**X**AATCTATCTTG-5′ 5′-Rh-ACIAC-TCAGTCAG-CCTTAGATAGAAC-3′
Rh-AITC$_{10}$	3′-TICTI-AITCAITCAI-G**X**TCTATCTTG-5′ 5′-Rh-ACIAC-TCAGTCAGTC-CCAGATAGAAC-3′
Rh-AITC$_{12}$	3′-TICTI-AITCAITCAITC-G**X**TATCTTG-5′ 5′-Rh-ACIAC-TCAGTCAGTCAG-CCATAGAAC-3′
Rh-AI$_2$	3′-TICTI-AI-G**X**TCTAATAATCTATCTTG-5′ 5′-Rh-ACIAC-TC-CCAGATTATTAGATAGAAC-3′
Rh-AI$_4$	3′-TICTI-AIAI-G**X**TAATAATCTATCTTG-5′ 5′-Rh-ACIAC-TCTC-CCATTATTAGATAGAAC-3′
Rh-AI$_6$	3′-TICTI-AIAIAI-G**X**ATAATCTATCTTG-5′ 5′-Rh-ACIAC-TCTCTC-CCTATTAGATAGAAC-3′
Rh-AI$_8$	3′-TICTI-AIAIAIAI-G**X**AATCTATCTTG-5′ 5′-Rh-ACIAC-TCTCTCTC-CCTTAGATAGAAC-3′
Rh-AI$_{10}$	3′-TICTI-AIAIAIAIAI-G**X**TCTATCTTG-5′ 5′-Rh-ACIAC-TCTCTCTCTC-CCAGATAGAAC-3′
Rh-AI$_{12}$	3′-TICTI-AIAIAIAIAIAI-G**X**TATCTTG-5′ 5′-Rh-ACIAC-TCTCTCTCTCTC-CCATAGAAC-3′

a. PhO= Anthraquinone or $[Rh(phi)_2(bpy')]^{3+}$ tethered as in Figure 4.1.

b. X= ^{CP}G or guanine.

trap, there is a constant three base sequence so that fraying of the ends do not affect results. In addition, guanine can serve as a thermodynamic well if placed near the rhodium intercalation site and although the trapping rate is slow, BET to rhodium is fast. Therefore, inosine was employed as a substitute for guanine to enhance ^{CP}G decomposition.[36] Note that the first four adenine tract sequences, **Rh-A$_2$** through **Rh-A$_8$**, are composed of 20 base pairs, while that of **Rh-A$_8$'** through **Rh-A$_{14}$** are slightly longer, with 26 base pairs. **Rh-A$_8$** and **Rh-A$_8$'**, both containing the 8 base pair long adenine tract but differing in length, yield equivalent decomposition profiles, and in subsequent results and figures, the data from **Rh-A$_8$'** are presented. In the **Rh-(AT)$_n$** and **Rh-(AI)$_n$** series, the repetitive bridge is composed of varying length alternating AT or AI base pairs, respectively. In the **Rh-(ATIC)$_n$** series, the repetitive bridge consists of ATIC repeats, and the **Rh-(AITC)$_n$** series contains duplexes with bridging AITC repeats. Derivatives of the **AQ-A$_n$** series with G replacing ^{CP}G were used for the gel electrophoresis experiments monitoring damage at double guanine sites.

For the fluorescence quenching studies, as shown in Table 4.2, the **Ap(AT)$_n$Y** series was synthesized in which Y is either guanine or inosine, and is separated from the Ap photooxidant by a variable number of ATs. The bases flanking Ap are kept constant throughout the series and, on either side of the repetitive bridge, six bases of random but constant sequence have been employed to ensure stability.

4.3.2. ^{CP}G decomposition as a probe of photooxidation in DNA duplexes with A-tracts. Figure 4.2 shows the variation in the decomposition yield (Y) as a function of bridge length for the **Rh-A$_n$** series. Y is determined by calculating the fraction of ^{CP}G-containing duplexes undergoing ring opening. The data were fit to an equation combining

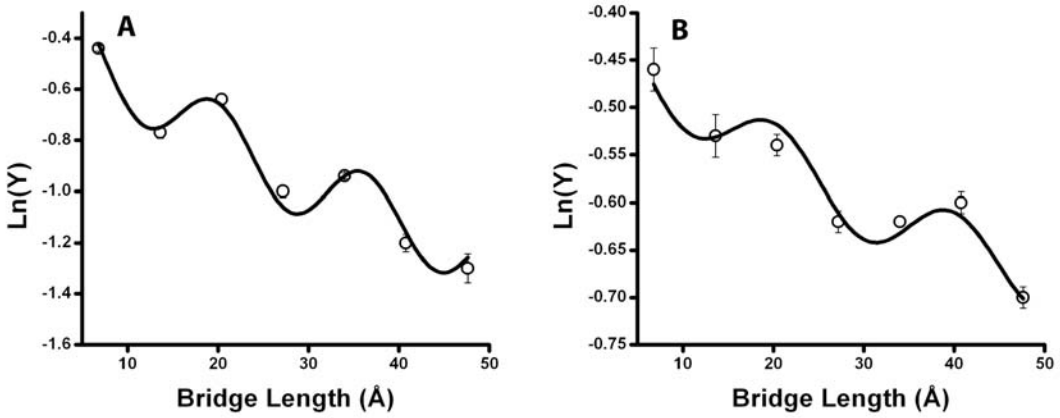

Figure 4.2. HT decays in yield as a function of bridge length for two photooxidants in the **Rh-A$_n$** series (**A**) and **AQ-A$_n$** series (**B**). Duplexes (10 μM) were irradiated at 365 nm in 20 mM sodium phosphate, 50 mM NaCl, pH 7.0 at 25 ^{o}C as described in the text. The bridge length is defined as the length of the repeating bases between the photooxidant and the trap. The experiments were repeated three times and the results averaged. The curves shown here and for all figures represent the best fit to the exponential decay with a sinusoidal term (equation 4.1), with correlation coefficients $\geq$ 0.99. The error bars are a result of three trials and represent 2 standard deviations from the mean for a 95% confidence level.

Table 4.2. DNA assemblies used for fluorescence quenching studies[a]

DNA #	Sequence
$Ap(AT)_1Y3$	5′-GTAATATCTTGATAAC T-TA-CCATAACTTATGTAATC-3′ 3′-CATTATAGAACTATTIAp-AT-YITATTGAATACATTAG-5′
$Ap(AT)_2Y3$	5′-GAATATCATGATAAC T-TATA-CCATAACAATGTAATC-3′ 3′-CTTATAGTACTATTIAp-ATAT-YITATTGTTACATTAG-5′
$Ap(AT)_3Y3$	5′-GAATATCTGATAAC T-TATATA-CCATAACAAGTAATC-3′ 3′-CTTATAGACTATTIAp-ATATAT-YITATTGTTCATTAG-5′
$Ap(AT)_4Y3$	5′-GAATCTGATAAC T-TATATATA-CCATAACATGTAATC-3′ 3′-CTTAGACTATTIAp-ATATATAT-YITATTGTACATTAG-5′
$Ap(AT)_5Y3$	5′-GAATCTGATAAC T-TATATATATA-CCATAACTGAATC-3′ 3′-CTTAGACTATTIAp-ATATATATAT-YITATTGACTTAG-5′
$Ap(AT)_1Y5$	3′-GTAATATCTTGATAAC T-TA-CCATAACTTATGTAATC-5′ 5′-CATTATAGAACTATTIAp-AT-YITATTGAATACATTAG-3′
$Ap(AT)_2Y5$	3′-GAATATCATGATAAC T-TATA-CCATAACAATGTAATC-5′ 5′-CTTATAGTACTATTIAp-ATAT-YITATTGTTRCATTAG-3′
$Ap(AT)_3Y5$	3′-GAATATCTGATAAC T-TATATA-CCATAACAAGTAATC-5′ 5′-CTTATAGACTATTIAp-ATATAT-YITATTGTTCATTAG-3′
$Ap(AT)_4Y5$	3′-GAATCTGATAAC T-TATATATA-CCATAACATGTAATC-5′ 5′-CTTAGACTATTIAp-ATATATAT-YITATTGTACATTAG-3′
$Ap(AT)_5Y5$	3′-GAATCTGATAAC T-TATATATATA-CCATAACTGAATC-5′ 5′-CTTAGACTATTIAp-ATATATATAT-YITATTGACTTAG-3′

a. Duplexes contain an aminopurine (Ap) base and either an inosine or guanine (Y) on one strand, separated by a bridge of increasing length AT base pairs. Fluorescence experiments were carried out using 50 μM duplex in 100 mM sodium phosphate pH 7.0.

geometric and periodic terms as shown:

$$\ln Y = A - \gamma * \ln(d) + B * \sin(2\pi/p * d), \quad (4.1)$$

where d is the distance between the photooxidant and the trap, γ is a monotonic fall-off parameter, and B and p are the amplitude and period respectively. The first term describes the logarithmic distance dependence that is expected for any incoherent process, with γ analogous to η, the hopping parameter.[16,24] The sinusoidal term is included to describe the observed periodicities.

The **Rh-A_n** series were also fit to a series of equations including an exponential decay, an exponential decay with a sinusoidal term, a geometric decay, a geometric decay with a sinusoidal term, a fourth order polynomial spline, and a four parameter step function as shown in Figure 4.3. None of the four fits that do not include a sinusoidal term have R values above 0.99. To account for the degrees of freedom, the R values are adjusted by

$$R_{adj} = \sqrt{1 - (1 - R^2)\left(\frac{n-1}{n-k-1}\right)}, \quad (4.2)$$

where n is the number of data points (7) and *k* is the number of parameters of a given fit. For a superexchange mechanism, one expects an exponential decay with a slope = β. For a hopping mechanism, the distance dependence is expected to decay geometrically, be more shallow, but certainly monotonic.[24] As is evident in Figure 4.2A, measurements of decomposition with distance of ^{CP}G in Rh-tethered assemblies exhibit non-monotonic periodic decays. The amplitude of the periodicities exceeds significantly that of the uncertainty in the measurement. When the data are fit to equation 4.1, a period of 4.8 bases, γ value of 0.72 (0.02), and a β = 0.0191 (0.0006) Å^{-1} results from the exponential

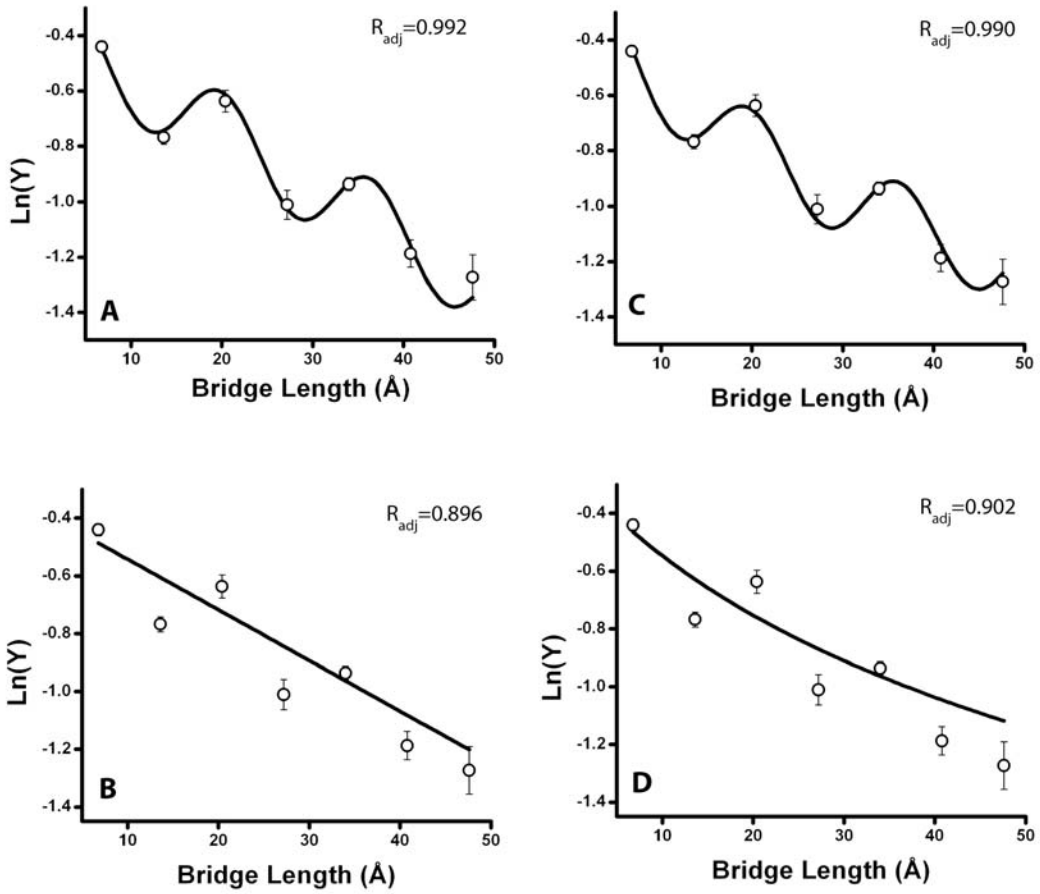

Figure 4.3. Selected fits of data from Figure 4.2A and corresponding R values, adjusted for the number of parameters. Fits include exponential decay with a sinusoidal term (**A**), exponential decay (**B**), geometric decay with a sinusoidal term (**C**), and geometric decay (**D**). Data were also fit to a four parameter step function and a fourth order polynomial spline with R values less than 0.99. See table 4.3. for the equations.

Table 4.3. Equations used in Figure 4.3

Model	Equation
Exponential decay	$\ln Y=m_1-m_2[(x/3.4)+5]$
Exponential decay with a sinusoidal term	$\ln Y=m_1-m_2[(x/3.4)+5]-m_3\sin[2\pi((x/3.4)+5)/m_4]$
Geometric decay	$\ln Y=m_1-m_2\ln[(x/3.4)+5]$
Geometric decay with a sinusoidal term	$\ln Y=m_1-m_2\ln[(x/3.4)+5]-m_3\sin[2\pi((x/3.4)+5)/m_4]$

fit.

It is noteworthy that this periodic decay with distance resembles that seen earlier in fluorescence quenching studies using Ap as the photooxidant and guanine as the trap separated by a bridge of increasing adenine base pairs.[31] In those measurements, we found a period of 4-5 bases and $\gamma = 2$ when the data were fit to equation 4.1.

In order to investigate whether this periodic distance dependence is specific to rhodium, we also synthesized the **AQ-A_n** series, which is identical to the **Rh-A_n** series but uses anthraquinone instead as the pendant photooxidant. Irradiations for the **AQ-A_n** series were carried out at ambient temperature. Semilog plots showing ^{CP}G decomposition as a function of the length of the adenine bridge can be seen in Figure 4.2B**.** As with the **Rh-A_n** series, photooxidation of the **AQ-A_n** assemblies show a shallow, non-monotonic periodic distance dependence in yield. Decay parameters are comparable. In the case of **AQ-A_n**, the β value is 0.005 (0.003) $Å^{-1}$, $\gamma = 0.25$ (0.02) and the period is 5 bases. The periodic behavior we observe is therefore independent of the photooxidant.

4.3.3. Variations in photooxidation with temperature. In the **Rh-A_n** duplexes, we also examined how the decomposition varies with temperature. As can be seen in Figure 4.4**,** increasing the temperature below the T_m of the duplex leads to increased ^{CP}G decomposition. Once the duplexes begin to melt, thus unstacking the base pairs, the decomposition efficiencies sharply drop to zero. This decrease in decomposition occurs between 50-60 ^{o}C, consistent with the T_m found for the duplexes at the equivalent concentration. These data may also be examined by plotting the decay in efficiency as a function of distance at several temperatures (Figure 4.4B). Again periodicities are

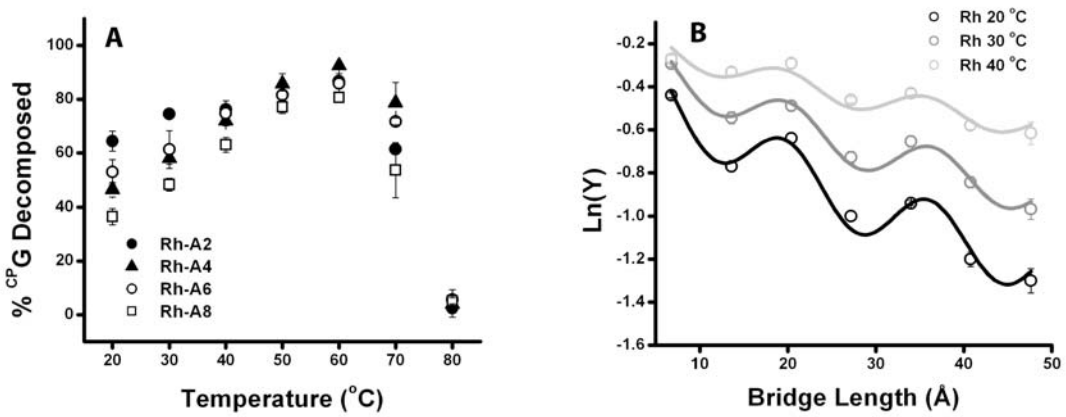

Figure 4.4. ^{CP}G decomposition as a function of temperature. For the Rh-A_n series, shown in (**A**) is the % ^{CP}G decomposition as a function of temperature and in (**B**) is the semilog plot of decomposition yield (Y) as a function of the length of the bridging adenine tract separating the photooxidant from the ^{CP}G trap. Conditions for these experiments are as in Figure 4.2. Note for these duplexes the melting temperatures determined by UV-visible spectroscopy are 55 – 60 ^{o}C.

consistently apparent with amplitudes exceeding the uncertainty in the measurement. It is furthermore evident that below the melting temperature, the periods remain essentially constant over the temperature range. These results also compare closely to those examined earlier by fluorescence quenching of Ap in A-tracts.[31]

4.3.4. Photooxidation of the $(AT)_n$, $(ATIC)_n$, $(AITC)_n$ and $(AI)_n$ sequences. We were interested in determining whether the periodic decay with distance was a phenomenon unique to A-tracts. Therefore, the **Rh-$(ATIC)_n$**, **Rh-$(AITC)_n$**, **Rh-$(AT)_n$**, and **Rh-$(AI)_n$** duplex series containing mixed or alternating base sequences were investigated. The **Rh-$(ATIC)_n$** series contains a bridge comprised of four different bases alternating evenly between purines and pyrimidines. The **Rh-$(AITC)_n$** series contains a bridge comprised of the same four bases as in the **Rh-$(ATIC)_n$** series, but with alternating purine-purine pyrimidine-pyrimidine repeats. The **Rh-$(AT)_n$** series and **Rh-$(AI)_n$** series contain bridges composed of alternating adenines and thymines or alternating adenines and inosines respectively. Distance dependent HT reactions for these duplexes were carried out at ambient temperature.

Inspection of the data in Figure 4.5 shows that for the **Rh-$(AT)_n$** series, periodicities are not apparent. Also, for the **Rh-$(AI)_n$** series, non-monotonic behavior is very slight, at most. However, the **Rh-$(ATIC)_n$** and **Rh-$(AITC)_n$** assemblies do show non-monotonic variations, although with periodicities less obvious than for the **Rh-A_n** series. In particular, in the **Rh-$(AITC)_n$** series there is an initial increase in decomposition followed by a sharp decrease when the bridge is extended from 4–6 bases. This non-monotonic behavior is again greater than the uncertainty in the measurement. If one fits the data for the **Rh-$(AI)_n$**, **Rh-$(ATIC)_n$** and **Rh-$(AITC)_n$** assemblies to equation 4.1,

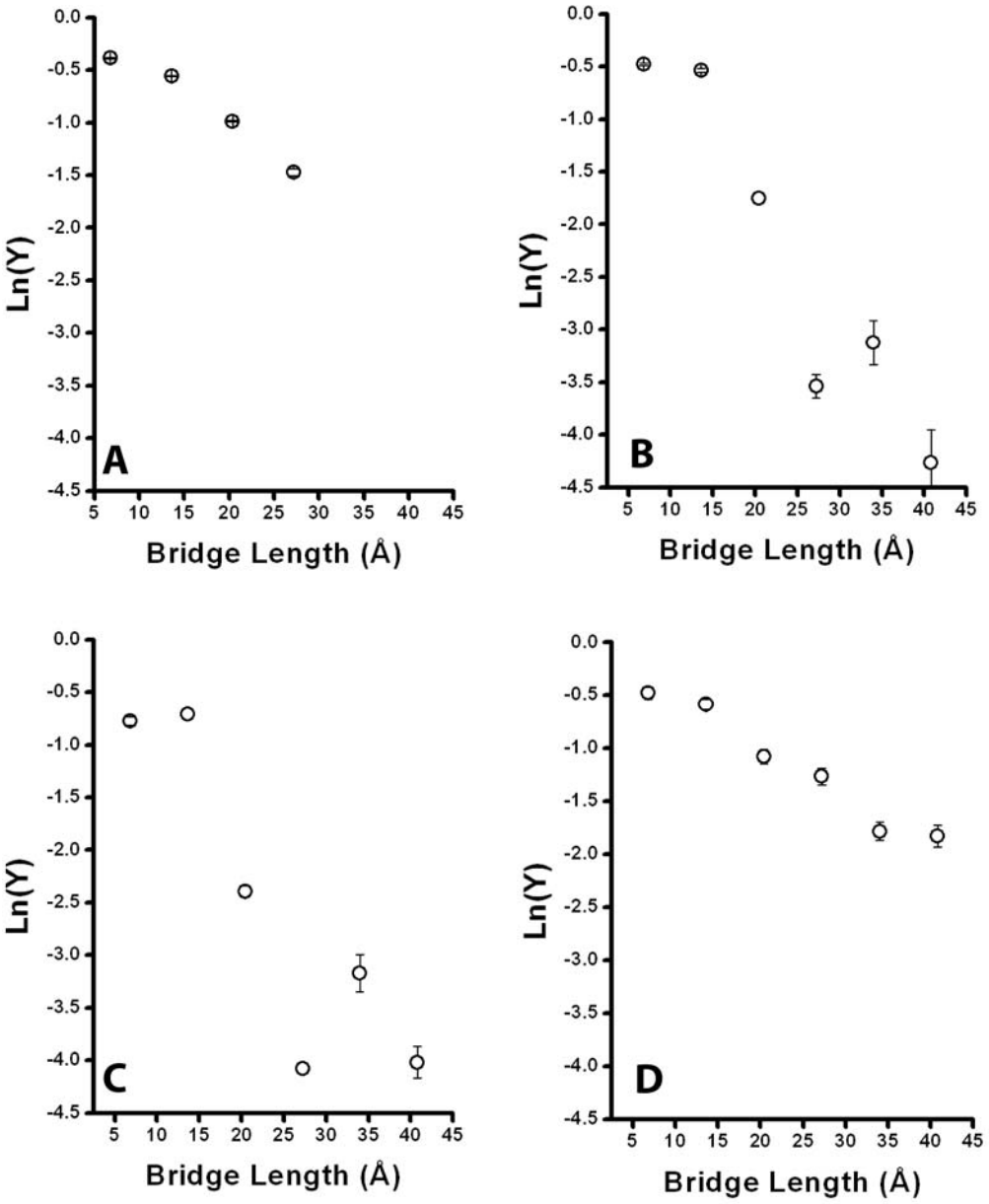

Figure 4.5. Semilog plots showing the distance dependence of HT yield (Y) through sequences containing various bridging bases. Experiments were repeated three times and the results averaged. Shown in (**A)** is the decomposition as a function of repeating bridge length for the $(AT)_n$ series, in (**B**), the $(ATIC)_n$ series, in (**C**), the $(AITC)_n$ series and in (**D**), the $(AI)_n$ series. Conditions are as in Figure 4.2.

periods of 4-7 base pairs are obtained. If the data for all the sequences are plotted on the same graph, simulating a random sequence, the decomposition behavior is very scattered, with an exponential decay fit equal to 0.05 $Å^{-1}$.

4.3.5. Photooxidations with guanine as the hole trap. Earlier systematic studies of long-range oxidative damage to unmodified guanine in our laboratory, as well as by others, had not shown any indication of periodic behavior.[10,11,25,43] To test this specifically using closely analogous sequences, we prepared **AQ-A_n** sequences with G rather than ^{CP}G as the hole trap, introduced a 5'-^{32}P end label, and carried out photooxidations. Following subsequent cleavage with hot piperidine to reveal oxidative base damage, the samples were eluted through a 20% denaturing polyacrylamide gel. Quantitation of the damage yield at the double guanine site is shown in Figure 4.6. Damage yields show a simple decrease in HT efficiency as a function of distance. The periodic behavior in **AQ-A_n** apparent with ^{CP}G is not evident with guanine, a much slower radical trap.

4.3.6. Fluorescence quenching of 2-aminopurine through AT-tracts. Hole injection into a DNA bridge can be studied by comparing the fluorescence quenching of aminopurine by redox-active guanine and redox-inactive inosine.[31,42] A series of 36 base pair duplexes were designed to contain both Ap and either guanine or inosine, separated by a bridge of varying length AT repeats. As shown in Table 4.2, **Ap$(AT)_nY$** (n=1-5) duplexes have either a guanine (Y=G) or inosine (Y=I) positioned n AT base pairs away from Ap. **Ap$(AT)_nY5$** and **Ap$(AT)_nY3$** duplexes contain the same sequence, but the polarity of the strands are reversed so as to note any effects of directionality on HT.

Steady-state fluorescence quenching of the **Ap$(AT)_nY$** series does not show a

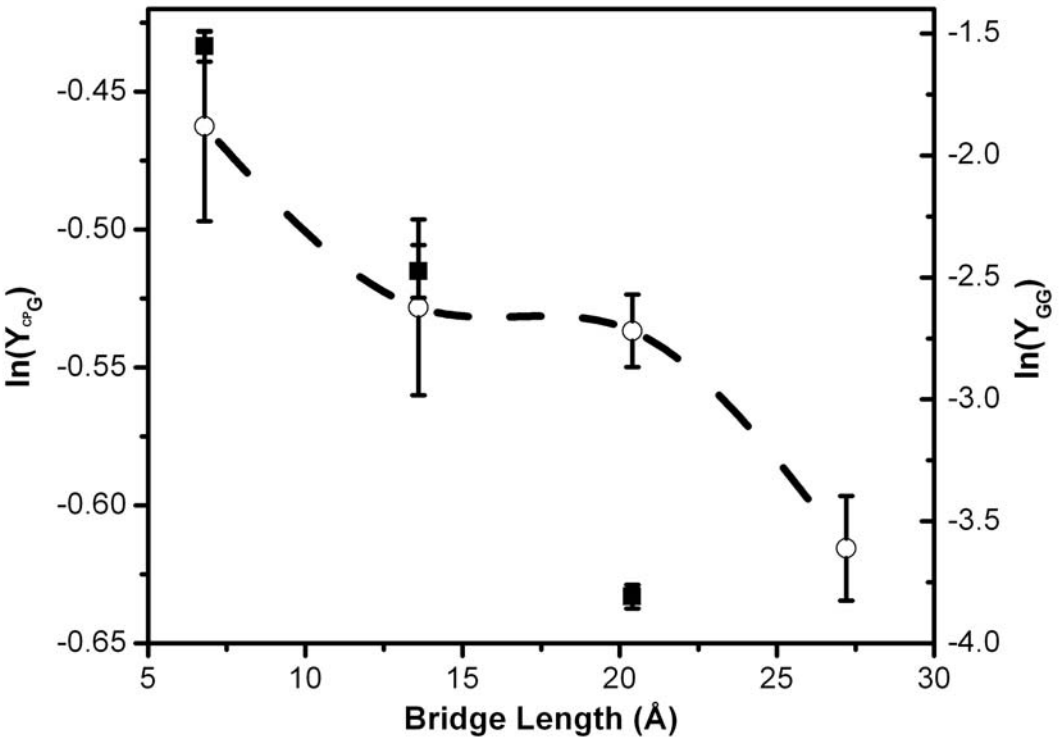

Figure 4.6. Semilog plot of the distance dependence of HT yield in the AQ-A_n series revealed with two oxidative traps, ^{CP}G (open circles) and guanine (closed squares). For the measurements of oxidative guanine damage, duplexes (4 μM) were irradiated at 350 nm in 20 mM sodium phosphate, 50 mM NaCl, pH 7.0 followed by piperidine treatment, gel electrophoresis and quantitation by phosphimagery as detailed in materials and methods.

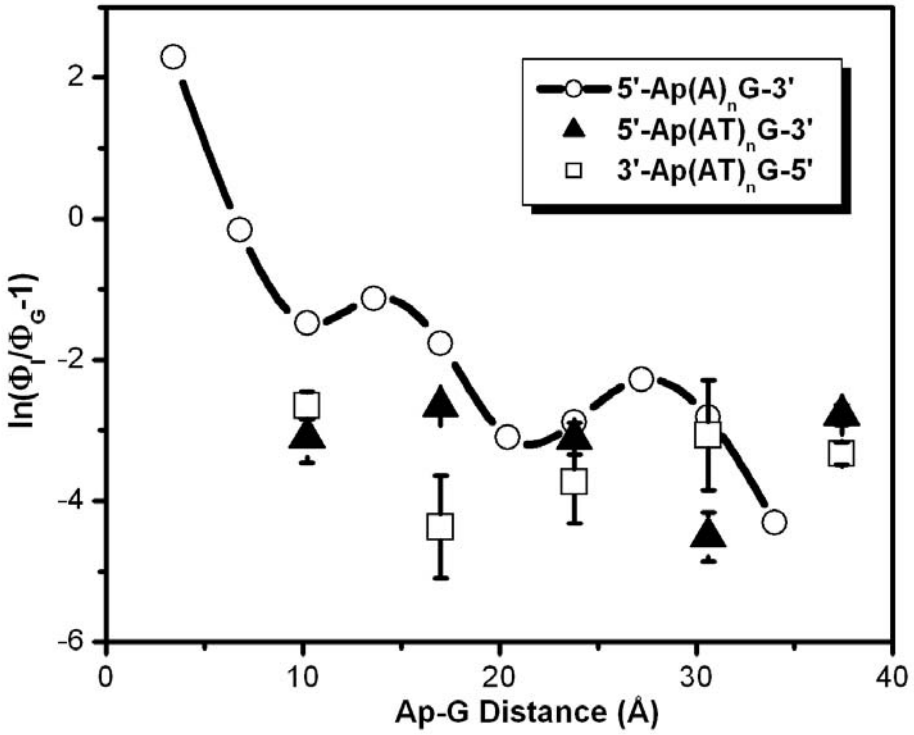

Figure 4.7. Comparison of distance dependence of hole injection into A- and AT-tracts at 25 ^{o}C. Data (open circles) for the **Ap(A)$_n$G** set are adapted.[31] The distance dependence of hole injection into AT-tracts from both directions, 5' to 3' (closed triangles) and 3' to 5' (open squares), are shown with errors determined from at least three experiments with each series.

similar trend in HT yield as a function of distance as compared with the $Ap(A)_nY$ series (Figure 4.7). Here the quenching yield is exceedingly low, although essentially constant with distance. Due to the low yield, periodicities that exceed the certainty in the measurement are difficult to establish. An equivalent low but consistent quenching is seen for duplexes with HT in the 5'- 3' direction and 3'- 5' direction.

4.4. Discussion.

4.4.1. Distance dependence of DNA HT through A-tracts using ^{CP}G. In this study, we examine the distance dependence of HT through increasing length A-tracts using the kinetically fast hole trap, ^{CP}G. Using $[Rh(phi)_2(bpy')]^{3+}$ and AQ as photooxidants, we observe shallow distance dependences over 50 Å. The decays observed with both the well stacked rhodium and the end capped anthraquinone show pronounced periodic variations in ring opening yield as a function of distance, which exceed the associated error in the measurement. The non-monotonic decay is not specific to the photooxidant. With both photooxidants, similar periods and decays with distance are observed. The significant periodic nature of these data is best fit with either an exponential (superexchange) or geometric (hopping) decay containing a sinusoidal component. When these data are fit to an exponential or geometric decay without this component, the R values are considerably lower, even after adjusting for the number of parameters. This strongly implies that superexchange and hopping mechanisms on their own are insufficient to explain the HT yields observed in this system.

4.4.2. Conformational gating by base dynamics. These periodicities are also apparent at higher temperatures, where the overall yield of HT increases and the distance

dependence becomes shallower (Figure 4.4). In a direct HT event, in which the donor and acceptor orbitals are already aligned, higher temperatures are likely to decrease the probability that the orbitals will remain aligned, and decreased HT results.[31] In contrast, when the donor and acceptor are separated by a bridge of dynamic base pairs, increasing the temperature allows a greater fraction of these duplexes to access a HT-active conformation resulting in enhanced HT. Indeed, in our system in which the rhodium photooxidant is intercalated at least 6 bases away from the trap, we observe increased HT for all bridge lengths as a function of temperature. Increased temperature has a more prominent effect on HT through longer adenine bridges because there is a lower initial probability of each base being aligned in a HT-active conformation. We have seen a similar periodic distance dependence of HT through A-tracts using a different system in which HT is monitored by fluorescence quenching of Ap by guanine.[31] The quenching event, which occurs on a subnanosecond time scale, is gated by base dynamics.[29] Here too, a periodic decay is seen as a function of distance but is an order of magnitude steeper than observed using the rhodium photooxidant and ^{CP}G trap. This is not surprising, given that our ^{CP}G trapping system does not monitor solely coherent HT events. As with the present experiment, HT yield is also enhanced at higher temperatures, as monitored by Ap quenching, due to increased base dynamics which facilitate a duplex conformation suitable for undergoing a HT event. This conformational gating, influenced by DNA sequence, controls the HT processes on extremely fast time scales governed by base motions.

4.4.3. Effects of base stacking on distance dependent HT. We have established that base dynamics can dramatically influence the DNA HT process. Hole transport,

which is exquisitely sensitive to the intervening bases, is also significantly influenced by the electronic coupling of the donor and acceptor to the intervening bridge. We have observed that increased stacking between the donor and acceptor enhances HT at longer distances such that shallower distance dependences are observed.[42] Hole injection into a duplex from a photooxidant that is not sufficiently electronically coupled to the orbitals of the DNA bases is strongly hindered and severely influenced by increasing distance. The steep distance dependences observed in systems associated with a superexchange mechanism result from poor coupling between the donor and the bridge. For example, when a distorted sugar radical, not electronically coupled with the DNA bases, is used as a photooxidant, a steep distance dependence is observed through the first three bases, as the injection is rate-limiting when the hole effectively tunnels from the photooxidant to the base orbitals.[43] Conversely, in a system in which the photooxidant is extremely well electronically coupled to the DNA and the trap is isoenergetic to the bridge, distance-independent HT results.[44] The shallow distance dependence we observe through A-tracts is expected, given the efficient coupling of the rhodium complex with the DNA, and the inherent coupling of the ^{CP}G trap to the bridge.

While the coupling between the donor, bridge, and acceptor has a profound influence on the distance dependence of DNA HT, we find that the intervening bridge sequence can significantly alter the decay profile as a result of changes in stacking. We investigated the distance dependence of HT through various bridging bases using the rhodium photooxidant and the ^{CP}G trap. Interrupting the electronic coupling by using non-homogeneous bridging bases decreases HT efficiency as a function of distance.[36] Indeed, when alternating AT sequences are inserted into the bridge, as is the case in the

Rh-(AT)$_n$ series, a steeper distance dependence is observed, and periodicities are not apparent. Additionally, when we observe the distance dependence through AT-tracts using Ap fluorescence quenching, periodicities are not observed. Here, the purine-pyrimidine stacking results in diminished coupling between the orbitals and leads to decreased HT efficiency with distance. Due to the flexible nature associated with AT-tracts,[45] increased base pair motion might lead to dampened periodicities. In contrast, a shallower distance dependence results for a bridge consisting of alternating adenine and inosine base pairs, as seen for the **Rh-(AI)$_n$** series. The purine-purine stacking can lead to more efficient coupling between the bases, yielding shallower HT as a function of distance. When mixed sequence bridges intervene between the rhodium photooxidant and the ^{CP}G trap, steeper, but still non-monotonic distance dependences are apparent. Interestingly, the **Rh-(ATIC)$_n$** and **Rh-(AITC)$_n$** series show similar decay profiles despite the fact that the base stacking between purines and pyrimidines is completely different in these duplexes. These results are consistent with studies in which A-tracts are interrupted by guanines and significant attenuation of HT yields are observed; homogeneous coupling and stacking of the intervening bridging bases are required for efficient HT over longer distances.[25,36,46]

4.4.4. The importance of time scale in monitoring HT processes through DNA. It is interesting to compare the results for the A-tracts monitored with the slow guanine trap to our fast ^{CP}G trap and fluorescent Ap probe. Distance dependences obtained from biochemical studies monitoring the guanine radical trapping here and in previous experiments show shallow decay profiles but lack the periodicities we find using our fast reporters.[25,43] Owing to its millisecond lifetime, the guanine radical can undergo

multiple reactions including BET prior to radical trapping, inevitably convoluting the HT process.[38,39] Indeed, when we compare HT yield for the **AQ-A_n** sequences as monitored by ^{CP}G ring opening to that monitored by guanine radical trapping, significantly different decay profiles are evident. It should be noted in this context that previous studies using rhodium as a photooxidant and guanine as a trap are complicated by fast BET.[35] Just as information as to rapid BET is lost with double guanines, it also appears that the periodicities in long-range DNA HT as a function of distance may also be dampened with the slower guanine radical trap.

In the present study, ring opening, occurring on the picosecond time scale, is competitive with BET and our results are therefore not limited by hole recombination. Our ring opening reaction is also faster than the overall transport process, since we observe differing decomposition yields as a function of sequence. Thus, the yield of ^{CP}G decomposition is an appropriate proxy for the HT rate. We have now seen in several experiments that DNA HT is gated by base pair motions on the picosecond time scale.[28-30] Both the Ap and ^{CP}G systems are sensitive to variations on this time scale and should not be affected by slow oxidative trapping at guanine. This underscores the lack of reliability in utilizing oxidative guanine damage in mechanistic studies of HT. Importantly, these differences highlight the sensitivity of DNA HT chemistry to DNA dynamics on a fast time scale.

4.4.5. Comparison with other DNA HT systems. It is now apparent that (i) coupling between the photooxidant, acceptor, and bridge, (ii) bridge homogeneity, and (iii) time scale are all critical in studying mechanistic DNA HT. Our current system utilizing a fast reporter which is well coupled to the bridge, a well intercalated

photooxidant, and a structurally homogeneous A-tract bridge results in efficient HT with a prominent periodic decay. There have been many reported studies investigating distance dependences through A-tracts, but with the exception of the Ap quenching experiment, a periodic distance dependence has not been observed. The lack of periodicities seen in these experiments can be reconciled by examining the time scale and stacking associated with the system. Majima and co-workers investigated yields of hole separation and rates of recombination as a function of bridge length using transient absorption spectroscopy with NDI as a hole donor and PTZ or 8-oxoguanine as the acceptor.[46] Here, no apparent periodicities are observed in transport yields, and the distance dependences are steeper than what we find using the ^{CP}G trap. However, the lack of error bars associated with these data make them difficult to interpret. Moreover, the hole separation yields as measured by formation of the NDI radical are inevitably convoluted by BET processes which will dampen any periodic behavior. Indeed, NDI radical formation was not observable in the absence of PTZ, indicating that BET dominates hole migration along the bridge. Our Ap quenching experiment is similar but because BET events cannot contribute to the quenching measurement, a prominent periodic distance dependence is evident.[31] Similarly, the slower rate of BET to rhodium and AQ obviates this process as the dominant contributor to our measured yields in the present work, such that periodicity is not dampened. Interestingly, a picosecond transient absorption study using stilbene-capped hairpins also found a shallow dependence over longer distances, but steeper variations were observed for shorter distances.[47] The data were interpreted as supporting three regimes of HT, such that the mechanism changes from superexchange to localized hopping to delocalized hopping with increasing

distance. Given the distortions in these doubly capped hairpins, it is likely that hole injection is rate-limiting near the stilbene. Further from the photooxidant, the DNA is less distorted, yielding the smooth transition to a weaker distance dependence. This process should obscure any periodicity from well coupled HT. Significantly, the profile with the stilbene hairpins is similar to that found using a modified sugar radical as the photooxidant and a double guanine site as the hole acceptor.[43] In this study, the radical must migrate from the sugar backbone to the π-stack, a slow process that leads to the initial superexchange regime. The subsequent shallow distance dependence is characteristic of faster transport once the hole occupies the bridge.

4.4.6. Conformational gating through delocalized domains. Previously, we have suggested that conformational gating by delocalized base pair domains naturally induces a periodic distance dependence.[31] The motions of neighboring bases depend upon the sequence-dependent dynamics of DNA, and for some sequences, these motions can become correlated, or coherent. This coherent collection of bases, existing on the time scale of HT, represents a domain, the size of which is limited by the persistence length of the coherent motion. When the base motions are coherent, the probability of consecutive groups of bases being in HT-active conformations also become correlated; the hole is delocalized over the domain. Note that electronically coherent HT beyond the length of a single domain requires that a second domain be present, and in a conformation that is HT-active with respect to the first domain.[48]

Ap quenching experiments, in which we first observed a periodic distance dependence, assay the coherent injection and transport processes in the DNA duplex but not the trapping event. In those experiments, the periodicities reflect the varying

probabilities of coherent HT with distance, which we ascribed to the varying probabilities of finding a coherent domain on the time scale of HT. It is interesting that delocalized exciton domains that depend upon coherent base motions have also been described for DNA A-tracts with a domain size of 3-4 bases.[49]

Coherent motions of the bases may also generate periodic behavior with incoherent HT, as we measure here through the yield of acceptor ring opening. In this case, each HT event depends upon the probability of bases aligning in a coherent domain. Transport occurs between two domains that acquire a mutually HT-active conformation, forming a larger domain, but only on the time scale of HT. Thus the two domains need *not* be in mutually HT-active conformations *at the same time*. Hence a similar periodic distance dependence should follow as with coherent HT but be shallower and dampened by incoherent steps. Note that base pair motions have also been considered in the context of HT through polarons.[11,18,19]

Base motions furthermore may be coherent on the time scale of HT but incoherent on the time scale of trapping. On this longer time scale, one or more bases in the domain may move out of the HT-active conformation, while other bases move in. The net result of such a process is a translation of the delocalized domain along the duplex. Such translations should also have a tendency to dephase the periodicities in the acceptor decomposition yield, lowering the amplitude of periodicities.

It is interesting to compare the distance dependence here to a system in which the A-tract length is fixed. This was accomplished by monitoring decomposition of cyclopropyladenine (^{CP}A) serially substituted at each position within a 14 base pair adenine tract.[44] In contrast to the guanine trapping situation, there is no periodic variation

of the yield with ^{CP}A position for a given A-tract length. This finding is consistent with our domain model, as a set length A-tract will accommodate a similar domain structure regardless of the placement of the trap.

4.4.7. Other theoretical predictions of periodic distance dependences. Periodic distance dependences have been predicted theoretically but not examined experimentally. In particular, when the energies of the donor, bridge, and acceptor are similar, on-resonant HT has been described in the context of a periodic distance dependence.[50-52] In theoretical studies of molecular wires, while an exponential distance dependence for off-resonance HT was described, for on-resonance coupling, smooth, bounded periodicities were predicted; energetic inhomogeneities along the bridge could attenuate the periodicities.[51] Although these studies modeled the wire between metals, it was theorized that the same analyses could apply to a sufficiently gated hole transfer system. It is possible that DNA fulfills that requirement based on the apparent conformational gating from temperature studies. Periodicities in on-resonant transfer have also been explored in a novel approach to determine the coupling across a molecular bridge by means of formulating the lengthening of the bridge as iterative perturbations.[52] Here, too, periodicities were predicted for on-resonant transfer, but the periods were unstable with respect to the coupling parameters.

Interestingly, Renger and Marcus have calculated a periodic distance dependence for HT across an A-tract DNA bridge when using a model that allowed delocalization of the electron hole over several bases.[53] These periodicities were eliminated by incorporation of a static disorder term. Though the result is intriguing, the physical basis for the periodicities was not clear.

4.4.8. Implications of the periodic distance dependence to mechanisms for DNA-mediated HT. The periodic distance dependence we observe using probes for HT on a fast time scale but not with slow guanine trapping is fully consistent with DNA HT being governed by coherent base motions. The periods are ~4-5 base pairs for A-tracts measured both by Ap quenching and ^{CP}G decomposition. The decay parameters are smaller for ^{CP}G decomposition, since multiple HT events should make the distance dependence more shallow. Long-range DNA-mediated HT measured by ^{CP}G decomposition appears to be at least partially an incoherent process. The decrease in amplitude at longer distances is furthermore indicative of dephasing by base motions.

We cannot establish whether the periodicities depend solely upon coherent base motion or also reflect underlying quantum periodicities due to on-resonance transfer within a domain. The periodicities are essentially constant with respect to their periods for different photooxidants, Ap, Rh, AQ, and with different measurements; this similarity would argue that correlated base motions are most important. Some variations are also apparent with sequence, notably in the absence of periodicities for Rh-$(AT)_n$. For quantum periodicities, changing the sequence should generate different bridge energies and different couplings, which should in turn affect the period. In the coherent motion model, however, the periodicities directly reveal the size of the domains over which base motion is correlated, and over which HT-active conformations are more readily achieved. Here we expect domain size to be roughly dictated by the local sequence-dependent DNA structure. Thus with both models, sequence variations are expected. Only the coherent motion model, however, predicts that serially inserting a ^{CP}A trap along an A-tract will

eliminate the periodicity;[44] a quantum or symmetry effect would be, if anything, more pronounced in such a system.

It is remarkable that we are able to observe these periodicities in DNA HT using disparate assays so long as the experiments assay events on a fast time scale. The observations here underscore the utility of applying cyclopropylamine-modified bases as fast traps for HT. Perhaps more importantly these results highlight the criticality of sequence-dependent motions of the DNA bases in defining HT.

4.5. References.

1. Hall, D. B., Holmlin, R. E., Barton, J. K. Oxidative DNA damage through long-range electron transfer *Nature* **1996**, *382*, 731-735.

2. Delaney, S., Barton, J. K. Long-range DNA charge transport *J. Org. Chem*. **2003**, *68*, 6475-6483.

3. O'Neill, M. A., Barton, J. K. Sequence-dependent DNA Dynamics: The regulator of DNA-mediated charge transport *Charge Transfer in DNA: From Mechanism to Application*, Wagenknecht, H.A., ed.; Wiley: New York, **2005**, 27-75.

4. Schuster, G. B. Long-range charge transfer in DNA: transient structural distortions control the distance dependence *Acc. Chem. Res.* **2000**, *33*, 253-260.

5. Schuster, G. B., Landman, U. The mechanism of long-distance radical cation transport in duplex DNA: ion-gated hopping of polaron-like distortions *Top. Curr. Chem.* **2004**, *236*, 139-162.

6. Giese, B. Long-distance charge transport in DNA: the hopping mechanism *Acc. Chem. Res.* **2000**, *33*, 631-636.

7. Giese, B. Hole injection and hole transfer through DNA: the hopping mechanism *Top. Curr. Chem.* **2004**, *236*, 27-44.

8. Nakatani, K., Saito, I. Charge transport in duplex DNA contaiing modified nucleotide bases *Top. Curr. Chem.* **2004**, *236*, 163-186.

9. Lewis, F. D., Wasielewski, M. R. Dynamics and equilibrium for single step hole transport process in duplex DNA *Top. Curr. Chem.* **2004**, *236*, 45-65.

10. Nuñez, M. E., Hall, D. B., Barton, J. K. Long-range oxidative damage to DNA: effects of distance and sequence *Chem. Biol.* **1999**, *6*, 85-97.

11. Henderson, P. T., Jones, D., Hampikian, G., Kan, Y. Z., Schuster, G. B. Long-distance charge transport in duplex DNA: the phonon-assisted polaron-like hopping mechanism *Proc. Natl. Acad. Sci. USA.* **1999**, *96*, 8353-8358.

12. (a) Drummond, T. G., Hill, M. G., Barton, J. K. Electrochemical DNA sensors *Nat. Biotechnol.* **2003,** *21*, 1192-1199. (b) Boon, E.M., Ceres, D.M., Drummond, T.G., Hill, M.G., Barton, J. K. Mutation detection by electrocatalysis at DNA-modified electrodes *Nat. Biotechnol.* **2000**, *18*, 1096-1100. (c) Boon, E.M., Salas, J.E., Barton, J.K. An electrical probe of protein-DNA interactions on DNA-modified surfaces *Nat. Biotechnol*. **2002**, *20*, 282-286.

13. Nuñez, M. E., Noyes, K. T., Barton, J. K. Oxidative charge transport through DNA in nucleosome core particles *Chem. Biol.* **2002**, *9*, 403-415.

14. (a) Boon, E. M., Livingston, A. L., Chmiel, N. H., David, S. S., Barton, J. K. DNA-mediated charge transport for DNA repair *Proc. Natl. Acad. Sci. USA.* **2003,** *100*, 12543-12547; **2004,** *101*, 4718; (b) Yavin, E., Boal, A. K., Stemp, E. D. A., Boon, E. M., Livingston, A. L., O'Shea, V. L., David, S. S., Barton, J. K. Protein-DNA charge transport: redox activation of a DNA repair protein by guanine radical *Proc. Natl. Acad. Sci. USA.* **2005,** *102*, 3546-3551; (c) Boal, A. K., Yavin, E., Lukianova, O. A., O'Shea, V. L., David, S. S., Barton, J. K. DNA-bound redox activity of DNA repair glycosylases containing [4Fe-4S] clusters *Biochemistry* **2005,** *44*, 8397-8407.

15. Jortner, J., Bixon, M., Voityuk, A. A., Rosch, N. Superechange-mediated charge hopping in DNA *J. Phys. Chem. A* **2002**, *106*, 7599-7606.

16. (a) Bixon, M., Jortner, J. Long-range and very long-range charge transport in DNA *J. Chem Phys.* **2002**, *281*, 393-408. (b) Bixon, M., Jortner, J. Hole trapping, detrapping, and hopping in DNA *J. Phys. Chem. B.* **2001**, *105*, 10322-10328. (c) Bixon, M., Jortner, J. Charge transport in DNA via thermally induced hopping *J. Am. Chem. Soc.* **2001**, *123*, 12556-12567. (d) Bixon, M., Jortner, J. Electronic coupling for charge transfer and transport in DNA *J. Phys. Chem. B* **2000**, *104*, 3906-3913.

17. (a) Berlin, Y. A., Burin, A. L., Ratner, M. A. Elementary steps for charge transport in DNA: thermal activation vs tunneling *Chem. Phys.* **2002**, *275*, 61-74. (b) Berlin, Y. A., Burin, A. L., Ratner, M. A. On the long-range charge transfer in DNA *J. Phys. Chem. A* **2000**, *104*, 443-445.

18. Conwell, E. M., Rakhmanova, S. V. Polarons in DNA *Proc. Natl. Acad. Sci. USA.* **2000**, *97*, 4556-4560.

19. Conwell, E. M. Charge transport in DNA in solution *Proc. Natl. Acad. Sci. USA.* **2005**, *102*, 8795-8799.

20. Grozema, F. C., Berlin, Y. A., Siebbeles, L. D. A. Sequence-dependent charge transfer in donor-DNA-acceptor systems: a theoretical study *Int. J. Quantum Chem.* **1999**, *75*, 1009-1016.

21. Tong, G. S. M., Kurnikov, I. V., Beratan, D. N. Tunneling energy effects on GC oxidation in DNA *J. Phys. Chem. B* **2002**, *106*, 2381-2392.

22. Li, X. Q., Zhang, H. Y., Yan, Y. J. A superexchange-mediated sequential hopping theory for charge transfer in DNA *J. Phys. Chem. A* **2001**, *105*, 9563-9567.

23. Zhang, H.Y., Li, X.Q., Han, P., Yu, X.Y., Yan, Y.J. A partially incoherent rate theory of long-range charge transfer in deoxyribose nucleic acid *J. Chem. Phys.* **2002**, *117*, 4578-4584.

24. (a) Bixon, M., Giese, B., Wessely, S., Langenbacher, T., Michel-Beyerle, M.E., Jortner, J. Long-range charge hopping in DNA *Proc. Natl. Acad. Sci. USA.* **1999**, *96*, 11713-11716. (b) Jortner, J., Bixon, M., Langenbacher, T., Michel-Beyerle, M.E. Charge transfer and transport in DNA *Proc. Natl. Acad. Sci. USA.***1998**, *95*, 12759-12765.

25. Williams, T. T., Odom, D. T., Barton, J. K. Variations in DNA charge transport with nucleotide composition and sequence *J. Am. Chem. Soc.* **2000**, *122*, 9048-9049.

26. Yoo, J., Delaney, S., Stemp, E. D. A., Barton, J. K. Rapid radical formation by DNA charge transport through sequences lacking intervening guanines *J. Am. Chem. Soc.* **2003**, *125*, 6640-6641.

27. Shao, F., O'Neill, M. A., Barton, J. K. Long-range oxidative damage to cytosine in duplex DNA *Proc. Natl. Acad. Sci. USA.* **2004**, *101*, 17914-17919.

28. Wan, C. Z., Fiebig, T., Kelley, S. O., Treadway, C. R., Barton, J. K., Zewail, A. H. Femtosecond dynamics of DNA-mediated electron transfer *Proc. Natl. Acad. Sci. USA.* **1999**, *96*, 6014-6019.

29. O'Neill, M. A., Becker, H. C., Wan, C., Barton, J. K., Zewail, A. H. Ultrafast dynamics in DNA-mediated electron transfer: base gating and the role of temperature *Angew. Chem. Int. Ed.* **2003**, *42*, 5896-5900.

30. O'Neill, M. A., Barton, J. K. DNA-mediated charge transport requires conformational motion of the DNA bases: elimination of charge transport in rigid glasses at 77K *J. Am. Chem. Soc.* **2004**, *126*, 13234-13235.

31. O'Neill, M. A., Barton, J. K. DNA charge transport: conformationally gated hopping through stacked domains *J. Am. Chem. Soc.* **2004**, *126*, 11471-11483.

32. Nakatani, K., Dohno, C., Saito, I. Design of a hole-trapping nucleobase: termination of DNA-mediated hole transport at N^2-cylcopropyldeoxyguanosine *J. Am. Chem. Soc.* **2001**, *123*, 9681-9682.

33. Dohno, C., Ogawa, A., Nakatani, K., Saito, I. Hole trapping at N_6-cyclopropyldeoxy-adenosine suggests a direct contribution of adnine bases to hole transport through DNA *J. Am. Chem. Soc.* **2003**, *125*, 10154-10155.

34. O'Neill, M. A., Dohno, C., Barton, J. K. Direct chemical evidence for charge transfer between photoexcited 2-aminopurine and guanine in duplex DNA *J. Am. Chem. Soc.* **2004**, *126*, 1316-1317.

35. Williams, T. T., Dohno, C., Stemp, E. D. A., Barton, J. K. Effects of the photooxidant on DNA-mediated charge transport *J. Am. Chem. Soc.* **2004**, *126*, 8148-8158.

36. Shao, F., Augustyn, K. E., Barton, J. K. Sequence dependence of charge transport through DNA domains *J. Am. Chem. Soc*. **2005**, *127*, 17445-17452.

37. Musa, O.M., Horner, J.H., Shahin, H., Newcomb, M. *J.* A kinetic scale for dialkylaminyl radical reactions *Am. Chem. Soc*. **1996**, *118*, 3862-3868.

38. Stemp, E. D. A., Arkin, M. R., Barton, J. K. Oxidation of guanine in DNA by $Ru(phen)_2(dppz)^{3+}$ using the flash-quench technique *J. Am. Chem. Soc*. **1997**, *119*, 2921-2925.

39. (a) Douki, T., Ravanat, J. L., Angelov, D., Wagner, R., Cadet, J. Effects of duplex stability on charge transfer efficiency within DNA *Top. Curr. Chem*. **2004**, *236*, 1-25. (b) Burrows, C. J., Muller, J. G. Oxidative nucleobase modifications leading to strand scission *Chem. Rev*. **1998**, 98, 1109-1152.

40. Holmlin, R. E., Dandliker, P. J., Barton, J. K. Synthesis of metallointercalator-DNA conjugates on solid support *Bioconjug. Chem*. **1999**, *10*, 1122-1130.

41. Gasper, S. M., Schuster, G. B. Intramolecular photoinduced electron transfer to anthraquinones linked to duplex DNA: the effect of gaps and traps on long-range radical cation migration *J. Am. Chem. Soc*. **1997**, *119*, 12762-12771.

42. Kelley, S. O., Barton, J. K. Electron transfer between bases in double helical DNA *Science* **1999**, *283*, 375-381.

43. Giese, B., Amaudrut, J., Kohler, A. K., Spormann, M., Wessely, S. Direct observation of hole transfer through DANN by hopping between adenine bases and by tunneling *Nature* **2001**, *412*, 318-320.

44. Augustyn, K. E., Genereux, J. C., Barton, J. K. Distance-independent DNA charge transport across an adenine tract *Angew. Chem. Int. Ed.* **2007**, in press.

45. (a) Dickerson, R. E. Structure, Motion, Interaction, and Expression of Biological Macromolecules **1998**, 17-36. (b) Dickerson, R. E. DANN bending: the prevalence of kinkiness and the virtues of normality *Nucleic Acids Res*. **1998**, *26*, 1906-1926. (c) Kim, J. L., Nikolov, D. B., Burley, S. K. Co-crystal structure of TBP recognizing the minor groove of a TATA element *Nature* **1993**, *365*, 520-527. (d) Kim, Y. C., Geiger, J. H., Hahn, S., Sigler, P. B. Crystal structure of a yeast TBP/TATA-box complex *Nature* **1993**, *365*, 512-520.

46. (a) Takada, T., Kawai, K., Cai, X., Sugimoto, A., Fujitsuka, M., Majima, T. Charge separation in DNA via consecutive adenine hopping *J. Am. Chem. Soc*. **2004**, *126*, 1125-1129. (b) Takada, T., Kawai, K., Fujitsuka, M., Majima, T. Direct observation of hole transfer through double-helical DNA over 100 Å *Proc. Natl. Acad. Sci. USA.* **2004**, *101*, 39,14002-14006. (c) Takada, T., Kawai, K., Fujistuka, M., Majima, T.

Rapid long-distance hole transfer through consecutive adenine sequence *J. Am. Chem. Soc*. **2006**, *128*, 11012-11013.

47. (a) Lewis, F. D., Zhu, H., Daublain, P., Fiebig, T., Raytchev, M., Wang, Q., Shafirovich, V. Croosover from superexchange to hopping as the mechanism for photoinduced charge transfer in DNA hairpin conjugates *J. Am. Chem. Soc.* **2006**, *128*, 791-800. (b) Lewis, F. D., Zhu, H., Daublain, P., Cohen, B., Wasielewski, M. R. Hole mobility in DNA A-tracts *Angew. Chem. Int. Ed.* **2006**, *45*, 7982-7985.

48. Note the distinction between coherent motion, where coherence refers to spatial correlation of consecutive bases, and coherent CT, where coherence refers to CT occurring as a single process.

49. Bucharov, I., Wang, Q., Raytchev, M., Trifonov, A., Fiebig, T. Electronic energy delocalization and dissipation in single and double-stranded DNA *Proc. Natl. Acad. Sci. USA* **2007,** *104*, 4794-4797.

50. Reimers, J. R., Hush, N. S. Electron transfer and energy transfer through bridged systems II. Tight binding linkages with zero asymptotic band gap *Chem. Phys.* **1990**, *146*, 89-103.

51. (a) Mujica, V., Kemp, M., Ratner, M. A. Electron conduction in molecular wires I: a scattering formalism *J. Chem. Phys.* **1994**, *101*, 6856-6864. (b) Kemp, M., Mujica, V., Ratner, M. A. Molecular electronics: disordered molecular wires *J. Chem. Phys.* **1994**, *101*, 5172-5178.

52. Hsu, C. P., Marcus, R. A. A sequential formula for electronic coupling in long range bridge-assisted electron transfer: Formulation of theory and application to alkanethiol monolayers *J. Chem. Phys*. **1997**, *106*, 584-598.

53. Renger, T., Marcus, R. A. Variable-range hopping electron transfer through disordered bridge states: application to DNA *J. Phys. Chem. A* **2003**, *107*, 8404-8419.

CHAPTER 5

Synthesis and Characterization of Iridium(III) Cyclometalated Complexes:

Insights into Redox Reactions with DNA Oligonucleotides

** Synthesis of Ir-1 was performed by Dr. Wei Lu.

5.1. Introduction

Various metallointercalators have been used extensively as pendant photooxidants to probe DNA oxidative chemistry with biochemical and spectroscopic assays.[1-8] In particular, both ruthenium and rhodium polypyridine complexes, such as $[Ru(phen)(bpy')(dppz)]^{2+}$ (dppz = dipyrido[3,2-a:2',3'-c]phenazine) and $[Rh(phi)_2(bpy')]^{3+}$ (phi = 9,10-phenanthrenequinone diimine), are covalently tethered to DNA strands and can initiate DNA-mediated hole transport (HT) upon photoactivation.[9] The distant oxidative damage is characterized by the thermodynamically favored guanine radical, followed by irreversible reactions with oxygen and solvents.[1,5] Guanine doublets and triplets are often adopted as thermal hole traps in response to photooxidation from Ru and Rh complexes.[10,11] However, the true mechanism of HT is often obscured by the slow trapping rate of the guanine radical, since multiple electron pathways, such as fast back electron transfer, occur during that time period.[12] In order to elucidate the mechanism of HT, several fast kinetic hole traps, such as N_2-cyclopropyl-guanine (^{CP}G)[13] and N_4-cyclopropyl-cytosine (^{CP}C)[14] have been developed to probe the transient hole occupancy on bridging bases. Since the cyclopropyl moiety can undergo a ring-opening reaction upon both oxidation and reduction, ^{CP}C is also a potential electron trap.[6] Until now, DNA-mediated HT has been investigated substantially by using transition metal complexes as photooxidants and a variety of bases as hole traps.[15-17]

Like HT, DNA-mediated electron transport (ET) is also an electron migration process except that distant DNA bases are reduced in the case of ET.[18] Unlike HT, ET has not been studied systematically, which is partially due to the lack of proper photoreductants with close interaction with DNA, as well as efficient electron traps.

Long-range reductive chemistry on DNA in solution has been demonstrated but only using organic reductants. [19-21] Flavin and aromatic amines are common electron donors in the study of ET.[22,23] However, organic reductants adopt different interaction modes with DNA than those metal complexes as photooxidants. Additionally, cyclobutane pyrimidine dimers can be repaired by both oxidation and reduction;[23,24] hence the thymine dimer (T^T) is often used as an electron trap to investigate the features of ET.

DNA-mediated ET and HT have always been investigated by using different photoredox probes and traps. Whereas, electron coupling mode of photoredox probe to DNA is very essential to DNA-mediated electron migration process,[25] we have been interested in studying both ET and HT with a uniform photoredox probe, which provides the exact same interaction and electron coupling to DNA when the probe photooxidizes and photoreduces DNA. In order to achieve that goal, a metal complex with a planar polypyridine intercalative ligand could be a good candidate if the complex has the proper redox potential to initiate oxidative and reductive chemistry onto the DNA duplex. The consequent redox reactions of DNA bases can be detected by the fast ring opening reaction of cyclopropylamine-substituted bases. Recently, a series of water soluble platinum complexes with dppz ligand were developed in our group.[6] $[(mes)_2Pt(dppz)]^{2+}$ (mes = N,N,N,3,5-pentamethylaniline) can simultaneously promote oxidatively the ring opening reaction of ^{CP}G and reductively decompose ^{CP}C in DNA. However, these Pt complexes are difficult to functionalize and covalently tether to DNA strands, making the parallel study of DNA-mediated ET and HT untenable.

Cyclometalated Ir(III) complexes are well known to be relatively stable upon irradiation and have been extensively applied in the design and preparation of high-

emiting diodes.[25,26] Recently, Ir(III) diimine complexes have also been developed as luminescent labels for biological applications.[27,28] Redox potentials of excited states in Ir(III) cyclometalated complexes can furthermore be tuned by substitutions of both ancillary and diimine ligands.[29] More specifically, positively charged $[Ir(ppy)_2(dppz)]^+$ (ppy = 2-phenylpyridine) has shown luminescence and avid DNA binding.[30] With the proper design of ancillary and intercalative diimine ligands, Ir(III) cyclometalated complexes would be able to trigger the redox reaction of DNA upon photolysis. Moreover, it is possible to introduce a monofunctional linkage to the Ir complex through modification of the dppz moiety, through which the further conjugation to DNA strands can be conducted.[30] In this chapter, three Ir(III) complexes with functionalized dppz ligands have been developed to initiate both oxidation and reduction of DNA oligonucleotides. Optical and electrochemical properties of Ir(III) complexes are used to determine the redox potentials of their excited states. Photoredox reactions of DNA with the Ir(III) complexes are studied in order to establish a donor-bridge-acceptor system suitable for the investigation of both ET and HT through DNA.

5.2. Experimental.

5.2.1. General materials preparation. All the starting materials were used as received and the reactions were conducted under argon. Compounds 1,10-phenanthroline-5,6-dione,[31] dipyrido[3,2-a:2'3'-c]phenazine[31] and cyclometalated Ir(III) μ-dichloro-bridged dimers ($[Ir(ppy)_2Cl]_2$, ppy: 2-phenylpyridine)[32] were prepared according to literature methods and confirmed by ^1H NMR and MALDI-MS. Unmodified DNA oligonucleotides were synthesized by standard phosphoramidite chemistry on an

ABI 392 DNA/RNA synthesizer. Cyclopropylamine modified DNA assemblies were synthesized as described in previous chapters.[10] DNA strands with a 5'-dimethoxy trityl (DMT) protecting group were purified by using a Hewlet-Packard 1050 reverse-phase (RP) HPLC on a Dynamax 300 Å C18 column (Varian) (95% 50mM NH_4OAc/5% acetonitrile, to 65% 50mM NH_4OAc/35% acetonitrile over 30 min). Afterward, DNA strands were deprotected in 80% acetic acid for 20 min and purified again by RP-HPLC (95% 50mM NH_4OAc/5% acetonitrile, to 80 % 50mM NH_4OAc/20% acetonitrile over 30 min). Aqueous buffer used in both spectroscopy and irradiation experiments was composed of 20 mM sodium phosphate, pH 7.0, 10 mM sodium chloride.

5.2.2. Methyl dipyrido[3,2-a:2',3'-c]phenazine-11-oxy-hex-5-ynoate (dppz1). *Methyl 6-iodohexanoate.* *ε*-caprolactone (2.28 g, 20 mmol) was added dropwise to a mixture of BBr_3 in CH_2Cl_2 (1.0 M, 20 mL), KI (4.98 g, 30 mmol) and *n*-Bu_4NI (40 mg, 0.1 mmol) under argon. The resulted suspension was stirred at room temperature for 16 h and then the reaction was quenched with anhydrous MeOH (5 mL). The solution was diluted with CH_2Cl_2 (50 mL) and washed subsequently with aqueous $NaHCO_3$ (50 mL), $Na_2S_2O_3$ (50 mL), and water (50 mL). The organic phase was dried over anhydrous $MgSO_4$ and evaporated to yield a brownish oil. The pure product can be isolated as a colorless oil after percolation of the brownish oil through a short silica gel column with hexane.

Methyl 6-(3-amino-4-nitrophenoxy)hexanoate (1). A mixture of 4-amino-3-nitrophenol (0.52 g, 3.4 mmol) and NaH (60% in mineral oil) (136 mg, 5.7 mmol) in anhydrous DMF (20 mL) was stirred at room temperature for 15 min under argon. A solution of methyl 6-iodohexanoate (0.87 g, 3.4 mmol) was added to the mixture. The

resulted solution was further stirred for 5 h at room temperature. The solvent was removed under reduced pressure, then the crude product was purified by neutral alumina chromatography with EtOAc/hexane = 1/5 (v/v) as eluant to yield the desired product (bright red solid). Yield: 90%. ^{1}H NMR (300 MHz, $CDCl_3$): δ 7.51 (d, 1H, *J* = 2.7 Hz), 7.03 (dd, 1H, *J* = 2.7 Hz, *J* = 9.3 Hz), 6.75 (d, 1H, *J* = 9.3 Hz), 5.90 (broad s, 2H), 3.91 (t, 2H, *J* = 9.3 Hz), 3.67 (s, 3H), 2.34 (t, 2H, *J* = 7.8 Hz), 1.80~1.72 (m, 2H), 1.70~1.65 (m, 2H), 1.51~1.48 (m, 2H). HRMS (FAB+): calcd. 282.1216 for $C_{13}H_{18}N_2O_5$, found 282.1214 (M^+).

Palladium carbon (10% loaded, 0.26g) was slowly added to a solution of **1** (1.0g, 13mmol) in MeOH (40 ml). The mixture was stirred at room temperature for 3 hours under H_2 atmosphere. During reaction, the orange color of the starting material disappeared and TLC indicated the end of reaction. The resulted suspension was filtered through a short Celite plug into a suspension of 1,10-phenanthroline-5,6-dione (0.75g) in absolute EtOH (40 ml) and the resulted mixture was refluxed for 12 h under argon. The reaction mixture was evaporated to dryness and purified with neutral alumina column (eluant: CH_3CN/CH_2Cl_2/MeOH = 10/10/1, v/v/v). To the resulting deep colored solid was added acetone (2 mL) and the suspension was sonicated for 30 s. The brownish solid was collected by filtration and washed with a little acetone. Yield: 33%. ^{1}H NMR (300 MHz, $CDCl_3$): δ 9.56~9.52 (m, 2H), 9.26~9.21 (m, 2H), 8.16 (d, 1H, J = 9.3 Hz), 7.78~7.73 (m, 2H), 7.55~7.49 (m, 2H), 4.22 (t, 2H, J = 6.3 Hz), 3.69 (s, 3H), 2.43 (t, 2H, J = 7.2 Hz), 1.99~1.94 (m, 2H), 1.81~1.76 (m, 2H), 1.63~1.61 (m). HRMS (FAB^+): calcd. 427.1770 for $C_{25}H_{23}N_4O_3$, found 427.1756 (M_+).

5.2.3. Ethyl dipyrido[3,2-a:2',3'-c]phenazine-11-zoate (dppz2). *Ethyl 3,4-diaminobenzoate (2).* 3,4-diaminobenzoic acid (500 mg, 3.3 mmol) was refluxed in 30ml ethanol. Concentrated sulfuric acid (1 ml) was added dropwise to the suspension. After 4 h, solvent was removed under vacuum. Reaction crude was dissolved in 30ml water and adjusted to pH 10 by 1N NaOH. The product was extracted over $CHCl_3$ (2 ∗ 50ml) and washed with brine and water. A yellow solid was obtained by removing the chloroform under vacuum. The crude was used without purification.

Boiling EtOH solution (10 ml) of **2** (0.11g, 0.6 mmol) was added dropwise to 5ml boiling EtOH of 1,10-phenanthroline-5,6-dione (0.115g, 0.6 mmol). Brownish precipitate came out during mixing process. The mixture was refluxed for 10 mins. The crude product was collected by filtration. The crude product was used without further purification. ^{1}H NMR (300 MHz, $CDCl_3$): δ 9.69 (d, 2H, J = 8.1 Hz), 9.34~9.32 (m, 2H), 9.11 (s, 1H), 8.53 (d, 1H, J = 7.2 Hz), 8.43 (d, 1H, J = 8.1 Hz) 7.86 (m, 2H), 4.55 (q, 2H, J = 7.5 Hz), 1.52 (t, 3H, J = 7.2 Hz). ESI-MS: calcd. 354.1 for $C_{21}H_{14}N_4O_2$, found 355.0 (M^+).

5.2.4. Ethyl (dipyrido[3,2-a:2',3'-c]phenazine-11-yl)-hex-5-ynoate (dppz3). *4-iodobenzene-1,2-diamine (3).* 5-iodo-2-nitroaniline (2.64 g, 10 mmol) and $SnCl_2$ (9.5g, 50 mmol) were dissolved in 70ml absolute ethanol. The reaction mixture was stirred under argon at 70 ^{o}C for 4 h and monitored by TLC (Alumina, 1:1 EtOAc/Hexanes). After the reaction was complete, the solution was neutralized by saturated $NaCO_3$ to pH 7~8. Solution color changed from yellow to brown color and precipitates came out. The crude was extracted over 100ml ethyl acetate and 100ml ethyl ether individually. The organic layer was then washed with 100ml brine twice and dried over anhydrous $MgSO_4$.

After the solvent was removed under vacuum, the crude was immediately used in the next step without further purification.

Tert-butyl 4-iodo-1,2-phenylenedicarbamate (4). **3** (~10mmol) and ditertbutyldicarbonate (6.54g, 30mmol)were dissolved in 50ml THF and stirred under argon at room temperature overnight. Extra sodium bicarbonate was added during the reaction in order to complete the protection of amine group. The crude product was purified by neutral alumina column (eluant: EtOAc/Hexanes = 22:78, v/v). Yield: 70%. ^{1}H NMR (300 Hz, DMSO-d_6): δ 8.59 (s, 2H), 7.85 (s, 1H), 7.37 (d, 1H, J = 10.5 Hz), 7.29 (d, 1H, J = 8.7 Hz) 1,45 (s, 18H). ESI-MS: calcd. 434.1 for $C_{16}H_{23}IN_2O_4$, found 435.0 (M^+).

Ethyl hex-5-ynoate (5). **5** was prepared as described previously with adaptions.[33] 20 drops of concentrated sulfuric acid was added to hex-5-ynoic acid (1.16g, 10 mmol) in 20ml EtOH. Reaction solution was refluxing at 100 ^{o}C for 2 h. Completion of the reaction was determined by TLC (silica 10:1 Hexane/Et_2O). The reaction solution was neutralized by saturated Na_2CO_3 and extracted with 100ml CH_2Cl_2. Organic phase was washed by 2 ∗ 50ml brine and dried over $MgSO_4$. Pure product was a transparent oil obtained by distillation at 65 ^{o}C under vacuum. Yield: 84.1%. ^{1}H NMR (300 Hz, $CDCl_3$): δ 4.08 (q, 2H, J = 7.2 Hz), 2.39 (t, 2H, J = 7.2 Hz), 2.21 (m, 2H), 1.93 (t, 1H, J = 2.7 Hz), 1.84~1.75 (m, 2H), 1.21 (t, 3H, J = 7.2 Hz). ESI-MS: calcd. 140.2 for $C_8H_{12}O_2$, found 140.8.

Ethyl 6-(3,4-bis(tert-butoxycarbonylamino)phenyl)hex-5-ynoate (6). **4 (**260 mg, 0.6 mmol) was mixed with $Pd(pph_3)_4$ (36 mg, 0.04 mmol) and CuI (14 mg, 0.08mmol) in a dry 25ml 2-neck round bottom flask under argon. 7.5 ml anhydrous THF was added to

dissolve the reaction mixture followed by 450 μl anhydrous triethylamine. **5 (**126 mg, 0.9 mmol) was added to the reaction solution dropwise. The solution underwent a color change from yellow to wine red to dark green to red. Finally, when the reaction was completed, the color went back to green again. The reaction was also monitored by TLC (Alumina, 1:4 EtOAc/Hexanes). Product was purified by a silica column (28% EtOAc/Hexanes). Yield: 65%. ^{1}H NMR (300 Hz, CD_2Cl_2): δ 7.50~7.32 (m, 2H), 7.08 (d, 1H, J = 8.6 Hz), 6.71 (broad s, 1H), 6.59 (broad s, 1H), 4.04 (q, 2H, J = 7.2 Hz), 2.48~2.29 (m, 4H), 1.90~1.74 (m, 2H), 1.43 (s, 18H), 1.17 (t, 3H, J = 7.2 Hz). FAB+: calcd. 446.2417 for $C_{24}H_{34}N_2O_6$, found 446.2439.

6 (1 g, 2.2 mmol) was dissolved in 20ml anhydrous dichloromethane under argon. 50 equivalents of anhydrous trifluoroacetic acid was added slowly into the solution. During the addition, the solution color changed from brown to deep red. The reaction was stirred at room temperature for 1.5 h to allow the reaction complete. The solvent was removed under vacuum to yield a deep brown oil. The crude product was neutralized by saturated Na_2CO_3 to pH 8 and extracted over ethyl acetate. The resulting oil was added to 0.8 equivalent of 1,10-phenanthroline-5,6-dione in 7ml boiling EtOH. The reaction mixture was refluxed for about 2 hours. After the solvent was removed under vacuum, the crude was purified by neutral alumina column (2% MeOH/CH_2Cl_2). Yield: 40%. ^{1}H NMR (300 Hz, $CDCl_3$): δ 9.64~9.62 (d, 2H, J = 10.5 Hz), 9.29~9.22 (m, 2H), 8.38~8.24 (m, 2H), 7.89~7.71 (m, 3H), 4.18 (q, 2H, J = 7.2 Hz), 2.66~2.56 (m, 4H), 2.11~1.94 (m, 2H), 1.29 (t, 3H, J = 7.2 Hz). FAB+: calcd. 421.1664 for $C_{26}H_{21}N_4O_2$, found 421.1678.

5.2.5. Synthesis of Ir(III) cyclometalated complexes with functionalized dppz. One equivalent of $[Ir(ppy)_2Cl]_2$ and 2 equivalents of corresponding functionalized dppz

moiety were suspended in 15ml 1:1 MeCN/$CHCl_3$ under argon. The reaction suspension was refluxed at 65^oC overnight. Red solids were yielded after removing the solvent under vacuum. The solids were dissolved in small amount of $CHCl_3$ and was filtered through a short silica column. A redish orange band was eluted by 1:1 MeCN/0.4N KNO_3. After the organic solvent was removed under vacuum, precipitate was collected by filtration and redissolved in $CHCl_3$. The solution was dried over $MgSO_4$ and the solvent was removed under vacuum. Relatively pure product was obtained by precipitating from $CHCl_3$ with copious amount of ether and applied directly to the next step. RP-HPLC (C18 column, 45% MeCN/55% H_2O ~ 80% MeCN/20% H_2O over 30min, both MeCN and H_2O contain 5% TFA) was applied for final purification for spectroscopy. The complexes were changed to chloride salt by eluting from an anion exchange column (Sephadex QAE A-25).

[Ir(ppy)$_2$(dppz1)]Cl (Ir1): ^{1}H NMR (300 MHz, $CDCl_3$): δ 9.82 (d, 1H, J = 8.1 Hz), 9.77 (d, 1H, J = 8.4 Hz), 8.35~8.24 (m, 3H), 7.94~7.10 (m, 4H), 7.72~7.70 (m, 4H), 7.65~7.26 (m, 4H), 7.11~7.06 (m, 2H), 7.00~6.98 (m, 4H), 6.41 (d, 2H, J = 7.5 Hz), 4.26 (t, 2H, J = 6.0 Hz), 3.69 (s, 3H), 2.41 (t, 2H, J = 7.2 Hz), 1.97 (m, 2H), 1.77 (m, 2H), 1.61 (m, 2H). HRMS (FAB+): calcd. 927.2635 for $C_{47}H_{38}IrN_6O_3$, found 927.2607 (M^+).

[Ir(ppy)$_2$(dppz2)]Cl (Ir2). ^{1}H NMR (300 MHz, $CDCl_3$): δ 9.87~9.83 (m, 2H), 9.12 (d, 1H, J = 2.1 Hz), 8.58~8.55 (m, 1H), 8.46 (d, 1H, J = 8.7 Hz), 8.38~8.37 (m, 2H), 8.04~7.99 (m, 2H), 7.93 (d, 2H, J = 7.8 Hz), 7.75~7.65 (m, 6H), 7.09 (t, 2H, 7.2 Hz), 7.03~6.96 (m, 4H), 6.41 (d, 2H, J = 7.2 Hz), 4.54 (q, 2H, J = 7.2 Hz), 1.51 (t, 3H, J = 7.2 Hz). HRMS (FAB+): calcd. 855.2059 for $C_{43}H_{30}IrN_6O_2$, found 855.2090.

[Ir(ppy)$_2$(dppz3)]Cl (Ir3). ^{1}H NMR (300 MHz, CD_2Cl_2): δ 9.83 (d, 2H, J = 8.4 Hz), 8.48~8.37 (m, 4H), 8.04~7.96 (m, 5H), 7.82~7.74 (m, 4H), 7.49 (d, 2H, J = 4.8 Hz), 7.15 (t, 2H, J = 7.5 Hz), 7.05~7.00 (m, 2H), 6.89 (t, 2H, J = 7.5 Hz), 6.43 (d, 2H, J = 7.5 Hz), 4.14 (q, 2H, J = 7.2 Hz), 2.64 (t, 2H, J = 7.2 Hz), 2.55 (t, 2H, J = 7.5 Hz), 2.01 (t, 2H, J = 7.5 Hz), 1.26 (t, 3H, J = 7.2 Hz). HRMS (FAB+): calcd. 921.2529 for $C_{48}H_{36}IrN_6O_2$, found 921.2521.

Deprotection of carboxylic acid on alkyl linker from Ir complexes. The suspension of Ir complexes (0.5 mmol) in aqueous 0.4M LiOH (50 mL) and THF (75 mL) was stirred at room temperature for 3 h. TLC (Alumina 7% methanol/CH_2Cl_2) was applied to monitor the reaction complete. The resulted mixture was adjusted to pH <7 by 1.0 M HCl. The solvent was removed under reduced pressure and the precipitates were collected by filtration and washed with copious water. The resulting solid was dissolved in 9ml 1:1:1 MeOH/CH_2Cl_2/MeCN and precipitated by 100 mL ethyl ether and collected by filtration. Reverse-phase (RP) HPLC was applied to purify the crude product for characterization and spectroscopy. Crude product can be used for DNA coupling without further purification.

[Ir(ppy)$_2$(dppz1-OH)]Cl (IrCOOH1): Yield: 66%. ^{1}H NMR: (300 MHz, dmso-d_6): δ 9.45 (d, 1H, J= 7.5 Hz), 9.35 (d, 1H, J = 7.5 Hz), 8.28~8.22 (m, 3H), 8.13~8.03 (m, 2H), 7.99~7.86 (m, 3H), 7.72 (d, 1H, J = 5.7 Hz), 7.61 (t, 1H, J = 5.4 Hz), 7.31 (s, 1H), 7.09~6.93 (m, 5H), 6.28 (d, 2H, J = 6.6 Hz), 4.03 (broad t, 2H), 1.89 (t, 2H, J = 6.9 Hz), 1.72 (m, 2H), 1.49 (m, 2H), 1.38 (m, 2H). HRMS (FAB+): calcd. 913.2478 for $C_{46}H_{36}IrN_6O_3$, found 913.2484 (M+).

[Ir(ppy)$_2$(dppz3-OH)]Cl (IrCOOH3): Yield: 75%. ^{1}H NMR: (300 MHz, CD_2Cl_2): δ 9.85 (t, 2H, J = 8.4 Hz), 8.50 (s, 1H), 8.42~8.34 (m, 3H), 8.05~7.94 (m, 5H), 7.82~7.41 (m, 4H), 7.48 (d, 2H, J = 4.5 Hz), 7.14 (t, 2H, J = 7.5 Hz), 7.05~7.02 (m, 2H), 6.42 (t, 2H, J = 7.8 Hz), 2.66~2.61 (m, 4H), 2.04~1.97 (m, 2H). ESI-MS: calcd. 893.2216 for $C_{46}H_{32}N_6O_2Ir$, found 893.2198.

5.2.6. Optical spectroscopy. All of the optical spectra were measured at ambient temperature. Absorption spectra of Ir complexes in either acetonitrile or aqueous buffer (10 mM NaCl, 20 mM sodium phosphate, pH 7.0) were obtained on a Beckman DU 7400 spectrophotometer. Steady-state fluorescence measurements of three Ir complexes were conducted using an ISS K2 fluorimeter (5 mm path length) equipped with a Peltier-controlled thermostated sample holder (Quantum Northwest). Emission spectra were obtained in CH_2Cl_2 by exciting at maximum absorption of MLCT band of Ir complexes (Ir-1: 373 nm; Ir-2: 412nm; Ir-3: 410nm). Excitation spectra in CH_2Cl_2 were monitored at the maximum emission wavelength for excitation wavelength from 300 to 550nm. Energies of triplet states of Ir complexes were determined by the overlap of emission and excitation spectra.

DNA titrations were conducted in aqueous buffer with 22 μM **Ir3** in order to achieve measurable absorption intensity at MLCT band. Various amounts of λ DNA/Hind III fragments (Invitrogen, 0.5 μg/μl) were added to **Ir3** solution to achieve desired DNA base pair (bp) concentrations and the absorption spectra of resulting solutions were measured.

5.2.7. Electrochemistry. Ground state oxidation and reduction potentials for the metal complexes were obtained on a Bioanalytical systems (BAS) Model CV-50W

electrochemical analyzer. A glassy carbon working electrode, Ag/AgCl reference electrode and Pt auxiliary electrode were used in a single cell sample apparatus. Solutions of Ir complexes (0.8mM) in dry acetonitrile (Fluka; stored over molecular sieves) containing 0.1M tetrabutylammonium hexafluorophosphate were degassed with argon prior to use and voltammagrams were collected using 100mV/s scan rate. $E_{1/2}$ values were taken as the average of the voltage of maximum current for the forward and reverse electrochemical processes. Potentials are adjusted to versus NHE using oxidation reaction of ferrocene as the standard.

5.2.8. Photoredox reaction of Ir complexes with DNA. Aliquots of ^{CP}C nucleoside or DNA duplexes with non-covalently bound Ir complexes (**Ir1**~**Ir3**) were irradiated at 380nm with a 1000-W Hg Xe lamp equipped with a 320-nm long pass filter and a monochromator. Light controls were conducted by irradiating duplexes in the absence of Ir complexes. Experiments reported here were carried out aerobically unless it is mentioned specifically. Anaerobic samples were prepared by utilizing the freeze-pump-thaw method in airtight cuvettes under argon. After irradiation, DNA duplex aliquots were digested by 37 °C incubation with phosphodiesterase (USB), and alkaline phosphatase (Roche) for 24 h to yield nucleosides. After incubation, RP-HPLC (Chemcobond 5-ODS-H, 4.6 × 100 mm, 2% MeCN/ 98% 50 mM NH_4OAc ~ 12% MeCN/ 88% 50 mM NH_4OAc over 30 min) was applied to analyze the decomposition of cyclopropylamine modified nucleosides.

5.3. Results and discussion.

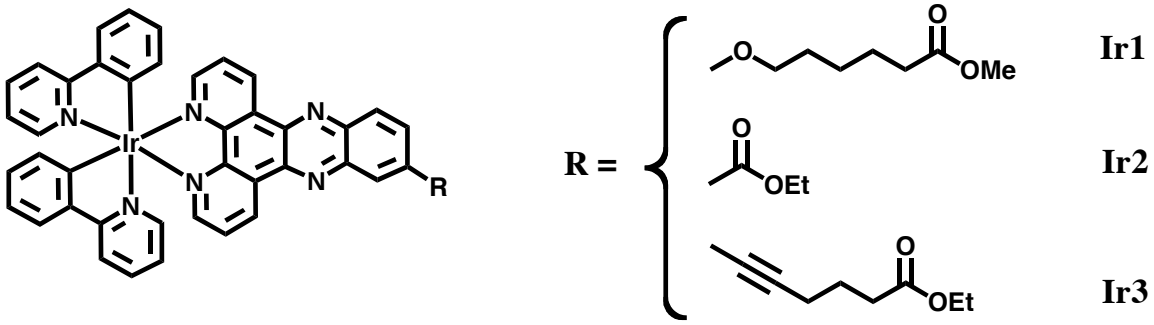

Figure 5.1. Structures of Ir(III) cyclometalated complexes with 2-phenylpyridine as auxiliary ligands and dppz or functionalized dppz as intercalation moiety.

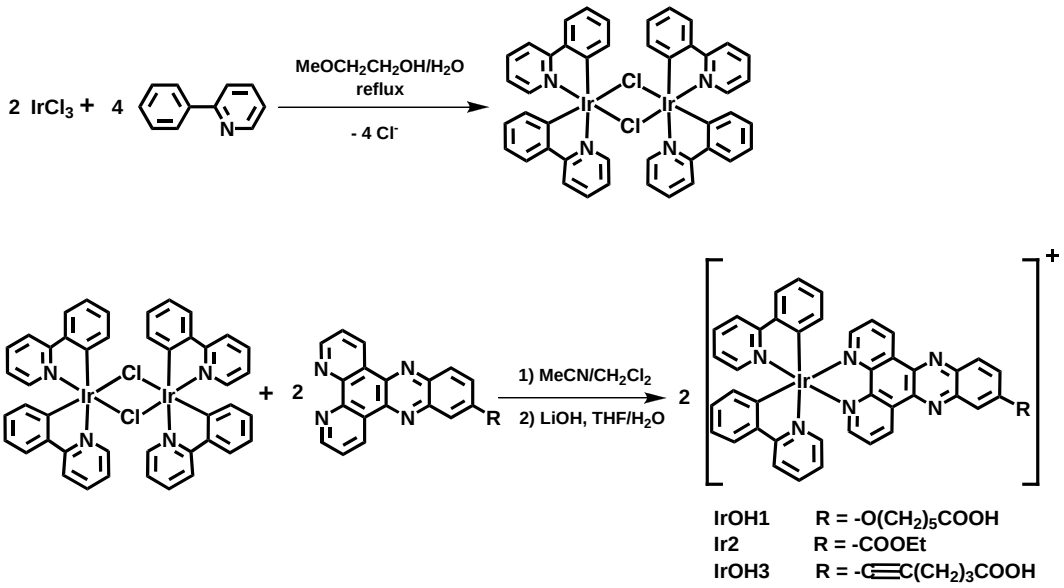

Figure 5.2. Synthetic scheme of Ir(III) cyclometalated complexes.

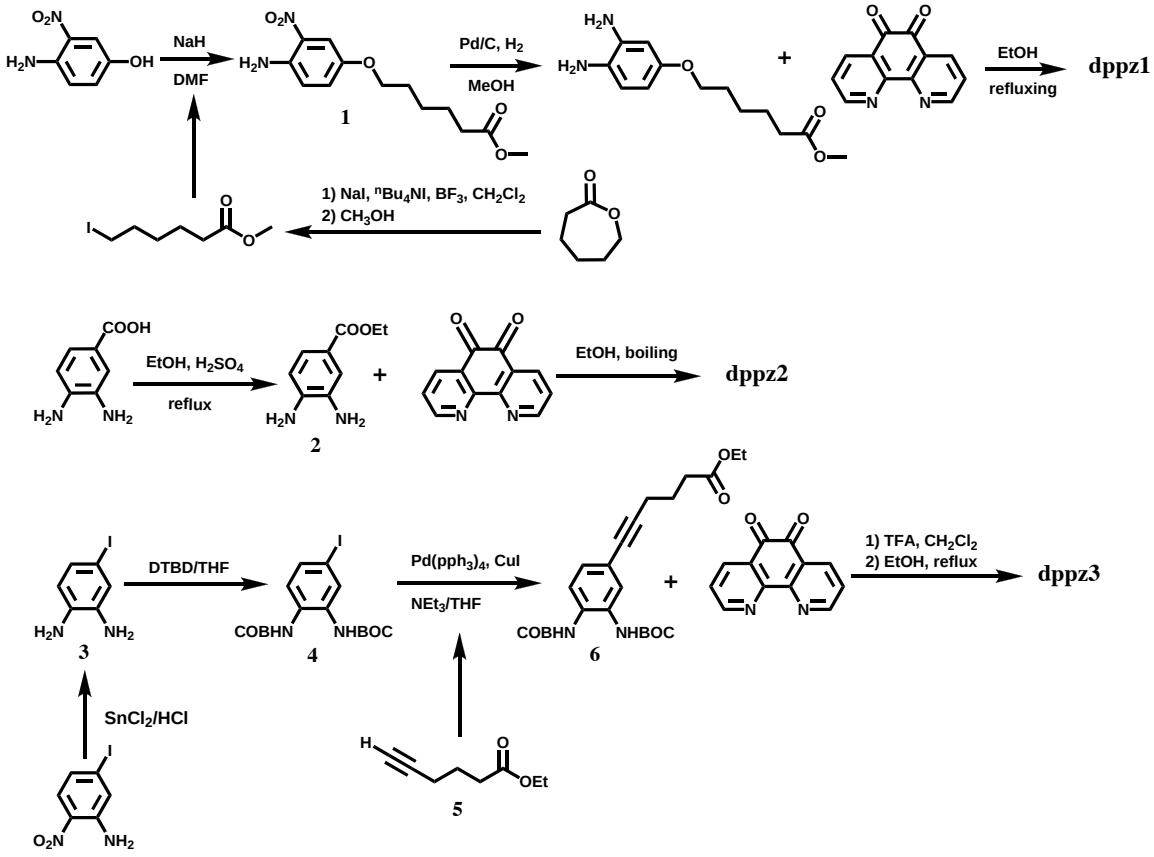

Figure 5.3. Synthetic scheme to functionalize dppz ligands.

Table 5.1. Summary of the optical and redox features of Ir(III) complexes

Feature			Ir1	Ir2	Ir3
Absorption			λ^{nm}, ε $M^{-1}cm^{-1}$	λ^{nm}, ε $M^{-1}cm^{-1}$	λ^{nm}, ε $M^{-1}cm^{-1}$
			290, 125770[a]	278, 104555	292, 94616
			388, 22293	369, 17371	385, 25610
			406, 25300	389, 15702	405, 30605
Emission			λ^{nm}	λ^{nm}	λ^{nm}
	CH_2Cl_2		600	676	634
- DNA[b]	MeCN		620	Q[c]	715
	Buffer[d]		Q	Q	Q
+ DNA	Buffer				Q
Redox reaction[e]					
^{CP}C	+ O_2[f]	Ox[g]	-[h]	+	-
		Red	+	+/-[i]	+
	- O_2	Ox/Red	+	+	+
^{CP}G	+ O_2	Ox	+	+	+
	- O_2	Ox	+	+	+

a. Uncertainty of ε is < 3%.
b. Emission spectra of Ir complexes in the absence (-DNA) and presence (+ DNA) of DNA are measured in the solvents indicated in the right column.
c. Luminescence of Ir complex is quenched under the indicated conditions.
d. Buffer condition: 10 mM NaCl, 20 mM sodium phosphate, pH 7.0.
e. Photolysis of Ir(III) complexes with ^{CP}C- and ^{CP}G-containing duplexes. Details are seen Table 5.2 and experimentals.
f. + O_2 and – O_2 represent that the experiments are conducted aerobically or anaerobically.
g. Ox and Red represent the oxidative and reductive decomposition of ^{CP}C and ^{CP}G induced by photolysis of non-covalently bound Ir(III) complexes. Details are seen in experimentals.
h. - represents no reaction and + represents positive reaction occurring under the indicated working conditions.
i. ^{CP}C decomposition is observed in both DNA assemblies, **I-^{CP}C** and **G-^{CP}C**. However, the origin of the decomposition is not clearly understood by current experiments. Neither reduction nor oxidation of ^{CP}C can be excluded.

Table 5.2. Redox potentials for ground and excited states of Ir complexes

Complex	$\lambda_{0\text{-}0}$(nm/eV)[a]	E_{ox} (V)[b]	E_{red} (V)[b]	E^*_{red}(V)[c]	E^*_{ox} (V)[d]
Ir1	504/2.47	1.48	-0.87	1.60	-0.99
Ir2	522/2.38	1.50	-0.62	1.76	-0.88
Ir3	522/2.38	1.49	-0.70	1.68	-0.89

a. Wavelengths of the 0-0 band ($\lambda_{0\text{-}0}$) are determined by overlap of the emission and excitation spectra in MeCN at room temperature. Energy of the triplet state is calculated from $\lambda_{0\text{-}0}$. Experimental details are given in experimentals. Uncertainty is ± 10 nm.
b. Potentials of Ir(III) complexes are determined by cyclic voltammetry in MeCN and are reported versus NHE ($Cp_2Fe^{+/0}$ = 0.59 V vs. NHE). Uncertainty is < 1%.
c. $E^*_{red} = E_{0\text{–}0} + E_{red}$.
d. $E^*_{ox} = E_{ox} - E_{0\text{–}0}$.

Table 5.3. Sequences of DNA assemblies for irradiation with non-covalently bound Ir complexes

DNA #	Sequences
G–^{CP}C	5′–ACATT GTTTTTTCAGTCAC–3′ 3′–TGTAA^{CP}CAAAAAAGTCAGTG–5′
I–^{CP}C	5′–ACATT ITTTTTTCAGTCAC–3′ 3′–TGTAA^{CP}CAAAAAAGTCAGTG–5′
^{CP}G	5′–ACATT CTTTTTTCAGTCAC–3′ 3′–TGTAA^{CP}GAAAAAAGTCAGTG–3′

5.3.1. Design and synthesis of Ir(III) complexes. Three cyclometalated iridium complexes (**Ir1**, **Ir2** and **Ir3**), as shown in Figure 5.1, were designed to serve as both a photooxidant and photoreductant to induce DNA redox reactions. Each Ir(III) complex has two 2-phenylpyridines as auxiliary ligands and one polypyridine ligand as an intercalative moiety for DNA base stacking. Since the final goal is to use these complexes to study DNA-mediated ET or HT, Ir(III) complexes are required to have a handle for covalently coupling to DNA oligonucleotides. However, the two ppy ligands cannot be coordinated to the metal center individually, because the intermediate tetrachloride Ir(III) complex is extremely labile. Thus, it is not feasible to add a monofuntional linker to Ir(III) complex through the auxiliary ligand, ppy. As a result, functionalization was introduced to the dppz ligand. An ether, carboxylic acid and acetylene group were introduced to the C11 position on dppz in **Ir1**, **Ir2** and **Ir3**, respectively. The functional groups in **Ir1** and **Ir3** were further elaborated to an alkyl linker and a carboxylic acid. In the chapter 6, the methodology for covalently attachment to DNA oligonucleotides is described.[34]

The three Ir(III) cyclometalated complexes are prepared by incorporating the functionalized dppz to a bisphenylpyridine Ir(III) μ-dichloro-bridged dimer as shown in Figure 5.2. The dinuclear Ir(III) complex was synthesized by the method reported by Lamansky,[32] which involves refluxing $IrCl_3 \bullet nH_2O$ with 2 equiv of 2-phenylpyridine in a mixture of 2-methoxyethanol and water. Figure 5.3 shows the synthetic strategy for modification of the dppz ligands. The functional groups on dppz are first introduced to an diaminobenzene moiety before the condensation reaction with phenanthrolinedione. The carboxylic acid at the end position of the alkyl chain is protected during the whole

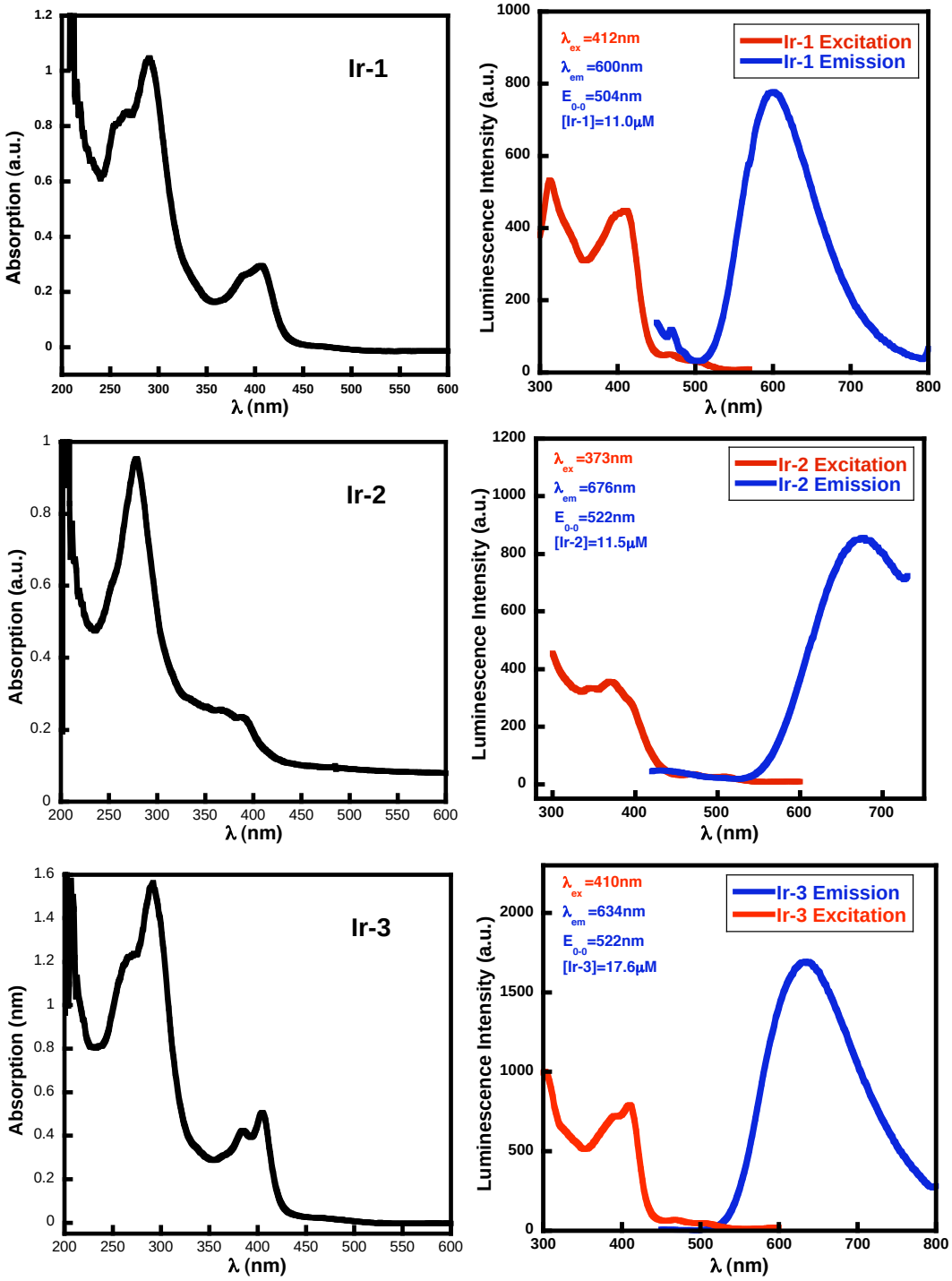

Figure 5.4. Optical spectra of Ir complexes are applied to determine the energy of the excited state. Absorption spectra in left column are obtained in MeCN. Luminescence spectra in right column are observed in CH_2Cl_2. Experimental details are described in materials and methods.

process for the synthetic purposes. In the last step after the entire complex is constructed, the ester is deprotected under basic condition.

5.3.2. Optical spectra of Ir complexes. UV-visible spectra of the three Ir(III) complexes are measured in acetonitrile as shown in Figure 5.4 and Table 5.1. Salient features of the absorption spectra of **Ir1** to **Ir3** are the high intensity peak at 280 ~ 290nm in MeCN, which corresponds to a $\pi \rightarrow \pi^*$ transition in ppy, and a modest band around 380nm to 410nm, which is assigned to a mixture of triplet [5d(Ir) → diimine] MLCT and an intraligand transition (IL) of dppz, which is well-known around ~380nm.[4] Based upon the modifications on dppz, the MLCT band emerges at 368nm for **Ir2** and 405nm for **Ir1** and **Ir3**, besides the IL(dppz) band at ~380nm. The redshift of the low-energy band among the Ir complexes is presumably related to the difference in electron withdrawing character of the functional groups on dppz.

Luminescence spectra of the three Ir complexes are observed in CH_2Cl_2 as shown in Figure 5.4. **Ir1**, **Ir-2** and **Ir-3** have a broad emission band between 500nm and 700nm. The feature of luminescence of the three complexes, like the absorption spectra, is affected by the functionalization of dppz. The peak wavelength (λ_{em}) redshifts from 600nm for **Ir-1** to 634nm for **Ir-3** to 676nm for **Ir-2**, while the electron withdrawing character of the functional groups increases. The excitation spectra of Ir complexes obtained by scanning the excitation wavelength and monitoring the luminescence at corresponding λ_{em}, have similar characteristics as the UV spectra of corresponding Ir complexes, which confirms the origin of the excited states. The overlap wavelength of excitation and emission spectra was used to determine the energies of the excited Ir

complexes. As listed in Table 5.2, $\lambda_{0\text{-}0}$ of **Ir1**, **Ir2** and **Ir3** are 504nm, 522nm and 522nm, respectively.

As shown in previous studies,[4] the luminescence of dppz complexes of Ru(II) is sensitive to solvent environment, because the protonation of the imine on dppz by solvent protons causes significant luminescence quenching. A similar phenomenon is observed for Ir complexes here. The luminescence of **Ir3** also exhibits apparent solvatochromicity. With the same concentration, the luminescence is the most pronounced in less polar solvent, CH_2Cl_2. As shown in Figure 5.5, the emission band of **Ir3** is weakened and the peak is redshifted from 634nm to 705nm in a more polar solvent, MeCN. The luminescence of **Ir3** is completely quenched by only 10% H_2O in MeCN (Figure 5.5). A solvatochromic shift also occurs in the absorption spectra (Figure 5.5). Apparent hypochromicity and loss of peak features are observed for both the high energy IL transition and MLCT bands upon varing solvents from MeCN to aqueous buffer.

5.3.3. Electrochemistry to determine the redox potentials of Ir(III) cyclometalated complex. Table 5.2 lists the reversible oxidation (E_{ox}) and reduction (E_{red}) potentials of the ground state Ir complexes obtained by cyclic voltammetry in MeCN. The potentials are given versus NHE, but are measured using ferrocene as a standard. Electrochemical profiles are shown in Figure 5.6. E_{ox} of **Ir1**, **Ir2** and **Ir3** are almost the same (~ 1.49 V), while the reduction potentials vary according to the functional group on dppz. **Ir-1** has the highest reduction potential, -0.87V, while **Ir2** has the lowest value at -0.62V.

The similar oxidation potentials reflect the common part, $Ir(ppy)_2$, among the three complexes. The variety of modifications on dppz adjusts the reduction potentials of

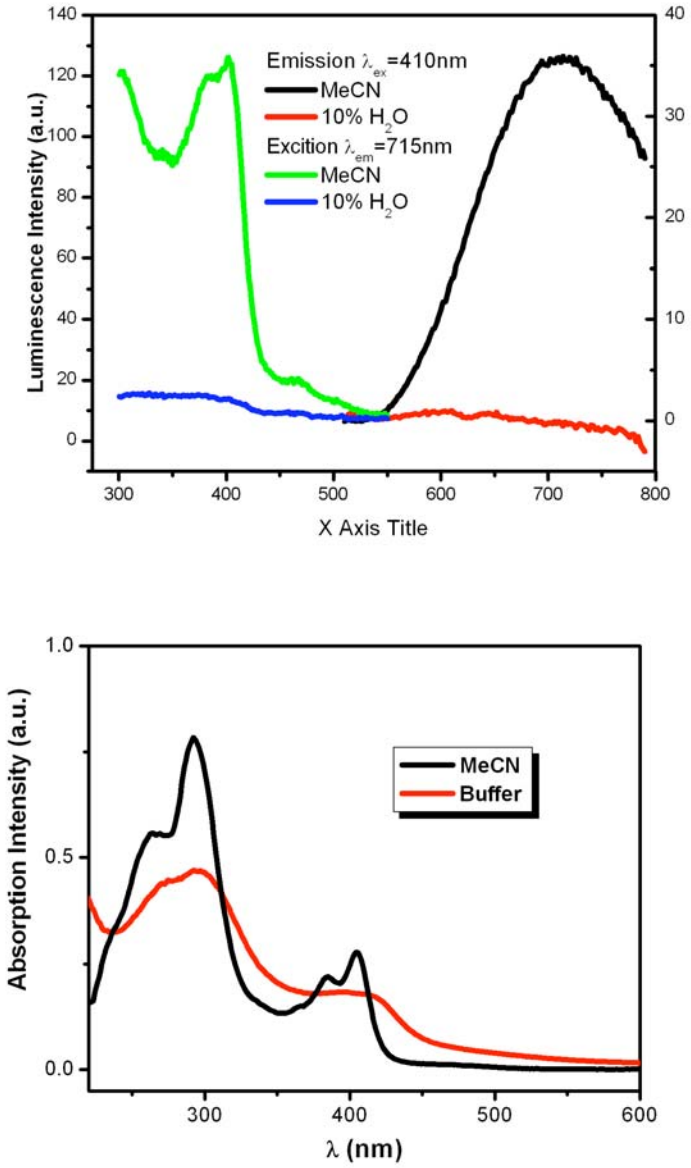

Figure 5.5. Solvatochromistic effects on optical spectra of Ir3. *Top:* Luminescent spectra in MeCN or 10% H_2O/MeCN. [Ir-3] = 20 μM. Spectra are taken anaerobically. *Bottom*: Absoprtion spectra of Ir-3 in MeCN and aqueous buffer. [Ir-3] = 10 μM. Buffer condition is 10 mM NaCl, 20 mM sodium phosphate pH 7.0.

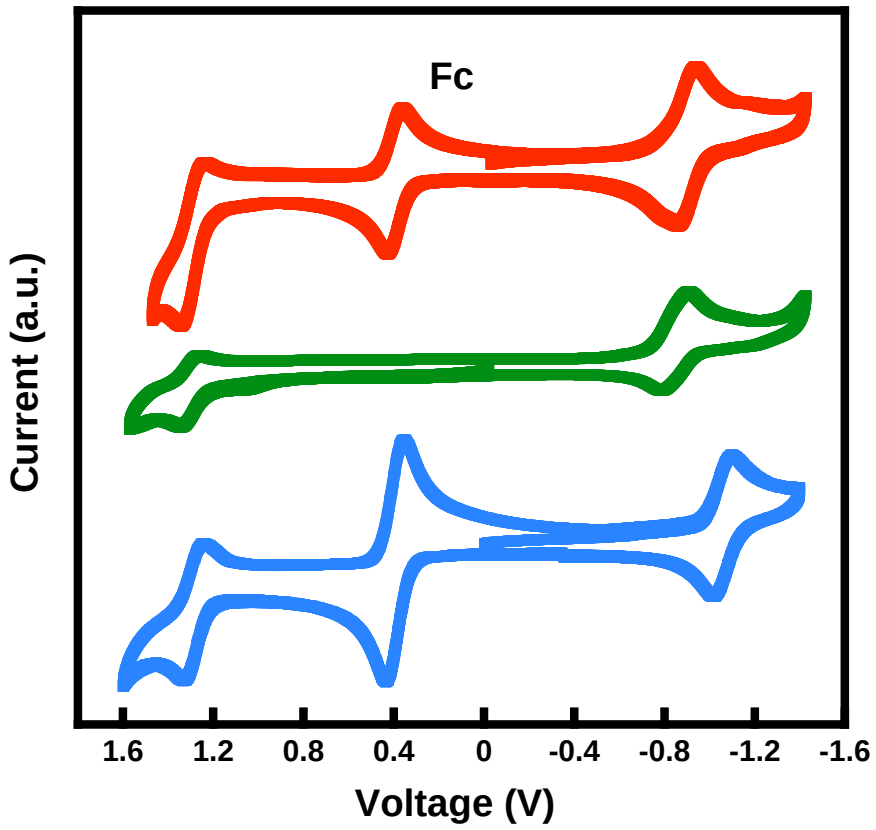

Figure 5.6. Comparison of redox potentials of Ir complexes. Red: Ir1; green: Ir2; blue: Ir3. Fc represents the oxidation peak of standard ferrocene. Working conditions are described in materials and methods.

ground state. Since the electron-withdrawing carbonyl group in **Ir2** can stabilize the extra electron density in the reduced complex, **Ir2** is more readily reduced than the other two complexes. Whereas, the ether group in **Ir1** has electro-donating features, which shifts E_{red} of **Ir1** to more negative values. The electronic properties of the functional groups on dppz agree with the trends of reduction potentials.

Redox potentials of excited Ir complexes are determined by both $E_{0\text{-}0}$ and redox potentials of the ground states:

$$E^*_{red} = E_{0-0} + E_{red}, \tag{5.1}$$

$$E^*_{ox} = E_{ox} - E_{0-0}, \tag{5.2}$$

E^*_{red} of three Ir complexes increase as **Ir-1**< **Ir-3** < **Ir-2** as listed in Table 5.2. **Ir-1** and **Ir-3** has E^*_{red} at 1.60 V and 1.68 V versus NHE, respectively. Based upon E_{ox} of the isolated nucleic acid bases,[35] E^*_{red} of **Ir-1** and **Ir-3** have enough driving force to oxidize purines but presumably not pyrimidines. **Ir-2** has a higher E^*_{red} at 1.76 V and is perhaps able to initiate oxidation of both purines and pyrimidines upon photoirradation. **Ir-1** has E^*_{ox} at -1.0 V versus NHE, while those of **Ir-2** and **Ir-3** are at -0.9 V. Both values are roughly in the same region as E_{red} of nucleic acid pyrimidine bases, which are ~ -1.0V versus NHE.[35] Thus, the three Ir complexes would be able to reduce pyrimidines in DNA.

The redox potentials of Ir complexes and DNA bases provide an estimate to predict the possible redox chemistry between Ir complexes and the DNA duplex. Both **Ir1** and **Ir3** have the sufficient driving forces only to oxidize purines and reduce pyrimidines upon irradiation. In contrary, **Ir2** may both oxidize and reduce pyrimidines with photoactivation, which could cause complications to interpret the origin of pyrimidine damage when the DNA is irradiated with **Ir2**.

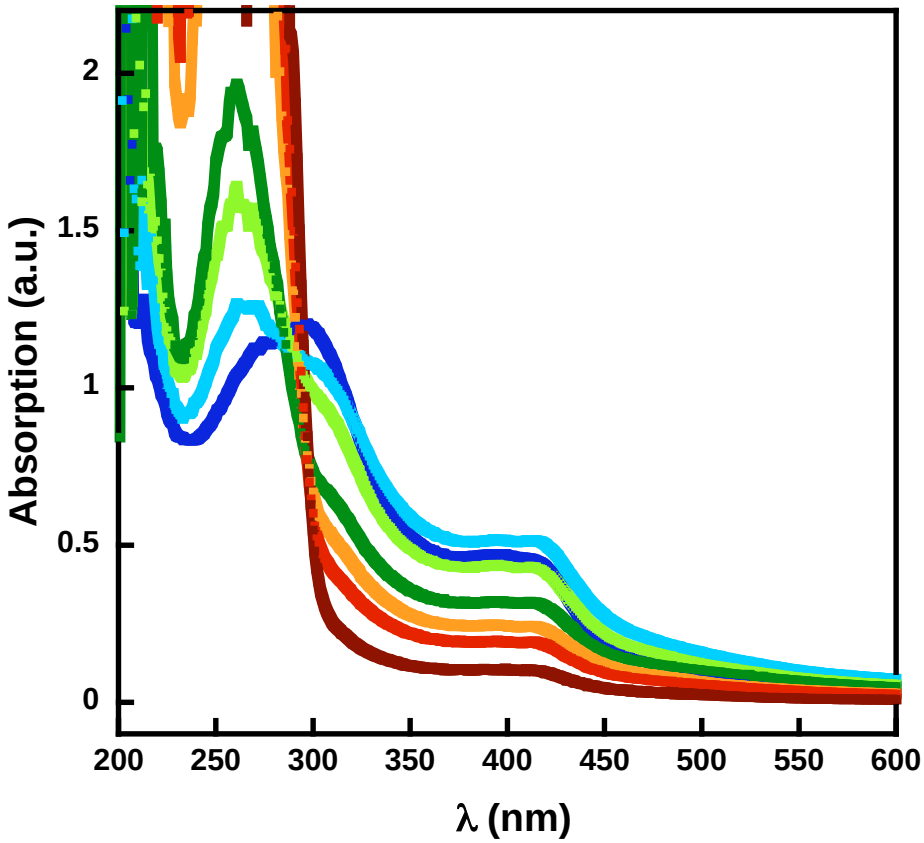

Figure 5.7. Absorption spectra of Ir3 in the presence or absence of λ DNA. DNA concentration increases from blue to green to brown. Concentration of Ir3 is kept constant at 22 μM, while [DNA] = 0 (blue), 50 μM (light blue), 100 μM (light green), 200 μM (green), 405 μM (orange), 540 μM (red) and 609 μM (brown). The buffer condition is 10mM NaCl, 20mM sodium phosphate (pH 7.0). Details are described in experimental.

5.3.4. Interactions of Ir complexes with duplex DNA. Optical spectra of **Ir3** in the presence of DNA are used to investigate the stacking of the complex with DNA. UV absorption spectra of **Ir3** are observed upon titration of λ DNA (0~600μM bp conc.) in aqueous buffer. As shown in Figure 5.7, the IL π→π* band at short wavelength (290nm) decreases upon addition of DNA, while the characteristic DNA band at 260nm emerges and become saturated at high DNA concentration. The similar variation upon addition of λ DNA or calf thymus DNA is also observed in the case of **Ir2** (data not shown). The absorption at the MLCT band varies in a more complicated fashion as a function of titration. The absorbance intensities of **Ir3** increase at first, when DNA bp concentration is less than 3 times of that of complex. Then, upon further addition of DNA, the normal hypochromicity at the low-energy band occurs (red lines in Figure 5.7), which is consistent with the intercalative stacking of dppz' ligand into DNA duplex. A similar effect is also observed for the $[Pt(mes)_2(dppz)]Cl_2$ complex and bulky $[Ru(bpy)_2(tpqp)]Cl_2$ (tpqp: 7,8,13,14-tetrahydro-6-phenylquino-[8,7-*k*][1,8]phenanthroline) complex.[6,36] The observation of an initial hyperchromic shift of the MLCT band is most likely due to, as suggested by the other complexes, the aggregation of **Ir3** in aqueous solution that the complex adopts to protect dppz' from the solvent molecules. At very low DNA concentrations (DNA bp concentration < 100 μl), the addition of DNA duplexes disrupts the aggregation of the complex and leads to the enhancement of the absorbance. Once the aggregation is disrupted, and the concentration of DNA is sufficiently high, the normal hypochromic shifts can be observed.

As has been seen in Figure 5.5, dppz complexes pf Ir do not luminesce in either aqueous buffer or organic/aqueous mixture. The similar luminescence quenching is observed for $[Ru(bpy)_2dppz]^{2+}$, which is due to the protonation of dppz imine by solvent.[4]

By intercalating into DNA, the luminescence of Ru complex can be switched on, because the imines are protected by the hydrophobic base pairs in the DNA helix. However, unlike the dppz complex of Ru(II), the similar restoration of luminescence in the presence of duplex DNA is not observed for Ir complexes. Luminescence of **Ir3** in aqueous buffer remains quenched both in the absence and presence of DNA. The lack of luminescence restoration here, is presumably due to the fact that the excited state of the Ir complex is quenched by HT and/or ET through DNA and has the lifetime too short to generate steady-state luminescence. Similar quenching is seen for highly oxidizing Ru(II) complexes.[37] Luminescent excited state of those complexes are indeed known to reductively quenched by guanine or adenine moieties. In the case of $[Ru(bpy)_2dppz]^{2+}$, the driving force is not sufficient ($E(Ru^{2+*}/Ru^{+}) \sim 0.6$ V vs NHE) for ET-induced quenching. Indeed the guanine radical is observed by EPR at room temperature when $[Ir(ppy)_2dppz]^{+}$ is irradiated with $[poly(dG\text{-}dC)]_2$.[38]

5.3.5. Photoredox reaction of ^{CP}C and ^{CP}G-containing DNA with non-covalently bound Ir complexes. DNA assemblies in Table 5.3 contain an A-tract composed of eight adenine-thymine base pairs. The flanking sequences are random and kept the same to avoid other effects, such as fraying ends. After the second adenine, either a ^{CP}C in ^{CP}C-containing assemblies (**I/G-^{CP}C**) or a ^{CP}G in **C-^{CP}G** is placed as a fast kinetic electron or hole trap. ^{CP}C is base paired to a guanine in **G-^{CP}C** or an inosine (I) in **I-^{CP}C** in order to study the base-pair effects on redox decomposition of ^{CP}C.[14] Due to the slightly higher oxidation potential of inosine (1.5 V vs NHE)[39] than that of guanine (1.29 V vs NHE), I is less competitive as a thermal hole trap than guanine. Higher efficiency of ^{CP}C decomposition has been observed when ^{CP}C is oxidatively ring opened via HT. This

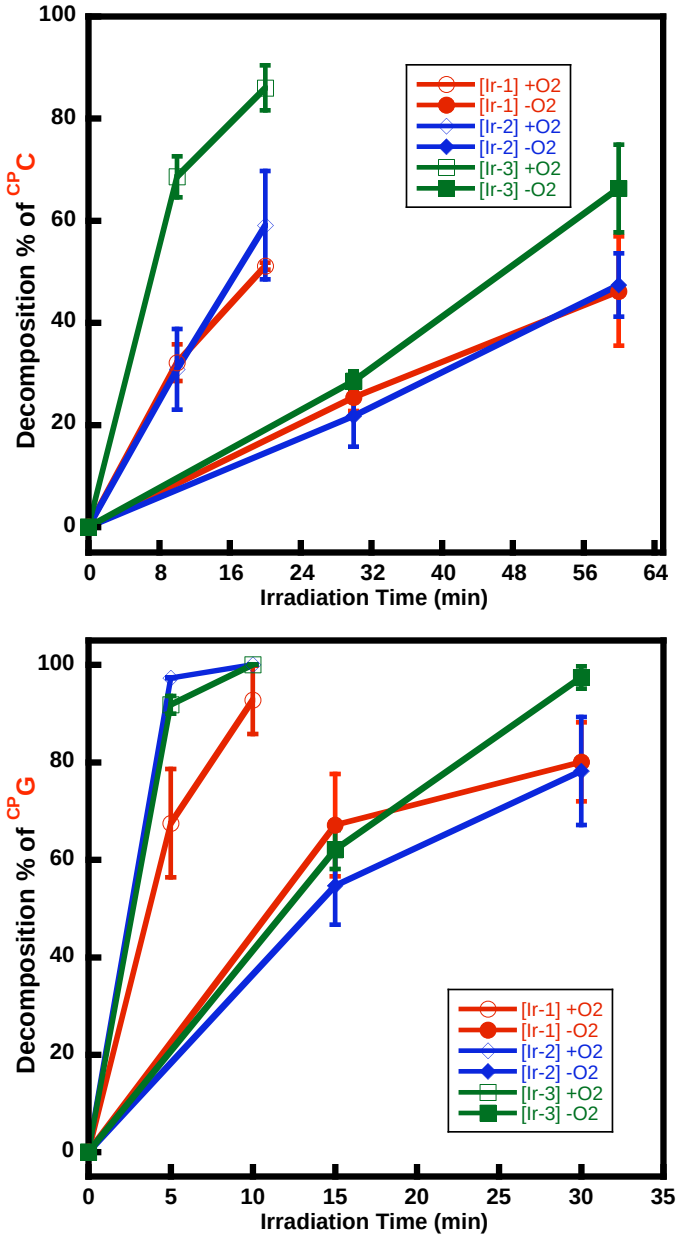

Figure 5.8. Redox decomposition of ^{CP}C in duplex **^{CP}C** or ^{CP}G in duplex **^{CP}G** with iridium complexes. Open symbols represent the aerobic data and close symbols represent the data obtained anaerobically. [DNA]=20μM, [NaCl]=10mM and [NaP]=20mM. Irradiation wavelength is 380nm. *Top*: decomposition data of ^{CP}C; *Bottom*: that of ^{CP}G.

enhancement of ^{CP}C decomposition by base paired to I is absent in case of ^{CP}C reduction.[6] Thus, the base-pair effects can be used to discern the redox reactions that causes the ring opening of ^{CP}C. Photoredox reactions of the traps in duplex **I/G-^{CP}C** and **C-^{CP}G** are carried out with non-covalently bound **Ir1**, **Ir2** and **Ir3**, respectively. Decomposition percentages of the traps are plotted versus irradiation time in Figure 5.8. ^{CP}C in duplex **I-^{CP}C** is decomposed by irradiating with each of Ir complexes. **Ir1** and **Ir2** induce redox ring opening of ^{CP}C with similar efficiency upon photoactivation. About 51% of ^{CP}C with **Ir1** and 59% with **Ir2** have decomposed after 20 mins of irradiation. Although **Ir3** has similar E^*_{red} to **Ir1** and **Ir2**, ^{CP}C decomposes more efficiently in the presence of **Ir3**. After 20 mins irradiation with **Ir3**, 86% of ^{CP}C is decomposed. In the case of ^{CP}G oxidation, the three complexes have similar reaction efficiencies. Nearly 100% of ^{CP}G in **C-^{CP}G** are consumed by photolysis with each Ir complex within 10 mins, while **Ir1** has slightly slower reactivity at short times as shown in Figure 5.8.

In order to eliminate the possibility of oxidation of cyclopropylamine substituent from singlet oxygen, which may be generated by energy transfer from the excited state of Ir complexes to O_2, the same photolysis experiments were also carried out under anaerobic conditions. Decomposition of ^{CP}C occurs with each Ir complex in the absence of oxygen. Although the reaction efficiency under anaerobic conditions is lower than that under aerobic condition, similar damage yields have been achieved under both conditions. 46%, 47% and 66% of ^{CP}C in **I-^{CP}C** are decomposed after 1 h irradiation with **Ir1**, **Ir2** and **Ir3**, respectively. Oxidative damage of ^{CP}G with non-covalently bound Ir complexes are also observed under anaerobic conditions. The overall decomposition

yields of ^{CP}G with Ir complexes can still reach above 80% within 30 mins irradiation. The similar damage yields of both cyclopropyl-modified traps under aerobic and anaerobic conditions imply that the redox decomposition of the two modified bases is not due to singlet oxygen. It is not unexpected because the luminescence of **Ir3** in the presence of DNA shows that the excited state has relatively a short lifetime and exists presumably not long enough to react with oxygen. The overall lower efficiency of ^{CP}C and ^{CP}G decomposition under anaerobic conditions likely reflects the poor stability of the complex in aqueous buffer, as well as under freeze-pump-thaw conditions.

5.3.6. Effects of paired bases on ^{CP}C decomposition triggered by irradiation of Ir complexes. DNA assemblies **I-^{CP}C** and **G-^{CP}C** have the same sequence, except for the base opposite to ^{CP}C. In **I-^{CP}C**, an inosine, a guanine analogue with higher oxidation potential, is base paired to ^{CP}C, while a guanine is substituted at that position in **G-^{CP}C**. As seen previously, when ^{CP}C is one-electron oxidized via DNA-mediated CT by the photoactivated Rh(III) complex, decomposition of ^{CP}C based paired with I is significantly more efficient than that base paired to guanine.[14] This enhancement is because hole competition from energetically less favored inosine is less than that from the thermal hole trap guanine. Contrary to the case of ^{CP}C oxidation, significant enhancement of ^{CP}C decomposition in I-containing duplex is not observed with **Ir1** and **Ir3**, as shown in Figure 5.9. Irradiated with **Ir1**, **I-^{CP}C** and **G-^{CP}C** yield comparable damage efficiency of ^{CP}C and the difference is within the experimental uncertainty. More remarkably, in the case of **Ir3**, ^{CP}C decomposes more efficiently in **G-^{CP}C** than in **I-^{CP}C**, which is opposite to the expected result for ^{CP}C oxidation. The lack of I-enhancement effect on ^{CP}C decomposition indicates that ^{CP}C is photo-reduced by non-covalently bound **Ir1** or **Ir3**.

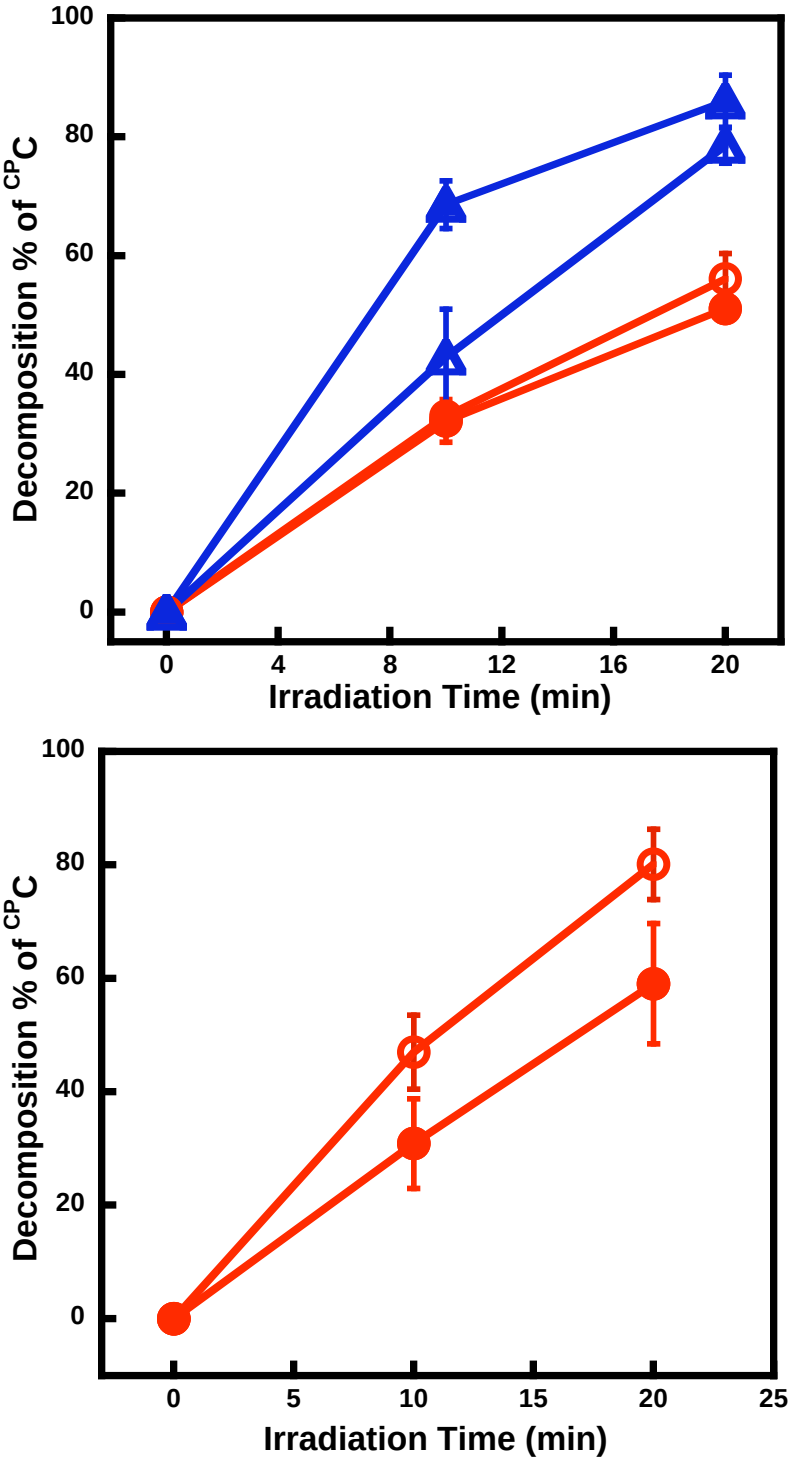

Figure 5.9. Effects of paired base on ^{CP}C decomposition triggered by irradiation of Ir complexes. *Top*: Time course of ^{CP}C decomposition with **Ir-1** (red) or **Ir-3** (blue). *Bottom:* Time course of ^{CP}C decomposition with **Ir-2** (red). Open symbols represent the data of duplex **I-^{CP}C**. Close symbols represent the data of duplex **G-^{CP}C.** Experiments were done under aerobic conditions. The details are described in materials and methods.

Thus, both **Ir1** and **Ir3** can only oxidize purines. They reduce pyrimidine, upon photo-excitation. However, **Ir2** triggers the decomposition of ^{CP}C in the similar way as canonical photooxidants. ^{CP}C in **I-^{CP}C** is consumed in a more efficient way than that in **G-^{CP}C**. Since **Ir2** has relatively higher E^*_{red} than **Ir1** and **Ir3**, it is more likely for **Ir2** that photooxidation would be the dominant reaction on DNA.

5.4. Summary and implication.

Three cyclometalated Ir(III) complexes were developed containing functionalized dppz ligands. Optical and redox features of the complexes are modulated by the functional group with different electron affinities. As listed in Table 5.1, the Ir(III) complexes exhibit unique features of excited state redox properties and can be applied to probing both oxidation and reduction of DNA bases. In particular, **Ir1** and **Ir3** electron donating functionality on the dppz ligand can serve as both a potent photooxidant to purines and photoreductant to pyrimidines. Redox decomposition of both ^{CP}C and ^{CP}G in DNA duplex is observed upon irradiation of non-covalently bound Ir complexes with DNA. Unlike oxidation, ^{CP}C base-paired with guanine in **G-^{CP}C** is decomposed in a comparably or more efficient way than in **I-^{CP}C** upon irradiation with **Ir1** or **Ir3**. The absent of I-enhancement on ^{CP}C decomposition points out that ^{CP}C has been reduced by excited **Ir1** and **Ir3**. Thus, both **Ir1** and **Ir3** can be used as electron and hole donor, and be further applied to the study of DNA-mediated ET and HT. With monofunctional linkage on dppz ligand, these iridium complexes could be covalently tethered to a DNA oligonucleotide and the resulting Ir-DNA conjugates would possess the same photooxidant and photoreductant which have identical intercalation mode, as well as

electron coupling to DNA. Thus, DNA assemblies with covalently-tethered **Ir1** or **Ir3** would be remarkably useful to investigate the features of ET and HT through the same DNA model system. The mechanisms of the two DNA-mediated electron migration processes can then be compared and presumably reconciled into a general model.

5.5. References

1. Hall, D.B., Holmlin, R.E., Barton, J.K. Oxidative DNA damage through long range electron transfer *Nature* **1996**, *382*, 731-735.

2. Núñez, M.E., Barton, J.K. Probing DNA charge transport with metallointercalators *Curr. Opin. Chem. Biol.* **2000**, *4*, 199-206.

3. Sitlani, A., Long, E.C., Pyle, A.M., Barton, J.K. DNA photocleavage by phenanthrenequinone diimine complexes of rhodium(III): shape-selective recognition and reaction *J. Am. Chem. Soc.* **1992**, *114*, 2303-2312.

4. Friedman, A.E., Chambron, J.C., Sauvage, J.P., Turro, N.J., Barton, J.K. Molecular 'Light Switch' for DNA: $Ru(bpy)_2(dppz)^{2+}$ *J. Am. Chem. Soc.* **1990**, *112*, 4960-4962.

5. Stemp, E.D.A, Arkin, M., Barton, J. K. Oxidation of guanine in DNA by $Ru(phen)_2dppz^{3+}$ using the flash-quench technique *J. Am. Chem. Soc.* **1997**, *119*, 2921-2925.

6. Lu, W., Vicic, D.A., Barton, J.K. Reductive and oxidative DNA damage by photoactive platinum(II) intercalators *Inorg. Chem.* **2005**, *44*, 7970-7980.

7. Yoo, J., Delaney, S., Stemp, E.D.A., Barton, J.K., Rapid radical formation by DNA charge transport through sequences lacking intervening guanines *J. Am. Chem. Soc.* **2003**, *125*, 6640-6641.

8. Holmlin, R.E., Stemp, E.D.A., Barton, J.K. $Os(phen)_2dppz^{2+}$ in photoinduced DNA-mediated electron transfer reactions *J. Am. Chem. Soc.* **1996**, *118*, 5236-5244.

9. Erkkila, K.E., Odom, D.T., Barton, J.K. Recognition and reaction of metallointercalators with DNA *Chem. Rev.* **1999**, *99*, 2777-2795.

10. Delaney, S., Yoo, J., Stemp, E.D.A., J.K. Barton Charge equilibration between two distinct sites in double helical DNA *Proc. Nat. Acad. Sci. USA* **2004**, *101*, 10511-10516.

11. Núñez, M.E., Hall, D.B., Barton, J.K. Long range oxidative damage to DNA: effects of distance and sequence *Chem. Biol.* **1999**, *6*, 85-97

12. Williams, T.T., Dohno, C., Stemp, E.D.A & Barton, J.K. Effects of the photooxidant on DNA-mediated charge transport *J. Am. Chem. Soc.* **2004**, *126*, 8148–8158.

13. Nakatani, K., Dohno, C., Saito, I. Design of a hole-trapping nucleobase: termination of DNA-mediated hole transport at N^2-cylcopropyldeoxyguanosine *J. Am. Chem. Soc.* **2001**, *123*, 9681-9682.

14. Shao, F., O'Neill, M.A., Barton, J.K. Long-range oxidative damage to cytosines in duplexes DNA *Proc. Nat. Acad. Sci. USA* **2004**, *101*, 17914-17919.

15. O'Neill, M.A., Barton, J.K. DNA charge transport: conformationally gated hopping through stacked domains *J. Am. Chem. Soc.* **2004**, *126*, 11471-11483.

16. Shao, F., Augustyn, K., Barton, J.K. Sequence dependence of charge transport through DNA domains *J. Am. Chem. Soc.* **2005**, *127*, 17445-17452.

17. Augustyn, K., Shao, F., Genereux, J., Barton, J.K. Periodicities in DNA charge transport probed with N_2-cyclopropylguanine, a kinetically fast hole trap *submitted*.

18. Behrens, C., Cichon, M.K., Grolle, F., Hennecke, U., Carell, T. Excess electron transfer in defined donor-nucleobase and donor-DNA-acceptor systems *Top. Curr. Chem.* **2004**, *236*, 187-204.

19. See also reductive chemistry on surfaces, for example: Kelley, S.O., Jackson, N.M., Hill, M.G., Barton, J.K. Long range electron transfer through DNA films *Angew. Chem. Int. Ed.* **1999**, *38*, 941-945.

20. Breeger, S., Hennecke, U., Carell, T. Excess electron-transfer-based repair of a Cis-Syn thymine dimmer in DNA is not sequence dependent *J. Am. Chem. Soc.* **2004**, *126*, 1302-1303.

21. Lewis, F.D., Liu, X., Miller, S.E., Hayes, R.T., Wasielewski, M.R. Dynamics of electron injection in DNA hairpins *J. Am. Chem. Soc.* **2002**, *124*, 11280-11281.

22. Ito, T., Rokita, S.E. Reductive electron injection into duplex DNA by aromatic amines *J. Am. Chem. Soc.* **2004**, *126*, 15552-15559.

23. Giese, B., Carl, B., Carl, T., Carell, T., Behrens, C., Hennecke, U., Schieman, O., Feresin, E. Excess electron transport through DNA: a single electron repairs more than one UV-induced lesion *Angew. Chem., Int. Ed.* **2004**, *43*, 1848-1851.

24. Dandliker, P. J., Holmlin, R. E., Barton, J. K. Oxidative thymine dimer repair in the DNA helix *Science* **1997**, *275*, 1465-1467.

25. Tamayo, A.B., Simona, G., Sajoto, T., Djurovich, P.I., Tsyba, I.M., Bau, R., Thompson, M.E. Cationic bis-cyclometalated iridium(III) diimine complexes and their use in efficient blue, green, and red electroluminescent devices. *Inorg. Chem.* **2005**, *44*, 8723-8732.

26. Lamansky, S., Djurovich, P., Murphy, D., Abdel-Razzaq, F., Lee, H., Adachi, C., Burrows, P.E., Forrest, S.R., Thompson, M.E. Highly phosphorescent bis-

cyclometalated iridium complexes: synthesis, photophysical characterization, and use in organic light emmtting diodes *J. Am. Chem. Soc.* **2001**, *123*, 4304-4312.

27. Lo, K.K., Ng, D.C., Chung, C. First examples of luminescent cyclometalated iridium(III) complexes as labeling reagents for biological substrates *Organometallics* **2001**, *20*, 4999-5001.

28. Lo, K.K., Chung, C., Lee, T.K., Lui, L. Tsang, K.H., Zhu, N. New luminescent cyclometalated iridium(III) diimine complexes as biological labeling reagents. *Inorg. Chem.* **2003**, *42*, 6886-6897.

29. Lepeltier, M., Lee, T.K., Lo, K.K., Toupet, L., Bozec, H.L., Guerchais, V. Synthesis, structure, and photophysical and electrochemical properties of cyclometallated iridium(III) complexes with phenylated bipyridine liands *Eur. J. Inorg. Chem.* **2005**, 110-117.

30. Lo, K.K., Chung, C., Zhu, N. Nucleic acid intercalators and avidin probes derived from luminescent cyclometalated iridium(III)-dipyridoquinoxaline and –dipyridophenazine complexes. *Chem. Eur. J.* **2006**, *12*, 1500-1512.

31. Dupureur, C.M., Barton, J.K. Structural studies of L- and D-$[Ru(phen)_2dppz]^{2+}$ bound to $d(GTCGAC)_2$: characterization of enantioselective intercalation *Inorg. Chem.* **1997**, *36*, 33-43.

32. Lamansky, S., Djurovich, P., Murphy, D., Abdel-Razzaq, F., Kwong, R., Tsyba, I., Bortz, M., Mui, B., Bau, R., Thompson, M. E. Synthesis and characterization of phosphorescent cyclometalated iridium complexes *Inorg. Chem.* **2001**, *40*, 1704-1711.

33. Duclos, S., Stoeckli-Evans, H., Ward, T.R. Design and synthesis of compartmental ligands and their complexes for the production of catalytic antibodies *Helvetica Chimica Acta* **2001**, *84*, 3148-3161.

34. O'Neill, M. A., Barton, J. K. *Charge Transfer in DNA: From Mechanism to Application*, Wagenknecht, H. A., ed., Wiley: New York, **2005**, 27-75.

35. Steenken, S., Telo, J. P., Novais, H. M., Candeias, L. P. One-electron-reduction potentials of pyrimidine bases, nucleosides, and nucleotides in aqueous solution. Consequences for DNA redox chemistry *J. Am. Chem. Soc.* **1992**, *114*, 4701-4709.

36. Rüba, E., Barton, J. K., $[Ru(bpy)_2(L)]Cl_2$: Luminescent Metal Complexes that Bind DNA Base Mismatches *Inorg. Chem.* **2004**, *43*, 4570-4578.

37. Elias, B., Kirsch, A. Photo-reduction of polyazaaromatic Ru(II) complexes by biomolecules and possible applications *Coordination Chem. Rev.* **2006**, *250*, 1627-1641.

38. Shao, F., Lu, W., Elias, B., Barton, J. K. *manuscription in preparation*.

39. Kelley, S. O., Barton, J. K. Electron transfer between bases in double heical DNA *Science*, **1999**, *283*, 375-381.

Chapter 6

Long range electron and hole transport through DNA triggered by covalently tethered Ir(III) cyclometalated complexes

6.1. Introduction.

The structural core of a DNA duplex is constituted by an array of heterocyclic aromatic nucleic acid base pairs.[1] This well-defined π-stacked structure provides an effective pathway for charge migration, which includes two types of charge propagation, hole transport (HT) and electron transport (ET).[2] In HT, a radical cation, a hole, is injected and migrates through the DNA duplex to oxidize distant bases. On the other hand, ET is affected by DNA reduction and an excess electron is transported along the double helix.

DNA-mediated HT has been extensively explored using a variety of photooxidants and hole traps with both biochemical and spectroscopic assays.[3-10] A conformationally gated domain model is proposed to reconcile most of HT data up until now.[11,12] Recently, it has been highly underscored that the interaction mode of photooxidants with the DNA duplex is one of the essential factors in terms of studying HT mechanisms.[13] For example, two fluorescent adenine analogues, 2-aminopurine (Ap) and 1,N^6-ethenoadenine (A_ε) with similar reactivity to oxidize nucleic acid guanine, yield striking differences in distance dependence of HT (β~1.0 $Å^{-1}$ for A_ε; β~0.14 $Å^{-1}$ for Ap).[14] The distinctly low HT efficiency triggered by A_ε is due to the significantly poor base stacking of the sterically bulky analogue within the double helix. With covalently tethered Rh(III) and Ru(II) complexes, which have exteneded intercalative ligands to achieve effective electronic coupling with DNA, efficient HT over long distances up to 200 Å in DNA is observed.[4] Thus, the critical ways in which photooxidants interact with the DNA helix can result in significant differences in HT. Additionally, DNA-mediated HT exhibits remarkably diverse features when probed on different time scales.[15] Due to

its long millisecond lifetime, the guanine radical cannot report HT event on faster time scale.[16] The development of cyclopropylamine substituted bases, such as N_4-cyclopropylguanine (^{CP}G)[17] and N_4-cyclopropylcytosine (^{CP}C)[18] allows for probing transient hole and electron occupancy on DNA during electron migration as the cyclopropyl ring can open with a rate of ~ 10^{12} s^{-1} upon both oxidation and reduction.[19] Thus this assay can report the yields of HT and ET on a picosecond time scale.

Photoreductants and electron traps are expected also to have the same sensitivity to the electronic coupling as photooxidants.[10b] However, today the knowledge about DNA-mediated ET is much less than DNA-mediated HT and still rudimentary due to the lack of model systems.[20] Currently covalently attached flavin analogues are used by Carell as photoreductants, and a thymine dimer (T^T) is employed as the electron trap.[21] Aromatic amines or pyrene-substituted uracil are also employed as electron donors in the model systems, while 5-bromouracil (^{Br}U) are utilized as the electron trap.[22-24] However, these organic small molecules have different interaction modes with DNA upon electron injection. Additionally, T^T is thought to have the cleavage rate of the dimer as ~10^9 s^{-1}.[25] The trapping rate of T^T is slower than electron transport rate through DNA,[25] which makes the traps less appropriate to study the mechanism of ET than cyclopropylamine modified bases, such as ^{CP}C. The difference of donor-DNA interaction and trapping rates of acceptors between ET and HT makes it difficult to compare these two inherently similar DNA-mediated electron migration processes by using existing model systems. A uniform photoredox probe for both HT and ET is necessary. More recently, several Ir(III) cyclometalated dypyridophenazine (dppz) complexes have been developed to trigger DNA redox reactions.[26] In this chapter, two of the Ir(III) complexes has been covalently

tethered to DNA oligonucleotides and serve as both an oxidant for HT and a reductant for ET upon irradiation. ^{CP}C- and ^{CP}G-containg DNA, as well as ^{Br}U-containing DNA, are used to explore the resulting electron propagation process.

6.2. Experimental.

6.2.1. DNA oligonucleotides. All DNA oligonucleotides were synthesized using standard phosphoramidite chemistry on an ABI DNA synthesizer. N_2-cyclopropylguanine (^{CP}G) and N_4-cyclopropylcytosine (^{CP}C) modified sequences with the trityl group on were first prepared by solid-phase DNA synthesis, using by 2-fluoroinosine (^{F}I) and 4-thiouridine (ThU) as precursors for the two substituted bases, respectively. The DNA oligonucleotides containing ^{F}I and ThU at the desired positions are then incubated in 6 M aqueous cyclopropylamine at 60 ^{o}C for 16 h for substitution reactions.[27] ^{CP}C- and ^{CP}G-containing oligonucleotides are also cleaved from the resin during this incubation. The cleaved strands were purified by reverse-phase (RP) HPLC and repurified after removing the trityl group by treatment in 80% acetic acid for 15 minutes. Oligonucleotides were characterized by MALDI-TOF mass spectrometry.

5-Bromouracil (^{Br}U) was incorporated into DNA by using a 5-bromouridine phosphoramidite (Glen Research) on the ABI DNA synthesizer. Afterward, ^{Br}U-containing strands were cleaved from the resin by incubation in NH_4OH at room temperature for 24 h and purified as standard oligonucleotides.

The photoredox probes, $[Ir(ppy)_2(dppz1)]^+$ (IrOH1) (ppy: 2-phenylpyridine; dppz1: dipyrido[3,2-a:2’,3’-c]phenazine-11-oxy-hex-5-ynoic acid) and $[Ir(ppy)_2(dppz3)]^+$ (IrOH3) **(**dppz3: dipyrido[3,2-a:2’,3’-c]phenazine-11-yl-hex-5-ynoic acid), were

synthesized as described previously in chapter 5.[26] IrOH1 was tethered to DNA oligonucleotides through a series of diamino-alkyl linker with 3, 4, 5 and 9 methylenes, respectively. The coupling method described previously[3] to prepare Rh-tethered DNA strands was applied here to tether IrOH1 to DNA. IrOH3 was covalently tethered to DNA oligonucleotides as follows: First, the detritylated resin-bound oligonucleotides with an amine-ended C_6-alkyl linker were prepared by phosphoramidite chemistry. The amine-modified strands were then reacted with $[Ir(ppy)_2(dppz')]^+$ in anhydrous DMF using *O*-(benzotriazol-1-yl)-*N*,*N*,*N'*,*N'*-tetramethyluronium hexafluorophophate (HBTU, Aldrich) and 1-hydroxybenzotriazole hydrate (HOBT, Aldrich) as the coupling reagent in the presence of diisopropylethylamine (DIEA). Cleavage from the resin was accomplished by incubation in NH_4OH at 60 ^oC for 6 hours. IrOH3 tethered strands were HPLC-purified using a Varian C_4 reverse-phase column. MALDI-TOF mass spectrometry was used to characterize the metalated DNA conjugates, e.g., calcd. 6557 for **Ir3G2**, found 6556 for $(M-H)^-$. DNA oligonucleotides were suspended in buffered aqueous solution (10mM sodium phosphate, 20 mM NaCl, pH 7) and quantitated by UV-visible spectroscopy.

6.2.2. Melting temperatures. Melting temperatures (T_m) of all the duplexes were measured using a Beckman DU 7400 spectrophotometer with a temperature control attachment. Absorption at 260nm (A_{260}) of equimolar DNA complements (1.5 μM in 10 mM NaCl, 20 mM sodium phosphate, pH 7.0) were measured every 0.5 ^oC from 90 ^oC to 15 ^oC with rate 0.5 ^oC/min. The reverse temperature traces were measured under the same conditions to confirm the reversibility of the DNA annealing process. The data were fit to a sigmoidal curve to determine the T_m. The absorption profile was also measured at

413 nm as a function of temperature for 20 μM Ir(III)-tethered DNA aliquots in the same buffer in order to measure the corresponding T_m of the Ir(III) complex within the duplex. The error of T_m over at least three sets of individual experiments was less than 1^oC.

6.2.3. Photolysis experiments. Aliquots (10μM DNA, 30μl) for irradiation were prepared by annealing equimolar amounts of the desired DNA complements on a DNA thermal cycler (Perkin Elmer Cetus) from 90 ºC to 15 ºC over a period of 2.5 hours. Sodium ascorbate is added to the samples after DNA annealing in the reductive flash-quench experiments. Aliquots of the Ir-tethered duplexes were then irradiated with a 1000W Hg/Xe lamp equipped with a 320 nm LP filter and a monochromator. After irradiation at either 365nm or 380nm (0, 30 min, 60 min), duplex samples were digested by 37 ºC incubation with phosphodiesterase I (USB) and alkaline phosphatase (Roche) for 24 h in order to yield the free nucleosides, and the samples were analyzed by reverse phase HPLC (Chemcobond 5-ODS-H, 4.6x100 mm, 2% ~ 14% MeCN in 50 mM NH_4OAc over 30 min; 0% ~ 14 % over 35 min for reductive flash-quench samples). The percentage decomposition of modified bases (Y) was determined by the ratio of the peak area of ^{CP}G, ^{CP}C or ^{Br}U in an irradiated sample over that in a non-irradiated sample. The peak area of deoxyadenosine is used as an internal standard for all HPLC traces. Irradiations were repeated three times and the results averaged.

6.3. Results and discussion.

6.3.1. Experimental design. The modified DNA assemblies utilized for these studies are shown in Figure 6.1. Upon photolysis, the tethered cyclometalated Ir(III) complex serves as both a photooxidant for HT and photoreductant for ET in the

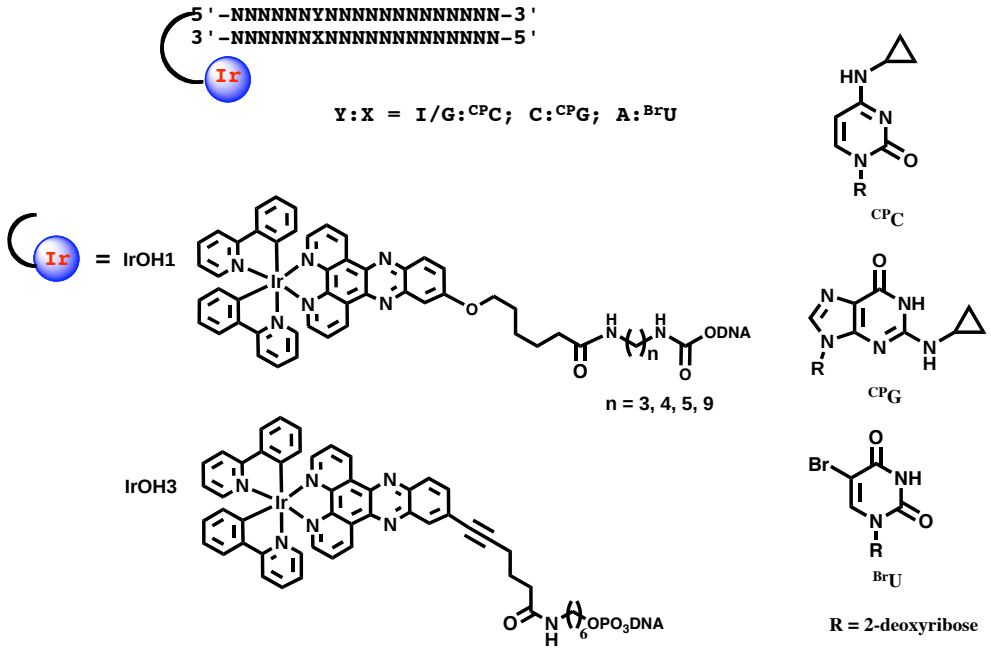

Figure 6.1. Scheme of Ir-tethered DNA assemblies for photoredox reaction. Sequences of DNA assemblies are listed in Tables 6.1 and 6.2. Ir complexes serve as both photooxidant and photoreductant. Ir1 is tethered to DNA oligonucleotides by a series of diamino-alkyl linker with various lenghs, while Ir3 is coulpled to DNA by a C6-alkyl amino-linker through a phosphate bond. Cyclopropylamine-substituted nucleosides, ^{CP}C and ^{CP}G, is incorporated to the complement of Ir-tethered strands as fast kinetic electron and hole traps, respectively. Structures of Ir(III) cyclometalated complexes (*left*) and cyclopropylamine modified bases and bromouridine (*right*) are shown at the bottom. Experimental details are described in materials and methods.

assemblies. Cylcopropylamine-modified bases, ^{CP}C and ^{CP}G, as well as 5-bromouridine (^{Br}U), are employed as fast kinetic traps to probe the transient electron and hole densities during both electron migration processes. The Ir(III) complexes are covalently tethered to the complementary strands of the cyclopropyl-substituted DNA oligonucleotides through an alkyl linker. In the case of IrOH3, the alkyl chain is connected to the 5'-end of DNA single strands through a phosphate linkage, which may better mimic the DNA backbone than the diamine alkyl linker used in Rh(III)-tethered DNA.[4,18]

In the IrOH1 tethered DNA assemblies (Ir1-DNA), a four-base segment, 5'GACT-3' is adopted from previous Rh(III)-tethered DNA as intercalation sites for IrOH1. As shown in Table 6.1, ^{CP}C and ^{CP}G are incorporated in the purine strands of an eight base pair (bp) adenine tract, while IrOH1 is tethered to the complementary pyrimidine strands. In **Ir1-G** and **Ir1-I**, ^{CP}C is positioned after the fourth adenine and ^{CP}G in **Ir1-C** is substituted at the end of the adenine tract.

Two sets of IrOH3-tethered DNA duplexes were prepared here to explore long range redox chemistry between the Ir complex and DNA (Table 6.2). All the duplexes have a three base pair segment, 5'-ACA-3' at the metal-tethering end to accommodate the intercalative dppz' ligand. An adenine tract with eight ATs follows the intercalation site in order to study the potential DNA-mediated ET and HT through the A-tract. On the distal side of the A-tract, a mixed seven base sequence is included and is constant to minimize any effects of fraying ends in the duplexes. In set #1, 8 adenines are placed in strands that are complementary to the Ir(III) tethered strands (**Ir3Y1**, Y = I, G, or C). Cyclopropyl-substituted bases, ^{CP}C and ^{CP}G are placed after the second adenine in **^{CP}C1** and **^{CP}G1**, respectively. DNA assemblies in set # 2 (**Ir3Y2**, Y = I, G, or C) have the same

Table 6.1. Sequence and melting temperatures of IrOH1-tethered DNA assemblies

DNA #	Sequences[a]	T_m (^oC)
Ir1-G	5′-Ir1-GATCTTTT GTTTTCAGTCAGCGTG-3′ 3′-CTAGAAAA^{CP}CAAAAGTCAGTCGCAC-5′	65 (60)[b]
Ir1-I	5′-Ir1-GATCTTTT ITTTTCAGTCAGCGTG-3′ 3′-GTAGAAAA^{CP}CAAAAGTCAGTCGCAC-5′	68 (63)
Ir1-C	5′-Ir1-GATCTTTTITTTT CAGTCAGCGTG-3′ 3′-GTAGAAAACAAAA^{CP}GTCAGTCGCAC-5′	

a. Ir1 represents the covalently tethered complex $[Ir(ppy)_2dppz1]^+$.

b. 1.5 μM of DNA assemblies in 50 mM NaCl, 20 mM sodium phosphate pH 7.0 were used to measure T_m. T_m of the DNA with same sequence but without tethered Ir complex is shown in periphrasis. Uncertainty of T_m under this working conditions is less than 1^{o}C.

Table 6.2. Sequence and melting temperatures of DNA assemblies in the studies of DNA-mediated ET and HT upon irradiation of the tethered Ir(III) complex

DNA		Sequence	T_m(DNA) (^oC)[a]	T_m(Ir) (^oC)[b]
Set #1	Ir3G1[c] ^{CP}C1	Ir-5′-ACATT GTTTTTTCAGTCAC-3′ 3′-TGTAA^{CP}CAAAAAAGTCAGTG-5′	52	61
	Ir3I1 ^{CP}C1	Ir-5′-ACATT ITTTTTTCAGTCAC-3′ 3′-TGTAA^{CP}CAAAAAAGTCAGTG-5′	50	60
	Ir3C1 ^{CP}G1	Ir-5′-ACATT CTTTTTTCAGTCAC-3′ 3′-TGTAA^{CP}GAAAAAAGTCAGTG-5′	52	59
Set #2	Ir3G2 ^{CP}C2	Ir-5′-ACAAAAAA GAACAGTCAC-3′ 3′-TITTTTTT^{CP}CTTGTCAGTG-5′	48	55
	Ir3I2 ^{CP}C2	Ir-5′-ACAAAAAA IAACAGTCAC-3′ 3′-TITTTTTT^{CP}CTTGTCAGTG-5′	46	52
	Ir3C2 ^{CP}G2	Ir-5′-ACAAAAAA CAACAGTCAC-3′ 3′-TITTTTTT^{CP}GTTGTCAGTG-5′	50	57
	G1 ^{CP}C1	5′-ACATT GTTTTTTCAGTCAC-3′ 3′-TGTAA^{CP}CAAAAAAGTCAGTG-5′	47	
^{Br}U	T^{Br}U	Ir-5′-ACAAA AAAGAACAGTCAC-3′ 3′-TITTT^{Br}UTTCTTGTCAGTG-5′		
	A^{Br}U	Ir-5′-ACATT ATTTTTTCAGTCAC-3′ 3′-TITAA^{Br}UAAAAAAGTCAGTG-5′		

a. T_m is determined by monitoring the UV absorption of 1.5 μM DNA in 20 mM sodium phosphate, pH 7.0, 10 mM NaCl at 260nm from 90 ^{o}C to 15 ^{o}C.

b. T_m is determined by monitoring UV absorption of 20 μM DNA in 20 mM sodium phosphate pH 7.0, 10 mM NaCl at 413nm from 90 ^{o}C to 15 ^{o}C.

c. Ir3 represents the covalently tethered complex $[Ir(ppy)_2dppz3]^+$.

A-tract, but the purine and pyrimidine strands are flipped between the complements. ^{CP}C and ^{CP}G are placed in the pyrimidine strand of the A-tract and after the fifth thymine in the corresponding sequences of set #2. These two sets of IrOH3-tethered DNA assemblies would allow us to compare the transient hole and electron distributions between the purine and pyrimidine strands during DNA-mediated HT and ET, respectively.

6.3.2. Intercalation of the tethered Ir(III) complex. UV-visible spectra of the DNA assemblies with covalently tethered IrOH1 (Ir1-DNA) and IrOH3 (Ir3-DNA) have characteristic bands at 260nm, primarily from the DNA bases, and around 380~430nm from a mix of intraligand transition of dppz and the metal-to-ligand charge transfer (MLCT) band of the Ir complex.[27] As we observed previously and as is evident in Figure 6.2, the absorption spectra of $[Ir(ppy)_2dppz3]^+$ shows significant solvatochromic effects. Hypochromicity, as well as loss of original features in absorption spectra of the Ir(III) complexes are observed at both high energy intraligand (IL) and the low energy bands by switching from organic solvent to aqueous buffered solution. Upon tethering to the DNA single strand, the features of the absorption spectrum of IrOH3 at low-energy band can be resolved in aqueous buffer. The wavelength of the low-engergy band in Ir-DNA appears in between those of Ir(III) in buffer and MeCN, which is redshifted from that of the Ir complex in MeCN but blueshifted from that of the complex in aqueous solution. Two absorption maxima at 393nm and 413nm, which are broadened out in aqueous solution, are present to some extent in the case of Ir3-DNA, although they are still not well resolved and have been red-shifted ~10 nm compared to MeCN. The spectral features of the Ir complex upon tethering to DNA, in particular the hypochromicity, suggests that the

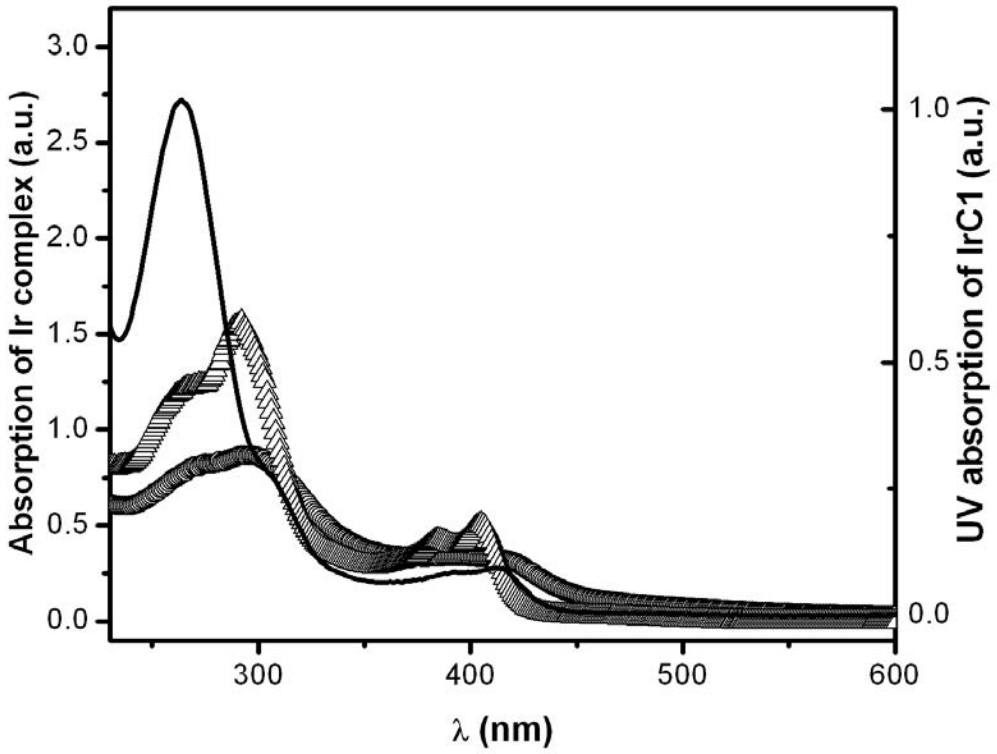

Figure 6.2. UV-vis spectra of Ir-DNA conjugate and free $[Ir(ppy)_2dppz']^+$ complex. Free Ir(III) complex (23 μM) in MeCN (triangle) and buffer (circle) (10 mM NaCl, 20 mM sodium phosphate, pH 7.0), as well as tethered to the DNA single strand **IrC1** (black line, 4.5 μM) in buffer, are used to measure the spectra.

dppz' may stack, at least partially, with the nucleic acid bases even in the single DNA strands, which, to some extent, may create a polar environment more like acetonitrile than water.

Melting temperatures (T_m) of Ir3-DNA assemblies also provide some evidence of intercalative stacking to stabilize the tethered duplex. Melting temperatures of DNA assemblies (1.5 μM) in set #1, as well as set #2, are found at 50 ~ 52 ^oC, by monitoring the characteristic A_{260} associated with base stacking from 90 ^oC to 15 ^oC reversibly. As shown in Figure 6.3 and Table 6.2, **Ir3G1/^{CP}C-1** has a T_m that is 5 ^oC higher than the same DNA sequence without tethered IrOH3, **G1/^{CP}C-1**. Furthermore, the absorption intensities at the MLCT band (A_{413}) of Ir3-DNA were measured at 413nm following the same temperature cycle. By fitting the data to a sigmoidal curve, the T_m(Ir) (temperature at half maximum of A_{413}) can obtained to characterize the melting of the Ir(III) complex from the DNA duplex. The T_m(Ir)s of Ir3-DNAs are observed around 60 ^oC as shown in Table 6.2. Remarkably, the T_m(Ir) increases an extra 7~8 ^oC from the T_m(DNA) of the same assemblies.[28] Interestingly, In the DNA assembly with a $[Ru(phen)_2dppz]^{2+}$ complex covalently tethered to DNA through a carboxylic acid functional group on the intercalative dppz ligand, similar T_m enhancement was observed and assigned to stabilization of the duplex due to the intercalation of dppz.[29] Additionally, hypochromicity at the MLCT band occurs upon DNA annealing. A_{413} decreases 13% when Ir3-DNA is annealed to form DNA duplex. Thus, the increase in T_m(Ir) indicates that the Ir complex stabilizes the end of the DNA duplex from separating even after much of the duplex has been denatured. Certainly the duplex stabilization and the hypochromicity in the MLCT band support the idea that the tethered IrOH3 complex can

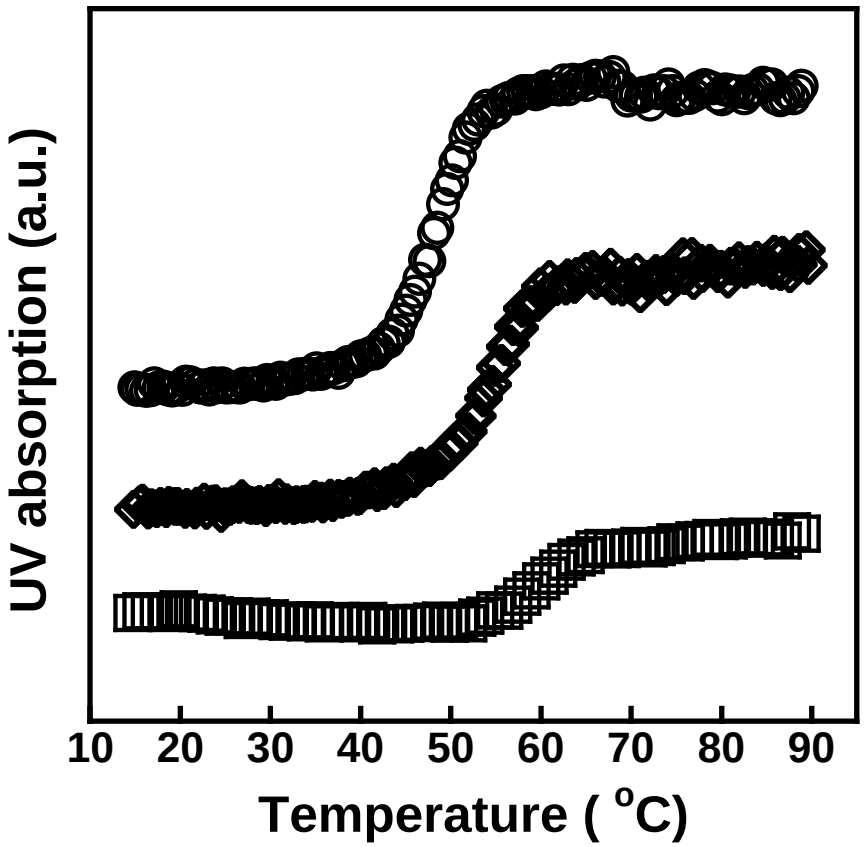

Figure 6.3. Melting temperatures of DNA duplexes with or without covalently tethered Ir(III) complex. (*top*) 1.5 μM of G-1/^{CP}C-1; (*middle*) 1.5 μM of IrG-1/^{CP}C-1; (*bottom*) 20 μM of IrG-1/^{CP}C-1. The UV absorption is monitored at 260nm for 1.5 μM DNA assemblies and at 413nm for 20 μM IrG-1/^{CP}C-1.

adopt an intercalation mode. Sigmoid melting temperature data are not available for IrCOOH1.

6.3.3. IrOH1 cannot promote electron migration upon being covalently tethered to DNA oligonucleotides. Irradiation of DNA assemblies (Table 6.1) with covalently tethered IrOH1 up to 1 h cause little damage of either ^{CP}C or ^{CP}G as shown in Figure 6.4. Only 2% of ^{CP}C decomposition is observed after 1 h irradiation of Ir1-DNA, which cannot compete with decomposition of ^{CP}C in the DNA assemblies without IrOH1. Moreover, no decomposition of ^{CP}G is observed in **Ir1-C**. Redox potentials of excited state of $[Ir(ppy)_2dppz1]^+$ have enough driving force to oxidize guanine and indeed non-covalently bound Ir1 has been observed to decompose both ^{CP}C and ^{CP}G upon UV irradiation. The lack of ring opening reaction in Ir1-DNA conjugates may be due to poor intercalation of dppz1. Dppz1 in IrOH1 has an ether functional group at C11 of dppz ligand, which has the tetrahedral sp^3 hybridization, instead of planar sp^2 orbitals in the carbonyl group of dppz2 in Ir2 or sp orbitals in acetylene group of dppz3 in Ir3. Tetrahedral glycol group may prevent dppz1 from intercalating deeply into DNA base stacking, especially in the case of Ir1-DNA conjugates, which have an extra hindrance associated with the tethering. Although the Ir1-DNA assemblies exhibit $T_m \sim 5^oC$ higher than those without tethered IrOH1 (table 6.1), this could reflect the groove binding of the complex or partial intercalation of dppz ligand within DNA, which cannot result electronic coupling efficient enough to trigger the electron and hole injection to DNA. Different lengths of the amino-end alkyl linkers are applied to the IrOH1-DNA coupling in order to improve the flexibility of the linkage and potentially the intercalation of IrOH1. However, C9, C5, C4 and C3 alkyl linker do not show much difference (data not

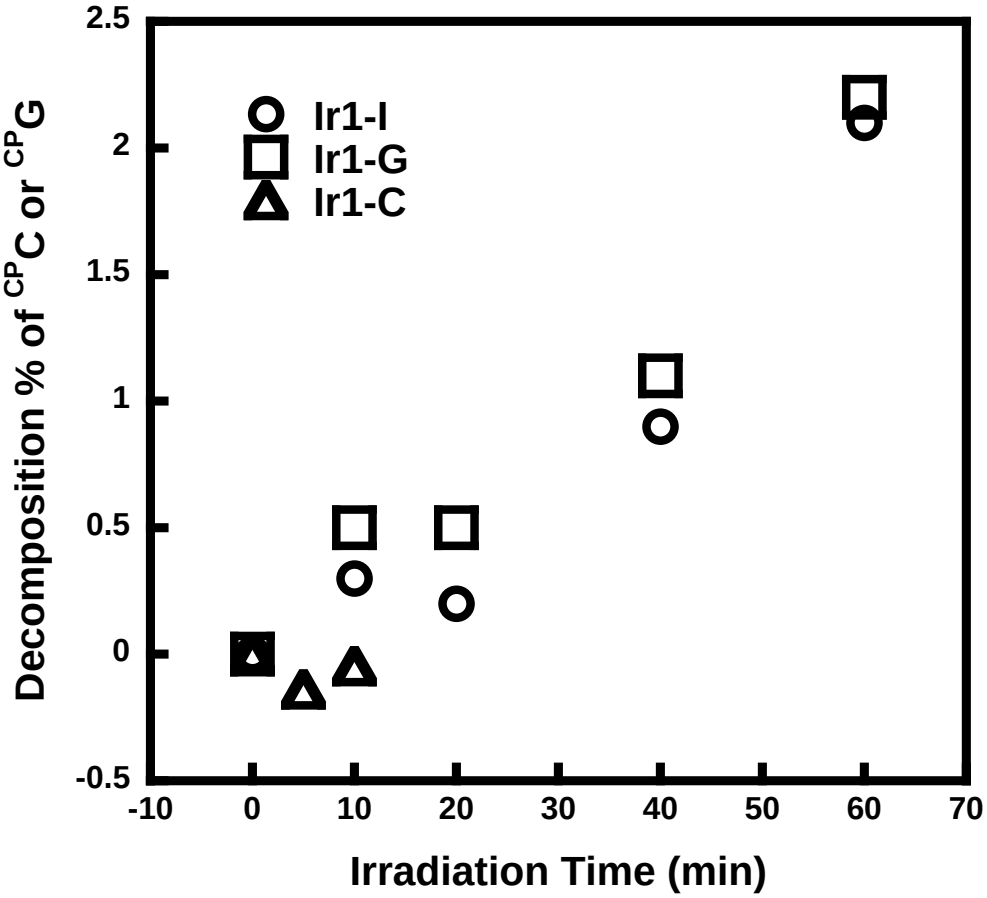

Figure 6.4. Photoredox reaction of ^{CP}C or ^{CP}G in Ir1-DNA. 5μM Ir1-DNA assemblies with C9 diamino-alkyl linker are irradiated at 380 nm in buffer (50 mM NaCl, 20 mM sodium phosphate, pH 7.0). Details are seen in experimental.

shown) in terms of ^{CP}C or ^{CP}G decomposition. No decomposition of either ^{CP}C or ^{CP}G is observed from photolysis of Ir1-DNA assemblies with various linkers.

6.3.4. IrOH3 initializes DNA-mediated hole transport. DNA assemblies with the covalently tethered IrOH3 complex in set #1 have either a ^{CP}C or a ^{CP}G positioned within the A-tract at least 3 base pairs away from ^{CP}C or ^{CP}G. Upon irradiation of IrOH3 at 380nm, in these assemblies both cyclopropylamine-substituted bases are seen to decompose linearly with an irradiation time of $\leq$1 h as shown in Figure 6.5. In **Ir3C1-^{CP}G1** 46% of ^{CP}G is decomposed after 1 h by the irreversible oxidative ring opening reaction. ^{CP}C decomposition is also observed in both assemblies, **Ir3I1-^{CP}C1** and **Ir3G1-^{CP}C1**. Notably, however, duplex **Ir3I1-^{CP}C1** exhibits more efficient decomposition (35% after 1 h) than does **Ir3G1-^{CP}C1** (10% after 1 h). The enhanced ^{CP}C decomposition in the duplex with base pairing to inosine, a guanine derivative of higher oxidation potential, is a characteristic feature of ^{CP}C oxidation.[18] The higher ring opening yield observed in **Ir3I1-^{CP}C1** versus **Ir3G1-^{CP}C1** is explained by the lower competition for low energy hole traps with the inosine-containing assembly versus the guanine-containing assembly. Efficient photooxidation of ^{CP}C by the IrOH3 complex might be surprising based upon the excited state reduction potential of the Ir complex (E^{*}_{red} = 1.64 V vs NHE).[26] However, previous studies have shown that purine stacking in the duplex can significantly reduce the oxidation potentials of the DNA bases.[27,30] Thus it is reasonable to consider that the oxidation potential of ^{CP}C in **Ir3I1-^{CP}C1** and **Ir3G1-^{CP}C1** is lowered enough to be oxidized by the excited state of the Ir complex. With photoactivation, then, using this tethered photooxidant both ^{CP}G and ^{CP}C can be oxidized from a distance through DNA-mediated HT.

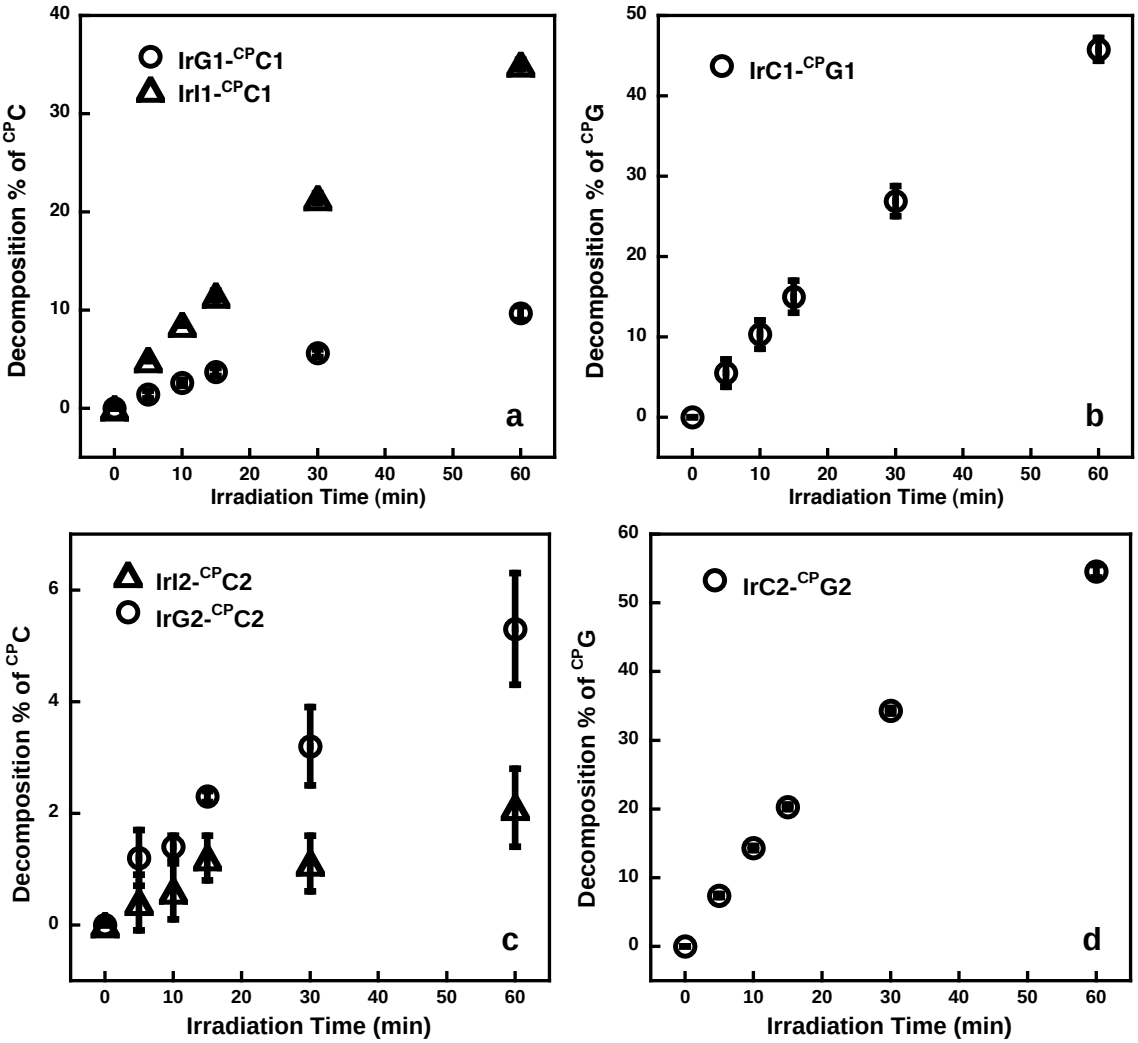

Figure 6.5. Redox decomposition of cyclopropylamine-substituted DNA bases upon photoirradiation of the tethered IrOH3. Percentages of decomposition in assemblies sets #1 (a) and #2 (c), as well as those of ^{CP}G in sets #1 (b) and #2 (d). The error bars are obtained over 3 sets of individual experiments.

6.3.5. DNA-mediated electron transport by photoexcited IrOH3. In set #2 versus set #1, with respect to the Ir(III)-tethered end, the A-tract is flipped between the two complementary strands. ^{CP}G and ^{CP}C are thus positioned in the pyrimidine strands of the A-tract and are located after the sixth thymine (Table 6.2). In this set of assemblies, oxidative decomposition of ^{CP}G in **Ir3C2-^{CP}G2** is observed upon irradiation at 380nm and has comparable efficiency (55% after 1 h) to that of **Ir3C1-^{CP}G1**. Photoexcitation of the Ir complex in set #2 thus shows similar decomposition yields to set #1. As expected, the variation in yield with distance is shallow and the electronic coupling between the bound Ir complex and the DNA base pairs certainly is not changed.

Interestingly, ^{CP}C in both **Ir3I2-^{CP}C2** and **Ir3G2-^{CP}C2** are also effectively decomposed upon irradiation of the distally tethered Ir(III) complex, but now the efficiency of charge transport in the inosine-containing duplex is equivalent to or lower than that of the guanine-containing duplex (Figure 6.5). Decomposition efficiencies of ^{CP}C in this series are significantly lower than for series #1 where the ^{CP}C is embedded within the purine strand. The increased separation from the Ir center may be a contributor to the lowered efficiency, but the switch in efficiency between the guanine-containing duplex and the inosine-containing duplex indicates that a different mechanism for charge transport must be involved. A similar phenomenon is observed in the case of photoactivation of a platinum diimine complex with ^{CP}C-containing duplexes.[30] The switch to give greater decomposition with ^{CP}C paired to guanine versus inosine supports the idea that for the transport through pyrimidines it is electron transport that occurs. In the pyrimidine series, set #2, ^{CP}C is reduced by the excited state of the distally bound IrOH3. The flanking pyrimidines likely do not efficiently decrease the oxidation potential

of ^{CP}C by base stacking[31] and the pyrimidine bridge provides a viable low energy path for electron transport. Hence, in the ^{CP}C-containing duplexes of set #2, the reductive ring opening reaction of ^{CP}C effectively competes with ^{CP}C oxidation. Therefore, upon direct irradiation, the covalently tethered Ir complex can promote both DNA-mediated HT and ET, probed by decomposition of ^{CP}G and ^{CP}C, respectively.

These results are reasonable to consider in the context also of other studies of DNA-mediated electron transport. Previous studies using a derivative of *N,N,N',N'*-tetramethyl-1,5-diaminonaphthalene (TMDN) as photoreductant and ^{Br}U as an electron trap have shown that ET through intervening a thymine doublet are ~3 times more efficient than through an adenine doublet.[32] An tentative proposal based upon LUMO overlap of nucleobases as electron carriers are introduced to explain both the sequence and direction dependence of ET through DNA. The relative low reduction potential and protonation rate of $T^{-\bullet}$ make thymine the major conduit for ET, which is presumably the reason why reduction of ^{CP}C via ET is preferred when it is stacking with thymines in the DNA assemblies of set #2.

6.3.6. ^{Br}U is reduced by IrOH3 with a reductive flash-quench technique.

Upon direct photolysis, Reductive ring opening on ^{CP}C is therefore observed in Ir3-DNA assemblies. However, the efficiencies of ^{CP}C reduction are not high enough to study the features of ET, e.g., distance and sequence dependence. Further optimization of Ir3-DNA system is required. One way to improve the efficiency of ET in Ir3-DNA is to use a flash-quench technique, which has been extensively applied to study protein electron transfer and DNA-mediated HT with Ru(II) complex.[16,33] Upon reductive quenching by sodium ascorbate, a reduced Ir complex $[Ir^{II}(ppy)_2(dppz3^-)]^+$ (Ir(II)) can be generated *in situ*. The

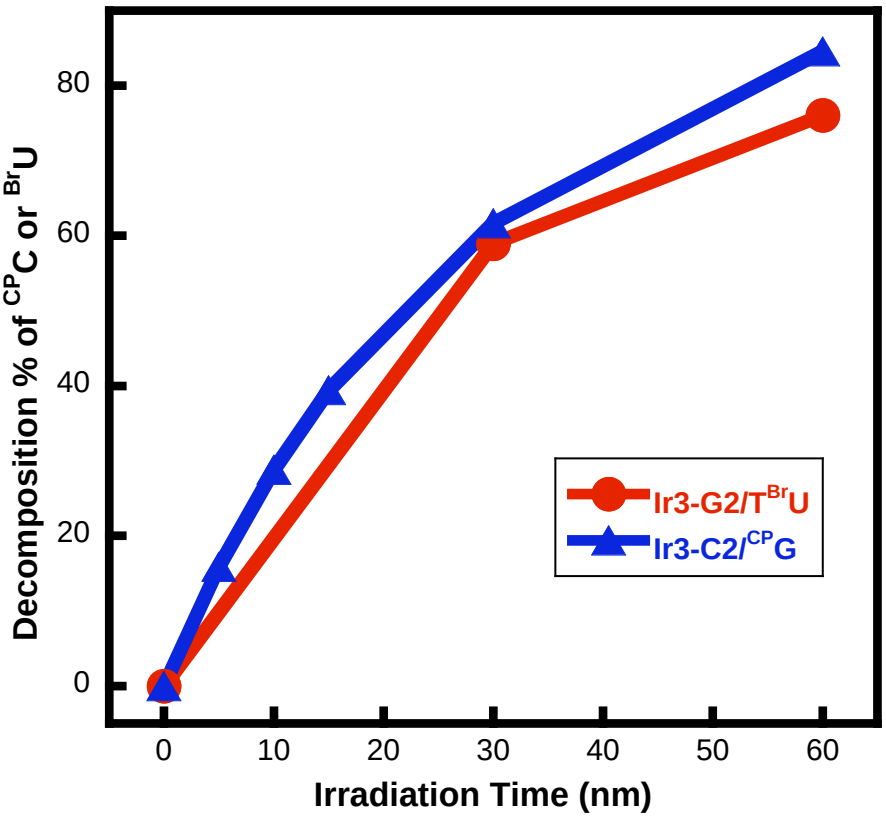

Figure 6.6. Oxidation of ^{CP}G and reduction of ^{Br}U via DNA-mediated HT and ET from distant Ir complex. Reductive flash-quench technique is applied to generate ground state **Ir(II)** complex *in situ* in order to trigger reductive chemistry of ^{Br}U to a comparable efficiency as oxidative decomposition of ^{CP}G. Irradiation is conducted at 365 nm in presence of 10 μM DNA and 200 mM sodium ascorbate.

ground state species should have much a longer lifetime than excited IrOH3 (Ir*), which may enhance the electron injection yield of Ir3-DNA. However, since the reduction potential (E_{red})of Ir(II) is shifted 200 mV to the positive field of Ir*, ^{Br}U with E_{red} 60 mV lower than that of thymine,[34] is incorporated into the Ir3-DNA assemblies (**T^{Br}U** and **A^{Br}U**) as the electron trap instead of ^{CP}C (Table 6.2). **T^{Br}U** contains the same sequence of Ir3G2-^{CP}C2, except that the third thymine in A-tract is substituted by ^{Br}U and ^{CP}C is replaced by a C. In **A^{Br}U**, the A-tract is flipped between the two complements and the third adenine in purine strand is substituted by ^{Br}U. **T^{Br}U** and **A^{Br}U** are thus designed to explore the sequence dependence of ET by this flash-quench assay. Upon reduction, ^{Br}U forms uridine radical by releasing bromide anion and leads to a strand break after a cascade reactions with piperidine.[32] In our reductive quenching essay, ^{Br}U-containing Ir3-DNA assemblies are irradiated in the presence of ascorbate followed by enzyme digestion to yield deoxynucleosides. Reduction of ^{Br}U is monitored by the peak area of ^{Br}U from HPLC analysis.

As shown in Figure 6.6, ^{Br}U is reduced by irradiating **T^{Br}U** in the presence of ascorbate. Decomposition efficiencies of ^{Br}U and ^{CP}G upon reduction and oxidation, respectively, are comparable. After 30 min and 1 h irradiation, 59.0% and 76.1% of ^{Br}U is reductively decomposed by Ir(II), respectively, while 61.7% and 84.6% of ^{CP}G is oxidatively ring-opened by Ir*. Thus, the observation window is enlarged wide enough to study the variations in ET.

The decomposition efficiency of ^{Br}U is correlated to both the intensity of incident light and the concentrations of ascorbate (Figure 6.7). The reduction efficiency of ^{Br}U is enhanced by irradiation with more intense incident light at 365nm (red line in Figure 6.7).

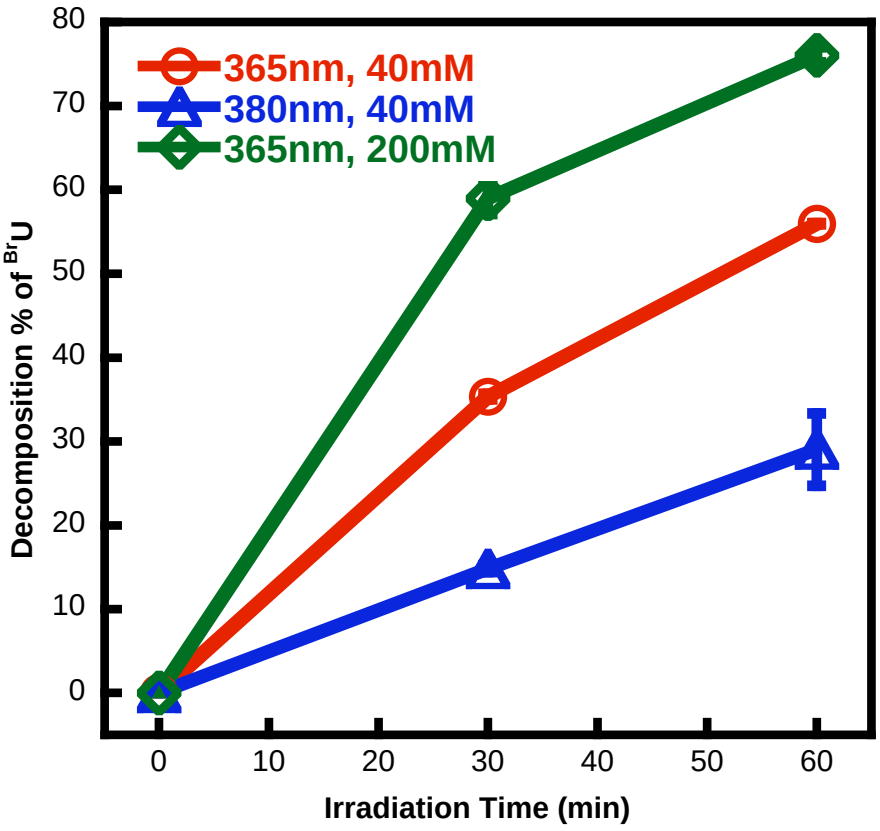

Figure 6.7. Reduction of ^{Br}U via flash-quench technique is correlated to the intensity of incident light and concentration of reductive quencher. The wavelength of incident light and [ASB] are indicated in the figure. Power of light at 365nm is 13mW and that at 380nm is 9 mW. Other experimental details are seen in materials and methods.

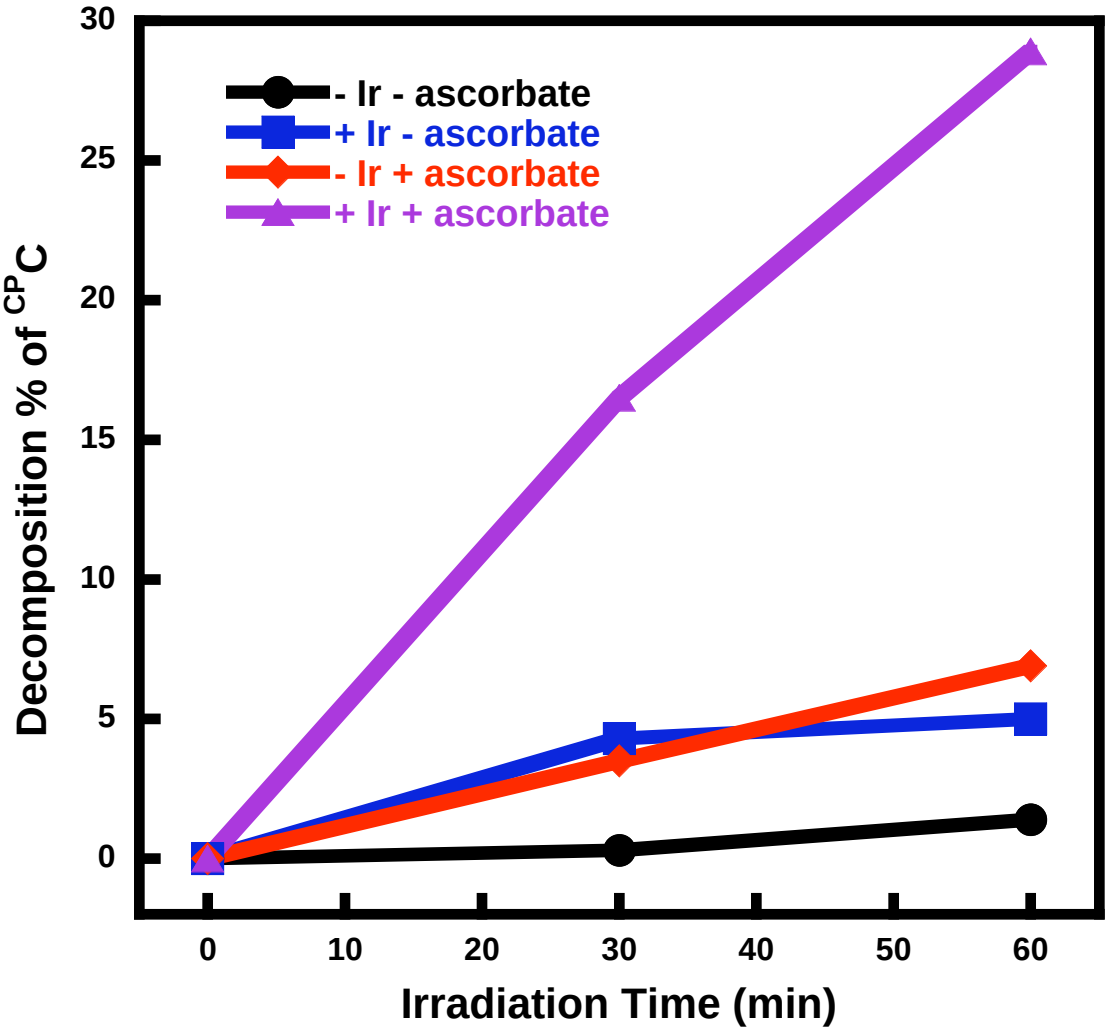

Figure 6.8. Control of reductive flash-quench experiments. -Ir and +Ir indicate the DNA duplex without and with the tethering Ir complex, respectively. - ascorbate and + ascorbate represent the presence and the absence of sodium ascorbate as a reductive quencher. Photolysis is conducted in the presence of 10 μM DNA and 40 mM sodium ascorbate if added. Other experimental details are seen in materials and methods.

Furthermore, the fluorescence of Ir3 in MeCN exhibits incremental quenching with higher concentration of ascorbate (data not shown), ^{Br}U is reductive decomposed more efficiently in presence of ascorbate with higher concentration. An extra 20% decomposition of ^{Br}U is observed after 1 h irradiation at 365nm by increasing the ASB concentration from 40 mM to 200 mM. The same flash-quench experiments are also conducted on the samples with or without tethered Ir complex and in the absence and presence of ascorbate as controls (Figure 6.8). No decomposition of ^{Br}U is observed in absence of either tethered IrOH3 or ascorbate or both. Efficient reduction of ^{Br}U requires the presence of tethered IrOH3 and ascorbate, which confirms that the distant decomposition of ^{Br}U is induced via ET from Ir(II) generated *in situ* by a reductive flash-quench technique. Thus as shown in Scheme 6.1, DNA-mediated ET and HT in Ir3-DNA assemblies can be triggered by either direct photolysis or a flash-quench technique. Upon direct photolysis, excited IrOH3 complex can undergo charge separation and inject an electron to reduce ^{CP}C or/and a hole to oxidize ^{CP}G over a long molecular distance. On the other side, in the presence of an external quencher, e.g. ascorbate, a reduced ground state Ir(II) is generated *in situ* and can serve as a reductant. Reduction of distant ^{Br}U is observed via DNA-mediated ET from tethered Ir(II).

Model system of ^{Br}U-containing Ir3-DNA is also applied further to study the features of DNA-mediated ET. In **T^{Br}U** and **A^{Br}U**, ^{Br}U is incorporated into thymine strand and adenine strand, respectively, in order to probe the transient electron occupancy on purine and pyrimidine strands of an A-tract during DNA-mediated ET. As shown in Figure 6.9, ^{Br}U decomposes apparently more efficiently in **T^{Br}U** than in **A^{Br}U**. 26.7% of ^{Br}U in the adenine strands is consumed after 1 h irradiation at 365nm, which is only one-third of the

efficiency observed in **T^{Br}U**. The decomposition of ^{Br}U reflects the transient electron occupancy on the complemetary purine and pyrimidine strands in the A-tract. The distinction of ^{Br}U reduction efficiency in **T^{Br}U** and **A^{Br}U** illustrates that during DNA-mediated ET electron is distributed onto both complementary strands. The same phenomenon is observed also in DNA-mediated HT. The decompositions of ^{CP}C in both the adenine strands and thymine strands of an A-tract are observed by photolysis of the DNA assemblies with tethered anthraquinone as a photooxidant.[26] However, the decomposition of ^{Br}U is more efficient in **T^{Br}U**, when ^{Br}U is stacked within pyrimidine strands. Thus, the favorable reduction of ^{Br}U demonstrates that opposite to what has observed in HT, ET prefers pyrimidine strands. The energetically low E_{red} of thymine makes the overlaped LUMO in thymine stacking more accessible to electron migration.

6.4. Summary and implications

Two cyclometalated Ir(III) complexes have been therefore been covalently tethered to DNA oligonucleotides and provide both a photooxidant and photoreductant for studying DNA-mediated HT and ET. However, IrOH1 cannot properly intercalate within base stacking upon covalently tethered to DNA, which is presumably due to the disturbance of planar dppz from the functional group. In the case of IrOH3-tethered DNA assemblies, melting temperatures monitored at both the DNA absorption band and the MLCT band of IrOH3 indicate stabilization of the DNA duplex by the tethered IrOH3 complex, consistent with intercalation by the functionalized dppz. Thus the Ir complex, IrOH3, with extended dppz π-system, can provide consistent and effective electronic coupling with the DNA base pairs for both HT and ET. Upon photolysis, both the

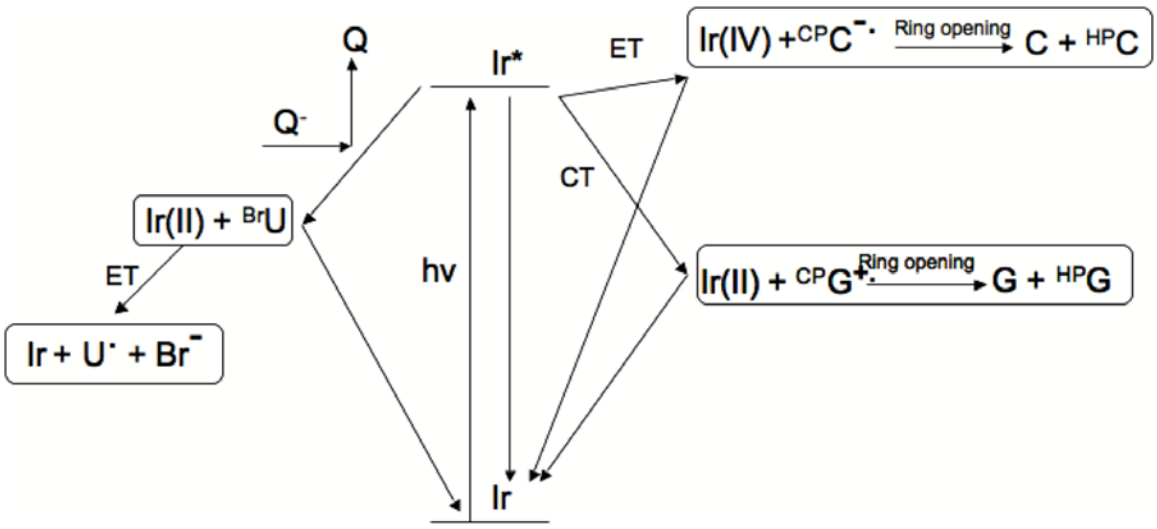

Scheme 6.1. DNA-mediated ET and HT in Ir3-DNA containing cyclopropyl-substituted bases or bromouracil (^{Br}U) as electron and hole traps. Upon direct photolysis, covalently tethered IrOH3 complex is excited to an excited state (Ir*). DNA-mediated ET is triggered by Ir* to reduce ^{CP}C and concomitantly HT is triggered to oxidize ^{CP}G over a long molecular distance. On the other side, in the presence of an external quencher, e.g., ascorbate, a reduced ground state Ir complex (Ir(II)) is generated *in situ* to serve as a reductant and reduction of distant ^{Br}U is observed via DNA-mediated ET from tethered Ir(II).

reduction of ^{CP}C and oxidation of ^{CP}G are promoted by DNA-mediated ET and HT from the distally DNA-bound IrOH3. Therefore, ET and HT can be initiated with the same photoredox probe and can be probed on a picosecond scale by ring-opening of cyclopropyl amine-substituted bases. The Ir-DNA assembly is a unique model system that allows us now to compare characteristics of DNA-mediated HT and ET directly in the same donor-bridge-acceptor system.

DNA-mediated ET is also studied by using ^{Br}U-containing Ir3-DNA duplexes. A reductive flash-quench technique is applied to generate reduced IrOH3 complex, Ir(II), as an *in situ* ground state reductant for DNA-mediated ET. Significant yield of ^{Br}U reduction in **T^{Br}U** is observed by ET from distally bound Ir(II) and is comparable to the efficiency of ^{CP}G oxidation in Ir3-DNA. Furthermore, this flash-quench assay is applied to explore the sequence dependence of DNA-mediated ET in an A-tract. Similar to HT through A-tract, electron radical is transiently distributed onto both complementary strands during migration. Interestingly, in the contrary to HT, ET prefers to the pyrimidine strands as a pathway for propagation. This preference in ET for the pyrimidine path is consistent with the lower energy of pyrimidines versus purine for reduction.

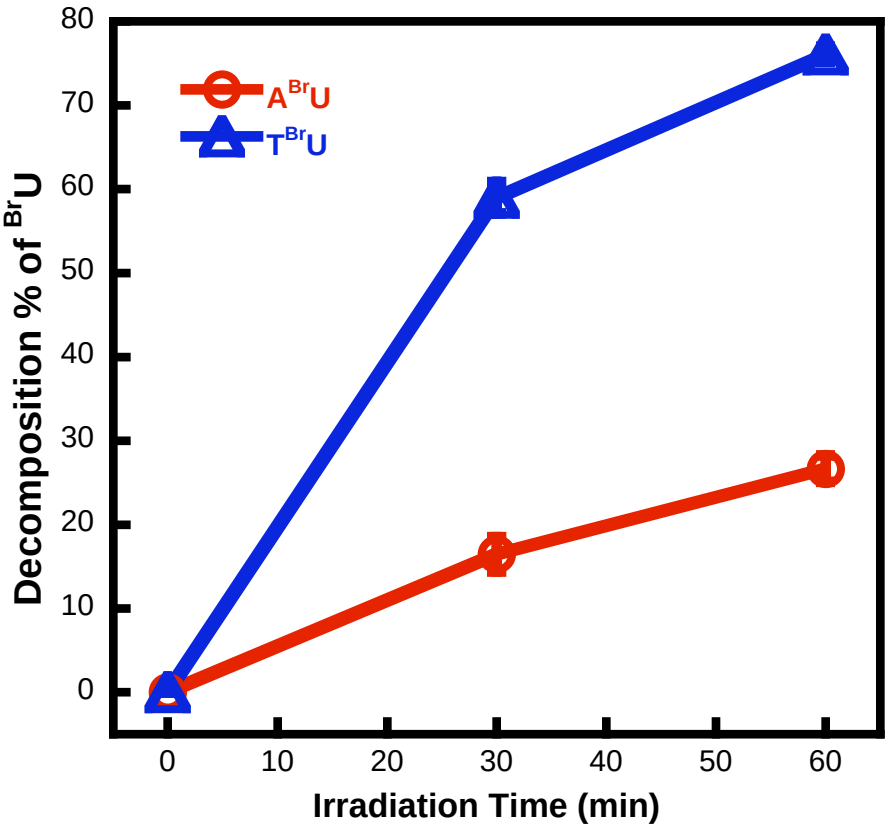

Figure 6.9. Sequence dependence of DNA-mediated ET probed by reduction of ^{Br}U. ET is initialized by reductive flash quenching technique with sodium ascorbate as a quencher. Photolysis is conducted in the presence of 10 μM DNA and 40 mM sodium ascorbate if added. Other experimental details are seen in materials and methods.

6.5. References

1. Watson, J.D., Crick, F.H.C. The structure of DNA *Cold Spring Harbor Symposia on Quantitative Biology* **1953**, *18*, 123-131.

2. Delaney, S., Barton, J. K., Long-range DNA charge transport *J. Org. Chem.* **2003**, *68*, 6475-6483.

3. Hall, D.B., Holmlin, R.E., Barton, J.K. Oxidative DNA damage through long range electron transfer *Nature* **1996**, *382***,** 731-735.

4. Núñez, M.E., Hall, D.B., Barton, J.K. Long range oxidative damage to DNA: effects of distance and sequence *Chem. Biol.* **1999**, *6*, 85-97.

5. Henderson, P.T., Jones, D., Hampikian, G., Kan, Y.Z., Schuster, G. Long-distance charge transport in duplex DNA: the phonon-assisted polaron-like hopping mechanism *Proc. Natl. Acad. Sci. USA* **1999**, *96*, 8353-8358.

6. Giese, B. Long-dstance electron transfer through DNA *Annu. Rev. Biochem.* **2002**, *71*, 51-70.

7. Takada, T., Kawai, K., Cai, X., Sugimoto, A., Fujitsuka, M., Majima, T. Direct observation of hole transfer through double-helical DNA over 100 Å *J. Am. Chem. Soc.* **2004**, *126*, 1125-1129.

8. Nakatani, K., Dohno, C., Saito, I. Modulation of DNA-mediated hole-transport efficiency by changing superexchange electronic interaction *J. Am. Chem. Soc.* **2000**, *122*, 5893-5894.

9. Yoo, J., Delaney, S., Stemp, E., Barton, J.K. Rapid radical formation by DNA charge transport through sequences lacking intervening guanines *J. Am. Chem. Soc.* **2003**, *125*, 6640-6641.

10. (a) Delaney, S., Yoo, J., Stemp, E.D.A., J.K. Barton Charge equilibration between two distinct sites in double helical DNA *Proc. Nat. Acad. Sci. USA* **2004**, *101*, 10511-10516. (b) O'Neill, M.A., Barton, J.K. Sequence-dependent DNA dynamics: The regulator of DNA-mediated charge transfer *Charge Transfer in DNA: From Mechanism to Application* Wagenknecht, H. A., ed.; Wiley: New York, **2005**, 27-75.

11. O'Neill, M.A., Barton, J.K. DNA charge transport: conformationally gated hopping through stacked domains *J. Am. Chem. Soc.* **2004**, *126*, 11471-11483.

12. O'Neill M.A., Barton, J.K. DNA-mediated charge transport requires conformational motion of the DNA bases: elimination of charge transport in rigid glasses at 77K *J. Am. Chem. Soc.* **2004**, *126*, 13234-13235.

13. (a) Williams, T.T., Dohno, C., Stemp, E.D.A, Barton, J.K. Effects of the photooxidant on DNA-mediated charge transport *J. Am. Chem. Soc.* **2004**, *126*, 8148-8158. (b) O'Neill, M.A., Becker, H.C., Wan, C., Barton, J.K., Zewail, A.H. Ultrafast dynamics in DNA-mediated electron transfer: base gating and the role of temperature *Angew. Chem. Int. Ed.* **2003**, *42*, 5896-5900.

14. Kelley, S.O., Barton J.K. Electron transfer between bases in double helical DNA *Science* **1999**, *283*, 375-381.

15. Augustyn, K., Shao, F., Genereux, J., Barton, J.K. Periodicities in DNA charge transport probed with N_2-cyclopropylguanine, a kinetically fast hole trap *Submitted* **2007**.

16. Stemp, E.D.A, Arkin, M., Barton, J. K. Oxidation of guanine in DNA by $Ru(phen)_2(dppz)^{2+}$ using the flash-quench technique *J. Am. Chem. Soc.* **1997**, *119*, 2921-2925.

17. Nakatani, K., Dohno, C., Saito, I. Design of a hole-trapping nucleobase: termination of DNA-mediated hole transport at N^2-cylcopropyldeoxyguanosine *J. Am. Chem. Soc.* **2001**, *123*, 9681-9682.

18. Shao, F., O'Neill, M. A., Barton, J. K. Long-range oxidative damage to cytosine in duplex DNA *Proc. Natl. Acad. Sci. USA* **2004**, *101*, 17914-17919.

19. Musa, O. M., Horner, J. H., Shahin, H., Newcomb, M. A kinetic scale for dialkylaminyl radical reactions *J. Am. Chem. Soc.*, **1996**, *118*, 3862-3868.

20. Carell, T., Meltzer, M.V. Excess electron transfer in DNA probed with flavin- and thymine dimer-modified oligonucleotides *Charge Transfer in DNA: From Mechanism to Application* Wagenknecht, H. A., ed.; Wiley, **2005**, 77-91.

21. Schwögler, A., Burgdorf, L.T., Carell, T. Self-repairing DNA based on a reductive electron transfer through the base stack *Angew. Chem. Int. Ed.* **2000**, *39*, 3918-3920.

22. Rokita, S.E., Ito, T. Chemical probing of reductive electron transfer in DNA *Charge Transfer in DNA: From Mechanism to Application* Wagenknecht, H. A., ed.; Wiley: New York, **2005**, 133-151.

23. Wagenknecht, H. A., Fiebig, T. Electron transfer and structural dynamics in DNA *Charge Transfer in DNA: From Mechanism to Application* Wagenknecht, H. A., ed.; Wiley: New York, **2005**, 197-223.

24. Ito, T., Rokita, S. E. Excess electron transfer from an internally conjugated aromatic amine to 5-bromo-2'-deoxyuridine in DNA *J. Am. Chem. Soc.* **2003**, *125*, 11480-11481.

25. (a) Giese, B., Carl, B., Carl, B, Carell, T., Behrens, C., Hennecke, U., Schiemann, O., Feresin, E. Excess electron transport through DNA: A single electron repairs more than on UV-induced lesion *Angew. Chem. Int. Ed.* **2004**, *43*, 1848-1851.

26. Shao, F., Lu, Wei., Elias, B., Barton, J.K. Synthesis and characterization of iridium (III) cyclometalated complexes: Insight into redox reactions with DNA oligonucleotides *manuscript in preparation*.

27. Shao, F., Augustyn, K.E., Barton, J.K. Sequence dependence of charge transport through DNA domains *J. Am. Chem. Soc*. **2005**, *127*, 17445-17452.

28. Lo, K.K., Chung, C., Zhu, N. Nucleic acid intercalators and avidin probes derived from luminescent cyclometalated iridium(III)-dipyridoquinoxaline and –dipyridophenazine complexes. *Chem. Eur. J.* **2006**, *12*, 1500-1512.

29. Although 20 μM solution of DNA samples, instead of 1.5 μM, are used in T_m(Ir) experiment in order to achieve measurable absorption intensities, the enhancement due to the concentration increments should be less than 4 ^oC by calculation.

30. Kitamura, Y., Ihara, T., Okada, K., Tsujimura, Y., Shirasada, Y., Tazaki, M., Jyo, A. Asymmetric cooperativity in tandem hydridization of enantiomeric metal complex-tethered short fluorescent DNA probes *Chem. Commun.* **2005**, 4523-4525.

31. Lu, W., Vicic, D.A., Barton, J. K. Reductive and oxidative DNA damage by photoactive platinum(II) intercalators *Inorg. Chem.* **2005**, *44*, 7970-7980.

32. Voityuk A. A., Jortner J., Bixon M., Rösch N. Energetics of hole transfer in DNA *Chem. Phys. Lett.*, **2000**, *324*, 430-434.

33. Ito, T., Rokita, S.E. Criteria for efficient transport of excess electrons in DNA *Angew. Chem. Int. Ed.* **2004**, *43*, 1839-1842.

34. Babini, E., Bertini, I., Borsari, M., Capozzi, F., Luchinat, C., Zhang, X. Y., Moura, G. L. C., Kurnikov, I. V., Beratan, D. N., Ponce, A., Di Bilio, A. J., Winkler, J. R., Gray, H. B. Bond-mediated electron tunneling in ruthenium-modified high-potential iron-sulfur protein *J. Am. Chem. Soc.* **2000**, *122*, 4532-4533.

35. Wagner, C., Wagenknecht, H. Reductive electron transfer in phenothiazine-modified DNA is dependent on the base sequence *Chem. Eur. J.* **2005**, *11*, 1871-1876.

CHAPTER 7

Methylation Effects on DNA-Mediated Hole Transport

7.1. Introduction.

A small proportion of DNA and RNA bases in mammalian genomes can undergo an enzyme-mediated chemical modification to generate methylated bases, such as 5-methylcytosine (mC) and N^6-methyladenine, by a variety of DNA methyltransferases.[1] Only 5-methylcytosine is physiologically methylated at the C5 of the pyrimidine, instead of exocyclic amines in other bases. Cytosine methylation occurs primarily at cytosines that are followed by a guanine (CpG); however, most of CpG islands in promoter region remain intact.[2] These non-random distributions of methylation patterns have profound effects on the mammalian genome, including transcriptional repression by inhibition of transcription factor binding or the recruitment of methyl-binding proteins, X chromosome inactivation, imprinting and the suppression of parasitic DNA sequences.[3,4] Furthermore, cytosine methylation defines hotspots for oxidative damage to DNA,[5] which is suspected of underlying aging and carcinogenesis.[6] Up to now, many human cancers have been found out to be related to abnormal methylation patterns, such as global hypomethylation companied with region-specific hypermethylation.[7]

One-electron oxidation of DNA over long distances have been studied for about 40 years.[8] Based upon results from our lab[9] and the others[10], distant guanine oxidation is triggered by a DNA-mediated hole transport (HT), which can propagate the hole, a cation radical, through DNA base stacking even over 200 Å.[11] The efficiency of hole migration is sensitive to the base stacking of DNA helixes.[12] One of the reasons is that the oxidation potentials of DNA base can be altered by stacking and base pairing to other bases. In

particular, guanines in G_n sequence (n = 2,3) are prone to oxidation because hole delocalization slightly lowers its energy, which facilitates trapping the hole at G_n sites.[13] Recently it has been reported that methylation reduces the ionization potential (I_P) of cytosine from 8.79 to 8.50 eV.[14] We were interested in determining the electronic effects on mC could be transmitted to paired guanine and cause a rate acceleration in the oxidation of guanine, which is partnered with mC.[15] Furthermore, mC could also affect the efficiency of oxidative damage at its paired guanine via proton coupled electron transfer (PCET).[16] One the other hand, abnormal DNA base pairs, such as DNA mismatches, affect the dynamic motion of base pairs and significantly attenuates HT through DNA duplex by disturbing the well-defined base stacking.[17]

5-Methylcytosine:guanine is not a normal Watson-Crick DNA base pair, although the hydrogen bonds between G:C have remained in G:mC. Methyl substitution on C5 of pyrimidine increases the hydrophobic area, which may influence the base stacking in DNA duplex[17] and lead an effect on HT. Since it is suspected that there is a relationship between the biological roles of mC and condensation of irreversible G damage by the DNA-mediated HT, it is intriguing to understand the methylation effects on HT, which may throw some light on both the mechanism of HT and biological behaviors of mC. In this chapter, a set of DNA assemblies with covalently tethered Rh complex as photooxidant, are substituted with mC strategically at a variety of positions, in order to investigate the effects of methylation on DNA-mediated HT.

7.2. Materials and methods.

7.2.1. Preparation of DNA Oligonucleotides. DNA strands without covalently tethered Rh complex were prepared by solid phase synthesis on an ABI 392 DNA/RNA synthesizer. After deprotection and spontaneous cleavage from the beads by NH_4OH at 60 ^oC, the strands with a 5'-trityl end were purified by reverse phase (RP) HPLC using a Dynamax 300 Å C18 reverse-phase column (Rainin) with method as 5% ~ 35% MeCN/50 mM NH_4OAc over 30 minutes. Then, the trityl group was deprotected by suspending the strands in 80% acetic acid at room temperature for 20 minutes. The strands were precipitated by ethanol and purified by RP-HPLC (5% ~20% MeCN/50 mM NH_4OAc over 30 minutes). The DNA strands were confirmed by MALDI-MS and suspended in 10 mM NaCl, 20 mM sodium phosphate buffer (pH 7.0). The concentrations of DNA strands were quantitated by UV-visible absorption spectroscopy on a Beckman DU 7400 Spectrophotometer. The extinction coefficients were determined by the sum of those of DNA bases in the strands. ε_{260} ($M^{-1}cm^{-1}$) are: adenine (A) = 15,400; guanine (G) = 11,500; cytosine (C) = 7400; thymine (T) = 8700; 5'-methyl-cytosine (mC) = 5700.

$[Rh(phi)_2(bpy')]Cl_3$ (phi, 9,10-phenanthrenequinone diimine; bpy', 4-methyl-4'(butyric acid)-2,2'-bipyridine) was synthesized and purified by following the established protocols.[18,19] The complex was confirmed by H^1-NMR and TOF-MS. The Rh-tethered strands (Rh-DNA) were synthesized as described previously[20] and were purified by reverse-phase (RP) HPLC. After resuspending in 10 mM NaCl, 20 mM

sodium phosphate buffer (pH 7.0), Rh-DNA samples were quantitated by either the extinction coefficients of DNA bases mentioned or that of the Rh complex at 350nm (ϵ= 23,600 $M^{-1}cm^{-1}$). DNA duplexes were prepared by annealing the same equivalents of the two complementary strands gradually from 90 ^{o}C to room temperature over 2 hours.

7.2.2. Melting temperatures. mC containing duplexes without tethered Rh complex were used to obtain melting temperatures. Absorbance at 260 nm of 1.3μM pre-annealed duplexes was measured at each degree from 10^{o}C to 90^{o}C on the Beckman UV-vis spectrometer by increasing the temperature (0.5^{o}C min^{-1}). The melting temperature (T_m) values reflect the midpoints of the transition by fitting the melting profiles with a sigmoidal expression in Origin.

7.2.3. Irradiation and gels. The complementary strands of Rh-DNA (approximately 100 pmol) were radioactively labeled at 5'-end by incubation γ-^{32}P-ATP with T4 polynucleotides kinase at 37 ^{o}C for 1 hr.[18] The labeled strands were treated with 10% piperidine at 90 ^{o}C for 30 mins and dried down before being purified by a preparative 18% denaturing polyacrylamide gel electrophoresis (PAGE) with 1∗ (TBE) buffer. Afterwards, the radioactive DNA was cut from the gel, extracted by 100mM Tris-Cl, 10 mM EDTA (pH7.5) buffer and eluted from a Nensorb 20 cartridge.

The labeled strands (500,000CPM) were annealed with Rh-tethered strands at a concentration of 4μM duplexes in 10mM NaCl and 20mM Na_3PO_4 (pH 7.5) by cooling gradually from 90 ^{o}C to room temperature over 2hr. As shown in Figure 7.1, 30μl aliquots were irradiated at either 365nm for 0 or 60 min or at 313nm for 10 min on a

1000W Hg(Xe) lamp equipped with a monchromator. Irradiation samples at 365nm were followed by 10% piperidine treatment at 90 ^{o}C for 20 min and washed with 20μl H_2O twice. Afterwards, all of the aliquots were suspended in dyes and heated at 90 ^{o}C for 5 min before loading on a 18% denaturing polyacrylamide gel in 1∗TBE buffer. The damage patterns of radioactive-labeled strands were visualized by phosphorimagery and quantitated by ImageQuant, v 4 (Molecular Dynamics). The yield of the oxidation at guanine sites was determined by substracting the intensity of the damage patterns in the sample without irradiation from those of the irradiated samples.

7.3. Results.

7.3.1. Design of DNA assemblies with various methylation patterns. A series of 24 mer DNA assemblies were synthesized with the covalently tethered Rh complex as shown in Table 7.1 and Figure 7.1. A four base segment (5'-ACGA-3') was placed at the tethering end to facilitate the intercalation of the Rh complex. Two guanine doublets (GG) in the complementary strands with difference distances to the charge injection site were placed as potential oxidation sites. Since it is interesting to observe HT efficiency through methylated CpG sequence, a 5'-GCG-3' (CpG) segment was inserted between the two guanine doublets. In order to focus on the effects of methylation on HT, all of the assemblies have the same sequence, except the locations and number of mC. **Rh-1** in section 0 is a control duplex with no mC. In section 1, **Rh-2** to **Rh-4** have mC opposite to either 5' or 3' or both guanines in the proximal doublets. Similar methylation patterns in

Table 7.1. DNA sequences for studying methylation effects on DNA-mediated HT

# Section	# DNA	Sequence
# 0 (no mC)	Rh-1	Rh-5′-ACGAGCCGTATCGCTATGCCGATA-3′ 3′-TGCTCGGCATAGCGATACGGCTAT-5′*[a]
	Rh-2	Rh-5′-ACGAGCXGTATCGCTATGCCGATA-3′[b] 3′-TGCTCGGCATAGCGATACGGCTAT-5′*
# 1 (proximal)	Rh-3	Rh-5′-ACGAGXCGTATCGCTATGCCGATA-3′ 3′-TGCTCGGCATAGCGATACGGCTAT-5′*
	Rh-4	Rh-5′-ACGAGXXGTATCGCTATGCCGATA-3′ 3′-TGCTCGGCATAGCGATACGGCTAT-5′*
	Rh-5	Rh-5′-ACGAGCCGTATCGCTATGCXGATA-3′ 3′-TGCTCGGCATAGCGATACGGCTAT-5′*
# 2 (distal)	Rh-6	Rh-5′-ACGAGCCGTATCGCTATGXCGATA-3′ 3′-TGCTCGGCATAGCGATACGGCTAT-5′*
	Rh-7	Rh-5′-ACGAGCCGTATCGCTATGXXGATA-3′ 3′-TGCTCGGCATAGCGATACGGCTAT-5′*
	Rh-8	Rh-5′-ACGAGCCGTATXGXTATGCCGATA-3′ 3′-TGCTCGGCATAGCGATACGGCTAT-5′*
# 3 (middle)	Rh-9	Rh-5′-ACGAGCCGTATCGCTATGCCGATA-3′ 3′-TGCTCGGCATAGXGATACGGCTAT-5′*
	Rh-10	Rh-5′-ACGAGCCGTATXGXTATGCCGATA-3′ 3′-TGCTCGGCATAGXGATACGGCTAT-5′*

a. * = ^{32}P.

b. X = mC.

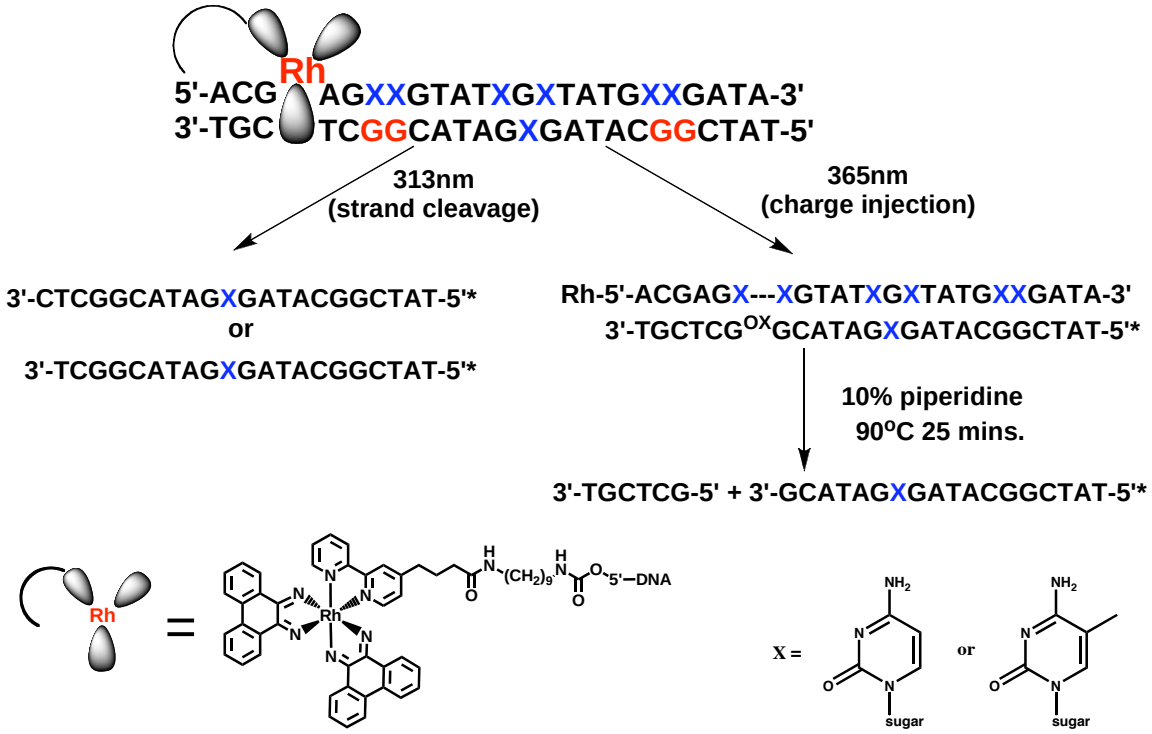

Figure 7.1. Methylation effects on oxidative guanine damage via DNA-mediated long-range hole transport is studied by UV irradiation of $[Rh(phi)2(bpy')]^{3+}$ at either 313nm or 365nm. Upon 313 nm irradiation, direct strand-cleavage occurs at intercalation site; while G damage is revealed by hot piperidine treatment after exciting the Rh complex at 365nm. In a generalized sequence of DNA duplexes with covalently tethered Rh complex, potential mC substitution sites are marked as X. Detail sequences of ten assemblies are listed in Table 7.1. Structure of the photooxidant $[Rh(phi)2(bpy')]^{3+}$ tethered to DNA through a diamino-functionalized nine carbon linker is shown on the left bottom. Structures of C and mC are shown at the right bottom.

distal guanine doublets are employed in **Rh-5** to **Rh-7** (section 2). In **Rh-8** to **Rh-10**, cytosines in CpG segment are methylated as shown in section 4.

7.3.2. Melting temperature. DNA assemblies, **Rh-1** to **Rh-10** show normal sigmoidal melting curves (data not shown) and the T_m of the ten assemblies are listed in Table 7.2. The T_m of **Rh-1**, the only duplex without mC, is 61.4 ^oC and relatively high for a 24mer duplex, probably due to the high content of GC base pairs. The T_m of the other methylated duplexes, **Rh-2** to **Rh-10**, are 3 to 5 ^oC higher than **Rh-1**. ΔT_m, which is the difference of T_m between **Rh-1** and the other methylated duplexes, are not found to be related to the number of mC in the duplexes. **Rh-4** and **Rh-7** with two mC, have similar or even lower T_m than the assemblies with one mC. However, multiple methylation at the middle GCG segment in **Rh-8** and **Rh-10** yields a relatively high ΔT_m, almost 5 ^oC in both cases. Enhancement of the T_m is more pronounced by methylation at CpG sequence, rather than mC doublets.

7.3.3. Damage patterns in mC-containing DNA duplexes via photoirradiation. As shown in Figure 7.1, irradiation of DNA assemblies, **Rh-1** to **Rh-10**, are conducted at both 313nm, which causes directly strands cleavage at the intercalation site, and at 365nm, which initializes charge injection to DNA base pair stacking and the guanine damage induced by HT is revealed by treating with hot piperidine. Based upon previous studies in our lab, DNA duplexes with the Δ diastereomer of Rh complex (Rh-Δ) are used in photoirradiation, because Rh-Δ can intercalate into right-handed DNA helix with higher affinity than Λ diastereomer and thus can achieve higher yields of HT at distant

Table 7.2. Melting temperatures of duplexes **Rh-1** to **Rh-10**

# DNA	T_m/^oC	ΔT_m/^oC[a]
Rh-1	61.4(17)[b]	--
Rh-2	64.4(5)	3.2
Rh-3	64.5(8)	3.1
Rh-4	64.5(5)	3.1
Rh-5	65.2(2)	3.9
Rh-6	65.1(8)	3.7
Rh-7	63.6(6)	2.2
Rh-8	66.1(13)	4.7
Rh-9	63.8(1)	2.4
Rh-10	66.5(1)	5.1

a. ΔT_m are T_m difference between Rh-n (n = 2~10) and Rh-1.

b. [duplex]=1.3μM, [NaCl]=10mM, [sodium phosphate]=20mM. Standard deviations are listed in parenthesis. Details are seen in methods.

Table 7.3. Yield of guanine damage via HT through mC-containing DNA duplexes

# DNA	Yield Ratio[a]			
	D/P[b]	Y_P	Y_D	Y_M
Rh-1	0.43(6)[c]	0.56(4)	0.24(2)	0.20(3)
Rh-2	0.49(1)	0.52(6)	0.26(1)	0.25(3)
Rh-3	0.37(1)	0.60(2)	0.22(1)	0.19(4)
Rh-4	0.60(1)	0.48(6)	0.28(3)	0.24(4)
Rh-5	0.50(1)	0.53(5)	0.26(4)	0.22(2)
Rh-6	0.40(1)	0.59(6)	0.23(4)	0.19(2)
Rh-7	0.33(8)	0.62(5)	0.20(4)	0.17(4)
Rh-8	0.55(1)	0.50(5)	0.27(4)	0.23(2)
Rh-9	0.50(9)	0.51(6)	0.25(22)	0.22(2)
Rh-10	0.60(1)	0.48(4)	0.28(4)	0.24(2)

a. [Rh-n] = 4μM (n = 1~10), [NaCl]=10mM, [sodium phosphate]=20mM; experimental details are seen in materials and methods. Yield ratios represent the ratio of oxidative damage at the indicated guanine sites.

b. Y_D, Y_P and Y_M represent the G damage yield at distal, proximal GG and middle CpG sites, respectively. D/P represents the yield ratio of distal over proximal GG.

c. Standard derivations (SD) over at least 3 sets of independent experiments are listed in parenthesis.

guanines.[9] Irradiation of **Rh-1** to **Rh-7** at 313nm (Figure 7.2 and 7.3), as well as the rest of DNA assemblies (data not shown), shows direct photocleavage between bases C3 and T4, the typical intercalation site for Rh-Δ, and confirms that in all of the assemblies, the photooxidant is located at a fixed position away from both guanine doublets. Upon 365nm irradiation, mC-containing duplexes yield similar damage patterns as unmethylated **Rh-1** (Figures 7.2 and 7.3). Oxidative guanine damages, visualized by PAGE after hot piperidine treatment, are observed at both proximal (G6G7) and distal (G19G20) guanine doublets, as well as the middle CpG site (G12,G14). In both guanine doublets, 5' G (G7 and G20) has higher damage yields than 3' G (G6 and G19), which is a characteristic factor of guanine oxidation due to DNA-mediated CT.

7.3.4. Methylation effects on DNA-mediated HT. HT-induced oxidation of guanines in unmethylated **Rh-1**, and mC-containing assemblies, **Rh-2** to **Rh-10**, are visualized by gel electrophoresis (data not shown) and quantitated by ImageQuant. DNA assemblies in sections # 2~#4 with mC substitution at different sequential guanine segments show the same damage patterns as **Rh-1**. The yields of guanine damage at proximal (Y_P), distal GG (Y_D) and middle CpG (Y_M) are quantitated using the equations shown:

$$Y_P = \frac{I_P}{I_P + I_D + I_M}; \qquad Y_D = \frac{I_D}{I_P + I_D + I_M};$$
$$Y_M = \frac{I_M}{I_P + I_D + I_M}; \qquad D/P = \frac{Y_D}{Y_P}; \tag{7.1}$$

where I_D, I_P and I_M is the sum of band intensities at distal, proximal GG and middle CpG

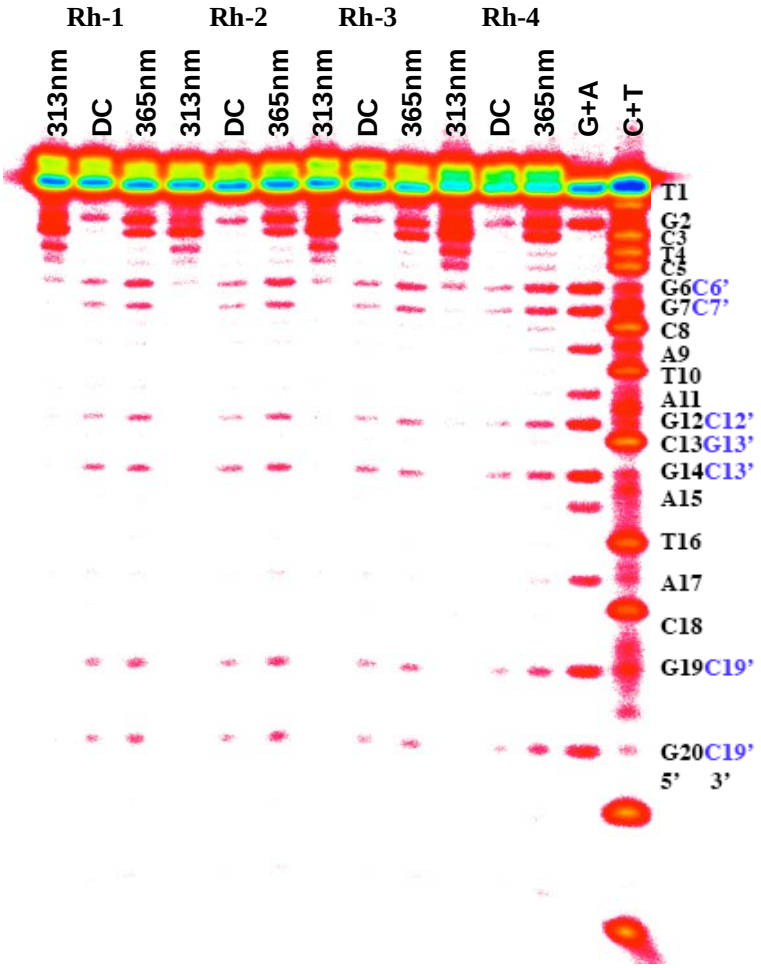

Figure 7.2. Damage patterns of of DNA assemblies in section #1 and #2 (**Rh-1** to **Rh-4)** after irradiation at either 365nm or 313nm are shown by a 20% PAGE. Sample identities are indicated in the figure. DNA sequence is shown on the right of Maxim-Gilbert land. Complementary bases to proximal (G6G7), distal guanine doublets (G19G20) and middle CpG site (G12C13G14) are indicated in blue. C6' in **Rh-2**, C7' in **Rh-3** and both C in **Rh-4** are substituted by mC. Complete sequences are listed in Table 7.1. Irradiation at 365nm is 0 or 60 minutes for dark control (DC) and 365nm samples, respectively. 313nm sample is irradiated for 10 minutes. Other working condition is listed in materials and methods.

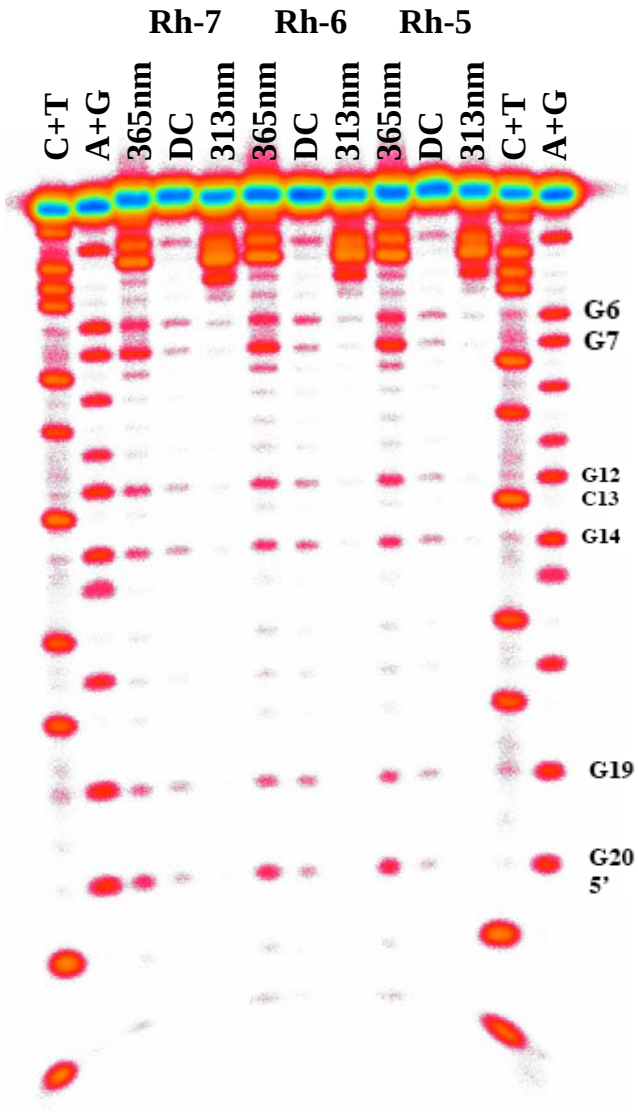

Figure 7.3. Damage patterns of of DNA assemblies in section #3 (**Rh-5** to **Rh-7)** after irradiation at either 365nm or 313nm are shown by a 20% PAGE. Sample identities are indicated in the figure. Potential G damage sites is shown on the right of Maxim-Gilbert land. Irradiation at 365nm is 0 or 60 minutes for dark control (DC) and 365nm samples, respectively. 313nm sample is irradiated for 10 minutes. The other working condition is listed in materials and methods.

sites, respectively. Another common parameter often adopted to show the efficiency of HT is the yield at distal over that at proximal GG (*D/P*). The values of these four parameters obtained for the ten DNA assemblies are listed in Table 7.3. The corresponding differential yields, which are obtained by subtracting the yield of **Rh-1** from those of the rest of the assemblies, are plotted in Figure 7.4. **Rh-1** shows Y_D and Y_M as 0.24(2) and 0.20(3), respectively, which is only half of Y_P (0.56(4)). The three yields of the mC-containing assemblies fluctuate, but not in an apparent correlation to the location of mC. Double substitution of mC at C6'C7' in **Rh-4** yields lower Y_P than that of **Rh-2** and **Rh-3** with monosubstitution at the same cytosine doublet; however, mC19'mC20' in **Rh-7** enhances Y_P for 5%~17% to the corresponding monosubstitution assemblies. After all, fluctuations of damage yields at three sequential G segments are all less than 15% of the yields observed in **Rh-1** and mostly do not exceed the errors.

The ratios of yield at distal GG over proximal GG sites are often used as a characteristic parameter reflecting HT efficiency. In each assembly section, *D/P* values do now show significant variation with DNA methylation; the variations do not exceed the uncertainty, except possiblely in **Rh-4, Rh-8** and **Rh-10**, as shown in Figure 7.4. In these three assemblies, *D/P* ratios are higher than that of **Rh-1**, which indicates that elevating amount of cation radical are propagated to the distal GG site in **Rh-4, Rh-8** and **Rh-10**.

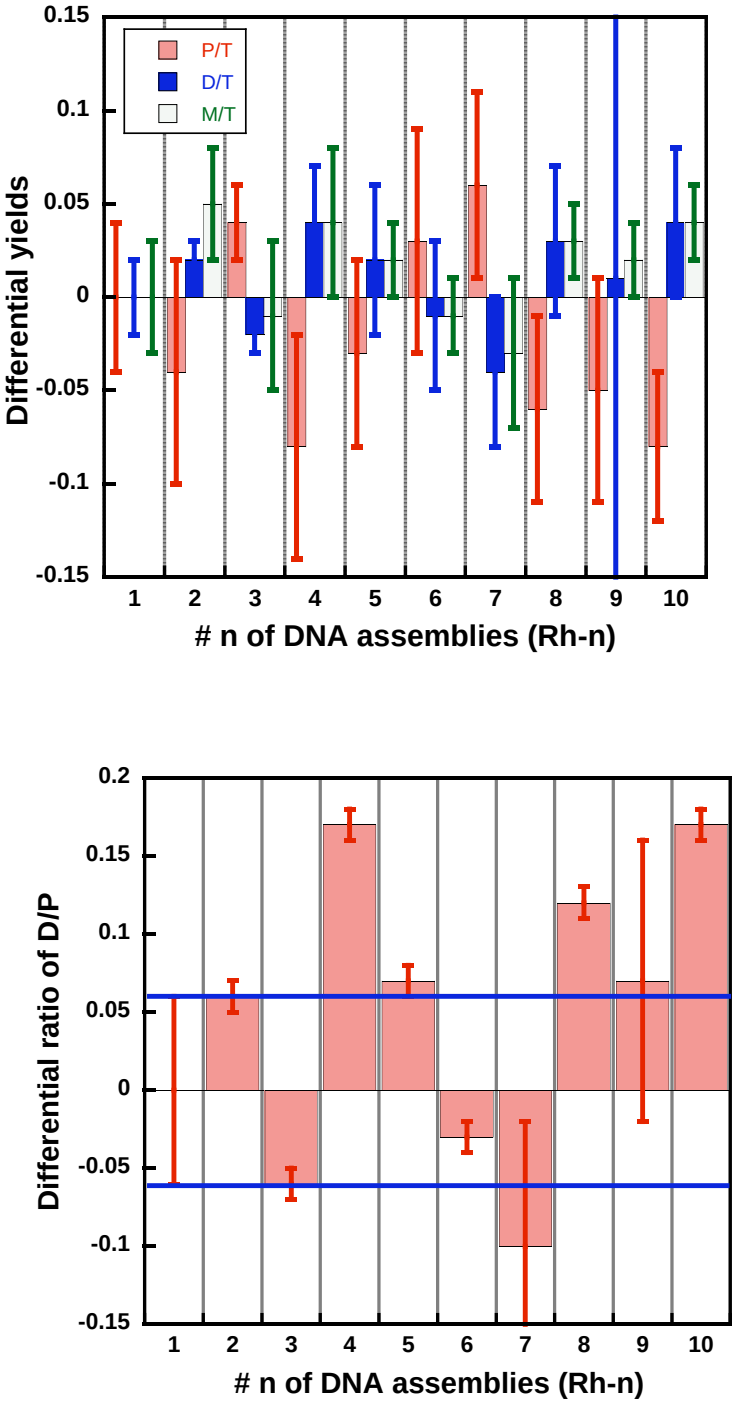

Figure 7.4. Methylation effects on DNA-mediated HT are investigated in mC-containing duplexes, **Rh-2** to **Rh-10**, comparing to **Rh-1.** *Top*: Differential yields of G damages at proximal (P/T), distal (D/T) GG and middle CpG (M/T) sites of assemblies, **Rh-1** to **Rh-10** are shown in red, blue and green, respectively with SD. *Bottom*: Differential ratio of D/P of the ten assemblies are shown with SD. SD are obtained over at least three sets of experiments. Details are in materials and methods.

7.4. Discussion.

In order to isolate the effects of methylation on DNA-mediated HT from other features, ten DNA assemblies were designed to have the same photooxidant and the same base sequence, except for the location and numbers of 5-methylcytosine substitution to cytosine. Upon UV irradiation followed by hot piperidine treatment, the guanine damage via HT can be discerned by PAGE and the roles that DNA methylation plays in HT may be revealed.

The extra methyl group on the C5 of mC increases the hydrophobicity of cytosine and extends the stacking area of G:mC along DNA base pair array. Although it is not correlated to the methylation pattern, alleviated T_m are observed in **Rh-2** to **Rh-10.** The enhancement of T_m in all of the mC-containing assemblies indicates that mC substitution makes DNA more stable in the duplex form than the unmethylated duplex, **Rh-1**.

5-Methyl-cytosine also affects the oxidative potential of the guanine base paired through hydrogen bonds.[13] Calculation results show that adiabatic I_p for G:C pair is about 0.75 eV lower than that of guanine itself. Since mC has lower I_p than cytosine, the electronic effect transmitted from mC to G would be more intense than C. Furthermore, PCET within base pairs separates the racial and charge on guanine cation radical ($G^{+\cdot}$) and presumably facilitates hole trapping at guanine sites. mC has an electron donating methyl group on pyrimidine to stabilize mC cation, which favors PCET between G and mC. Based upon above the three factors mentioned above, mC might be expected to contribute to HT by accelerating hole trapping at the base-paired guanine site. Kawai, *et.*

al. observed addendum of ET quenching rate of triplet N,N'-dibutylnaphthyldimide by switching from G:C to G:mC.[15] However, the HT yield revealed by guanine damage through PAGE in this chapter, as well as investigated by Kanvah, *et. al.*, do not show apparent effects of mC substitution. Similar G damage patterns occur in both mC containing duplexes and unmethylated **Rh-1**.[21] The fluctuation of oxidative guanine damage at three potential damage sites, proximal, distal GG and middle CpG, is not significant. Doubly mC substitution opposite to proximal and distal GG in **Rh-4** and **Rh-7**, respectively, even reduces the G damage yields at the corresponding methylation sites. Although the enhancement of D/P ratio in **Rh-4, Rh-8** exceeds the uncertainty, which may imply that mC substitution at proximal GG and middle CpG sites facilitates HT, the effect is less than 20% and not apparent in the other assemblies with mC substitution in the same section.

The failure to observe the methylation effects by guanine radical technique here is probably due to the slow trapping rate (k_{tr}) of guanine radical, which limits the detection of HT yield in mC-containing DNA. Even though mC may be able to accelerate k_{tr} of $G^{+\cdot}$, the alleviation is not great enough to make k_{tr} out-compete other electron pathways, such as back electron transfer. Thus effects of mC substitution on DNA-mediated HT are probably convoluted with the other faster electron pathways and cannot be revealed by guanine radical trapping technique.

7.5. Conclusion

Methylation effects on DNA-mediated HT are investigated in assemblies with a variety of mC substitution patterns. Enhancement of melting temperature in mC-containing duplexes shows that mC can stabilize the base stacking, probably due to the extended hydrophobic interaction from the methyl group. However, no apparent effects of methylation are observed by using guanine radical as a thermal hole trap here. This may imply that the slow trapping rate of guanine radical, as a rate-limiting step, overwhelms the contribution from mC substitution and obscures the potential effects that mC may have on DNA-mediated HT. In order to elucidate that, fast hole traps should be applied in future studies.

7.6. References

1. Adams, R., Burdon, R. *Molecular biology of DNA methylation*; Springer-Verlag: New York, 1985.

2. Razin, A., Cedar, H., Riggs, A. D. *DNA methylation, biochemistry, and biological significance*; Springer-Verlag; New York, 1984.

3. Robertson, K. D., Jones, P. A. DNA methylation: past, present and future directions *Carcinogenesis* **2000**, *21*, 461-467.

4. Antequera, F. Structure, function and evolution of CpG island promoters *CMLS, Cell. Mol. Life. Sci.*, **2003**, *60*, 1647-1658.

5. Denissenko, M. F., Chen, J. C., Tang, M. S., Pfeiffer, G. P. Cytosine methylation determines hot spots of DNA damage in the human P53 gene *Proc. Natl. Acad. Sci. U.S.A.* **1997**, *94*, 3893-3898.

6. Poulsen, H. E., Prieme, H. E. Cancer risk and oxidative DNA damage in Man *J. Mol. Med.* **1996**, *74*, 297-312.

7. Momparler, R. L., Bovenzi, V. DNA methylation and cancer *J. Cell. Physiol.* **2000**, *183*, 145-154.

8. (a) Eley, D. D., Spivey, D. I. Semiconductivity of organic substances. Part 9.—Nucleic acid in the dry state *Trans. Faraday Soc.* **1962**, *58*, 411-15. (b) Smart, R. S. Effect of oxygen on the optical and electrical properties of nucleic acids *Trans. Faraday Soc.* **1963**, *59*, 754-60.

9. Hall, D. B., Holmlin, R. E., Barton, J. K. Oxidative DNA Damage through Long Range Electron Transfer *Nature*, **1996**, *382*, 733-35.

10. (a) Henderson, P. T., Jones, D., Hampikian, G., Kan, Y. Z., Schuster, G. B. Long-distance charge transport in duplex DNA: the phonon-assisted polaron-like hopping mechanism *Proc. Natl. Acad. Sci. U.S.A.* **1999**, *96*, 8353-58. (b) Giese, B. Long-dstance electron transfer through DNA *Annu. Rev. Biochem.* **2002**, *71*, 51-70.

11. Nunez, M. E., Hall, D. B., Barton, J. K. Long range oxidative damage to DNA: effects of distance and sequence *Chem. Biol.* **1999**, *6*, 85-97.

12. O'Neill, M. A., Barton, J. K. DNA charge transport: conformationally gated hopping

through stacked domains *J. Am. Chem. Soc.* **2004**, *126*, 11471-11483.

13. Close, D. M., Oxidative damage to cytosine: implication for the study of radiation-induced damage to DNA *J. Phys. Chem. B* **2003**, *107*, 864-867.
14. Steenken, S., Electron transfer in DNA? Competition by ultra-fast proton transfer. *Boil. Chem.* **1997,** *378*, 1293-1297.

15. Kawai, K., Wata, Y., Hara, M., Tojo, S., Majima, T. Regulation of one-electron oxidation rate of guanine by base paring with cytosine derivatives *J. Am. Chem. Soc.* **2002,** *124*, 3586-3590.

16. Junicke, H., Kisko, J., Glebov, O., Kirsch, I. R., Barton, J.K. A rhodium(III) complex for high-affinity DNA base-pair mismatch recognition *Proc. Nat. Acad. Sci. U.S.A.* **2003**, *100*, 3737-3742.

17. Leitner, D., Schröder, W., Weisz, K. Influence of Sequence-Dependent Cytosine Protonation and Methylation on DNA Triplex Stability *Biochemistry* **2000**, *39*, 5886-5892.

18. (a) Hall, D. B., Barton, J. K. Sensitivity of DNA-mediated electron transfer to the intervening pi-stack: A probe for the integrity of the DNA base stack *J. Am. Chem. Soc.* **1997,** *119*, 5045-5046. (b) Dandliker, P.J., Holmin, R.E., Barton, J.K. Oxidative thymine dimer repair in the DNA helix *Science*, **1997,** *275*, 1465-1468.

19. Holmlin, R. E., Dandliker, P. J., Barton, J. K. Synthesis of Metallointercalator-DNA Conjugates on a Solid Support *Bioconjugate Chem.* **1999,** *10*, 1122-1130.

20. Sambrook, J., Fritsch, E. F., Maniatis, T. *Molecular Cloning: A Laboratory Manual*, 2nd ed, Colding Spring Harbor Laboratory Press: Plainview, NY.

21. Kanvah, S., Schuster, G. B. One-electron oxidation of DNA: the effect of replacement of cytosine with 5-methylcytosine on long-distance radical cation transport and reaction *J. Am. Chem. Soc.* **2004**, *126*, 7341-7344.